



University of
Nottingham
UK | CHINA | MALAYSIA

Colour polymorphism in the terrestrial snail *Cepaea nemoralis*: from genetics and genomics to spectroscopy and deep learning

Daniel Ramos Gonzalez, MBIolSci

Thesis submitted to the University of Nottingham for the
degree of Doctor of Philosophy

December 2020

Supervisors: Dr. Angus Davison and Dr. Sara Goodacre

Thesis abstract

Colour variation in the animal kingdom has been important in science to determine the principles of biology, especially in genetics and evolution. In the past decades, much effort has been targeted at the evolutionary, ecological and genetic basis of colour variation. Although land snails have been relatively neglected, especially in latter years, a comprehension of genetics and the evolution is important to understand colour variation precisely because snails may be representative of many species. When studying colour polymorphism, one of the remaining challenges is to describe colour. Generally, colour is described manually, relying on the judgment of human perception, classifying them into a discrete types. The main issue, then, is that human perception is subjective and colour is continuous. Fortunately, technology has enabled new techniques to score colour, which may help to investigate colour polymorphism.

This thesis aims to contribute to the knowledge of the maintenance of colour polymorphism by firstly, understanding the genetics and genomics and secondly, developing new methods for the scoring of colour. To achieve this, the grove snail *Cepaea nemoralis* was selected as a model species. *Cepaea nemoralis* was chosen due to their highly polymorphic shell, its easy collection, is widely distributed in all variety of habitats and the colour and banding morphs showing Mendelian inheritance (Cain & Sheppard, 1950, Cain & Sheppard, 1952, Cain & Sheppard, 1954, Lamotte, 1959, Jones et al., 1977).

In the first part, I aimed for a better understanding of the inheritance of colour. Hence, new crosses of *C. nemoralis* were used, with flanking restriction site-associated DNA sequencing (RAD-seq) markers used to identify putative instances of recombination with the supergene that determines colour and banding. No evidence of the predicted recombinants was found. Instead, a better explanation could involve incomplete penetrance and epistasis (Gonzalez et al., 2019). The findings therefore challenge the previous assumption of the supergene architecture and provides a new resource for the future creation of a fine mapping of the supergene (Gonzalez et al., 2019).

In the second part, I aimed to understand the evolutionary history of *C. nemoralis*, by investigating the relationship of the genomic and supergene variation with the geographic distribution over Europe. High-throughput genome-wide genotyping was achieved via a double digest restriction-site associated DNA sequencing (ddRADseq) method. A broad phylogenomic relationship showed geographic structure. However, no relationship between the geographical distribution and colour variation was found. Furthermore, possible genomic regions under selection, which may be driving the genomic variation, were identified. In addition, the phylogeny described the evolution of *C. nemoralis* and indicated how the Pyrenean lineages colonised Europe after the Pleistocene. The results suggest new roads of research into the evolutionary and genomic mechanisms that have led the geographical genomic and supergene variation of *C. nemoralis*.

In the third part, colour manual scoring was tested using new quantitative methods to describe colour to better understand colour variation. Therefore, a comparative study with historical and present shell colour patterns of *C. nemoralis* in the Pyrenees was used. Prior studies manually scored shell ground colour into three discrete colours; yellow, pink or brown. However, colour is continuous and the description of discrete colours may incur potential error and biased results. Thus, a quantitative method to score shell colour and to test manual scoring, comparing patterns of *C. nemoralis* shell colour polymorphism was used. Similar altitudinal trends irrespective of the method were found, even though quantitative measures of shell colour reduced the possibility of error. Moreover, a remarkable stability in the local shell patterns over five decades were found. This study determined that both methods remains valuable illustrating several advantages and disadvantages. In the future, a combination of both methods may be a possible solution.

Finally, and as continuation of the third part, a new visual recognition and classification method for *C. nemoralis* based on spectrophotometry and deep learning was created. Firstly, colour of the shells were quantified by spectrometry, and secondly, pictures were taken of the measured shells, in different backgrounds. Those pictures were used to train and test a Region-based Fully Convolutional Networks (R-FCN). Furthermore, public domain pictures were collected from iNaturalist database (<https://www.inaturalist.org/>), to validate the model. The results illustrate that this

method can achieve high accuracy of detection and classification of snails into the right morph. This work may facilitate the way of how colour polymorphism was investigated, illustrating new avenues for future research.

In conclusion, this thesis evaluates the limitations found in prior studies and generates new data for the genetic and genomic understanding of *C. nemoralis* colour polymorphism. It also produced viable solutions, using new technologies, to score the diverse colour morphs. I also contributed to the geographic evolutionary genomic diversity knowledge.

Publication

Gonzalez, D. R., Aramendia, A. C., & Davison, A. (2019). Recombination within the *Cepaea nemoralis* supergene is confounded by incomplete penetrance and epistasis. *Heredity*. doi:10.1038/s41437-019-0190-6

Additional manuscripts in review

Ramos-Gonzalez, D, Davison, A. Qualitative and quantitative methods show stability in patterns of *Cepaea nemoralis* shell polymorphism in the Pyrenees over five decades. *Ecol Evol*. 2021; 00: 1– 17. <https://doi.org/10.1002/ece3.7443>

Declaration of own work

Although the use of passive voice throughout this thesis have been applied in agreement of the academic scientific writing, all the practical experiments and data analysis were conducted by myself, with the exception of clearly mentioned procedures.

Chapter contributions

Chapter 2: This work was originally conceived by Angus Davison, with the laboratory work conducted by Amaia Caro Aramendia and myself. The published paper was also jointly written by Angus Davison and myself.

Chapter 3: This work was originally conceived by myself in discussion with Angus Davison. The majority of the snails used were collected by Adele Grindon as part of her PhD. The remainder were collected by a team on a trip to the Pyrenees, led by myself and with the help of Angus Davison, Hannah Jackson and Alejandro Garcia Alvarez. The unpublished reference genome was kindly provided by Suzanne Saenko. The analysis was carried out by myself, in discussion with Angus Davison. The work was first drafted by myself, and then reviewed by Angus Davison.

Chapter 4: This work, including the sampling design and the comparison between qualitative and quantitative methods, was originally conceived by myself in discussion with Angus Davison. The Pyrenean samples were collected by a team led by myself, with the help of Angus Davison, Hannah Jackson and Alejandro Garcia Alvarez. The analysis was carried out by myself, in discussion with Angus Davison. The work was first drafted by myself, and then reviewed by Angus Davison.

Chapter 5: This work was originally conceived by myself, in discussion with Angus Davison and Alejandro Garcia Alvarez. All images were generated by myself. The deep learning algorithm was developed by Alejandro Garcia Alvarez, in discussion with me. The analysis was carried out and the work was first drafted by myself, and then reviewed by Angus Davison.

Acknowledgements

The completion of this thesis has been possible to a great extent by the guidance, help, collaboration and moral support of many people, both in Nottingham and elsewhere on the planet. First and foremost, I would like to thank my supervisor Dr. Angus Davison. I really appreciate your understanding, guidance and attention from the first days to the last of this PhD. I also would like to thank Dr. Sara Goodacre, the members of the staff and all the other students and academics for showing support and invaluable experiences, when I most needed it.

Moreover, I would like to thank University of Nottingham and the Biotechnology and Biological Sciences Doctoral Training Programme to give me the chance, first, and the financial support and resources to accomplish this thesis.

A special thanks to Alejandro Garcia Alvarez for joining my fieldwork expedition to the Pyrenees, for providing guidance in the development of the deep learning algorithm and for the moral support. I also would like to thank Hannah Jackson for joining my fieldwork expedition to the Pyrenees. Thanks to both Sheila Keeble and Julie Rodgers for help with the care of snails, to Amaia Caro Aramendia to contribute in the genotyping of the snail crosses and to Sophie Poole who helped with some of the shell colour measurements. Thanks to the SNPsaurus team to deliver the RAD-sequencing. Moreover, the analysis of the genomic data would have not been possible without the guidance of Dr. Mark Ravinet, Dr. Joana Meier and Dr. Simon Martin.

I would also like to thank Jonathan Silvertown and the Evolution Megalab team who provided the historical data used in the comparative study. Thanks to Dr. Adele Grindon for providing the European sampling collection and Dr. Suzanne Saenko who provided an unpublished *Cepaea nemoralis* reference genome. Also, thanks to Dr. Laurence Cook as well as three anonymous referees for comments on the genetics manuscript, and to Dr. Robert Cameron and Dr. Małgorzata Ożgo for comments on the Pyrenean chapter. Additionally, to Anne Clarke and the University of Nottingham for access to the archive of Professor Bryan Clarke.

Finally, I would like to express my endless gratitude to my family, especially to my mother Marisa Gonzalez Ventoso, my sister Judit Ramos Gonzalez, my grandmother Maria Luisa Ventoso Bofill, my uncle Juanjo Gonzalez Ventoso, my cousins and my aunt-cousin Hortensia Gonzalez de la Fuente, for being just the nicest people ever. Also thanks to Noemi Contreras Marmol for caring and supporting me, Marc Gallardo Lombarte to keep me fit, Carlos Dominguez Puig because of his “repechitos”, Adrian Perez Martinez because of his resilient encouragement, Isaac Vidal Valdivia and his medical approach to live, Cristian Bejarano del Olmo due to his life challenges, Guillermo Arranz Bernal to teach me how to relax and many others to believe in me. To the DTP crew, especially Pierre Reitzer and his board-game nights, James Reekes and his runs at Uni park and Nottingham handball club to make these four years fantastic. Ultimately, thanks to my supportive bubble during this lockdown times, Giada Pedretti and her plank challenges, Louise Nathalie Vingert Silveira and her coffee breaks and excellent motivation, Samantha Paterson and the cow vision of life, Fotini Iacovou keeping my feet in the ground, Mark Palmieri and his Italian way of life and Bruna Falgueras Vallbona for your hope, your energy, your joy and your great support.

“In the long history of humankind (and animal kind, too) those who learned to collaborate and improvise most effectively have prevailed.”— Charles Darwin, The descent of man, 1871.

List of figures

1.1. <i>C. nemoralis</i> illustration	8
1.2. CIE 1931 chromaticity diagram	16
2.1. Representation of shell offspring and putative recombinant	34
3.1. European map of the genomic sampling collection	47
3.2. Genomic structure of <i>C. nemoralis</i> across Europe	54
3.3. Correlation of F_{st} versus geography	58
3.4. Density graphs of genetic differentiation	59
3.5. PCA analysis to the supergene-linked dataset	65
4.1. Overview of Pyrenean sampling locations	76
4.2. Colour distribution in the Central Pyrenees	82
4.3. Banding distribution in the Central Pyrenees	83
4.4. Comparison of changes in the shell frequencies	85
4.5. Present-day relationship of shell features and altitude	87
4.6. PC3 and altitude relationship	89
4.7. Relationship between altitude and colour variation	91
5.1. Bounding box pictures	107
5.2. General organization of R-FCN	109
5.3. Prediction result examples	112
5.4. Examples of prediction failures	113
5.5. Prediction test results	115
5.6. Background accuracy results	116
5.7. Pink banded variation	120

List of tables

2.1. Phenotypes and genotypes of <i>C. nemoralis</i> crosses	26
2.2. Summary of linked loci phenotypes	29
2.3. Summary of RAD-seq markers genotyping	37
3.1. Genomic samples summary	48
3.2. Four population test (D-statistic) results	56
3.3. F_{st} mean between all populations comparisons	60
3.4. Genbank homology sequences	63

4.1. Sampling collection summary	80
4.2. Statistical summary of shell geographical distribution	84
4.3. Fisher r-to z-transformation summary	88
5.1. Summary of picture datasets	104
5.2. Summary of accuracy metrics	114

Table contents

Thesis Abstract	i
Publication	iv
Additional manuscripts in review	iv
Declaration of own work	v
Chapter contributions	v
Acknowledgements	vi
List of figures	viii
List of tables	viii
Chapter 1: General introduction	1
1.1. Evolutionary genetics and genetic polymorphism	1
1.2. The grove snail (<i>Cepaea nemoralis</i>) in evolutionary genetics	4
1.3. Synthesis of the genetics and genomics of <i>C. nemoralis</i>	9
1.4. Characterising colour polymorphism	15
1.5. Citizen science	18
1.6. Thesis aims	19
Chapter 2: Recombination within the <i>Cepaea nemoralis</i> supergene is confounded by incomplete penetrance	22
Abstract	22
2.1. Introduction	23
2.2. Materials and methods	25
2.2.1. The culture of <i>Cepaea</i> and crosses	25
2.2.2. DNA extraction, quantification and amplification	30
2.3. Results	32
2.3.1. Segregation of Mendelian loci that determine shell phenotype	32
2.3.2. Putative recombinants between colour, banding and lip and band pigmentation loci	33
2.3.3. Genotyping of offspring using RAD-seq derived loci	36
2.4. Discussion	38
2.4.1. Incomplete penetrance and epistasis	38
2.4.2. Future progress	41
2.5. Acknowledgements	41

Chapter 3: Exploring the divergence of genomic variation and geographical structure in *Cepaea nemoralis* **42**

Abstract	42
3.1. Introduction	43
3.2. Materials and Methods	47
3.2.1. Dataset collection	47
3.2.2. Genomic methods	50
3.2.3. Sequence analysis and datasets	50
3.2.4. Analyses of genomic variation	51
3.3. Results	53
3.3.1. Western European phylogenomics of <i>C. nemoralis</i>	53
3.3.2. Different genomic evolutionary history of the colour and geographic variation	64
3.4. Discussion	66
3.4.1. Colour and genomic geographic variation	67
3.4.2. Evolutionary history, genomic diversity and population structure of <i>C. nemoralis</i>	69
3.5. Acknowledgments	71

Chapter 4: Qualitative and quantitative methods show stasis in patterns of *Cepaea nemoralis* shell colour polymorphism in the Pyrenees over five decades **72**

Abstract	72
4.1. Introduction	74
4.2. Materials and methods	77
4.2.1. Shell samples and human-scoring of shell phenotypes	77
4.2.2. Quantification of shell colour	78
4.2.3. Analysis of phenotype frequencies and correlation	79
4.3. Results	80
4.3.1. Past and present-day geographic distribution of colour and banding morphs	80
4.3.2. Quantitative measures of shell colour and banding and associations with altitude	88

4.3.3. Past and present-day associations, using qualitative and quantitative methods	89
4.4. Discussion	92
4.4.1. Quantitative versus qualitative methods to score shell phenotype	92
4.4.2. Past and present-day geographic distribution of colour and banding morphs	93
4.4.3. From phenotype to genotype	94
4.4.4. Conclusion	95
4.5. Acknowledgements	96
Chapter 5: A new <i>C. nemoralis</i> recognition and shell morph classification system using deep learning	97
Abstract	97
5.1. Introduction	98
5.2. Materials and methods	102
5.2.1. Image datasets	102
5.2.2. Training inputs	106
5.2.3. System overview	108
5.3. Results	111
5.4. Discussion	117
5.5. Conclusion	121
5.6. Acknowledgements	121
Chapter 6: General discussion and conclusions	122
6.1. <i>Cepaea nemoralis</i> colour polymorphism, a multidisciplinary challenge	122
6.2. Future steps towards understanding <i>Cepaea nemoralis</i> shell polymorphism	125
6.2.1. Mapping <i>Cepaea nemoralis</i> genome	125
6.2.2. Citizen science, the future of ecological and evolutionary genetics	128
6.3. Final conclusion	132
References	135
Supporting information	150
Chapter 2	150
Chapter 3	169
Chapter 4	218

Chapter 1:

General introduction

1.1. Evolutionary genetics and genetic polymorphism

Historically, ecological and evolutionary genetics studies have focussed on two patterns found in nature: adaptation, which refers to the relationship of the “fit” between environment and individuals, and genetic polymorphism (Dobzhansky et al., 1970). In the natural world, a genetic polymorphism occurs when phenotypic variation within and between populations of the same species is maintained and caused by two or more alleles each with considerable recurrence (Ford, 1975). Thus, ecological and evolutionary genetic studies focus on changes in the frequency of genotypes within populations, which ultimately may lead to speciation. Hence, the longstanding aim in evolutionary genetics has been to understand how the evolutionary factors affect the variation of biodiversity observed in nature.

There are four main evolutionary forces acting among and within populations of the same species: random genetic drift, gene flow, natural selection and mutation. Random genetic drift occurs in any population of finite size, due to random sampling of individuals (Masel, 2011; Wright, 1937), with smaller populations more affected. This effect is most pronounced in a bottleneck or founder event (Star et al., 2013; Wright, 1937). Gene flow is defined as the transmission of genetic material among populations. Normally, this event is caused by migration between populations (Star et al., 2013). In the case of populations illustrating high levels of genetic material transmission with similar allele frequencies, both populations can be considered as a single population. Natural selection pressures are described as the survival and the production of offspring to some individuals displaying specific morphs within populations due to their more adapted features for those environmental conditions (Darwin, 1859; Star et al., 2013). Finally, mutations are modifications in the DNA sequence of the genome of an individual (Beadle et al., 1941).

These evolutionary forces vary in their influence upon populations. While the majority of genetic mutations are neutral, which means that they do not have either positive or negative effects on the fitness of the individuals (Ford, 1975), when a positive or negative mutation occurs, other factors are known to act. For example, the pressure of directional selection often may cause that a new active genetic mutations becomes widespread over long periods due to 'survival of the fittest' (Wade, 2008), or random genetic drift may also contribute to the increase of the new active genetic mutations. However, also other forces may challenge the new effective genetic mutations. For instance, high levels of gene flow may contribute to the maintenance of the previous characteristics of the species. The higher the migratory frequency, the greater the probabilities of maintaining pre-established genetic conditions (Star et al., 2013). These evolutionary processes can interact and oppose each other as they may operate simultaneously causing alterations in the allele frequencies (Svensson, 2017). All these factors can be determined by mathematical theories of population genetics, which were generated by examining the evolutionary forces effects on genetic variation in species (Cook et al., 1996; Fisher, 1947; Ford, 1975; Wright, 1948).

In addition, there are other evolutionary process causing genetic polymorphism besides the genetic drift and directional selection. For example, frequency-dependent selection, which the fitness of the genotype depends on their abundance in the given population, may increase the frequency of rare morphs (Ayala et al., 1974; Jones et al., 1977). Either disruptive selection, which favours the extreme types of a normal distribution in a population as a consequence of a balance between gene flow among subpopulations and natural selection acting in diverse directions (Jones et al., 1977). Alternatively, also heterozygous advantage (stabilizing selection), which the heterozygote morph are fitter than the homozygote ones (Cain et al., 1963; Cain et al., 1954; Jones et al., 1977).

The emphasis of past research has been on attempting to determine whether polymorphism was genetic or not, the identification of each morph frequency and understanding its maintenance by examining natural selection and other evolutionary factors acting upon it (Fisher, 1930; Ford, 1975). During the beginning of the past century, the earliest ecological geneticists primary aim was to target natural selection as the main justification to explain the maintenance of a balanced polymorphism,

which is the coexistence and constancy of frequencies of several morphs in a given population (Fisher, 1930; Ford, 1975). Therefore, selective forces such as climate selection, predation or habitat were considered the main interpretation to explain morph frequency variation. For example, in the land snails *Theba pisana*, the absorption of heat by exposure to the sun by their shells depended on the colour, with the lighter colours absorbing the least heat (Cain, 1984; Cowie, 1990; Scheil et al., 2012a). Moreover, predation and habitat, together, can play a key role in the distribution of shell morphs, creating a mosaic of different frequencies among neighbouring populations (Cain, 1984; Cowie, 1990; Heller, 1981; Scheil et al., 2012a). The song thrush (*Turdus philomelos*) is known as one of the main predators of *Theba pisana* discriminating conspicuous shells depending on the background (Heller, 1981). For example, lighter shells in darker backgrounds are more exposed to predation affecting the fitness of the morphs (Johnson, 2011).

Then, from the 1960s and subsequent years, the introduction of molecular biology techniques changed the field of evolutionary genetics, raising new questions. As a result, researchers started focusing on understanding the genetic inheritance and genetic and genomic patterns driving the polymorphism. In recent decades, as DNA sequencing became more accurate, efficient and widely available to all researchers, novel methodologies were created, which opened up more precise conclusions. For instance in evolutionary biology, genome-wide sequencing is used to investigate complex evolutionary processes. For example in the House sparrows (*Passer domesticus*), this technology helped to comprehend the causes of new rapid genetic adaptations due to links with human development (Ravinet et al., 2018).

Among all kinds of polymorphism found in nature, one of the most studied is colour polymorphism. Traditionally, colour polymorphism was used to understand the functional meaning and ecological circumstances of all morphs due to the ease of recognising and describing their different phenotypes (Svensson, 2017). For example, some of the most common species used were butterflies and snails. These species exhibited clear visible phenotypic variation and can easily be raised in captivity, which made them model species in the earlier studies of natural selection (Fisher, 1930; Müller, 1879).

There are many examples of colour polymorphic model species. One of the classic colour polymorphic model species are the butterflies with mimicry rings (e.g. *Heliconius numata* and *Consul fabius*) (Müller, 1879). These species have been broadly studied to determine, for example, natural selection, aposematic selection, in which some morphs mimic dangerous or distasteful species for the predator (Joron et al., 1998), or to test gene flow and speciation (Martin et al., 2013). Another classic example used in evolutionary and ecological genetics is the Scarlet tiger moth (*Panaxia dominula*). *P. dominula* displays wing colour variation from a metallic-green sheen with white and orange or yellow signs, to red hindwings with variable black marks. This species was a target of one of the longest and continuous surveys in a single population (Fisher, 1947). Fisher (1947) examined possible annual fluctuations in morph frequency variation of *P. dominula* to explain whether natural selection or random genetic drift showed more influence in those changes. Fisher found that the observed fluctuations were driven by natural selection concluding that selection could be tested in wild populations (Fisher, 1947).

Other species, such as avian model species have also been at the centre of evolutionary research. For instance, hundreds of bird species including *Strigiformes*, *Ciconiiformes*, *Cuculiformes* and *Galliformes*, which show a range of colour polymorphic plumage (Galeotti et al., 2003) are used to understand the maintenance of the polymorphism due to its variety of possible selective scenarios where birds can be prey, predators and competitors at the same time. In this case, in evolutionary genetics, birds became model species, for example, to comprehend selection (Clarke, 1969; Paulson, 1973), to study disruptive selection (Baker et al., 1979; Rohwer, 1990), or to determine sexual selection among individuals (Endler, 1987).

1.2. The grove snail (*Cepaea nemoralis*) in evolutionary genetics

Terrestrial land snails can be considered as rather inconspicuous fauna in nature. However, some snail taxa exhibit an extensive shell variation, from patterning, shell shape or chirality to ground colour, making them useful to study genetic polymorphism. Studies focused on the genetic mechanisms and micro-evolutionary events caused by

selective factors in land snail species have been carried out over a century. With the main aim to understand the evolution and maintenance of shell polymorphism.

Land snails have, undoubtedly, played an important role in understanding genetic polymorphism resulting into the establishment of the modern ecological and evolutionary genetic discipline (Murray et al., 1978). Previous to the modern evolutionary synthesis, a great variety of studies were carried out based on the acquisition of the intrinsic knowledge of shell polymorphism. For example, land snail genera such as *Theba*, *Trochulus*, *Partula* or *Cepaea* (Clarke et al., 1971; Jones et al., 1977; Proćków et al., 2018; Scheil et al., 2012b), with a huge range of colour and banding shell patterns, were selected as models to understand its mechanisms. In French Polynesia the *Partula* genus was surveyed in the search of the understanding of the selective forces acting upon its shell colour variation (Clarke et al., 1971). Furthermore, recent research examples in land snails showed how colour and its thermic capacities of heat absorption are involved in *Theba pisana* shell variation, illustrating a correlation between shell type distribution and climatic selection (Scheil et al., 2012b); or habitat and shell morphology relations in the European *Trochulus hispidus* and *Trochulus sericeus* (Proćków et al., 2018).

In particular, the famous land snail *Cepaea nemoralis* was perceived as an excellent model species to study colour polymorphism due to its apparent non-adaptive and random diversity in wild populations (Lamotte, 1951). As mentioned above, the classic studies examined whether natural selection prevailed as the principal cause of shell banding and colour variation (Cain et al., 1950, 1952, 1954). Thereafter, other comparative surveys brought out other selective factors such as predation, variety of habitats and other evolutionary forces illustrating correlations with shell morph frequencies (Jones et al., 1977). Nowadays, *C. nemoralis* has become a traditional case study of adaptive evolution, attracting a growing interest from both, professionals and citizen scientists (Chapters 4 and 5; Cameron et al., 2012; Kerstes et al., 2019; Silvertown et al., 2011). Additionally, the development of new molecular protocols brings new avenues in the understanding of evolutionary forces and non-selective mechanisms related to the roots of natural variation in terrestrial land snails (Davison, 2002; Richards et al., 2013).

Overall, *C. nemoralis* is a good case to study in evolutionary genetics for a broad range of reasons (Figure 1.1). Firstly, it occupies a variety of different habitats, from woodland and grassland to sand dunes (Jones et al., 1977). Secondly, simple Mendelian inheritance is shown in the major loci that establishes shell polymorphism (Chapter 2 and 3; Cook, 1967; Jones et al., 1977). Thirdly, it has a highly polymorphic shell, which show three main inherited features. On one side, shell ground colour (C) can be dark brown, pink or yellow with deduced genotype dominance (brown > pink > yellow). On the other side, shells may have a wide range of dark bands (B) from zero to five, with its deduced genotype dominance (absence > presence). Moreover, bands may differ in their pigmentation (P), usually being fully pigmented bands, but sometimes unpigmented, interrupted (I), or spread (S). The genotypic dominance, in this case, being normal pigmentation dominant (Chapter 2, 3, 4 and 5; Jones et al., 1977). Fourthly, shape and coiling illustrate clear variation. All these traits together may be associated with environmental parameters and their intrinsic genetics can be a possible practical genetic marker themselves, which are genes with known location that can be used to recognise species (Figure 1.1, Davison, 2002; Murray et al., 1978). Finally, *C. nemoralis* can sometimes be crossed to obtain offspring and are easily maintained in laboratory. This is certainly helpful in the molecular studies (Davison, 2002; Richards et al., 2013).

In addition, at least nine loci involved in the expression of shell polymorphism have been identified, from which at least five are considered to be tightly linked together into a 'supergene' (Jones et al., 1977; Richards et al., 1975; Richards et al., 2013), a supergene is a group of neighbouring genes that inherited together (Ernst, 1936). Consequently, band presence, ground colour, pigmentation, interruption and fusion are thought to be linked in the supergene. Moreover, band suppression, which is supposed to have two loci, the intensity and colour banding seems to be unlinked loci (Richards et al., 2013). All these loci showed epistatic interactions among them and with the unlinked loci. Furthermore, the recombination frequencies within the *C. nemoralis* supergene have been estimated empirically (Cain et al., 1960; Cook, 1967; Richards et al., 2013). The conclusions hypothesised of a very tight linkage cluster composed by shell ground colour, band presence and band interruption showing recombination rates of ~0–2%. Other loci such as the spread banding and band pigmentation may be slightly less than the C-B linkage cluster, with respective

recombination rate estimations of ~3–4% and ~4–15% (Cain et al., 1960; Cook, 1967; Richards et al., 2013). Finally, Richards 2013 were able to generate RAD markers linked to the *C. nemoralis* supergene creating the basis for forthcoming research in molecular ecology.

In addition, museums, universities and digitised projects recorded and stored an abundant historical data from the 20th century on *C. nemoralis*, which continue to be available to the modern days (Silvertown et al., 2011).



Figure 1.1. Illustration of the variation of *Cepaea nemoralis* shell colour and banding in wild-collected individuals.

1.3. Synthesis of the genetics and genomics of *C. nemoralis*

As mentioned above, the historical evolutionary processes of colour polymorphic species have been a focus of research in evolutionary biology. One common approach to contribute to the study of colour polymorphism is the use of molecular biology methods due to their many attributes as mentioned in section 1.1 of this chapter (Cuthill et al., 2017; McKinnon et al., 2010; McLean et al., 2014; San-Jose et al., 2017). The objective of molecular biology in polymorphic evolutionary genetics, therefore, is to understand the molecular mechanisms and processes driving the evolution and maintenance of polymorphisms.

Pulmonate snails, like the genus *Cepaea*, have been presented as good model species candidates when researching environmental and evolutionary genetics due to the abundance of ecological data as also reviewed in section 1.2 of this chapter (Davison, 2002). Many efforts have been made in the understanding of the historical evolutionary processes of *C. nemoralis*. However, only a small number of studies used genetic data, even though molecular biology research in evolutionary biology and especially in evolutionary genetics started in the 1960's. Historically, the study of the maintenance of *C. nemoralis* colour polymorphism were based on the generation of crosses, and comparative surveys (morph frequencies) rather than molecular research, which were and are commonly used to create a broad picture of the understanding of the maintenance of the polymorphism. Originally, the shell morph diversity was thought to be non-adaptive and due to local events (Cameron, 1998; Goodhart, 1963). Nonetheless, the following 30 years of morph frequency research concluded that the shell polymorphism was, indeed, adaptive and that their morph frequencies could be influenced by natural selection (Jones et al., 1977). These studies provided important knowledge and insights on how evolutionary forces influence populations in local or larger areas. However, there are many unresolved questions, which need to be investigated from other perspectives.

In subsequent years, molecular population genetics was revolutionised by the development of genetic data collections and subsequently, academic developments. These new developments allowed the first measures of genetic variation in *C.*

nemoralis, to occur using alloenzymatic and enzymatic loci, opening a new era of research in population genetics. These studies enabled researchers to assess differences between adjacent populations contributing to their understanding of the evolutionary history, gene flow and selection in 'area effects' cases (Johnson, 1976; Ochman et al., 1983). The term 'area effects' is associated to the *Cepaea* genus and refers to the stability of morph frequencies over extensions bigger than a panmictic unit despite the visual selection, which these effects are caused by selective forces not related directly to the topography (Cain et al., 1963). For example, in the Pyrenees, where Caugant et al. (1982) and Ochman et al. (1983) sampled the region and generated local phylogenies using enzymatic variation, both authors identified a polymorphic morphological and molecular geographic structure in Pyrenean populations due to 'area effects'. Their findings suggested that the described 'area effects' were due to the temporary geographic isolation during the last glaciation. Subsequently, Valdez et al. (1988) and Guiller et al. (1993) sampled the same and other areas of the Pyrenees with similar hypothesis, results and conclusions reported. Other authors used enzymatic variation to evaluate 'area effects' in other geographical regions. For example in the Lambourn Downs, Johnson (1976) hypothesised of several causes of 'area effects' found due to lack of evidences not giving a clear explanation of the patterns found (Johnson, 1976). Another study in the lowlands of England used molecular enzymatic variation to test 'area effects' by visual selection in *C. nemoralis* populations finding instead, a correlation with altitude (Wilson, 1996).

Moreover, the employment of mtDNA and small numbers of genetic markers to assess phylogenetic relationships started to be used in evolutionary biology. In *C. nemoralis*, molecular biological studies aimed to understand either the genetic inheritance of *C. nemoralis* (Davison, 2000b; Terrett et al., 1996; Thomaz et al., 1996; Yamazaki et al., 1997), or whether to infer the genetic evolutionary history and the factors acting within and between populations (Davison, 1999, 2000a; Davison et al., 2000; Ellis, 2004; Grindon et al., 2013a; Neiber et al., 2015). For example, Davison, in a series of consecutive studies, performed the first few studies based on genetic data in *C. nemoralis* (Davison, 1999, 2000a, 2000b; Davison et al., 2000). Initially, the first microsatellite primers and mtDNA (16S rRNA locus) were created for *C. nemoralis* individuals striving to set the foundation for future research in the population relationships of the grove snails (Davison, 1999, 2000b). Subsequently, the

microsatellite and the mitochondrial DNA were used to assess 'mysterious' geographical patterns of shell polymorphism both locally in the famous Marlborough Downs in Wiltshire (Davison et al., 2000). As well as a more broadly study to evaluate the distribution of *C. nemoralis* from East to West in the islands of Britain and Ireland finding that the origin of the Irish populations may not come from the Britain island (Davison, 2000a). Moreover, mtDNA was used to infer the mitochondrial genomic inheritance discarding the possibility of a doubly uniparental inheritance, as it happens in other species like *Mytilus*, where maternal and paternal mitochondrial lineages coexist (Garrido-Ramos et al., 1998).

Furthermore, various authors used the molecular variation in *C. nemoralis* mitochondrial DNA to infer the genetic geographic divergence in European populations. In a notable example, Neiber et al. (2015) generated a molecular phylogeny combining mtDNA and nuclear sequences to study the ancestry of the genus *Cepaea*. The *Cepaea* genus was thought to be monophyletic and comprised of four pulmonate species; *C. nemoralis*, *C. hortensis* "*Cepaea sylvatica*" and "*Cepaea vindobonensis*". However, molecular phylogeny, using mitochondrial and nuclear sequences and comparing to another 20 genera of *Helicidae*, revealed that the supposed *Cepaea* genus is polyphyletic and that *C. sylvatica* is more closely related to *Macularia* genus and *C. vindobonensis* to the genus *Caucasotachea* (Neiber et al., 2015). Complementary, other research using mtDNA of just *C. nemoralis* populations, helped to reveal the expansion of snail populations after the Pleistocene. For instance, Grindon et al. (2013a) surveyed Europe to determinate the Irish ancestry using *C. nemoralis*. Interestingly, a mitochondrial lineage (C) was found only in the central and Eastern Pyrenees, Ireland, the western area of Great Britain and the Isle of Man. Grindon et al. (2013a) argued that vessels brought these populations through the Noguera Pallaresa – Garonne River to the Irish island, from the Pyrenees. In addition, Ellis (2004) evaluated the molecular pattern distribution of *C. nemoralis* populations in a local area, the Pyrenees. In this instance, mitochondrial DNA together with enzymatic variation were used to examine the relationship of shell patterns with their geographic distribution. Due to a lack of association, therefore, Ellis (2004) argued that the molecular and shell pattern variations were likely "relics of history" rather than variations caused by molecular area effects.

Whereas the use of few genetic markers and mtDNA have undoubtedly been informative when testing phylogenetic associations. The use of these methods has revealed several limitations. Firstly, mapping single genes may generate variations from the general species phylogeny (Nichols, 2001); biased results may occur due to many reasons such as population level relationships, bottlenecks, high mutation rates, introgression or to the low representation of the species when using individual or few genes. This is consistent with Davison et al. (2000) who showed how genetic markers could differ among them due to events like 'area effects'. Secondly, even though mtDNA can add information in the study of the genetic variation, it needs to be taken cautiously. As Funk et al. (2003) reported, mtDNA phylogenies can be strongly influenced by incomplete lineage sorting and introgression at species level. Thirdly, positive selection on mtDNA may affect the neutrality of known genetic markers as Parmakelis et al. (2013) indicated. Finally, and specifically in pulmonate snails, the rate of mtDNA evolution is remarkably elevated compared to other animal families (Thomaz et al., 1996), making outcomes uncertain. Previously, several authors thought that this mtDNA high rate was due to result of selection, high mutation rate or even population demography (Davison, 2002; Thomaz et al., 1996). However, these explanations may be insufficient to explain the high mitochondrial genetic diversity in pulmonate snail rising the ovotestis effect. The ovotestis effect occurs in hermaphrodite species where both reproductive cells (ova and sperm) accumulated similar mutation frequency increasing the mtDNA diversity (Davison, 2006). This hypothesis is founded in the theory of both reproductive cells undergo to approximately the same cell divisions showing similar accumulated mutation rates (Davison, 2006).

Currently, evolutionary genetics is entering an interesting prolific period. Technological progress in population-scale sequencing are developing rapidly. They are driving scientists to useful data sources, which are influencing and transforming the studies in genetic polymorphism. Consequentially, recent studies in *C. nemoralis* started using population genomics, proteomics, and transcriptomics and epigenomics techniques. All these molecular procedures enhance the knowledge of microevolution in individuals contributing to determine the demography of a population and its phylogenetic history. Thus, the use of one or another method depends on the hypothesis being tested. For instance, proteomics is frequently used to understand the expression of pigments. In molluscs, there are a lot marine snail shell-proteomes

characterised (Kocot et al., 2016). In land snails, next generation sequencing and high throughput proteomics has been used to characterise the first pulmonate of *Cepaea nemoralis* shell-proteome (Mann et al., 2014). The advantage of using proteomics instead of transcriptomics to describe a protein is that transcriptomics gives a rough estimation of the protein expression while proteomics confirms and quantifies the presence of a protein.

Moreover, the transcriptomics high-throughput method to study the genome are useful to unravel local adaptation processes in several time and temporal scales (Hendricks et al., 2018). Recent advances in RNA-seq library techniques provides accurate measurement of transcription, increases the use of transcriptomic analysis and enhances the accessibility of these methods to ecological and evolutionary studies (Stahlke et al., 2020). However, they are still in the development process due to technical limitations such as high-quality RNA isolation, pooling samples or the balance between biological replications and sequencing depth, demonstrating, nonetheless, good potential in the future for studies of population genomics (Le Luyer et al., 2017; Lim et al., 2020; Stahlke et al., 2020). These methods are widely used, for example, to identify changes in gene expression to enable adaptation to different environmental conditions in species such as *Oncorhynchus mykiss gardieri* known as redband rainbow trout (Chen et al., 2018; Garvin et al., 2015) or corals (Bay et al., 2017; Pratlong et al., 2015). In the case of *C. nemoralis*, transcriptomics has been used to identify and validate reference genes, and in particular, the candidate genes involved in shell colour polymorphism (Affenzeller et al., 2018; Kerkvliet et al., 2017).

Finally, whole genome sequencing and reduced representation methods such as restriction-site associated DNA-sequencing (RADseq) have grown as a common methodology in this field (Hohenlohe et al., 2018). Genomic variation in species is caused by many factors having an effect among and within populations of a particular species. These technologies, therefore, offer the possibility to investigate extrinsic and intrinsic forces equally (Campbell et al., 2018). Thus, detailed questions such as inter and intra population interactions or genome architecture can be approached to find out which forces drive these effects. Moreover, while past genetic techniques generated limitations when building phylogenies due to strong biases results found using limited number of genetic markers as stated above, the availability of generating

de novo genome assemblies and the access to a growing number of already sequenced reference genomes will help overcome biased results (Campbell et al., 2018). Finally, the genomic architecture generated using genome-scale data may bring solutions to unresolved questions when genetic-scale data and transcriptomics cannot answer the cause of polymorphic frequency stasis or divergence. To date, there have been only two studies using genomic data in *C. nemoralis* (Richards et al., 2013; Saenko et al., 2020). In one, Richards 2013 used RAD-seq sequencing to flank and create genetic markers to the shell colour and banding supergene aiming at helping future genome mapping (Richards et al., 2013). In the other one, Saenko et al. (2020) build the first draft of a reference genome of the target species.

The field of genetic and genomic studies is growing, becoming richer and more complex. Thanks to that, researchers are able to find, describe and understand the interplay among processes, patterns and features of the genome, together with ecological factors of the species. It is definitely becoming clear that the study of ecological evolutionary genetics is more complicated than analysing one single factor and that the field will push towards future multidisciplinary insights into natural, non-model populations stories throughout the Tree of Life.

1.4. Characterising colour polymorphism

The study of animal colouration has been a crucial part in the comprehension of the biological fundamentals in ecology, evolution and biology (Cuthill et al., 2017; McKinnon et al., 2010; McLean et al., 2014; San-Jose et al., 2017). Colour in biology emerges from a combination of nanoparticles and pigments (Stuart-Fox et al., 2018), being in species a complex attribute to describe. Colour is, therefore, remarkably visible but at the same time complex to understand. Sometimes, it is easy to identify colour in nature and relate it with species evolution, production and function. Other times, colour can be a complicated feature to use in the recognition of species. In land snails, for example, colour is fundamental in the thermoregulation of species. Lighter shell colours may survive better in hotter areas due to lighter shell colours absorbing less radiation compared with darker shells (Cameron et al., 2013; Mazon et al., 1987; Ramos, 1984; Richardson, 1974). In birds, colour is also known to play a crucial role in sexual selection. For instance, colourful plumage is used in signalling of courtship (Galeotti et al., 2003).

However, even though colour is easy to spot, it is difficult to describe and quantify. Colour is a quality, which can be described by its lightness, saturation and hue. Isaac Newton was the first scientist to demonstrate in his prism experiment, that the colour was a consequence of reflectance spectra. He also described the continuity of colour, rejecting the theory of the existence of discrete colours (de Andrade Martins et al., 2001). Besides, colour also depends on the visual perception of the receptor involving physics, psychology and physiology. In the animal kingdom, each species has different mechanisms to process colours, and within species, each individual perceives colours differently. For example, birds have four different photoreceptor cell types to perceive colour with different sensitivities; long (L), medium (M), short (S), and very short (VS), which all together generate a tetrachromatic colorimetric system (Davison et al., 2019a; Delhey et al., 2015). By contrast, humans possess three groups of photoreceptor cells in the retina: L (long wavelength, peaking at 560 nm), M (medium wavelength, peaking at 530 nm), and S (short wavelength, peaking at 420 nm) (Chapter 5, Hunt, 2004). For humans, the International Commission on Illumination (CIE), created the foundations to define the human colorimetric system,

based on the stimulation of the different photoreceptor cells of the retina (Smith et al., 1931; Westland et al., 2012).

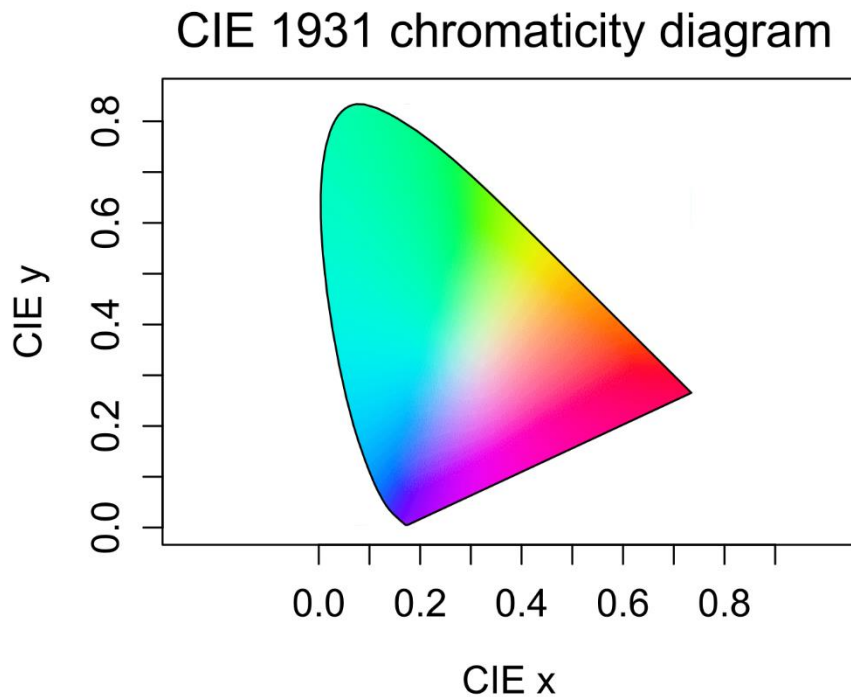


Figure 1.2. The chromaticity diagram system of the CIE 1931 colour convention. Wavelengths measured in nanometres illustrated the spectral boundary curved (monochromatic) locus. Colours shown in the diagram are translated into RGB chromaticity coordinates. The diagram was made using Pavo 2.2.0 R package in R version 3.4.1 (2017-06-30).

Since the 1931 convention (CIE), the definition of chromaticity is determined by the quantitative distributions of wavelengths in the visible spectrum (Figure 1.2). Colour-space mathematical equations are the basis to quantify the spectra and translate into the human chromatic visible spectrum to further test colour variation. As mentioned above, the human visual is captured by three different cone cells. Thus, the CIE commission agreed on three parameters representing each type of cone cells called the Tristimulus values (XYZ). This system corresponds to the primary colours, red, green and blue, and is based on an observer's point of view, which was standardised to the 2° arc of the fovea to reduce the number of variables (Smith et al., 1931; Westland et al., 2012). These Tristimulus values provide a standard reference to other colour spaces such as the well-known RGB (red, green and blue), CIE-LAB (abbreviated as Lab) and, HSV (hue and saturation value).

Throughout the past century, biological studies involving colour features were scored manually, using the expert perception of a trained biologist. Traditionally, in the ecological and evolutionary genetics fields, colour description has been subjective. For instance, pure genetic studies, demonstrating the basic Mendelian genetic theories in species (Staples-Browne, 1908; Wheldale, 1907), or biogeographic surveys aiming to deduce natural and sexual selection operating in nature (Delhey et al., 2015; Delhey et al., 2017) used manual scoring instead of quantitative methods (Endler, 1990). This may lead to potential error and biased results when scoring colour. The next step was to move to quantitative colour descriptions by using quantitative procedures. Thus, spectrophotometry rose as one of the most accurate and sophisticated tools to approach this issue. Spectrophotometry exposes objects to a certain light and compares the amount of light emitted to that received. Consequently, it measures the light absorption from the irradiated object (Germer et al., 2014).

In genetics, ecology, and evolution, the employment of quantitative techniques to analyse colour, specifically spectrophotometry, grew to become one of the conventional colour extractors (Delhey et al., 2015; Endler, 1990; Maia et al., 2013; Maia et al., 2018). One of the reasons for the success is that spectrophotometers can provide a significant variation of measurements showing under different lighting conditions and observing at various angles. The effective use of spectrophotometry in evolutionary genetics has been properly exemplified by Surmacki et al. (2013), firstly, and secondly by Delhey et al. (2015). In the first case, Surmacki et al. (2013) used chromatic and achromatic physiological avian models to test the avian predators view of different prey colours in various matching backgrounds. The main goal was to contribute in the comprehension of avian predation as a selective factor maintaining shell polymorphism (Surmacki et al., 2013). In the second case, Delhey et al. (2015) generated a large-scale colour quantitative and descriptive study testing 555 Australian bird species to analyse colour variation in animals. He found striking disparity of the distribution throughout the colour variety. Nonetheless, these methods are time-consuming and expensive (Leighton et al., 2016).

Like in birds or other fauna, spectrophotometry has also been applied in the study of *C. nemoralis* colour polymorphism. A recent ambitious study in *C. nemoralis* assessed shell ground colour of samples collected across Europe (Davison et al., 2019a). They defined the European shell chromatic variation based on a psychophysical model of a closely related species (the blackbird, *Turdus merula*) of its main avian predator song thrush (*Turdus philomelos*). They found that colour, in *C. nemoralis* shells, fall into a cluster in a multivariable space and detected geographical patterns of shell colour distribution in Europe (Davison et al., 2019a). These findings highlight the necessity of quantitative measurement of colour in other systems such as in citizen science projects.

1.5. Citizen science

Citizen science is increasing due to its potential to obtain a broad temporal and spatial biological data. Citizen science is defined as the contribution from public participation of non-professional scientist in the collection of data that do not demand additional training or material (Riesch et al., 2014). Riesch et al. (2014) describes the phenomena “as a win–win” because the scientist obtains huge amount of data and/or the participants get involved in real science, usually related to their hobbies. The most common activities related to citizen science are birdwatching with global projects like Macaulay Library project (<https://www.macaulaylibrary.org/>) holding over 19 million bird pictures, and fauna and flora observations like iNaturalist (www.inaturalist.org; Horn et al., 2018). The iNaturalist project became one of the largest social networking service for ecological and evolutionary biology. This database detected and classified more than 60 million species collected by more than 3.5 million citizen-scientist from pictures around the world. This is a clear example of how citizen science efforts are expanding the range of geographic and temporal data records (Pocock et al., 2015).

It has become clear that scientists need large-scale and long-term studies to study colour variation in macro-ecology and macro-evolution. This rises an issue of investment in labour, funding and time to be able to gather enough data (Zeuss et al., 2014). Ergo, considering the fact of current urge in colour data availability and the growth of social media (i.e., photographs), the implementation of citizen science is

necessary. However, this innovative resource must be taken carefully as it presents some limitations. As non-experts of the field, citizen scientists, can sometimes, misclassify species or colour pigmentation. Moreover, the absence of standards, filters or controls in the citizen inputs, entails many potential risks. This is clearly exemplified in photography, where variation in the user's camera features such as lighting, noise or camera exposure levels may condition the colour and influence in its quantification (Byers, 2006).

This reflection leads to a question of whether to use the traditional method (Arnold, 1968; Cameron et al., 1973) of spectrophotometry (Davison et al., 2019a; Delhey et al., 2015) or citizen science data (Cameron et al., 2012; Silvertown et al., 2011; Worthington et al., 2012). Two approaches could be used to address this question: either taking into account the studied hypothesis or combining several mentioned methods, such as a mixture of citizen science and spectrophotometry.

In *C. nemoralis*, the most useful and famous citizen science database was Evolution Megalab (Cameron et al., 2012; Silvertown et al., 2011; Worthington et al., 2012). This database provided frequencies of *C. nemoralis* shell polymorphism in groups of samples collected from throughout a broad geographical range during the past century. However, the database inputs were manually scored and added to the website as it is reviewed in chapter 4. In the future, with the increasing use of digital cameras to capture and record species presence and the expansion of online citizen science projects, colour and banding data may be extracted from the images uploaded to public databases and apps such as iRecord, iNaturalist and SnailSnap (Harvey, 2018; Horn et al., 2018; Kerstes et al., 2019).

1.6. Thesis aims

The study of colour polymorphism embraces many fields, from the fundamental genetics and evolutionary studies, to simple concepts such as the characterization of phenotypes. The aim of this thesis, therefore, is multifaceted. It contributes to the understanding of *C. nemoralis* shell polymorphisms through the use of different approaches and new procedures.

Therefore, this thesis explores new perspectives towards a better procedure in the understanding of the pulmonate *Cepaea nemoralis* in its ecological and evolutionary genetics and genomics over the next few years. Hence, understanding the *Cepaea nemoralis* genome will probably provide the key to interpret its shell colour polymorphism. Consequently, in chapter 2 (Gonzalez et al., 2019), I reviewed the underlying genetics in prior studies related to the recombination events occurring in the referred supergene and aimed to understand recombination within the *C. nemoralis* supergene. Previously, it was assumed that certain shell phenotypes occurred in the offspring due to putative instances of recombination between loci within the supergene (Richards et al., 2013). The underlying genotype was only possible to verify by breeding further generations of snails from the 'recombinant' offspring. Thus, the main objective, therefore, was to provide a more reliable method to identify recombination events, which either flank the supergene or are between loci within the supergene.

In chapter 3, I endeavoured to understand genomic variation of *C. nemoralis* and its relationship with shell polymorphism. Therefore, I reviewed what is known about *C. nemoralis* phylogenies and I provided more evidences on *C. nemoralis* origin and its European expansion by using the reference genome provided by Saenko et al. (2020) and Rad-seq high-throughput genome-wide sequencing methodology. Thus, I attempted to investigate the expansion of snails from the Pyrenees across Europe after the Pleistocene by creating a genomic phylogeny, and comparing the genomic phylogeny to the mitochondrial phylogeny generated (Grindon et al., 2013a). Moreover, there is a visible shell colour variation, which is thought to be related to geographic variation due to better environmental fitness (Arnold, 1968; Cameron et al., 1973; Jones et al., 1977; Richardson, 1974). However, two local enzymatic studies found no correlation between shell patterns and genomic variation (Ellis, 2004; Ochman et al., 1983), rising a question on whether colour variation and geographical genomic variation are related.

The characterization of colour represents a challenge for ecological and evolutionary genetic studies involved in colour polymorphism. Colour is a continuous variable and its scoring is subjective to the individual. Prior research scored colour

manually incurring both potential error and biased results in comparative studies. Therefore, with the development of new technologies regarding colour, scoring techniques are in the need of an upgrade. To this end, in chapter 4, I aimed to evaluate manual scoring by using a colour quantitative method based on Davison et al. (2019a). Moreover, I reviewed whether using spectrophotometric scoring or traditional manual scoring generates better outputs in a local comparative study in the Pyrenees. In addition, I also reviewed how comparative studies of shell pattern frequencies, whether local and long-scale, plays a vital role in the study of ecological, evolutionary and genetic procedures underlying the preservation of polymorphism in wild populations of *C. nemoralis*, specifically in the Central Pyrenees.

In chapter 5, I aimed to examine the emerging role of deep learning in ecological and evolutionary biology. There is an increasing potential to use digital technology like cameras to capture and record species presence and consequentially extract colour and banding data from public databases and apps such as iRecord, and iNaturalist and SnailSnap (Harvey, 2018; Horn et al., 2018; Kerstes et al., 2019). Therefore, the objective of this research is to explore the use of deep learning algorithms to test whether the mentioned technologies are effective in the recognition of *C. nemoralis* snails from pictures, and in its shell type classification. Moreover, this study intended to remove the human subjectivity when scoring colour, by training the algorithm with quantified colour spectra of the shells colours based on the method mentioned in chapter 4 to standardised colours. Thus, the main objective is the creation of a non-disruptive method, which will reduce time-consumption of the manual task. The novel method should make an important contribution to the field on understanding the maintenance of the colour phenotype of *C. nemoralis* and the natural factors acting upon it.

Chapter 2:

Recombination within the *Cepaea nemoralis* supergene is confounded by incomplete penetrance

This chapter was published in Heredity on 14/02/2019

DOI: 10.1038/s41437-019-0190-6

Abstract

Although the land snail *Cepaea nemoralis* is one of the most thoroughly investigated colour polymorphic species, there have been few recent studies on the inheritance of the shell traits. Previously, it has been shown that the shell polymorphism is controlled by a series of nine or more loci, of which five make a single ‘supergene’ containing tightly linked colour and banding loci and more loosely linked pigmentation, spread band and punctate loci. However, one limitation of earlier work was that putative instances of recombination between loci within the supergene were not easily verified. We therefore generated a new set of *C. nemoralis* crosses that segregate for colour, banding and pigmentation, and several other unlinked shell phenotype loci. The snails were genotyped using a set of RAD-seq-derived loci that flank the supergene, and instances of recombination tested by comparing inferred supergene genotype against RAD-marker genotype. We found no evidence that suspected ‘recombinant’ individuals are recombinant between loci within the supergene. As point estimates of recombination between both colour/banding, and colour/pigmentation loci are zero, incomplete penetrance and epistasis are a better explanation for the apparent ‘recombinant’ phenotype of some snail shells. Overall, this work, therefore, shows that the architecture of the supergene may not be as previously supposed. It also provides a resource for fine mapping of the supergene and other major shell phenotype loci.

2.1. Introduction

Historically, some of the most important animals in studying colour polymorphism have been the land snails *Cepaea nemoralis* and the sister taxon, *C. hortensis*, because it is straightforward to collect them and record the frequencies of the different morphs in different locations and habitats (Cain et al., 1950, 1952, 1954; Jones et al., 1977). There is also the benefit that the major loci that determine the polymorphism show simple Mendelian inheritance (Cook, 1967; Jones et al., 1977). However, while ongoing and long-term studies on these animals continue to provide compelling evidence for the fundamental role of natural selection in promoting and maintaining variation in natural populations, as well as the impact of modern-day habitat change (Cameron et al., 2012; Cook, 2017; Silvertown et al., 2011), the last research on the inheritance of the loci that determine the polymorphism dates to the late 1960s. This is a problem because now that there is finally some progress towards identifying the genes involved (Kerkvliet et al., 2017; Mann et al., 2014; Richards et al., 2013), it is important that laboratory crosses are available, to validate prior knowledge on the inheritance and for use in fine mapping recombination break-points.

Previous work has shown that the shell polymorphism is controlled by a series of nine or more loci, of which five or more make a single ‘supergene’, containing linked shell ground colour (C), banding (B), band/lip pigmentation (P/L), spread band (S) and punctate (or ‘interrupted’; I) loci. In most studies, colour and banding have been found to be tightly linked, with recombination typically towards the lower end of 0–2% (Cain et al., 1960; Cook, 1967). The exceptions are a study by Fisher et al. (1934), which reported recombination of ~20% between C/B, and two crosses in Cain et al. (1960) which showed recombination of ~16%, also between C/B. Although there have been fewer studies, pigmentation, spread band and punctate are believed more loosely linked, showing rates of recombination between 3 and 15% (Cain et al., 1968; Cain et al., 1960; Cook, 1967). The main other loci that make up the shell phenotype are various forms of band-suppressing loci, all unlinked to the supergene, including the mid-band locus, U (unifasciata), and another that suppresses the first two bands, T (trifasciata).

One unavoidable limitation of prior works was that putative instances of recombination between loci within the supergene could not be verified, except by breeding further generations of snails from the 'recombinant' offspring to confirm the underlying genotype. This was rarely possible, perhaps due to logistics combined with the fact that many pairs do not produce offspring. Nonetheless, it was recognised that incomplete penetrance might be an alternative explanation for the phenotype of recombinants. Chance arrangements of alleles at other loci might sometimes interact to prevent expression of a particular phenotype, causing individuals to appear as if they are 'recombinant' (Cook et al., 1966).

To further understand the frequency of recombination within the supergene, and to generate further material for fine mapping, we made a new set of *C. nemoralis* crosses that segregate for several shell phenotype loci. The offspring were then genotyped using a set of linked RAD-seq loci that flank either side of the supergene (Richards et al., 2013), and instances of recombination confirmed or refuted by comparing inferred supergene genotype against RAD-marker genotype. The underlying idea is that individuals that show recombination within the supergene should also be recombinant by RAD-marker. Overall, we found that the phenotype of 'recombinant' individuals is better explained by incomplete penetrance and epistasis.

This work, therefore, provides a method to identify recombination events that either flank the supergene or are between loci within the supergene. The results also show that recombination within the supergene may be considerably rarer than supposed.

2.2 Materials and methods

2.2.1. The culture of *Cepaea* and crosses

A mixture of oat, hydrated grass pellet and chalk, accompanied with lettuce were used to feed *C. nemoralis* snails as explained in prior research (Davison, 2000b). Firstly, large virgin juveniles from the UK, Ireland and Spain, were kept in isolation and raised to adulthood in individual tanks. Secondly, with the purpose of breeding adult snails were introduced to a partner. Thirdly, tanks with ~4 cm soil were used to keep those snail couples until oviposition started. Progeny from both parents were kept due to *C. nemoralis* being a simultaneous hermaphrodite. Fourthly, egg batches were isolated, and the offspring reared to adulthood under the same feeding regime, with the time from egg to adult being ~6 months. Finally, all individuals, ones used to breed and raise, were kept in the -80°C freezer.

Adulthood was achieved successfully for most of the snails. Main shell features such as ground shell colour, banding, band pigmentation and lip colour phenotypes were marked and registered. Some individuals presented complications when describing their traits. In consequence, detailed indications explained by Cain (1988), were followed and those were represented in table 2.1. Italics symbols were used to differentiate phenotype to genotypes. 14 crosses were generated. Only original snails were used in crosses 1 to 6 and 8. Crosses 7 and from 9 to 14 were set up using snails from the first group of crosses. Crosses from 1-8 were acquired from Richards et al. (2013), and further crosses were made by AD with the purpose of finding recombinants.

Table 2.1. Phenotypes and genotypes of *C. nemoralis* shell features used in this research.

Phenotype				Genotype		
Character	Description	Notation		Locus	Allele	Notation
Ground colour	Brown		B	Ground colour	Brown	C ^B
	Pink		P		Pink	C ^P
	Yellow		Y		Yellow	C ^Y
Banding	Unbanded	00000	O	Banding	unbanded	B ^O
	First two bands missing	00345			normal banded	B ^B
	First band missing	02345		Band pigmentation	normal	P ^N
	Mid-banded	00300	M		hyalozonate	P ^H
	Banded	12345	B	Lip pigmentation	normal	L ^L
					white lip	L ^A
	Spread-banding		S	Spread-banding	spread	S ^S
			normal		S ⁻	
Band pigmentation	Normal pigmented bands		N	Mid-banding (aka unifasciata)	mid-banded	U ³
	Unpigmented bands (aka hyalozonate)		H		normal banded	U ⁻
Lip pigmentation	Normal pigmented lip		L	Trifasciata	first two bands missing	T ³⁴⁵
	White lip		A		normal banded	T ⁻
	(aka albolabiate)			Hypothesised	first band missing	X ²³⁴⁵
				normal banded	X ⁻	

The ground colour, banding, band pigmentation, spread band, and lip pigmentation loci are linked in a supergene. The other loci are unlinked. Alleles are shown in dominance order.

Previous and current studies have shown that quantitative methodologies to measure colour variation are necessary as this trait has multiple continuous options in *C. nemoralis* (Davison et al., 2019a). To create simple crosses a non-accurate description is sufficient as colour can be explained directly. Consequently, scoring of either yellow (Y), pink (P) or brown (B) was used to report basic shell ground colour. Further, genotype dominance is deduced as follows $C^B > C^P > C^Y$ (Jones et al., 1977), and connections and repulsions with other traits were also noted (Table 2.1).

Additionally, shell banding was also scored. Three main groups were chosen to divide banding options such as unbanded (O; 00000), mid-banded (M; 00300) or having various options of banding (B; generally 12345, but all combinations as an exception of 00300). In this case, dominance was deduced by unbanded dominant; $B^O > B^B$ (Jones et al., 1977). In case of mid-band loci, several crosses segregated with its deduced dominance (mid-band dominant; $U^3 > U$). Furthermore, another cross targeted two different options, one for band-suppressing locus, T (Lack of the first two bands: 00345; $T^{345} > T^-$) and another alternative loci, called X (Lacking first band or very faint: 02345; $X^{2345} > X^-$). Other traits like lip colour pigmentation were not clarified by the literature in terms of whether separate loci or an allelomorphic part of the band pigmentation loci. As a result and to avoid errors, both were treated as separate loci. Hence, normal (N) or hyalozonate (H) with its corresponding genotype dominance deduced as $P^N > P^H$ were the band pigmentation phenotype alleles. The morph hyalozonate known as the band and lip with no pigmentation, is identified by contrasting shell ground colour to the “discrete bands” with paler background colour. Two different morphs were found in several crosses for the trait lip colour. On one hand, dark lip colour recognised as normal (L) and, on the other hand, white lip colour (A – albolabiate) as non-common. Genotypic dominance were deduced ($L^L > L^A$). In other crosses, lip pigmentation showed quantitative variation and so was difficult to score. One cross also showed variation in spread-banding, another locus of the supergene, for which the spread band allele, SS, is dominant to normal banding, S-.

Some of the adults used were wild-collected from either the UK, Ireland or Spain; others were derived from prior laboratory crosses (Table 2.2). The adults used in crosses 10, 11, 12 and 13 were derived from offspring of cross 9, so the shell genotype could be inferred with extra confidence. This was aided by full-sib inbreeding

in producing crosses 10, 11 and 12, and another round of inbreeding to produce cross 13.

Table 2.2. Summary of linked loci phenotypes from *C. nemoralis* crosses

Cross	Parent		Offspring					Linked Loci					Unlinked	Putative	Chi-squared				
	phenotype		n	phenotype					C	B	L	P	S	U	T	X	recombinant?	p value	
1	PO	YM		PM	YO													0.38	0.38
	C100	C101	103	56	47			103	103										
2	PO	YM		PO	YM	YO													
	C102	C103	43	20	20	3		43	43							C/B		0.65	0.65
3	PO	YM		PO	YM														
	C104	C105	46	27	19			10	10									0.24	0.24
4	PO	YB		PB	YO														
	C110	C111	27	17	10			27	27									0.18	0.18
5	PO	YB (12345)		PB (00345)	PB (12345)	PB (02345)	YO	PM											
	C112	C113	109	27	12	16	53	1											
									109	109			55	28				0.85	0.85
6	PO	YB		PO	YB	YM													
	C114	C115	34	18	8	8			34	34			17					0.73	0.73
7	PM	YM		PM	YM														
	C119	C118	75	37	38				75									0.91	
8	POL	YML		PML	YOL	YOA	POL												albolabiate
	C108	C109	50	26	11	12	1		50	50	25					C/B		0.57	0.78
9	PMN	YBH		PMN	PBN	YMN	YBN											1	0.62
	C116	C120	16	4	4	3	5		16				16						
10	Inb PMN	YBN		PMN	PBN	YMN	YBNYMHYBH												
	C450	C449	12	5	2	2	1	2	0		6		12					0.56	0.08
11	Inb PMN	YBN		PMN	PBN	YMN	YBNYMHYBH	PMH											
	C451	C452	116	34	28	12	22	10	6	4		28	116			C/P		0.14	0.71
12	Inb PMN	YBN		PMN	PBN	YMN	YBNYMHYBH	PMH											
	C662	C665	146	39	46	7	19	15	12	8		73	146			C/P		0	0.51
13	Inb PMN	YBH		PMN	PBN	YMN	YBNYMHYBH	PMH											
	C825	C841	63	14	18	0	0	20	9	2		63	63	63		C/P		0.53	0.26
14	YBS	YO		YBS	YO														
	C568	C569	44	28	16														
									44		44								
Total			884						804	420	25	170	44	370	55	28			

Phenotypes that may be due to a recombination event in a parent are highlighted in bold. Inferred genotypes of offspring are detailed in Supplementary Table 1. Key: P pink, Y yellow, O unbanded, M mid-banded, B all other banding patterns; N normal band pigmentation; H hyalozonate banding (nearly always with white lip—see text); S spread-banding; L normal lip pigmentation; A albolabiate (white lip). Cross 5 also showed segregation for another one or two band-suppressing loci, T and X, so the detailed banding notation is also shown. Crosses 10-13 were inbreeding.

2.2.2. DNA extraction, quantification and amplification

The DNA of progenitors and their progeny was extracted and genotyped by using RAD markers. The goal was to create a base for future mapping of the supergene and the possible identification of other shell trait genes close to or within the supergene. Furthermore, we wished to identify individuals that show evidence of recombination, ideally either close to a shell-character locus, or between loci within the supergene. Past research achieved isolation of flanking RAD-seq markers near the supergene (Richards et al., 2013). Those markers were used with the objective to accept or reject possible recombinant phenotypes within the supergene features. To do so, frozen snail tissue was used to extract genomic DNA as explained (Richards et al., 2013).

Two extraction methods were used. Foot tissue was chosen as it is known as a good resource of high molecular weight DNA. Foot samples were cut in tiny slices and added into 15ml Falcon tubes. 5ml of extraction solution (3% CTAB, 100mM Tris-HCl, pH 7.5, 25mM EDTA, pH 8, 2M NaCl) and 60µl Proteinase K (0.2 mg/mL) was inserted. The culture was incubated at 60-62 °C inverting gently occasionally overnight. Next day, RNAase A (80 µg/mL) was added to each tube and was incubated for 1 hour to remove RNA. The mixture was cooled down at room temperature. Upon lysis, a chloroform extraction was conducted, then three volumes of CTAB dilution solution was inserted (1% CTAB, 50 mM Tris-HCl, pH 7.5, 10mM EDTA, pH 8). Samples were combined until a precipitation emerged, then the supernatant was removed. The pellet was washed twice in 0.4M NaCl in TE (0.4M NaCl, 10 mM Tris-HCl, pH 7.5, 1 mM EDTA, pH 8), re-dissolved in 1.42M NaCl in TE (1.42M NaCl, 10mM Tris-HCl, pH 7.5, 1 mM EDTA, pH 8), then ethanol was used to precipitate DNA, followed by centrifugation and drying. Latterly, a few samples were lysed in lysis buffer (10 mM Tris, 0.1 M EDTA, 0.5% SDS), then extracted using the standard phenol-chloroform protocol. Protocol changed due to the product availability and sample conditions.

With the aim to flank the supergene, groups of samples from the key crosses were genotyped by following personalized assays from the RAD-seq markers. Therefore, two standard PCR methods were performed depending on the RAD-seq

marker. One option was the Amplitaq Gold polymerase (Invitrogen) that allows with very high sensitivity or specific amplification of DNA targets. The PCR programme applied for this polymerase was a single cycle of 95 °C for 10 min were used, followed by 35 cycles of 95 °C for 30 s, 58 °C for 30 s, and 72 °C for 1 min. The other PCR option was Clontech Advantage 2 PCR, which it is an extremely versatile polymerase mix that has three times higher fidelity than other Taqs. This PCR method started with an initial denaturation of 95 °C for 1 min, followed by 35 cycles of 95 °C for 15 s, 65 °C for 1 min, 68 °C for 1 min, and 72 °C for 1 min.

The genotyping and the particular primers used in each assays were based on the prior characterised RAD-seq loci (Richards et al., 2013). These varied depending on each cross. Primers applied were RAD06F 5'-GCCTATCCGTCATTGTTGGT-3', RAD06R 5'-GTCAAGGCTTGCTTCTTTGG-3', RAD9F 5'-TTTCTCGGAACGACGGAGT-3', RAD9R 5'-GGTCTCGTCAATGGCACTTT-3', RAD11F 5'-AAGAAGCGTCCTTCTGGAAA-3', RAD11R 5'-CACCTTCCCCATTCTTCAAA-3'. Then, a restriction enzymatic digestion was performed by 1-hour incubation usually at 37°C. Subsequently, the scoring of the genotype were carry out in agarose electrophoresis gel. The details of the respective of enzymes used with each assay and each cross are shown in the Supplementary Table 2.3. Finally, the recombination rates were estimated by calculating the recombination fraction estimation of the offspring (Ott, 1999).

2.3 Results

2.3.1. Segregation of Mendelian loci that determine shell phenotype

Shell colour, locus C, showed segregation in crosses 1–13 (Table 2.2; Supplementary Table 2.1, 2.2, 2.3), only deviating significantly from expected Mendelian segregation ratios in cross 12, with fewer yellow shells than expected.

Crosses 1–6 and 8 showed segregation for the band presence/absence locus, B, with no deviations from expected Mendelian ratios.

Crosses 6 and 9–13 showed segregating variation for the mid-band phenotype, coded by the unlinked U locus. The observed phenotype frequencies did not differ from the expected frequencies.

Crosses 10 to 13 showed segregation for the pigmentation (hyalozonate; P) locus, with no deviations from expected Mendelian ratios.

Cross 8 showed segregation for the putative lip colour locus, L. The offspring phenotype frequencies would be consistent with single locus, assuming that L is part of the supergene and treating lip colour phenotypes as either normal (N) or albolabiate lip (A); there was no deviation from expected Mendelian ratios. Offspring in several of the other crosses, especially 10–13, showed considerable and apparently continuous variation in lip colour. We, therefore, tried to score the lip phenotype in the conventional manner, having a phenotype as normal, pale, or albolabiate, and reconcile this with a knowledge of the parental phenotypes and genotypes (parents in crosses 8 and 9). No scheme that we devised fitted a simple Mendelian model. This fits with previous studies (Cain Arthur James 1968; Cook, 2003). Unfortunately, it was not possible to quantitatively measure the lip colour, as we have done for shell ground colour (Davison et al., 2019a), because the coloured part of the lip was frequently too small and also on a curved surface.

Cross 14 showed segregating variation in the spread band phenotype. However, as one parent was homozygous for the dominant spread band allele S^S , the cross was non-informative for recombination with other supergene loci.

Finally, cross 5 showed segregating variation for the locus that suppresses the first two bands, converting a five-banded snail (12345) to three-banded (00345). The offspring phenotype frequencies would be consistent with single locus, with T^{345} dominant to T^- , with both parents being heterozygote, except that this would require both parents to have a T^{345} allele; apparently not possible because one of the parents is 12345. As five of the offspring with suppressed bands have 02345 phenotype and eleven a 0:345 (: = trace) phenotype, then the results are consistent with their being two band-suppressing loci, one that causes the 00345 phenotype and another that causes the 02345/0:345 phenotype (see Supplementary Table 2.3 for inferred genotypes).

2.3.2. Putative recombinants between colour, banding and lip and band pigmentation loci.

Previously, the colour (P/Y) and banding (B/O) phenotype for six crosses (1, 4, 5, 6, 7, 8) and 398 offspring was reported, and the genotype of flanking RAD-seq loci reported for cross 1 (Richards et al., 2013). In this new work, we raised a further 486 offspring from eight more crosses, and genotyped six further crosses using flanking RAD-seq loci. The combined data set of parent and offspring phenotypes, alongside inferred genotypes, is presented here together, summarised in Table 2.2, S2.1, S2.2, and presented in full in Supplementary Table 2.3.

Offspring in several crosses (2, 8 and 10-13) produced snails with phenotypes that could be explained by a recombination event within the supergene of the heterozygous parent (Fig. 2.1).

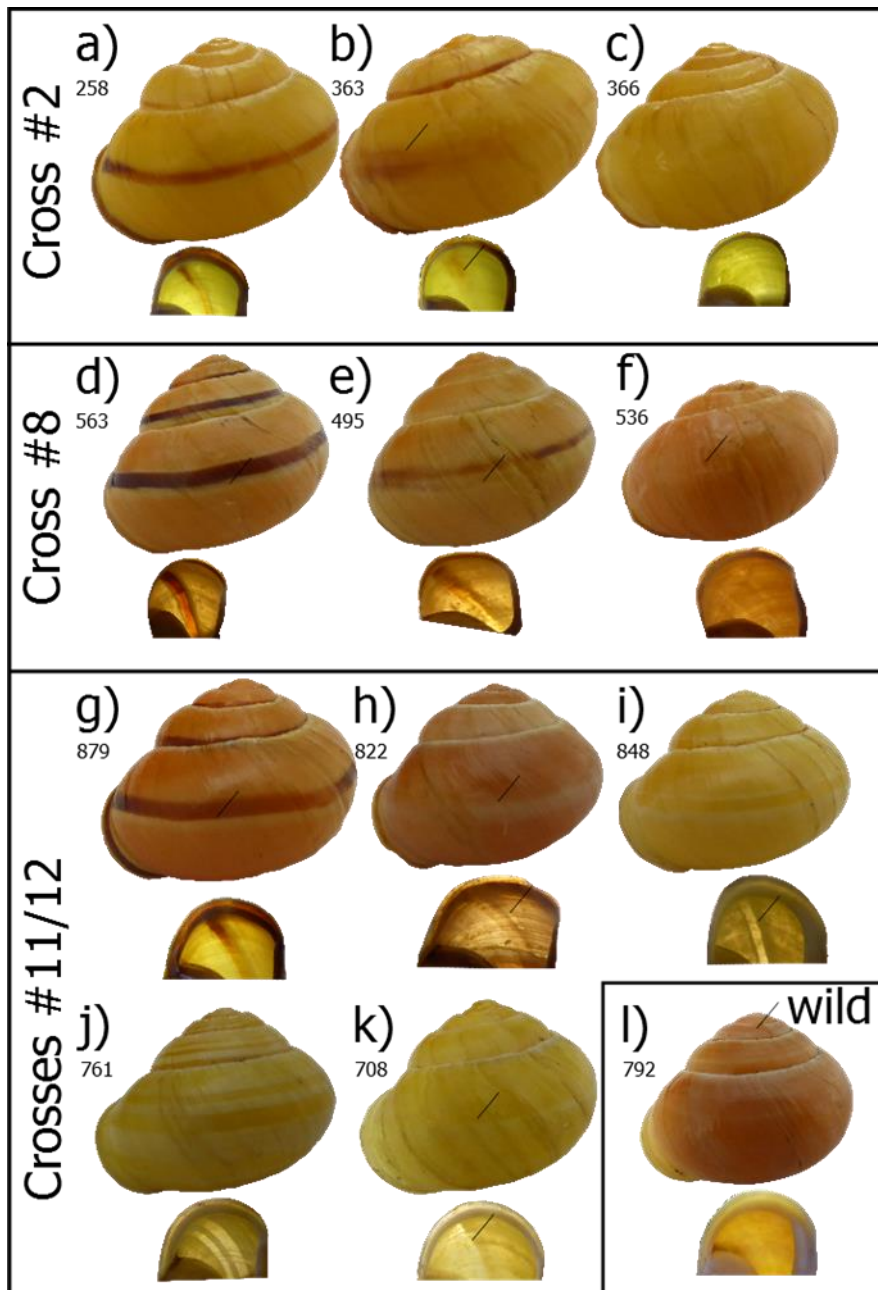


Figure 2.1. Shells of offspring from crosses, including putative recombinant individuals, and one wild collected individual. A) Normal yellow mid-band, b) yellow, trace of banding, c) yellow, no band. An absence of banding suggests that individual 366 is a putative recombinant. D) normal pink mid-band, showing evidence of white “highlighting” of pigmented band e pink, trace of banding, some highlighting f) pink, no band, very faint mark where band would be. An absence of banding suggests that individual 536 is a putative recombinant. G) Normal pink mid-banded, showing evidence of white highlighting of pigmented band h) pink, no band, white highlighting i) yellow, mid-band hyalozonate, j) yellow, banded hyalozonate (02345) k) yellow, mid-band hyalozonate. An absence of dark pigment suggests that 822 is a putative recombinant; however, the shell has retained the white highlighting pigment. Hyalozonate shells generally lack both dark and light pigment, see i) and j); this is not always easily visible, see k). In a wild-collected pink hyalozonate, l) the lack of pigment is just visible on some whorls, and not at all on some upper whorls, or from the inside.

Cross 2 produced three yellow unbanded snails (e.g., Fig. 2.1c), a phenotype that might be produced by recombination between the colour (C) and banding (B) loci; one of these individuals, a sub-adult with a damaged shell, has a very faint trace of a band. A few other snails in the same cross have much-reduced banding (e.g., Fig. 2.1b).

Cross 8 produced a single pink unbanded snail, a phenotype that is also best explained by recombination between the colour (C) and banding (B) loci (Fig. 2.1f). Very few of the snails in this cross have reduced banding. This cross also segregated for the lip pigmentation locus, L. As the recombinant snail has a pigmented lip (see Fig. 2.1f, lip image), then this cross in theory informs upon the order of loci within the supergene (but see below).

Cross 5 produced a single pink mid-banded snail. This phenotype is very difficult to explain by recombination, based on the known genotypes (Supplementary Table 2.3 and 2.4). As the pink colour of this snail is qualitatively different from the other pink-banded snails in this cross, the best explanation is that it is a likely a contaminant from another cross.

The remaining crosses produced offspring that suggest possible recombination between the colour C and band pigmentation P loci. Crosses 11, 12 and 13 produced several unbanded pink individuals, with pigmented lips (e.g., Fig. 2.1h). These were initially scored as hyalozonate, because the mid-band was evident but not pigmented. However, closer inspection revealed that the banding phenotype of these shells is not the same as the yellow hyalozonate shells. Specifically, the unbanded pink individuals retain the white highlighting pigment of a normal shell, but lack the dark pigment (compare Fig. 2.1h with 2.1g). This difference is especially evident when viewed from the underside: hyalozonate shells have cleared bands which are entirely lacking pigment whereas the white pigment of 'unbanded' snails shows a silhouette (compare Fig. 2.1h with 2.1i, j). Not all of the hyalozonate shells show such a clear pattern (e.g., Fig. 2.1k). For comparison, in a wild collected pink hyalozonate, the cleared bands are only evident on the upper whorls (Fig. 2.1l); in another shell they are not evident at all.

2.3.3. Genotyping of offspring using RAD-seq derived loci

Individual offspring from crosses 1, 2, 8, 9, 10, 11, 12, and 13 were genotyped using custom assays derived from RAD-seq loci that flank either side of the supergene, using RAD06/RAD11 on one side and RAD09 on the other side (Table 3; Supplementary Table 2.3). Unfortunately, the RAD-seq loci in cross 5 lacked polymorphism so no assay was possible. To confirm or refute individual recombination events, we inspected the genotype of the putative recombinant offspring. In theory, individuals for which we have inferred recombination within the supergene should also show recombination by one of the RAD-markers.

None of the three individuals from cross 2 showed evidence of recombination from the flanking loci RAD11 and RAD09. Similarly, the single individual in cross 8 did not show evidence of recombination for the same RAD-seq loci. All eight putative recombinants in cross 12 and all three in cross 13 showed no evidence of recombination using RAD06 and RAD09; in cross 11, three individuals did not show evidence of recombination, with one single individual (804) showing recombination between RAD06 and the supergene and apparent recombination between the colour and pigmentation loci (C/P). If this were correct then it would inform the order of loci within the supergene. However, the phenotype of this snail is exactly the same as the other refuted recombinants (Fig. 2.1h). It is most likely not a hyalozonate, and therefore a coincidence that it also shows recombination between RAD06 and the supergene.

Thus, overall, while there is incomplete evidence in some cases, we were not able to confidently confirm any recombination events within the supergene. This puts the point estimate on recombination between C and B at 0/376 (<0.27%), between C and P at 0/170 (<0.60%) and between C and L at 0/25 (<4%). Therefore, the upper confidence limit for the mean rate of recombination, assuming that the probability of observing zero recombination events is 5%, is 0.80% for C/B, 1.76% for C/P, and 12.0% for C/L. Of course, as there are no recombination events, then this work does not inform the order of loci within the supergene; the higher upper limits for C/P and C/L are due to smaller sample sizes.

Table 2.3. Summary of RAD-seq marker genotyping, putative number of supergene recombinants and actual number.

	Cross				Genotypes			Recombinants between supergene and:			Putative supergene recombinants	Actual supergene recombinants
	Snails and phenotypes				RAD11	RAD06	RAD09	RAD11	RAD06	RAD09		
1	C100	C101	P O	Y M	101	102	102	1	10	1	0	0
2	C102	C103	P O	Y M	38		43	0		2	3	0
8	C108	C109	P O L	Y M L	44		50	2		1	1	0
9	C116	C120	P M N	Y B H		16	16		2	0	0	0
10	C450	C449	P M N	Y B N		12	12		2	1	0	0
11	C451	C452	P M N	Y B N	103		104		4	2	4	1?
12	C662	C665	P M N	Y B N	127		132		3	6	8	0
13	C825	C841	P M N	Y B H	44		49		4	1	3	0

RAD06 and RAD11 flank one side of the colour and banding loci of the supergene; RAD09 flanks the other side. Full genotypes are in Supplementary Table 2.3.

2.4. Discussion

For future mapping and the precise identification of the supergene, it would be useful to identify individuals that are known to have a recombination break-point close to, or within the supergene. In this study, we initially identified four putative recombination events between the colour and banding loci (C/B) and fourteen putative recombination events between the colour and pigmentation loci (C/P). This is as expected because historic studies have indicated that C/B are more tightly linked than C/P. We also used genotyping of RAD-seq loci that flank the supergene in several of the crosses to reveal individuals that show recombination between a linked RAD-seq marker and the supergene. These RAD-seq markers may, therefore, be used for future recombination break-point mapping. However, the same RAD-seq genotyping did not find any evidence of recombination thereby refuting the putative recombinants detected above. This is also supported by a close analysis of the phenotype of the shells, including variable penetrance of the mid-band phenotype (Fig. 2.1; crosses 2, 8, 11–13) and a comparison of true hyalozonate shells against shells that partially lack pigmentation (Fig. 2.1; crosses 8, 11–13).

Therefore, in contrast to previous studies that have reported rates of recombination between C/B of 0–2% and between C/B and the pigmentation locus, P, of 3–15%, which were not supported by genetic data. We found zero recombinants, putting upper limits on the rate of recombination at 0.8 and 1.8%, respectively. This does not mean that previous inferences of recombination within the supergene were incorrect. However, as the ‘recombinants’ in this study are better explained by other means, then we would suggest that there is an absence of modern-day evidence for recombination within the *C. nemoralis* supergene. The structure of the supergene may not be as has previously been supposed.

2.4.1. Incomplete penetrance and epistasis

Four individuals in crosses 2 and 8 were initially identified as putative recombinants, because they lacked the mid-band, or had only very faint traces of a band. If these snails had been true recombinant individuals then they would most likely be

homozygous for colour and heterozygous for banding (genotype B^0B^b). Incomplete penetrance of the dominant B^0 allele could mean that some individuals show evidence of banding (e.g., Fig. 2.1b, e). Instead, the genotyping shows that these individuals are not recombinant, and so must be genetically homozygous for colour and banding (B^bB^b). Therefore, the best explanation for their phenotype is that other loci are interacting epistatically to prevent full penetrance of homozygous banding alleles.

Similarly, up to fourteen individuals were identified that were putative recombinants between the colour and pigmentation loci. If they had been true recombinants, then they would most likely be heterozygous for colour and homozygous for pigmentation ($C^PC^Y P^H P^H$). However, close analysis of the phenotype and the genotyping together show that they are not recombinants and therefore, more likely they were heterozygous for both colour and pigmentation ($C^PC^Y P^N P^H$). These same snails are homozygous for the banding locus (B^bB^b), but segregate for mid-band phenotype (U^3U^- , U^-U^-); the putative recombinants were always mid-banded (U^3U^-), rather than fully banded (U^-U^-). The same explanation may apply, as above. Other loci sometimes interact to prevent full penetrance of the mid-banded phenotype.

The observation that the absence of a mid-band does not always have a simple genetic basis may shed some light on previous findings. For example, both Fisher et al. (1934) and Cain et al. (1960) reported individual crosses that showed elevated rates of recombination between the C/B loci.

Cain et al. (1960) reported two crosses derived from the same mother that showed seven colour/banding recombinants in 43 snails, for which six were pink mid-banded snails. The expectation is that putative recombinants would have been homozygous for the banding locus ($C^PC^Y B^bB^b$) and non-recombinants heterozygous ($C^PC^Y B^0B^b$). However, if the six snails were not actually recombinants, then incomplete dominance of the band-suppressing allele (B^0), or else epistatic interactions with other loci, may be an alternative explanation.

Similarly, Fisher and Diver (1934) described unexpectedly high recombination (20%) between colour and banding in one cross. Unfortunately, they did not report whether the snails used were mid-banded or not. However, in their specific case, doubt

has been raised as to whether the individuals used were virgins before paired together (Cain et al., 1960; Ford, 1971; Lamotte, 1954). In researching this work, we were fortunate to find copies of letters between Fisher and Diver in the archive of Bryan Clarke (Supplementary Material). In letters from April/May 1934 that describe the preparation of the correspondence that was published in Nature in June 1934, there is clear admission that the snails used in the crosses were adult and not virgin. The authors partly acknowledge that this may be a problem. Referring to possible previous matings (“experience”), Fisher writes that “on fairly strong ground, which is not weakened by previous experience, but is not absolutely critical”. Our interpretation of the text is that Fisher acknowledges that the snails may have previously mated, but discounts this as being a problem, because the offspring ratios approximate to that expected with limited recombination. There are therefore perhaps two errors, which together invalidate the conclusions of the published work.

Epistasis could also explain other earlier data on recombination between the C/B loci and the pigmentation locus. For example, in our study, we initially scored some pink individuals as hyalozonate, even though they had a lightly pigmented lip, only later realising our error. Other authors may have made the same mistake. Unfortunately, it is difficult to be certain from the previous literature whether pink hyalozonate recombinant individuals had an unpigmented lip, though if this was not the case then it might have been explicitly noted (e.g. p404 in Cook, 1967). However, just as it is hypothesised that epistasis makes brown shelled individuals less likely to be banded, then it is reasonable to suppose that epistasis might mean that pink hyalozonates more rarely have a wholly unpigmented lip.

Evidently, further crosses are required, especially with respect to the other major loci, especially pigmentation, spread band and punctate loci in the supergene, and the various band-modifying genes. It is possible that some of these phenotypes, especially those for band-modification (Wolda, 1969), are under multi-factorial control and/or dependent upon genetic background. A further general consideration is that the genetics may differ depending upon the location of origin of the snails. In our study, the snails are derived from the UK, Ireland or Spain, and hybrids between them. As a previous mitochondrial DNA study has shown that the *Cepaea* snails in the West of Ireland are at least partly derived from snails from the Pyrenees, and genetically

divergent from those of the UK, then perhaps location should be more properly considered (Richards et al., 2013).

2.4.2. Future progress

Overall, this research proposes an alternative explanation to the putative non-recombinant phenotypes found. However, future steps are necessary to confirm that these results are due to incomplete penetrance or epistasis. Perhaps, an epistasis mapping method using, for example, QTL mapping studies to determine the expression of the genes involved may be a clever next step to verify this explanation. Moreover, this work also provides a resource for fine mapping of the supergene, and the other major shell phenotype loci. On the one hand, we have shown that phenocopies may be a problem in using the shell phenotype alone to detect recombination events within the supergene. On the other hand, the genotyping methods that we have introduced enable a means to avoid this problem.

Jones et al. (1977) (in)famously questioned whether understanding polymorphism in *Cepaea* is “a problem with too many solutions?” The intention of that work was to emphasise the perfect case study provided by *Cepaea*. We hope that these crosses may soon be used with new long-read DNA sequencing methods to assemble the *C. nemoralis* genome and to identify the supergene. Perhaps soon, polymorphism in *Cepaea* may instead be considered “a solution to many problems.

2.5. Acknowledgements

This work was supported by the University of Nottingham; the Biotechnology and Biological Sciences Research Council [grant number BB/M008770/1], via a studentship to Daniel Ramos Gonzalez; and the Dept. of Education, Universities and Research of the Basque Government [grant numbers PRE_2015_2_0191, EP_2015_1_33], via a visiting fellowship awarded to Amaia Caro Aramendia. Thanks to both Sheila Keeble and Julie Rodgers for help with the care of snails, and to Laurence Cook as well as three anonymous referees for comments on the manuscript, and to Anne Clarke and the University of Nottingham for access to the archive of Professor Bryan Clarke.

Chapter 3:

Exploring the divergence of genomic variation and geographical structure in *Cepaea nemoralis*.

Abstract

Colour variation is considered a driver in the adaptation to the environments in many species. In *Cepaea nemoralis*, it is well-known different shell ground colour are under various forms of selection and in to different environments. To what extent does this selection impact on the wider genome and across different environments? To begin to understand these factors, double digest restriction-site associated DNA (ddRADseq) was conducted to comprehend hidden patterns of its genomic variation, diversity and structure. Surprisingly, even though there was an association between genomic variation and the geographical distribution, colour variation was unrelated. The genomic areas leading the geographic variation were examined and several candidate sequences under selection were found. However, these candidates need further analyses to confirm which their involvement in the environmental adaptation. In addition, the phylogenomic structure of West European populations of *C. nemoralis* was inferred leading to an interpretation of how Pyrenean snails colonised Europe after the Pleistocene. The results may launch new roads of research into the evolutionary and genomic mechanisms that have led the geographical genomic variation and the supergene variation.

3.1. Introduction

Over the past century, the study of animal colour has been key in providing evidence for some of the central tenets of biology, especially with respect to genetics and evolution. For example, early work on the inheritance of colour traits contributed to an initial understanding of Mendelian genetics (Staples-Browne, 1908; Wheldale, 1907). Subsequent studies on the distribution and predation of colour morphs shaped our understanding of how natural selection may operate in wild populations, with perhaps some of the most important insights coming from moths and snails (Cain et al., 1950; Cook, 2003). In the 21st century, next-generation DNA sequencing technologies, such as genotyping-by-sequencing, have been used to identify the underlying genes that determine variation in colour morphs within species, and their evolutionary history (Wellenreuther et al., 2014). These same methods have also enabled the sub-discipline of phylogeography to move away from the use one or a few molecular markers to a genomic overview, usually involving thousands of genetic markers (Dusseix et al., 2020; Kotlík et al., 2018; Lucena-Perez et al., 2020). Such studies have revealed how connectivity between populations – or lack of – shapes the genetic structure of species, and critically, how regions of the genome respond differently depending upon the nature of selection and the genetic architecture of a particular colour trait (e.g. Pardo-Diaz et al., 2012; Poelstra et al., 2014).

Historically, some of the most important animals in studying colour polymorphism have been the *Cepaea* species, *C. nemoralis* and *C. hortensis*. This is partly because they are relatively easy to collect, but also because the different colour and banding morphs (Figure 1.1) show straightforward inheritance (Cook, 2017; Jones et al., 1977) – the shell polymorphism is controlled by a series of nine or more loci, of which five make a single ‘supergene’ containing tightly linked colour, banding and other loci. In these two species, we now have some understanding of the pigments and shell proteome (Affenzeller et al., 2020; Mann et al., 2014; Williams, 2017) and have begun to use new genomic methods to identify the genes involved (Kerkvliet et al., 2017; Richards et al., 2013).

However, while ongoing studies on snails in general continue to provide evidence for the relative role of various forms of natural selection and random drift in promoting and maintaining variation, as a group they are generally poorly represented in phylogeographic or population genomic studies. For example, most studies of phylogeography and/or population structure in terrestrial snails have been limited to using just one or a few genes, with a few notable exceptions (Chueca, 2020), and better representation for aquatic snails, especially *Littorina* (Hirano et al., 2019; Miura et al., 2020; Westram et al., 2018). This is a problem because if the ultimate aim is to understand the role of natural selection in promoting and maintaining colour polymorphism, then we require an understanding of the history of populations in general, and more precisely, a gene-by-gene account of how historical contingencies, including drift, and selection have impacted upon the genome.

One issue for *Cepaea* is that Steve Jones and colleagues (1977) questioned whether understanding the polymorphism is “a problem with too many solutions?”, which led to difficulties arguing the case for these snails as a study organism. Actually, the misunderstood intention of that work was to emphasise the perfect case study provided by *Cepaea*. Simple explanations for phenotypic variation, including colour, are likely an exception, so they were making the point that it is important to study organisms for which polymorphism may be explained by a variety of processes, precisely because they are more realistic. Given that present-day genomic technologies should allow us to uncover the relative contributions of each of these processes in making contemporary diversity, this point is perhaps just as prescient now.

Unfortunately, a second general issue is that is DNA from snails is sometimes difficult to work with (Adema, 2021), and snails in general have large and repetitive genomes, which are difficult to assemble. Advances in the understanding of the colour polymorphisms of snails have therefore tended to lag behind other species, especially invertebrates with relatively small genomes (Davison et al., 2020).

Historically, studies on the colour polymorphism of *Cepaea* have mainly been based on comparisons of morph frequencies between different habitats. More recently, data from much of the 20th century collections were digitised by the

“Evolution Megalab” project (Silvertown et al., 2011), so that comparisons can be made across the generations. Some of these comparative studies found that discrete colour variation were associated with geographic variables such as latitude, longitude, altitude and even by regions. For example, in larger studies yellow snails were commonly found at mid-latitudes (Jones et al., 1977; Silvertown et al., 2011). Moreover, in local surveys discrete colour patterns were mostly associated by the regions. For instance in the Pyrenees, each valley showed sharp frequency discontinuities in colour variation due to different selective pressures such as climatic or predation (Arnold, 1968; Cameron et al., 1973; Jones et al., 1975).

There have also been some genetic studies, first using allozymes and latterly mitochondrial DNA and microsatellites (but only at a local geographic scale; Davison & Clarke, 2000). Of most relevance here, Ochman et al. (1983) showed using allozymes that the Pyrenees contains three deeply differentiated sets of populations, or “molecular area effects”, for which the geographic patterns did not correlate with the shell ground colour and banding frequencies. Latterly, we surveyed much of Europe using a mitochondrial marker (Grindon et al., 2013a). As with Ochman’s study, high differentiation was found within the Pyrenees and the North of Spain. However, the main finding was that of the seven deep mitochondrial lineages, one was found only in Ireland and in a region of the Eastern Pyrenees in southwest Europe. As the oldest *C. nemoralis* fossils in Ireland date to about 8,000 years ago, around the time that modern humans began to inhabit the island after the glaciations, the suggestion was that ancient humans might have carried the edible snails with them as they moved between the Mediterranean and the Atlantic, following the Garonne river (Grindon et al., 2013a).

In this study, we take advantage of a first draft genome sequence (Saenko et al., 2020) and restriction-site associated DNA sequencing methods (ddRAD) to understand the phylogeographic and population genomic structure of *C. nemoralis*. Using samples from across Europe, the specific aim is to understand the post-glacial history of the species, at both the level of the whole genome, and more specifically, with respect to the supergene that is responsible for a large part of the colour and banding polymorphism. The ultimate aim is to provide context for subsequent studies on the evolutionary origins of the supergene, and the relative roles that natural

selection and drift may play in the establishment and loss of colour polymorphism in local populations.

3.2. Materials and Methods

3.2.1. Dataset collection

In previous work, we collected *C. nemoralis* from across Europe, euthanising snails by freezing at -80°C upon arrival at the University of Nottingham. In this study, we strategically sampled from this prior collection, including individuals from Germany, Belgium, France, Hungary, Denmark, Spain, UK and Ireland, as well as a 2017/2018 collection from three valleys in the Pyrenees, Valle de Vielha, Valle de Jueu and Valle Noguera Ribagorzana. Individuals were selected to ensure a wide geographic spread, and to include representatives of most of the major mitochondrial lineages reported in a prior study (Figure 3.1, Table 3.1; Grindon et al., 2013a).

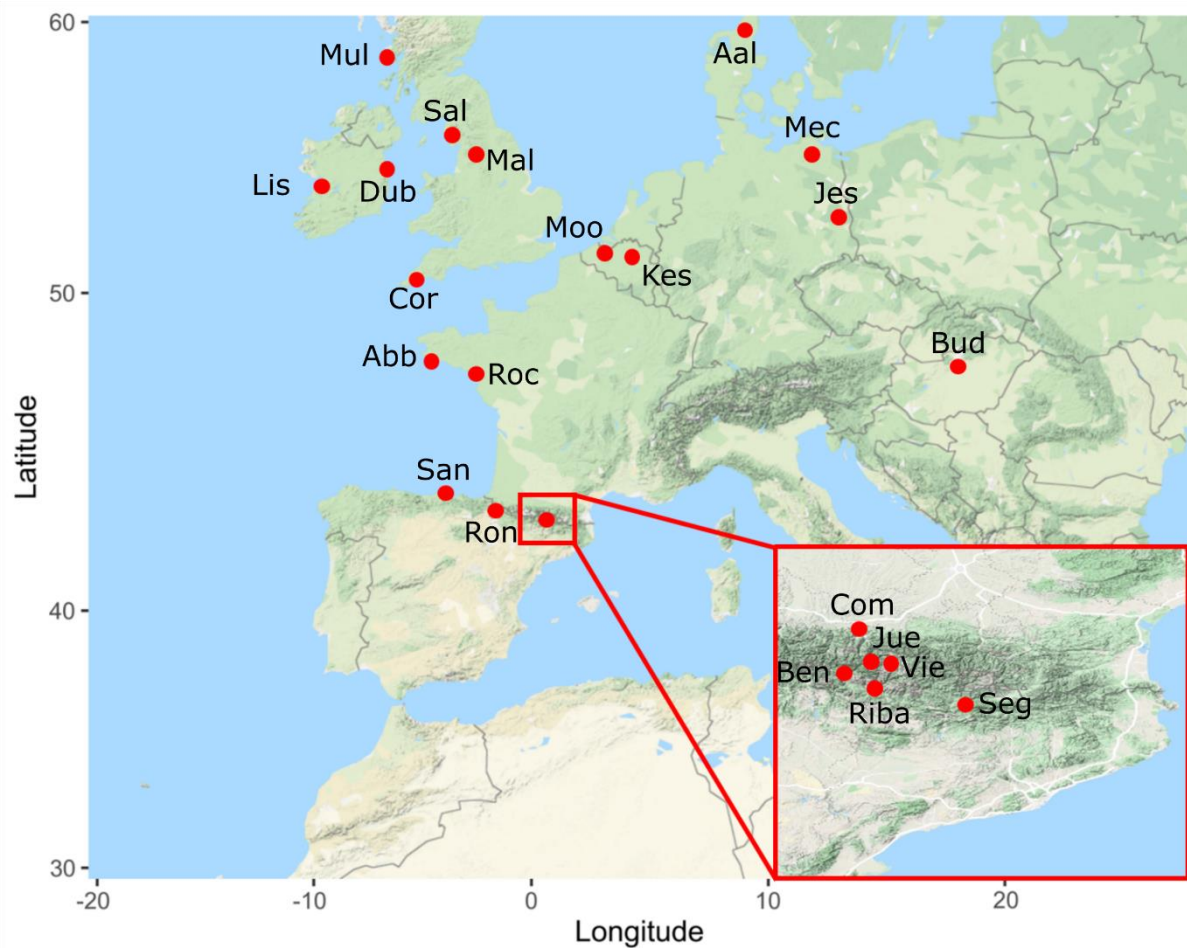


Figure 3.1. European map shows the geographical coordinate points of the sampling sites collected by Grindon and Davison (2013). Each population (red dots) is labelled by its abbreviation. In addition, an Eastern Pyrenean map is added. Three valleys from the Central Pyrenees were sampled in 2017; Vielha, Jueu, N. Ribagorzana. The other three; Comitges, Segre and Benasque were acquired from Grindon and Davison (2013).

Table 3.1. Summary showing the locations and phenotypes of the samples used in this study, including mitochondrial haplotype from Grindon and Davison (2013).

Location	ID	Grindon ID	Abbreviation	Latitude	Longitude	Mitochondrial Haplotype	Colour	Banding
Belgium / Moortsele	48	Ooscn2	Moo	50.9588	3.7798	A27	Yellow	12345
Denmark / Aalborg	46	Aal2cn5	Aal	57.0518	9.8728	A51	Yellow	12345
	47	Aal2cn7	Aal	57.0518	9.8728	A22	Pink	12345
England / Cornwall	26	Coascn3	Cor	50.2535	-5.0404	A87	Yellow	00000
	66	Coascn5	Cor	50.2535	-5.0404	A87	Yellow	00000
France / Pont L'Abbe	28	Abbecn1	Abb	47.884	-4.1826	A58	Pink	00300
	29	Abbecn3	Abb	47.884	-4.1826	A85	Yellow	00300
Germany / Jessern	49	Jesscn1	Jes	52.0167	14.1833	A11	Brown	00000
	51	Jesscn9	Jes	52.0167	14.1833	A40	Pink	00300
Scotland / Mull Isle	27	Muulcn4	Mul	56.5785	-6.2775	A47	Pink	12345
England / Malham	53	Malcn3	Mal	54.0618	-2.1467	B16	Yellow	12345
	54	Malcn5	Mal	54.0618	-2.1467	B8	Yellow	00000
England / Saltmill	52	Saltcn9	Sal	54.4893	-3.5895	B3	Pink	00300
France / La Roche	31	Berncn2	Roc	47.5118	-2.2857	B23	Brown	12345
Ireland / Dublin-Ranelagh	38	Dublincn4	Dub	53.3185	-6.2514	C15	Pink	12345
	39	Dublincn2	Dub	53.3185	-6.2514	C15	Yellow	00345
Ireland / Lisdoonvarna	36	Liscn1	Lis	53.0263	-9.2902	B27	Yellow	12345
	37	Liscn2	Lis	53.0263	-9.2902	C8	Yellow	12345
Spain / Benasque	61	Bencn3	Ben	42.5994	0.527	C18	Yellow	12345
	62	Bencn1	Ben	42.5994	0.527	C17	Pink	00000
Spain / Commitges	63	Romancn5	Com	43.028	0.7223	C57	Brown	00345
	64	Romancn7	Com	43.028	0.7223	C56	Pink	00000
Spain / Jueu	34	-	Jue	42.6779	0.7055	-	Yellow	00000
	56	-	Jue	42.6779	0.7055	-	Pink	00000
Spain / Ribagorzana	57	-	Rib	42.4792	0.714	-	Yellow	00000
	58	-	Rib	42.4792	0.714	-	Pink	00000

Spain / Segre	59	Serge2cn1	Seg	42.3598	1.4796	C1	Yellow	12345
Spain / Vielha	32	-	Vie	42.6905	0.8742	-	Yellow	12345
	33	-	Vie	42.6905	0.8742	-	Pink	00000
Belgium / Leuven	40	Kesscn5	Leu	50.8835	4.7225	D39	Yellow	00300
	45	Kesscn8	Leu	50.8835	4.7225	D8	Yellow	00000
Germany / Mecklenburg	50	Robcn2	Mec	53.5817	12.985	D33	Pink	00300
Spain / Santander	60	Santacn8	San	43.4144	-3.7413	F24	Yellow	00000
	65	Santacn9	San	43.4144	-3.7413	F25	Pink	00000
	30	Playacn9	San	43.487067	-3.792683	D49	Yellow	00000
	35	Playacn10	San	43.487067	-3.792683	D47	Yellow	00000
	55	Playacn7	San	43.487067	-3.792683	F24	Yellow	00000
Spain / Roncesvalles	41	Roncscn3	Ron	43.0093	-1.3191	F41	Pink	12345
Hungary / Budapest	42	Hungcn4	Bud	47.4258	19.4483	G11	Yellow	12345
	43	Hungcn5	Bud	47.4258	19.4483	G13	Yellow	00300
	44	Hungcn1a	Bud	47.4258	19.4483	G12	Yellow	00300

3.2.2. Genomic methods

High molecular weight genomic DNA was extracted from frozen snail tissue, similarly to the method described previously in Chapter 2.2 section (Gonzalez et al., 2019; Richards et al., 2013), using foot because it is a good source of high molecular weight DNA. In brief, slices of snail tissue were incubated at 65 °C in lysis buffer (10mM Tris, 0.1M EDTA, 0.5% SDS), with proteinase K (0.2 mg/mL), with occasional inversion. RNAase A (80 µg/mL) was added, and then each tube was incubated for one more hour to remove RNA. The mixture was cooled to room temperature, and then extracted using the standard phenol/chloroform/iso-amyl ethanol (25:24:1) method, with ethanol precipitation. DNA quality was visually verified by agarose gel electrophoresis, and then quantified and further checked using a spectrophotometer (Nanodrop 2000c) and a fluorometer (Qubit 2.0 Fluorometer). RAD-seq libraries were generated by SNPsaurus (<https://www.snpsaurus.com/>), using the method of Russello et al. (2015) and 75 ng of input DNA. One lane of a HiSeq4000 (University of Oregon) was used to generate 150 bp sequence reads, which were then demultiplexed and stored as fastq files.

3.2.3. Sequence analysis and datasets

FastQC software was used to check the quality of the reads, then adapters removed using Trimmomatic (Bolger et al., 2014) with the following settings; ILLUMINACLIP: trimmomatic/adapters/NexteraPE-PE.fa 2:30:10 (prefixNX/1:AGATGTGTATAAGAGACAG, prefixNX/2:AGATGTGTATA AGAGACAG, trans1:TCGTCGGCAGCGTCAGATGTGTATAAGAGACAG, trans1_rc:CTGTCTCTTATACACATCTGACGCTGCCGACGA, trans2:GTCTCGTGGGCTCGGAGATGTGTATAAGAGACAG, trans2_rc:CTGTCTCTTATACACATCTCCGAGCCCACGAGAC), and the trimmomatic specific parameters; LEADING:5, TRAILING:5, SLIDINGWINDOW:5:10 and MINLEN:50 – 150. Files were then checked again using FastQC. The trimmed fastq files were aligned to the *C. nemoralis* draft genome (~3.5Gb, Saenko et al., 2020) using Burrows-Wheeler Alignment Tool (Roodi et al., 2019). Bcftools v1.10 (Danecek et al., 2017) was then used to transform the sam output files to bam files, and then Bam tools was then used to call variants and genotypes (Li, 2011). Vcftools was used

to extract bi-allelic loci, while only retaining those with less than 25% missing data, a mean sequencing depth greater than 0.25 to a maximum of 25 reads, minimum quality score of 20 and minor allele frequency (MAF) of 0.1 (Danecek et al., 2011). Finally, allelic balance at heterozygotes test was used to detect contamination (Supporting information).

Approaching the challenge to understand the genetic basis of the colour and banding polymorphism in *C. nemoralis*, a set of 60 contigs from the draft genome were identified to be tightly linked to the supergene that determines the colour and banding of the shell. Contigs containing the supergene (~2.9 Mb) were found by Pool-seq technique using colour variation (Saenko et al., 2020), and verified by finding within them the flanking RAD-seq markers of the supergene (Richards et al., 2013). Two different datasets were, therefore, generated from the filtered bi-allelic loci: 1) the whole-genome RAD-seq dataset (hereafter “whole-genome”) 2) the subset of RAD-seq loci that are putatively linked to the supergene (“supergene-linked”).

3.2.4. Analysis of genomic variation

To understand the broad phylogenomic relationship between individuals, a principal component analysis (PCA) was performed. The filtered variant calling file was first pruned using a linkage genotyping analysis in plink v1.9 (Purcell et al., 2007), then linkage-pruned sites were used to generate eigenvalues and vectors. The PCA output was plotted in R version 3.4.1 (2017-06-30) using the tidyverse v1.3.0 package. To identify clusters within the genomic data, Gaussian finite mixture modelling was undertaken using Mclust 5.4.6 (Scrucca et al., 2016), assuming 1 to 20 possible clusters from the PCA results. The best fitting model was, then, determined by the highest Bayesian Information Criteria (BIC), with significant differences established by using a bootstrap likelihood ratio test, assuming varying orientations and homogeneity of variance.

To understand the distribution of genomic variation by geography, pairwise values of Weir & Cockerham’s F_{st} were estimated using Vcftools (Li, 2011). Genome-wide F_{st} was used directly by plotting against geographic distance, or transformed into a dissimilarity matrix, and again plotted against geographic distance. Geographic

distances were calculated in miles using the great circle formula in McSpatial 2.0 package in R (McMillen et al., 2013). Significance was tested using a Mantel test based on Spearman's rank correlation and 9999 permutations, using the vegan 2.5-6 community ecology package in R (Jari Oksanen et al., 2018). Then, to understand how individual genome contigs shape the overall geographic variation, the same analyses were carried out on each of the individual contigs, again testing significance using a Mantel test.

Thus, to identify the possible RAD genomic regions under selection, the mean of F_{st} pairwise estimation in each contig were calculated and Mantel statistic test were executed as previously mentioned. The estimation of higher or lower genetic differentiation than the expected under neutrality were evaluated by a simple histogram of the F_{st} (Akey et al., 2002; Narum et al., 2011). Subsequently, the outliers were determined using quantile range outliers statistic set at 97%. Finally, each sequence selected was aligned and compared with the Genbank dataset looking for homology with already described genes (Korf et al., 2003).

The whole-genome RAD-seq data was used to generate an unrooted phylogeny, using randomized accelerated maximum likelihood (raxml) v8.2.9 with the GTRGAMMA model and 100 bootstrap replicates (Stamatakis, 2014). An admixture test was performed to group and cluster allocations for each individual and to estimate the *C. nemoralis* ancestry (Alexander et al., 2011), computing the fivefold cross-validation error to determinate the best number of clusters (K). Finally, D statistics were calculated to identify evidence of introgression among targeted *C. nemoralis* populations over Europe using Admixtools version 6.0 (Patterson et al., 2012) and Admixr version 0.7.1 (Petr et al., 2019). To test robustness of the D statistics, different populations were used as outgroup. In addition, the significance of the D statistics test was evaluated using block jackknife and the Z-score.

3.3. Results

RAD-seq libraries were prepared from 41 snails and 22 locations across Europe. (Table 3.1). A contamination and genotyping quality test were performed and two samples were discarded due to a low number of reads (S57 and S58 both from Ribagorzana valley in Spain; Supplementary material and Table S3.1). 39 individuals were put through to the main analysis. An average of 95% of reads mapping to the reference genome (Table S3.1). After filtering, the whole-genome dataset was reduced to 8689 bi-allelic loci contained on 2323 genome contigs (out of 28,538 in the reference), with a mean of 3.74 SNPs per contig (Figure S3.1). There was a correlation between contig length and number of SNPs ($r = 0.11$, $p < 0.001$; Figure S3.2). Of the 60 contigs that are putatively linked to the supergene, 27 were represented in the RAD-seq data, but only 7 had variants in the final dataset (Table S3.2). The supergene-linked dataset was, thus, 31 bi-allelic SNPs found on 7 contigs.

3.3.1. West European phylogenomics of *C. nemoralis*

A principal components analysis of the whole-genome data showed that individuals of *C. nemoralis* broadly cluster according to geography (Figure 3.2a-c); PC1, PC2, and PC3 together explained 37% of the variance; Figure S3.3). Gaussian finite mixture modelling returned ten clusters as the best-fitting model (EII, spherical, equal volume; BIC 349.2 and ICL 349.2; $p < 0.001$ compared with 2nd best model).

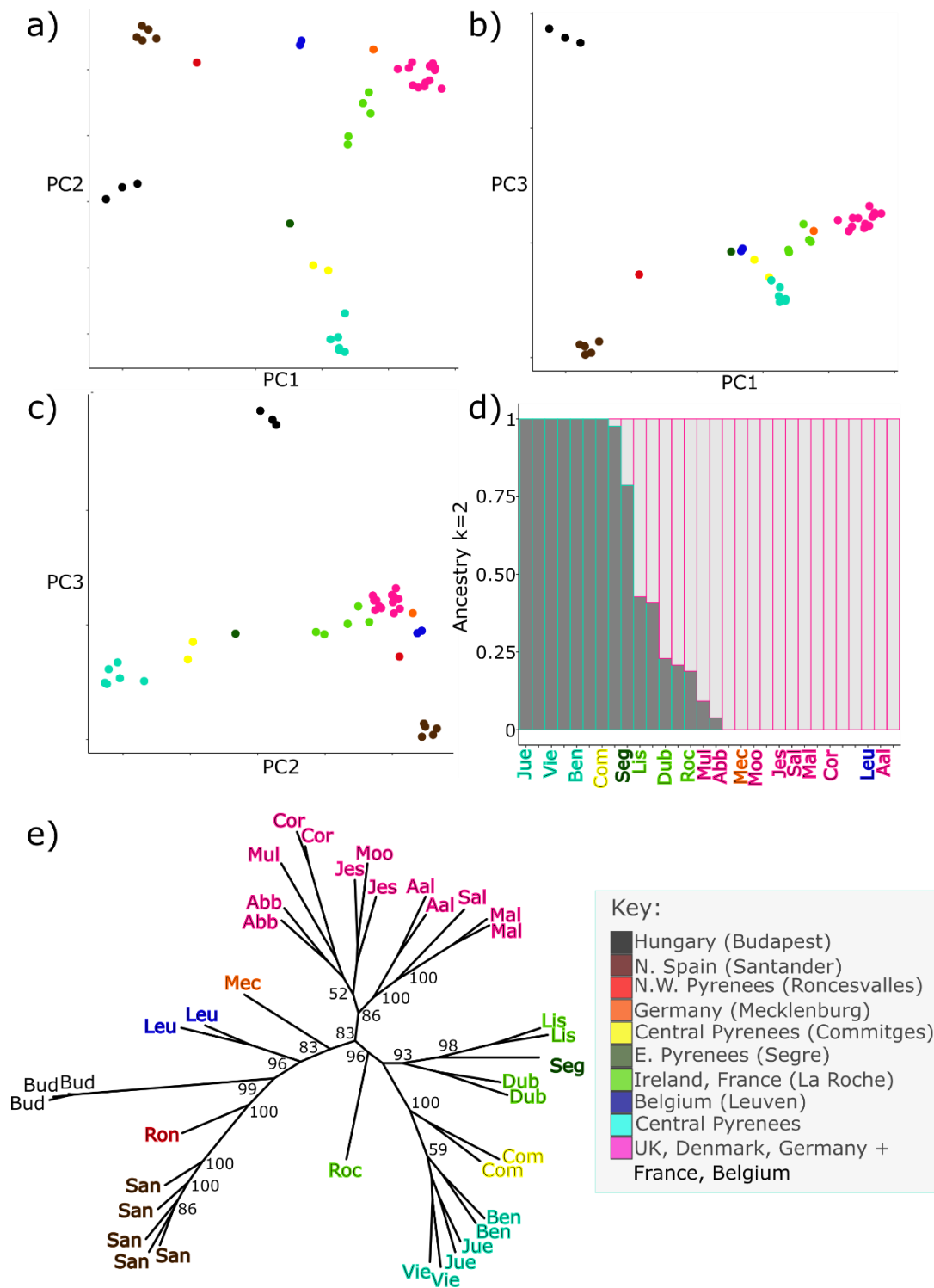


Figure 3.2. Relationship between individual *Cepaea nemoralis* snails across Europe based on 8689 biallelic loci using the whole-genome dataset. Figures are coloured according to the clusters defined by Gaussian finite mixture modelling. a), b), c) First three axes of a principal component analysis of the whole-genome data. d) Admixture analysis ($K = 2$), excluding the divergent individuals from Hungary (Budapest), North Spain (Santander) and West Pyrenees (Roncesvalles). Each vertical bar represents an individual, with the proportion of each colour representing the inferred ancestry e). Unrooted Raxml phylogeny, showing bootstrap support. Region abbreviations are shown in table 3.1.

The principal component analysis showed that the Hungarian (Budapest, n =3) samples and the North-West Iberian samples (Santander, n = 5; Roncesvalles, n = 1) were different from the other samples, and also each other. This is because PC1 separated the Hungarian samples and North-West Iberian samples from the rest of European populations (Figure 3.2a; PC1 = 15%), with PC3 separating the Hungarian samples from the North-West Iberian samples, with the others somewhat intermediate (Figure 3.2c; PC3 = 10%). PC2 separated the populations found in the central Pyrenees (Vielha, Jueu & Benasque, n = 6; Commitges, n = 2; Segre, n = 1) from samples found in central Europe and the UK (Figure 3.2b; PC2 = 12%), with samples from Ireland (Dublin, n = 2; Lisdoonvarna, n = 2) and the West of France (Roche, n = 1) closest to the Central Pyrenean samples.

An unrooted phylogeny based on the whole-genome data corroborated the principal components analysis, in recovering a North-West Iberian group, a Hungarian group, a central European group (French, German, Danish and British) and a central Pyrenean group, with the Irish populations closest to the latter (Figure 3.2e). Admixture analyses using the whole-genome data were, then, used to understand prior gene flow between the central European, Pyrenean and Irish populations. North-West Iberian and Hungarian individuals were removed from the admixture analysis due to the lack of shared ancestry. Admixture K =1 (0.91), 2 (1.00) were most strongly supported as the best cluster values according to the cross-validation error test (Figure S3.4). For K =2, individuals from the west of Ireland show mixed ancestry between the central Pyrenees and Europe. Dublin, Roc and Mul also showed mixed ancestry. Finally, D-statistical analysis using the whole-genome data were used to corroborate the admixture analyses (Table 3.2). Firstly, the comparison between the European populations (British, French, German and Danish) and Eastern Pyrenean did not illustrate significant introgression. These results illustrated that both populations had similar genetic introgression. However, significant introgression was shown when comparing the above-mentioned populations to the Iberian populations (Table 3.2, $3 < Z\text{-score} < -3$). According to D-statistic La Roche and the Irish populations are significantly (Table 3.2, $3 < Z\text{-score} < -3$) admixed between the Eastern Pyrenean and European populations (British and Danish).

Table 3.2. Four population test (D-statistic) results with its jack-knife significance test are illustrated admixture population candidates.

Population W	Population X	Population Y	Population Z	D-statistic	std-error	Z-score	BABA	ABBA	SNP's
Lisdoonvarna:									
Cornwall	Lisdoonvarna	Vielha	Budapest	-0.09	0.04	-2.32	178	215	3447
Malham	Lisdoonvarna	Jueu	Budapest	0.01	0.03	0.21	278	275	5074
Aalborg	Lisdoonvarna	Benasque	Budapest	-0.07	0.05	-1.44	133	152	2708
Cornwall	Lisdoonvarna	Jueu	Budapest	0.00	0.04	-0.08	186	187	3684
Malham	Lisdoonvarna	Benasque	Budapest	-0.06	0.04	-1.50	155	177	3228
Aalborg	Lisdoonvarna	Vielha	Budapest	-0.04	0.04	-1.08	245	265	4106
Cornwall	Lisdoonvarna	Benasque	Budapest	-0.05	0.05	-1.01	114	126	2296
Malham	Lisdoonvarna	Vielha	Budapest	0.01	0.03	0.40	281	274	4693
Aalborg	Lisdoonvarna	Jueu	Budapest	0.00	0.04	-0.05	260	261	4404
Santander	Lisdoonvarna	Vielha	Budapest	-0.25	0.03	-7.82	211	355	4441
Santander	Lisdoonvarna	Jueu	Budapest	-0.23	0.03	-7.35	225	360	4751
Santander	Lisdoonvarna	Benasque	Budapest	-0.19	0.04	-4.35	130	193	2887
Santander	Lisdoonvarna	Cornwall	Budapest	-0.21	0.03	-6.16	215	327	4407
Santander	Lisdoonvarna	Malham	Budapest	-0.19	0.03	-5.67	230	337	4688
Santander	Lisdoonvarna	Aalborg	Budapest	-0.15	0.03	-4.67	256	345	4922
Dublin:									
Cornwall	Dublin	Vielha	Budapest	-0.15	0.05	-3.37	122	166	2550
Malham	Dublin	Jueu	Budapest	-0.03	0.04	-0.90	192	206	3931
Aalborg	Dublin	Benasque	Budapest	-0.07	0.06	-1.19	96	110	1999
Cornwall	Dublin	Jueu	Budapest	-0.06	0.05	-1.36	136	155	2745
Malham	Dublin	Benasque	Budapest	-0.03	0.05	-0.57	114	121	2489
Aalborg	Dublin	Vielha	Budapest	-0.13	0.04	-2.82	141	182	3079
Cornwall	Dublin	Benasque	Budapest	-0.04	0.06	-0.70	96	104	1712
Malham	Dublin	Vielha	Budapest	-0.12	0.04	-3.09	164	210	3630

Aalborg	Dublin	Jueu	Budapest	-0.01	0.04	-0.28	160	164	3314
Santander	Dublin	Vielha	Budapest	-0.34	0.04	-9.12	135	272	3392
Santander	Dublin	Jueu	Budapest	-0.32	0.04	-8.99	146	281	3653
Santander	Dublin	Benasque	Budapest	-0.29	0.05	-6.09	92	166	2281
Santander	Dublin	Cornwall	Budapest	-0.33	0.04	-9.29	152	301	3443
Santander	Dublin	Malham	Budapest	-0.41	0.03	-11.58	127	301	3510
Santander	Dublin	Aalborg	Budapest	-0.29	0.03	-8.38	177	319	3815
La Roche:									
Cornwall	Roche	Vielha	Budapest	-0.12	0.04	-3.04	177	223	3854
Malham	Roche	Jueu	Budapest	0.06	0.03	1.88	316	281	5661
Aalborg	Roche	Benasque	Budapest	-0.15	0.05	-3.36	129	175	3000
Cornwall	Roche	Jueu	Budapest	-0.08	0.04	-2.26	196	232	4096
Malham	Roche	Benasque	Budapest	-0.03	0.04	-0.67	163	172	3500
Aalborg	Roche	Vielha	Budapest	-0.07	0.04	-1.82	237	270	4704
Cornwall	Roche	Benasque	Budapest	-0.11	0.05	-2.44	116	144	2558
Malham	Roche	Vielha	Budapest	0.08	0.03	2.40	295	251	5287
Aalborg	Roche	Jueu	Budapest	0.01	0.03	0.15	270	267	5024
Santander	Roche	Vielha	Budapest	-0.24	0.03	-6.95	183	298	4146
Santander	Roche	Jueu	Budapest	-0.19	0.03	-6.45	257	380	5296
Santander	Roche	Benasque	Budapest	-0.22	0.04	-5.22	139	216	3152
Santander	Roche	Cornwall	Budapest	-0.33	0.03	-11.37	212	426	4938
Santander	Roche	Malham	Budapest	-0.28	0.03	-9.44	248	436	5232
Santander	Roche	Aalborg	Budapest	-0.19	0.03	-6.49	279	412	5474

A significant positive (but shallow) relationship between F_{st} between individuals and the geographic and Haversine distance using the whole-genome dataset were found (Figure 3.3a,b, $r = 0.16, 0.06$ respectively and $p < 0.05$). Across all pairwise population comparisons, the mean genome-wide F_{st} calculated from the whole-genome data was 0.13, but with a wide range of individual values (0.00 to 0.44; S.D. = 0.10; Table 3.3). The frequency distribution revealed three groups, with peaks of F_{st} at approximately 0.05, 0.2 and 0.3 (Figure 3.4a). Hungarian was the most different, then Santander.

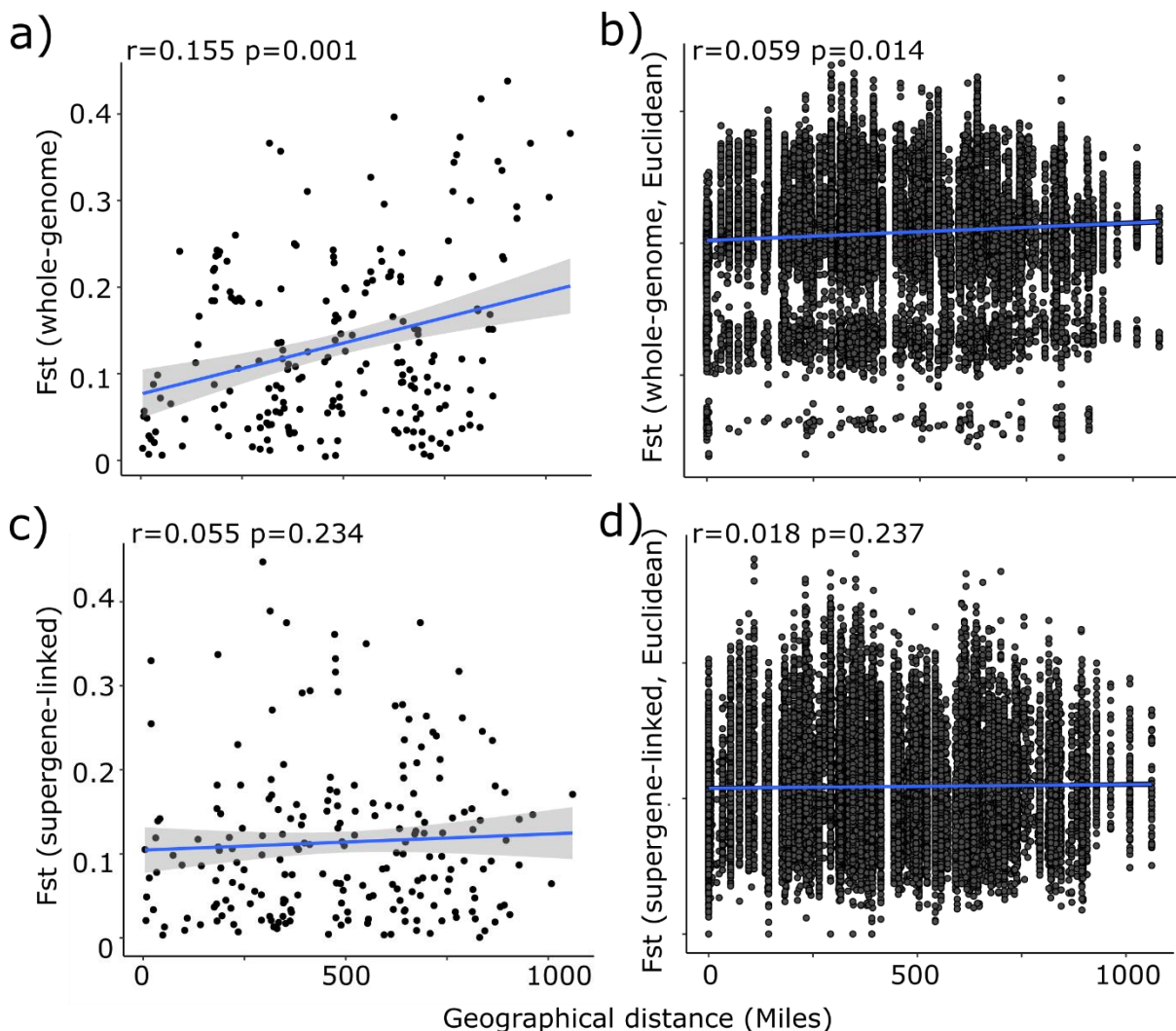


Figure 3.3. Correlations of F_{st} between individuals versus geographic distance using the whole-genome data, a) and b), and the supergene-linked data, c) and d). Left-hand plots, a) and c), show the F_{st} (averaged across all loci) versus geographic distance. Right-hand plots, b) and d), derive from the same data but transformed to represent a Euclidian genetic distance and geographic Haversine distance.

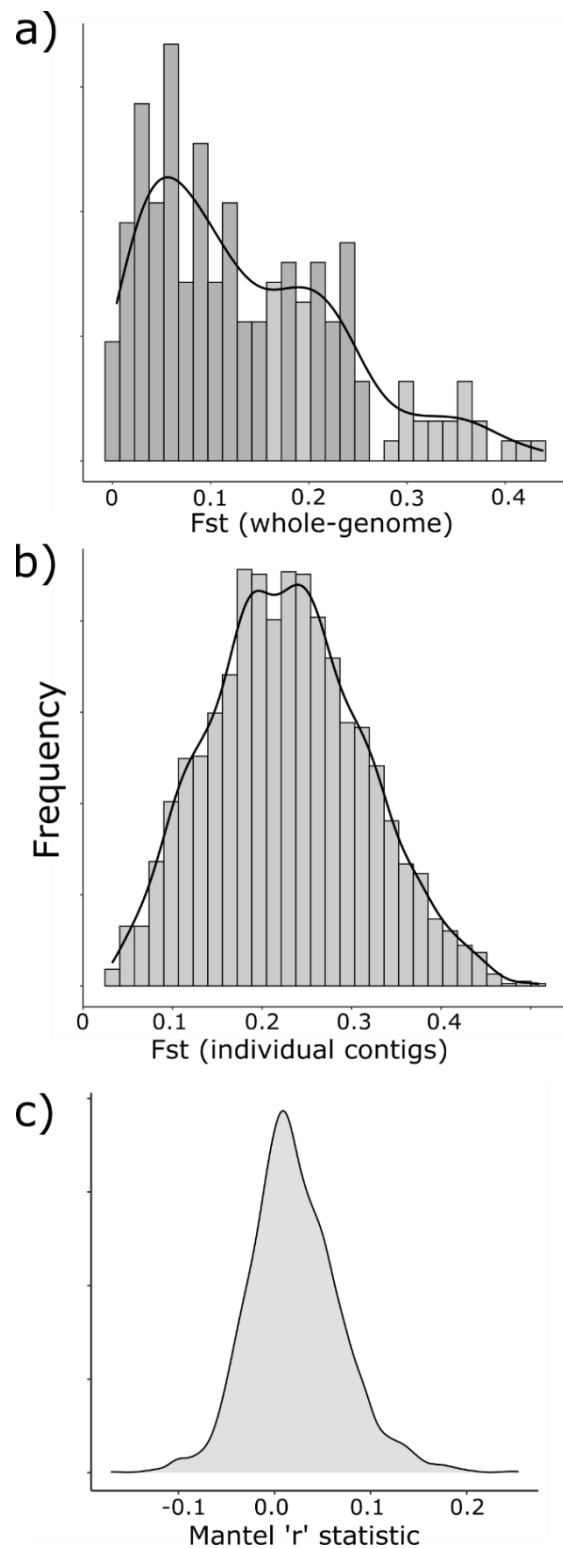


Figure 3.4. Histograms showing how genetic differentiation varies between individuals and between loci. a) Estimates of F_{st} between individuals based on whole-genome data. b) Estimates of F_{st} between individuals for each of the 2323 genome contigs c) Estimated Mantel r statistic, derived by testing correlation of F_{st} for each of the 2323 genome contigs against geographic distance, using Euclidean Haversine distances.

Table 3.3. Fst mean across all loci between all populations comparisons.

Fst mean	Vielha	Jueu	Benasque	Segre	Commitges	Budapest	Kessel.lo	Dublin	Lisdoonvarna	Santander_1	Santander_2
Vielha											
Jueu	0.051										
Benasque	0.049	0.057									
Segre	0.088	0.033	0.099								
Commitges	0.028	0.007	0.024	0.072							
Budapest	0.344	0.353	0.373	0.253	0.311						
Kessel.lo	0.161	0.168	0.164	0.062	0.119	0.327					
Dublin	0.090	0.113	0.099	0.033	0.035	0.366	0.096				
Lisdoonvarna	0.136	0.151	0.146	0.005	0.086	0.378	0.146	0.016			
Santander_1	0.238	0.236	0.219	0.195	0.184	0.293	0.170	0.205	0.208		
Santander_2	0.241	0.243	0.222	0.188	0.200	0.279	0.168	0.193	0.218	0.014	
Pont L'Abbe	0.117	0.136	0.083	0.032	0.072	0.345	0.105	0.043	0.135	0.184	0.185
Aalborg	0.151	0.168	0.151	0.074	0.115	0.397	0.108	0.078	0.160	0.232	0.235
Cornwall	0.228	0.243	0.235	0.126	0.184	0.438	0.198	0.184	0.230	0.248	0.250
Jessern	0.114	0.121	0.087	0.025	0.079	0.366	0.056	0.054	0.117	0.211	0.213
Malham	0.206	0.212	0.240	0.105	0.166	0.418	0.181	0.134	0.187	0.230	0.244
Mull	0.041	0.053	0.081	0.038	0.037	0.304	0.139	0.088	0.080	0.210	0.205
Saltmill	0.083	0.094	0.061	0.007	0.035	0.335	0.055	0.048	0.064	0.213	0.212
Moortsele	0.062	0.069	0.006	0.023	0.004	0.296	0.021	0.034	0.055	0.198	0.199
Mecklenburg	0.063	0.084	0.032	0.014	0.020	0.311	0.012	0.031	0.060	0.173	0.175
La Roche	0.038	0.050	0.013	0.041	0.016	0.300	0.041	0.067	0.014	0.184	0.185

Fst results from 0.2 to 0.3 are highlighted in yellow, whereas higher results are highlighted in red.

Fst mean	Pont L'Abbe	Aalborg	Cornwall	Jessern	Malham	Mull	Saltmill	Moortsele	Mecklenburg
Vielha									
Jueu									
Benasque									
Segre									
Commitges									
Budapest									
Kessel.lo									
Dublin									
Lisdoonvarna									
Santander_1									
Santander_2									
Pont L'Abbe									
Aalborg	0.033								
Cornwall	0.113	0.218							
Jessern	0.017	0.023	0.152						
Malham	0.127	0.125	0.260	0.111					
Mull	0.088	0.073	0.060	0.096	0.038				
Saltmill	0.031	0.022	0.106	0.058	0.006	0.166			
Moortsele	0.087	0.059	0.055	0.111	0.036	0.114	0.083		
Mecklenburg	0.048	0.028	0.090	0.241	0.054	0.131	0.103	0.357	
La Roche	0.065	0.015	0.059	0.055	0.038	0.145	0.094	0.115	0.113

Finally, to further understand geographic and genomic variation, we estimated Mantel's r statistic for the F_{st} for each contig and all pairwise comparisons of populations in the whole-genome data. Although the mean r was greater than zero, (Figure 3.4c; mean = 0.021), only ~1/3 of the genome contigs showed a significant association. Mantel ' r ' statistic outlier using a quantile range (97%) were found, which these contigs may lead the geographical genomic variation. Subsequently, the 70 sequences, the coding regions containing the SNPs located for these putative genes, were compared to GenBank database. 27 sequences found homologous sequences across the other species of the database, which 15 were uncharacterised/genome assembly/microsatellites and only 12 were characterised genes. The remaining outliers did not show homology (Table 3.4).

However, homology were found in some cases. The most relevant gene/protein found were Ig-like and fibronectin type-III domain-containing protein (FIB3) and Potassium voltage-gated channel subfamily KQT member 1 (KCHP) from *C. nemoralis* (Table 3.4, $p < 0.001$). Sulfatase 1 precursor (SULF1) and Cd-specific metallothionein gene from *Helix pomatia* (Table 3.4, $p < 0.001$). Serine/threonine-protein phosphatase 6 regulatory ankyrin and Arylsulfatase B from *Aplysia californica* (Table 3.4, $p = 0.01$ and $p < 0.001$ respectively). Carbonic anhydrase VA from *Latimeria chalumnae* (Table 3.4, $p < 0.001$). Finally, Zinc finger protein 239-like (ZNF239) from *Petromyzon marinus* (Table 3.4, $p < 0.001$).

Table 3.4. Contigs showing genomic similarities from the quantile range (97%) results of *C. nemoralis* genome are reported.

Contig	Mantel r	P-value	Species similarity	Genomic Feature	E-value	Identity
tig00006227	0.192	1E-04	<i>Apteryx australis</i>	Genome assembly	0.03	83.7
ctg4256	0.185	1E-04	<i>Cepaea nemoralis</i>	Ig-like and fibronectin type-III domain-containing protein (FIB3)	0.00	84.2
ctg12338	0.179	1E-04	<i>Arianta arbustorum</i>	Microsatellite C3 sequence	0.00	88.0
ctg34396	0.168	1E-04	<i>Helix pomatia</i>	Sulfatase 1 precursor (SULF1)	0.00	84.5
tig02175166	0.157	1E-04	<i>Scophthalmus maximus</i>	Chromosome 8	0.01	85.4
tig00395657	0.154	1E-04	<i>Cepaea nemoralis</i>	Potassium voltage-gated channel subfamily KQT member 1 (KCHP)	0.00	86.3
ctg21626	0.150	1E-04	<i>Ovis aries</i>	ATP binding cassette subfamily C member 1 (ABCC1)	0.00	89.8
ctg6440	0.149	1E-04	<i>Aplysia californica</i>	Serine/threonine-protein phosphatase 6 regulatory ankyrin	0.01	80.4
ctg7939	0.149	1E-04	<i>Helix pomatia</i>	Cd-specific metallothionein gene, complete cds	0.00	87.0
tig00047492	0.144	1E-04	<i>Polistes canadensis</i>	Putative uncharacterized protein DDB_G0289963 (LOC106785457)	0.03	91.7
ctg8829	0.142	1E-04	<i>Helix aspersa</i>	Microsatellite 8/17 sequence	0.00	78.6
ctg16452	0.140	2E-04	<i>Salmo trutta</i>	Genome assembly, chromosome: 35	0.03	79.7
tig00047947	0.140	1E-04	<i>Plectropomus leopardus</i>	DNA, chromosome 17, nearly complete sequence	0.00	83.5
ctg12268	0.137	1E-04	<i>Aplysia californica</i>	Arylsulfatase B (LOC101852069)	0.00	76.4
contig_25543	0.136	2E-04	<i>Anolis bartschi</i>	Partial HoxA11 gene, HoxA11-HoxA10 IGS and partial HoxA10 gene	0.00	93.3
tig00058036	0.135	1E-04	<i>Lateolabrax maculatus</i>	Linkage group 20 sequence	0.03	76.0
ctg852	0.134	1E-04	<i>Homo sapiens</i>	BAC clone RP11-8P17 from 4, complete sequence	0.03	91.4
contig_6378	0.133	1E-04	<i>Schistosoma mansoni</i>	Genome assembly, chromosome: 2	0.01	76.5
ctg8445	0.133	1E-04	<i>Arianta arbustorum</i>	Microsatellite Aa5 sequence	0.00	92.0
ctg27349	0.132	1E-04	<i>Helix aspersa</i>	Microsatellite 8/17 sequence	0.00	78.2
ctg11469	0.129	1E-04	<i>Aplysia californica</i>	Uncharacterized LOC101848590 (LOC101848590)	0.00	83.3
contig_22489	0.128	1E-04	<i>Cepaea nemoralis</i>	Potassium voltage-gated channel subfamily KQT member 1 (KCHP)	0.00	80.2
contig_27828	0.127	5E-04	<i>Latimeria chalumnae</i>	Carbonic anhydrase VA, mitochondrial (CA5A)	0.00	71.9
ctg15101	0.125	2E-04	<i>Apteryx australis</i>	Genome assembly AptMant0, scaffold scaffold50	0.03	84.8
tig00034653	0.123	4E-04	<i>Oryzias latipes</i>	Strain Hd-rR chromosome 8 sequence	0.00	86.8
ctg9955	0.123	4E-04	<i>Danio aesculapii</i>	Genome assembly, chromosome: 2	0.03	96.7
ctg18711	0.123	1E-04	<i>Petromyzon marinus</i>	Zinc finger protein 239-like (LOC116958600)	0.00	80.7

3.3.2. Different genomic evolutionary history of the colour and geographic variation

The same PCA analysis was also carried out on the supergene-linked data, with the first four axes represented 57% of the variance. In comparison to the whole-genome analysis, there was no clustering by geography (Figure 3.5), with the Gaussian finite mixture modelling returning one cluster (XII, spherical multivariate normal; BIC 110.5 and ICL 110.5).

No relationship was found for the geographic distance comparison using only supergene-linked data (Figure 3.3c). The same overall result was returned when using a Haversine distance matrix of F_{st} (Figure 3.3d). Moreover, while there was also considerable variation of F_{st} by contig, with a mean of 0.23 (range 0.03 to 0.51; S.D. = 0.09; Figure 3.4b), in the mean F_{st} for the supergene-linked contigs was about average, 0.24.

a) Gaussian Mixture clusters b) Shell colour background

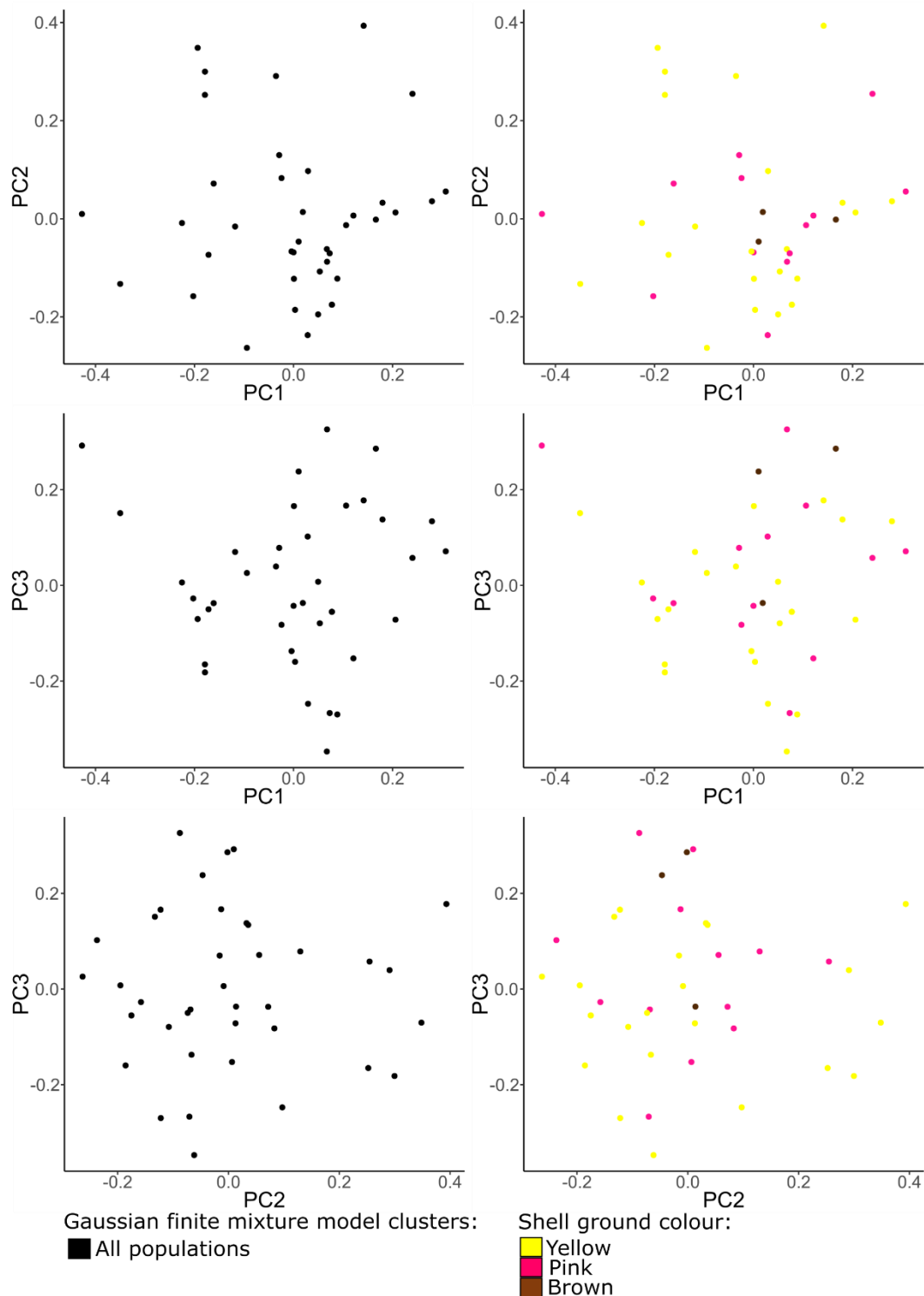


Figure 3.5. Relationship between individual *Cepaea nemoralis* snails across Europe based on 31 biallelic loci using the supergene-linked dataset. First three axes of a principal component analysis of the supergene-linked data are compared. A) Figures are coloured according to the clusters defined by Gaussian finite mixture modelling and b) to the individual shell ground colour. No clusters are found.

3.4. Discussion

Investigating the phylogeography of *Cepaea nemoralis* – and the relative degree of gene-flow between populations – is an important step towards understanding the relative roles that natural selection and drift have to play in the evolutionary history of the colour and banding polymorphism. In this study, we used a newly available draft genome (Saenko et al., 2020) and the ddRAD method, with a primary aim to understand the post-glacial history of the species, but also to provide context for future studies on the evolutionary origins of the supergene, and the roles that selection and drift have in determining the local colour polymorphism. The study is relatively novel, partly because the only genome assemblies available in land snails are for *Cepaea* and two species of *Achatina* (Guo et al., 2019; Liu et al., 2021; Saenko et al., 2020); the reality is that although phylogeographic and genomic studies are relatively common in other invertebrates, there are remarkably few similar studies in snails, or even the wider group of molluscs.

Broadly, the results corroborate previous studies, in that populations showed a high degree of genetic structuring, sometimes over short geographic distances. For example, the maximal genetic distance was between snails in Hungary and the rest of Europe ($F_{st} > 0.3$; Table 3.3) In comparison, much of Europe, including the UK, Denmark, Germany, France and Belgium, contains a relatively homogenous group of snails for which differentiation between populations is typically around 0.05 to 0.15 (excluding e.g. Mecklenburg and Leuven), sometimes irrespective of geographic distance.

One of the key characters of most population genetic studies of land snails is that they show high population structure, and deeply diverged mitochondrial lineages, the latter frequently considerably greater than 5% within species (Chiba, 1999; Thomaz et al., 1996). In *Cepaea*, one of the most striking findings from previous work, using mitochondrial DNA, was that some Irish *C. nemoralis* are most likely derived from a post-glacial colonisation event from the Pyrenees (Grindon et al., 2013a). In this study, an analysis of the whole-genome data shows a more nuanced view. The present-day snails in Ireland are likely descendants of hybridization between

Pyrenean-derived snails and individuals from the population that colonised most of central Europe. There is also a possible hint of this same hybrid genetic signature in a snail from the North-West of France (La Roche) and another from Mull in Scotland. Similar findings showing mixed ancestry have been reported for other species (especially those involving the "Celtic fringe"; Brace et al., 2016; Kotlík et al., 2018; McDevitt et al., 2011; Searle et al., 2009). Altogether, these new results contribute to the ongoing debate regarding the uncertain origins of the Irish biota (eg, McDevitt et al., 2020). Although not proven, we think that the most likely scenario is that *C. nemoralis* snails arrived directly from the Pyrenean region, likely assisted by humans (in the same way that mice are transported by humans; Jones et al., 2013).

Finally, even though the use of DdRAD-seq approach contributed towards understanding the relative roles that natural selection and drift have to play in the evolutionary history of the colour and banding polymorphism. This method conducive to a reduction in dataset due to a high amount of missing data allowed. Some researchers have argued that reducing dataset sizes due to missing data may show biased results of mutations among the screened loci (Huang et al., 2014). However, other authors found high genomic structure accuracy using a large proportion of missing data (Rubin et al., 2012; Wagner et al., 2013). In this case, the reduction of the dataset was not a great obstacle to deepen in the understanding of the post-glacial history of the species. I hope that in the future, a chromosomal level assembly of the *C. nemoralis* genome should enable subsequent studies on the evolutionary origins of the supergene, and the relative roles that natural selection, recombination and drift may play in the establishment and loss of colour polymorphism in species as a whole and, more specifically, local populations.

3.4.1. Evolutionary history, genomic diversity and population structure of *C. nemoralis*.

A revision of the taxonomy means the genus *Cepaea* now contains only two species, *C. nemoralis* and *C. hortensis*, with *C. sylvatica* and *C. vindobonesis* removed to another genus (Kajtoch et al., 2017). As the sister taxa *Iberus*, *Pseudotachea* and *Allognathus* are Iberian (Neiber et al., 2015; Neiber et al., 2016), then a best-guess is that the ancestor of *Cepaea* itself may have originated in Iberia, subsequently

colonising the whole of Europe. Unfortunately, the genomic data presented here do not easily inform on the origination of the genus, or the evolution of the polymorphism. In comparison, the data presented here is more informative of relatively recent events. Certainly, there are multiple divergent lineages in Iberia, which may imply origination there, but there are also divergent populations and lineages in other potential refugia, such as the Balkans (Hungary and Croatia sampled in Grindon et al., 2013b), and Italy (three sites in Grindon et al., 2013b). Much of mainland Europe was likely colonised by snails from the same glacial refugium, although the precise location of that refugium is not clear. In the future, further sampling is required in Italy, the Balkans, Alps, Mediterranean coast, western coast of France and the northern flanks of the Pyrenees. As mentioned already, human-aided migration remains the best explanation for the presence of snails in some locations. Both the mitochondrial and genomic data are consistent with the inference that snails were transported by Mesolithic humans from the Pyrenees to Ireland, via land, river and coastal routes (Grindon et al., 2013b). In perhaps a similar manner, modern-day populations of *C. nemoralis* have been founded in parts of Poland (Ožgo et al., 2019), Sweden (Cameron et al., 2020) and Russia (Egorov et al., 2021).

Moreover, the genome scan approach identified possible loci showing evidence of divergent selection among populations (Table 3.4). These candidate regions may be involved in the geographic genomic structure among the European populations (Table 3.3). However, this results must be taken with caution, as isolation by distance (Mantel test) results are susceptible to false positive outcomes due to the recombination rate differentiation (Diniz-Filho et al., 2013; Hoban et al., 2016). When conducting a large spatial sampling, like in this case across Europe, populations with closer distances are influenced by similar environmental parameters, predation, habitats etc... These methods assumed independent populations, which it may generate high false positive rates (Hoban et al., 2016).

All the homologous sequences found in the whole genome dataset aligned to evolutionary conserved protein. Interestingly, there are three main different functions proposed among these proteins; snail growth, cell structure and adaptation to stress due to polluted environments. For instance, Fibronectin (FIB3) is necessary in the embryogenesis process (Affenzeller et al., 2018; Wang et al., 2017), KCHP is a

transmembrane channels potassium specific and sensitive to voltage changes in the cell's membrane potential. In addition, other genes are known to be involved in adaptation to cellular stress or polluted environments such as SULF1 or arylsulfatase B enzyme, Cd-specific metallothionein gene, or Carbonic anhydrase VA (Affenzeller et al., 2018; Bradshaw et al., 2009; Dallinger et al., 1997; Erlichman et al., 1994; Grace et al., 2006; Robinson et al., 2019; Wang et al., 2017). The origination of genomic structure linked to the geographical distribution in nature can be derived from adaptations to environmental factors due to climate change or pollution (Stange et al., 2020). In *C. nemoralis*, genetic variation and shell morphology and strength association with different content of heavy metals were also found in past studies (Jordaens, De Wolf, Van Houtte, et al., 2006; Jordaens, De Wolf, Vandecasteele, et al., 2006). In this case, Jordaens (2006) studies showed possible adaptations to soil pollution due to *C. nemoralis* changes in feeding and reproduction processes in regions with soils polluted by heavy metals (Notten et al., 2006a; Notten et al., 2006b). The present genome scan findings may provide context for future studies on the association between the geographical and genomic variation.

In the future, we hope that a chromosomal level assembly of the *C. nemoralis* genome proposed above should also address the same phylogeographic and population genomic questions to the sister species *C. hortensis*, which has a more northerly distribution, and so is absent from Iberia. This species also colonised North America, possibly more than 7000 years ago (Pearce et al., 2004), and is long present in Iceland, and perhaps once present in Greenland (Johnson, 1906). It is not known how this species colonised these locations, but population genomics would reveal whether it was from one or several sources, and whether a “stepping-stone” was involved (e.g. Europe – Iceland – North America). Moreover, a proper genome scan with a more accurate dataset and analysis needs to be done to give an explanation to the genomic divergence among the European populations.

3.4.2. Colour and genomic geographic variation

One of the characters of the genus is that all, or nearly all, populations of *Cepaea* show some degree of colour or banding polymorphism, across the native range and also in introduced populations (Cook, 2017; Jones et al., 1977). The origin

of the colour differentiation is unclear and may be considered to be originated before of the Pleistocene glaciation as “relics of history” (Ellis, 2004), since during the last ice age the snails took refuge in the valleys of the Pyrenees and the genetic variation found was not related to the corresponding colour variation (Ellis, 2004; Ochman et al., 1983). Therefore, the lack of correlation with colour may lead to a possible anterior origination.

Large-scale and local surveys of the geographical distribution of shell ground colour showed clear geographical patterns (Cameron et al., 2012; Cook, 2014; Davison et al., 2019a; Ožgo et al., 2012; Silvertown et al., 2011; Worthington et al., 2012). Although our methods are still relatively blunt, relying upon a few loci that are linked to the supergene, there is no suggestion from the genomic data that large-scale trends in morph frequencies are the result of clines in frequencies of discrete haplotypes at supergene-linked loci. This is because the supergene-linked dataset showed no associations with geography; this situation that could come about because of diversifying natural selection and subsequent gene-flow but this remains to be proven.

Nonetheless, the whole-genome data does enable a more nuanced understanding. The genomic survey shows that European-wide patterns of differentiation are primarily due to three or more groups of snails between which recent gene-flow is apparently low or lacking – the species is made up of a central European population, a Hungarian population and two or more populations in Iberia (although further sampling is required, especially in the Balkans and Italy). Future studies that aim to test trends in shell variation may therefore wish to take account of this knowledge in analyses.

Perhaps unsurprisingly, large-scale differentiation due to isolation-by-distance is mainly driven by about a third of the genome (Figure 3.4c). The present data set lacks power (partly due to the lack of contiguity of the genome assembly), so it is premature to understand if this pattern is due chance events, or else gene-flow. Similarly, the apparent lack of differentiation at supergene-linked loci must also be taken with caution, especially given a lack of knowledge of precise linkage. A further note of caution is that isolation-by-distance (Mantel test) results are susceptible to

false positive outcomes, for a variety of reasons as mentioned above (Diniz-Filho et al., 2013; Hoban et al., 2016).

In the future, it should be possible to identify the genes involved in determining the polymorphism, in which case it would be fruitful to compare associations of colour alleles with geography. For example, it is our impression that the yellows, pinks and even browns of many Pyrenean (and Irish) populations are somewhat different – more ‘exuberant’ (Franks et al., 2009) – compared with other populations (Figure 1.1). A possible explanation is that the coding alleles for colour are long diverged, which should be evident in any phylogeny. As previous work showed that colour is ‘indiscrete’, and not three separate colours (Davison et al., 2019b), further sequence analysis of colour alleles will also be informative. In some other species, such as *Heliconius* butterflies, the colour differences are not continuous; phylogenies based on colour-linked loci show strong associations with the wing-colour. This is especially the case when markers are tightly linked, and occurs irrespective of the species (e.g. Pardo-Diaz et al., 2012).

3.5. Acknowledgments

This work was supported by the University of Nottingham; the Biotechnology and Biological Sciences Research Council [grant number BB/M008770/1], via a studentship to Daniel Ramos Gonzalez. Thanks to Dr. Adele Grindon providing the European sampling collection; Thanks to the SNPsaurus team to deliver the RAD-sequencing. Thanks to Thanks to Dr. Mark Ravinet, Dr. Joana Meier and Dr. Martin Simon for helping to solve genomic analysis issues; and thanks to Dr. Suzanne Saenko who provided preliminary full genome used in this research.

Chapter 4:

Qualitative and quantitative methods show stasis in patterns of *Cepaea nemoralis* shell colour polymorphism in the Pyrenees over five decades

This chapter has been published in Ecology and Evolution on 24/03/2021

DOI: 10.1002/ece3.7443

Abstract

One of the emerging strengths of working with the land snail genus *Cepaea* is that historical collections can be compared against modern day samples, for instance to understand the impact of changing climate and habitat upon shell morph frequencies. However, one potential limitation is that prior studies scored shell ground colour by eye, usually in the field, into three discrete colours yellow, pink or brown. This incurs both potential error and bias in comparative surveys. In this study, we therefore aimed to use a quantitative method to score shell colour, and evaluated it by comparing patterns of *C. nemoralis* shell colour polymorphism, using both methods on present day samples, and against historical data gathered in the 1960s using the traditional method. The Central Pyrenees were used as an exemplar, because intensive surveys sometimes show sharp discontinuities of morph frequencies within and between valleys (Arnold, 1968; Cameron et al., 1973; Jones et al., 1975). Moreover, selective factors, such as climate or the human impact in the Pyrenees, have significantly changed since 1960s.

The main finding was that while quantitative measures of shell colour reduced the possibility of error, and standardised the procedure, the same altitudinal trends were recovered, irrespective of the method. Therefore, although subject to error, human-scoring of snail colour data remains valuable, especially if persons have appropriate training. In comparison, while there are benefits in taking quantitative measures of colour in the laboratory, there are also several practical disadvantages, mainly in terms of throughput and accessibility. In the future, we anticipate that both

methods may be combined, for example, using automated measures of colour taken from photos generated by citizen scientists conducting field surveys. Moreover, a comparative studies of shell pattern frequencies was made to discover the factors acting on the ecological, evolutionary and genetic procedures in the wild populations of *C. nemoralis* of the Central Pyrenees. There was a remarkable stability in the local shell patterns over five decades, with the exception of one valley that has been subject to increased human activity. The lack of enough evidences to explain the stasis found rose a discussion about direct explanations.

4.1 Introduction

Historically, two of the most important species in studying colour polymorphism have been the west European land snails *Cepaea nemoralis* and *C. hortensis*, because individuals are relatively easy to collect and study, and the colour and banding morphs show straightforward inheritance (Cain et al., 1950, 1952, 1954; Jones et al., 1977; Lamotte, 1959). In the present day, one of the continuing benefits of working with *Cepaea* is an ability to compare the frequencies of shell morphs in historic collections against modern day samples, to infer the potential impact of natural selection and/or drift in changing shell morph frequencies. Of particular use, the “Evolution Megalab” project digitised a large set of 20th century samples (Cameron et al., 2012; Silvertown et al., 2011; Worthington et al., 2012). These records, and others deposited in museums, are now being used with modern surveys to produce an increasing number of comparative papers (Cameron et al., 2012; Cameron et al., 2013; Cook, 2014; Cowie et al., 1998; Silvertown et al., 2011; Worthington et al., 2012).

In nearly all comparative studies of *Cepaea* reported to date, absolute change in frequencies of the main shell morphs, colour and banding, have been reported, but the direction is not always consistent. The conclusions are in part dependent upon the geographic scale and the precision of resampling, whether exact or nearest neighbour. To fully understand changes – or stasis – in shell polymorphism, both global and local surveys are needed (Berjano et al., 2015). For instance, large-scale surveys illustrate the broad picture of the changes in the spatial variation of the polymorphism. In the largest study, a historical dataset of more than six thousand population samples of *C. nemoralis* from collections between 1950 and 1990 recorded in the Evolution Megalab, was compared with new data on nearly three thousand populations (Silvertown et al., 2011). A historic geographic cline among habitats in the frequency of the yellow shells was shown to have persisted into the present day. However, there was also an unexpected decrease in the frequency of unbanded shells, and a corresponding increase in frequency of banded and mid-banded morphs in particular (Silvertown et al., 2011). A UK-wide study used Evolution Megalab data, but reported a somewhat different pattern of change. Yellow and mid-

banded morphs had increased in woodland, whereas unbanded and mid-banded increased in hedgerow habitats (Cook, 2014).

In comparison to these large surveys, the majority of comparative studies have been at a more local scale. The benefit of these is that resampling is often precise (Cameron et al., 2013; Cook et al., 1999; Cowie et al., 1998; Ożgo et al., 2017; Ożgo et al., 2012), and it is also possible to take local factors into account. Most of the original historic studies took place in the UK. Following resampling, modern comparative surveys have tended to find an increase in yellow and mid-banded shells (as above) (Cameron et al., 2012; Ożgo et al., 2017; Ożgo et al., 2012; Silvertown et al., 2011), but with exceptions (Cameron et al., 2012; Cook et al., 1999; Cowie et al., 1998), depending upon the precise scale of comparison. Moreover, patterns of change are not always consistent within the same study.

One potential limitation of all of these works is that shell ground colour was scored by eye, usually in the field, into three discrete colours yellow, pink or brown. Even if persons are trained, there is still bias and error, and potential for dispute over what defines each colour. In practise, it is frequently difficult to distinguish the colours, and define different shades of the same colour. Therefore, to understand whether colour variation is in reality continuous, and to investigate how the variation may be perceived by an avian predator, we previously applied psychophysical models of colour vision to shell reflectance measures, finding that both achromatic and chromatic variation are continuously distributed over many perceptual units in indiscrete in *Cepaea nemoralis* (Davison et al., 2019a). Nonetheless, clustering analysis based on the density of the distribution did reveal three groups, roughly corresponding to human-perceived yellow, pink and brown shells.

This prior work raises the possibility that reproducible, quantitative shell colour measures, based on spectrophotometry in the laboratory, can be used to compare and test regular shell colour data, avoiding the requirement to bin measures into colour categories. In this study, we therefore aimed 1) to use the quantitative method to score shell colour, and 2) evaluated it by comparing patterns of *C. nemoralis* shell colour polymorphism using both methods on present day samples, and against historical data gathered using the traditional method.

To achieve this aim, the Central Pyrenees were used as an exemplar location, because they were intensively surveyed during the 1960s and 70s (Figure 4.1), sometimes showing sharp discontinuities of morph frequencies within and between valleys (Arnold, 1969; Arnold, 1968; Cameron et al., 1973; Jones et al., 1975). They are also particularly interesting for their geographic and ecological variation, including a diverse range of different microclimates, within and among the valleys, due to the interaction of three main climates, Atlantic, Mediterranean and Alpine, as well as a large altitudinal differences and incidence of precipitation. Moreover, selective factors, such as climate or the human impact in the Pyrenees, have significantly changed since the 1960s (García-Ruiz, 2015).

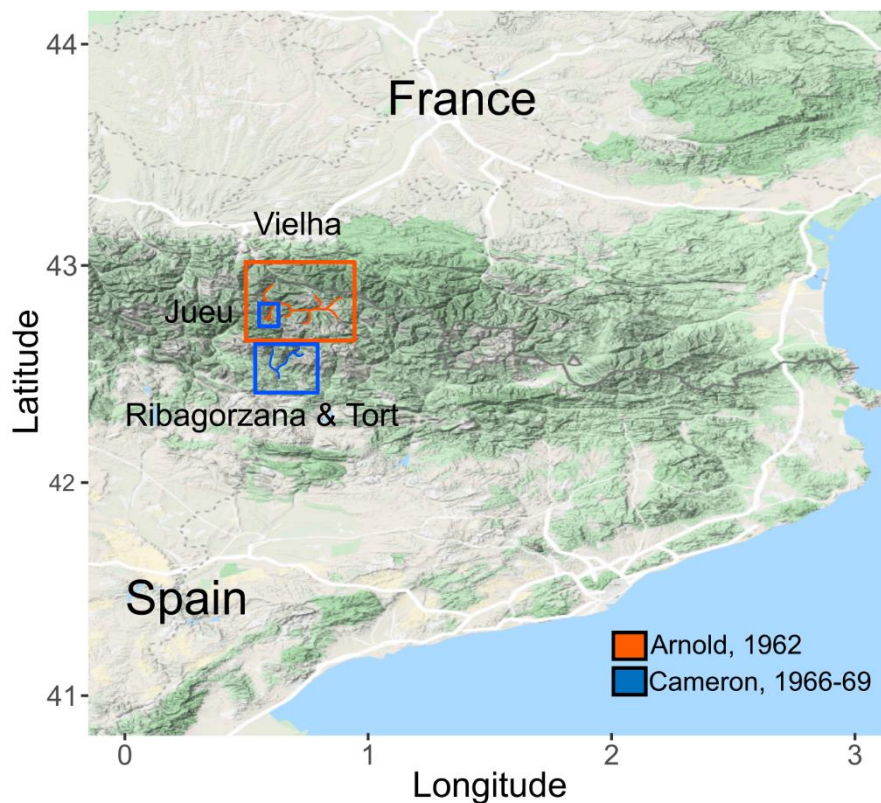


Figure 4.1. Overview of sampling locations in the Pyrenees, including this work, and previous work by others in the 1960s (Arnold, 1968, Cameron et al., 1973).

In this chapter, we aimed to evaluate manual scoring by using a colour quantitative method based on Davison et al. (2019) and using a comparative studies of shell pattern frequencies. Thus, a comparison of past and present patterns of the main shell features were tested by the two methods above mentioned to bring more insides on the ecological, evolutionary and genetic procedures happening in the underlying in the wild populations of *C. nemoralis* of the Central Pyrenees.

4.2. Materials and Methods

4.2.1. Shell samples and human-scoring of shell phenotype

The Valle de Vielha, Valle de Jueu, Valle Noguera de Tort and Valle Noguera Ribagorzana, hereafter abbreviated as “Vielha”, “Jueu”, “Tort” and “Riba”, were selected for sampling (Figure 4.1). This is because they had been previously sampled in 1962 by Arnold (1968), and in 1966 and 1969 by Cameron et al. (1973), with the colour and banding data made available via the Evolution Megalab database. New samples were collected in October 2017 and June 2018. By choice, we aimed to sample in the same location as described in past surveys, using the coordinates recorded in the Megalab database; when this was not possible, alive and empty shell samples were collected from the nearest adjacent site with suitable habitat for snails.

Snail shell colour was qualitatively scored in the laboratory as either yellow, pink or brown, by DRG, after training and discussion with AD. Similarly, following previous convention, shells were scored as “unbanded” (00000), “mid-banded” (00300) or “banded” (all shell banding versions except mid-banded). These three categories were used in all subsequent analyses. As *C. nemoralis* in the Pyrenees is polymorphic for other characters, we also scored the lip colour, as either pale (usually white) or any other colour (usually black or dark brown), and measured the shell “height” (H) and “width” (W) using a Vernier calliper with 0.05 mm precision, then calculating the “shape” as H/W.

4.2.2. Quantification of shell colour

The ground colour of adult snail shells from Vielha and Jueu valley were chosen to extract the colour spectra due to the presence of the two discrete colours, which PC3 tended to separate (Davison et al., 2019a), in the majority of the sample sites and the association with altitude. Shells were measured using an Ocean Optics spectrometer (model USB2000+UV-VIS-ES) and a Xenon light source (DT-MINI-2-GS UV-VIS-NIR), as described previously (Davison et al., 2019a). Briefly, the shell underside was used because it is generally unbanded and the least damaged/exposed to sunlight, holding the probe at a 45° incident angle, ~2 mm from the shell. Each sample was quantified three times, non-consecutively, recalibrating using light (WS-1) and dark standards after 2 to 5 quantifications, software was recalibrated by using light standards (Davison et al., 2019a). Data was collected using Ocean Optics SpectraSuite 2.0.162, using an integration time of 750 msec, boscar width of 5, and scans to average 10. Reflectance spectra were analysed following a modified protocol described below (Davison et al., 2019a; Delhey et al., 2015), using Pavo 2.2.0 R package to bin raw reflectance spectra (1 nm) (Maia et al., 2013; Maia et al., 2018), and then R version 3.4.1 (2017-06-30) for further analyses (Delhey et al., 2015).

In a previous analysis, we wished to understand how an avian predator might perceive the shell colours, so the tetrachromatic colorimetric standards of a blackbird (*Turdus merula*) were used (Davison et al., 2019a). In this new analysis, the main aim was to compare human qualitative scores of shell colour against quantitative scores, so as to better understand any biases. Reflectance spectra analysis were therefore analysed using human CIE colour trichromatic coordinates (Smith et al., 1931; Westland et al., 2012), as follows.

CIE standards are based on the stimulation of the different photoreceptors' cells (cones) of the retina. In humans, three main groups of cones are found, L (long wavelength, peaking at 560 nm), M (medium wavelength, peaking at 530 nm), and S (short wavelength, peaking at 420 nm) (Hunt, 2004). The visual colour spectra (300-700 nm) were converted using the three chromatic coordinates of the visual space, xyz, where Euclidean distances between points reflect perceptual differences, generated from quantum catches for each photoreceptor (Cassey et al., 2008). The

human trichromatic coordinates (xyz), determined from the tristimulus values (XYZ), were calculated by Pavo 2.2.0 R package, a colour spectral and spatial perceptual analysis, organization and visualization package, and the “standard daylight” (d65) irradiance spectrum (Maia et al., 2018; Smith et al., 1931). Then, a principal component analysis (PCA) was undertaken as described previously (Davison et al., 2019a; Delhey et al., 2015; Scrucca et al., 2016).

4.2.3. Analysis of phenotype frequencies and correlation

To compare past and present-day datasets, the change in the frequencies of colour and banding traits for each sample site were calculated. To detect any overall trends in each valley, any differences were evaluated using independent paired T-student (parametric) or paired rank Wilcoxon Test (non-parametric), selected according to normality (Shapiro-Wilk normality test) and homogeneity (F-test).

Linear mixed regression models were conducted for colour and banding from past and present datasets. Outliers were removed following the interquartile range method, using a Shapiro-Wilk normality test to test for deviations from normality. The Pearson correlation (parametric) or Kendall rank correlation test (non-parametric) were performed to evaluate correlation and any significance with altitude. Kendall rank correlation coefficient “Tau” were transformed into Pearson “r” coefficient to evaluate correlation and to conduct Fishers’ Z-transformation (Fisher, 1921; Walker, 2003). Correlation breached the assumption of normality required in the standard comparative test. Therefore, Fishers’ Z-transformation were applied to calculate the significance of the difference between the past and current correlation coefficients against altitude.

Maps, plots and statistical tests were made using R version 3.4.1 (2017-06-30), the ggplot2 3.2.1 package for data visualization, and the ggmap 3.0.0 R package, to generate maps. Maps were acquired from the Geo-location APIs platform in Google maps source (<https://console.cloud.google.com/apis/dashboard>).

4.3. Results

4.3.1. Past and present-day geographic distribution of colour and banding morphs

In general, snails were found in open areas such as hedgerows, scrubs, meadows and grass, and were rare in woodlands. In high altitude areas, snails were discovered mostly on meadows or screes. In total, 2633 snails were collected from 138 sample sites ranging from 823 m to 1921 m above sea level. Only 108 sites and 2633 individuals were used for the analysis, as we only considered sites with ten or more individuals collected (Tables 4.1). Of the filtered 108 sites, 87 were judged to be the same as a previous study, based on previous coordinates, or up to 50 m distance away.

In comparison, in the previous surveys, Arnold (in 1962) collected 5006 snails from 123 sites in the Vielha and Jueu valleys (Arnold, 1968). Cameron (in 1966 and 1969) sampled 2177 and 2145 snails from 48 and 55 sites located in Jueu, Ribagorzana and Tort respectively (Cameron et al., 1973). Therefore, a total of 226 historical sample sites and 9328 individuals were available for comparison (Table 4.1). Full details of all sample sites are in the supporting information (Tables S4.1, S4.2).

Table 4.1. Sampling summary; number of sites and snails for each valley.

Valley	Past		Present		Spectrophotometry	
	Sample sites	No. shells	Sample sites	No. shells	Sample sites	No. shells
Vielha	119	4756	43	942	43	607
Jueu	49	1862	17	637	12	206
Riba	34	1545	21	518		
Tort	24	1165	27	536		
Total	226	9328	108	2633	55	813

As in previous studies from the Pyrenees, the new survey showed that the pattern of shell morph distribution depends upon the specific valley, frequently showing associations with altitude (Figures 4.2, 4.3). Yellow and unbanded shells tended to predominate in the higher regions of the Vielha and Jueu valleys. In the intermediate or lower sites (below ~1200m), pink and yellow shells had similar frequencies, with most shells also having bands. In Ribagorzana yellow shells were commonly distributed in all sites, whereas pinks were usually found in the upper valley and brown morphs in the intermediate and lower valley. Brown populations were only found in the Ribagorzana and Tort valleys. In addition, unbanded morphs prevailed in Ribagorzana. In contrast, in the adjoining Tort valley, yellow predominated in all sites, with banded morphs predominant in almost the entire valley.

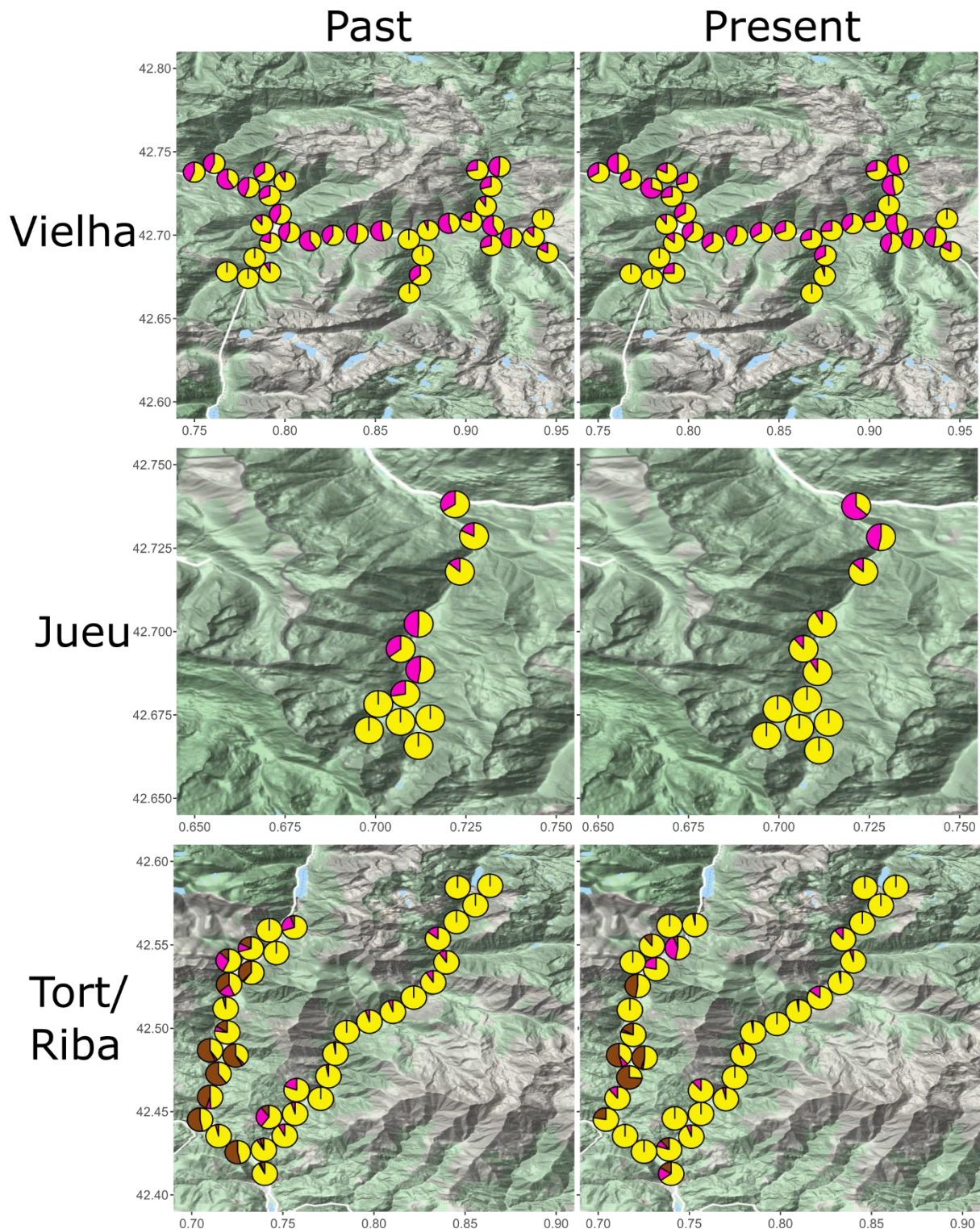


Figure 4.2. Past and present distribution of yellow, pink and brown shell morphs in Pyrenean valleys, based on sampling in the 1960s (Cameron et al., 1973, Arnold, 1968) and 2017/18. Pie charts show frequencies of yellow (yellow), pink (pink) and brown (brown) morphs in each location. Valle Noguera de Tort is the left valley and Valle Noguera Ribagorzana is the right valley.

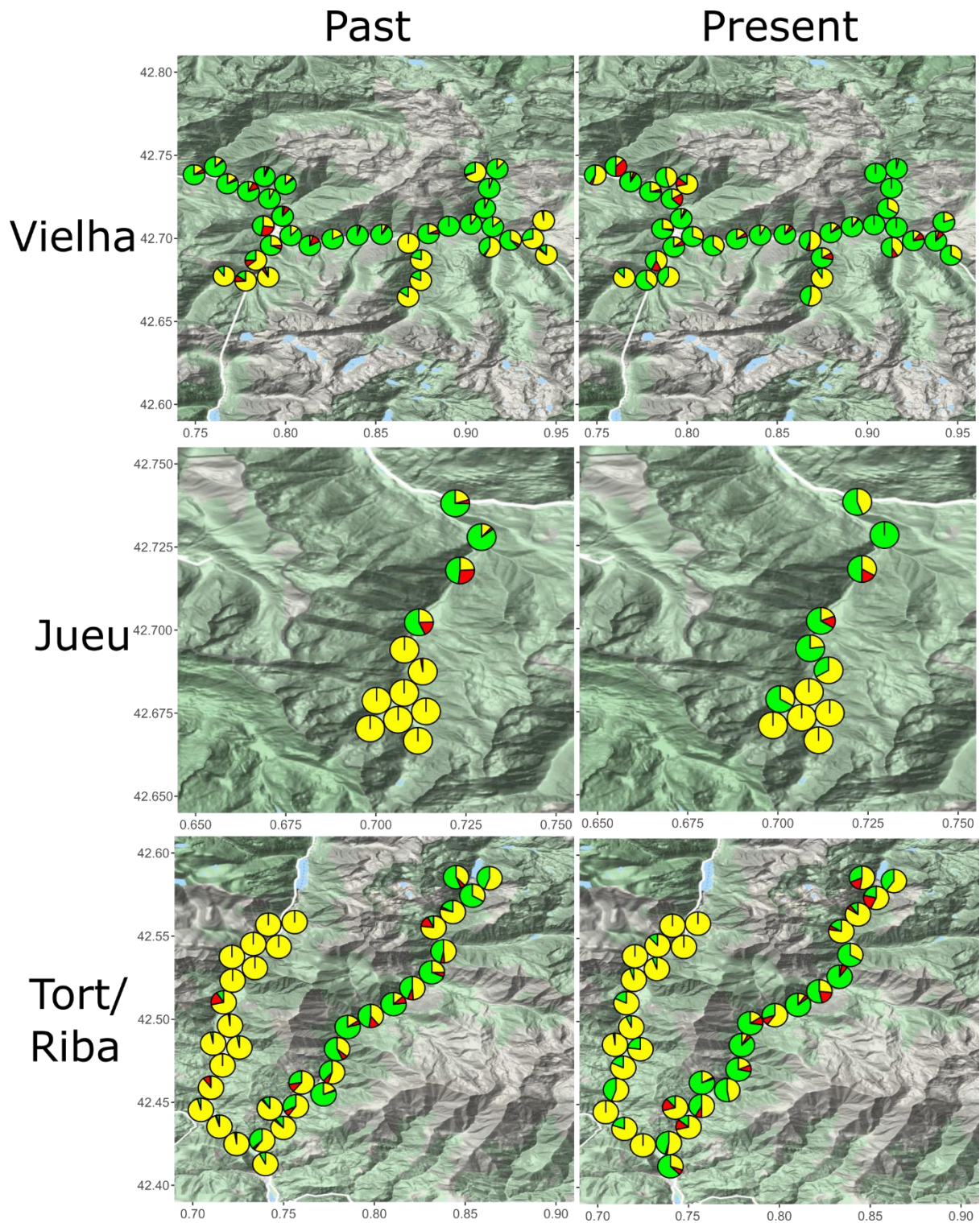


Figure 4.3. Past and present distribution of banded, mid-banded and unbanded shell morphs in four Pyrenean valleys, based on sampling in the 1960s (Cameron et al., 1973, Arnold, 1968) and 2017/18. Pie charts show frequencies of banded (green), mid-banded (red) and unbanded (yellow) morphs in each location. Valle Noguera de Tort is the left valley and Valle Noguera Ribagorzana is the right valley.

Spatial patterns of variation in morph frequencies were largely the same as recorded in the past, including colour and banding (Figures 4.2, 4.3) as well as lip-colour (Figure S4.1). To formally test this, directional changes in the mean frequencies of shell types at each location between the 1960s and the present-day were tested using independent paired T-student or paired rank Wilcoxon tests (Table 4.2; Table S4.3). This confirmed little overall change in the distribution of the main colour and banding types in Vielha, Jueu, and Tort (Table 4.2; Table S4.3; and Figure 4.4). The exception was in Ribagorzana valley, where the proportion of banded shells has risen from ~3% to 14%, with substantially fewer brown shells recorded and more yellow shells (Table 4.2).

Table 4.2. Statistical summary of shell geographical distribution in each valley; independent paired comparison (Student's t-test (parametric), Wilcoxon signed-rank test (non-parametric)).

	Vielha				Jueu			
	Mean	S.E.	Mean % change	P-value	Mean	S.E.	Mean % change	P-value
Present (2017/2018)								
Yellow	70.9	3.1	0.4	0.933	87.1	6.1	5.8	0.427
Pink	29.0	3.1	0.3	0.923	12.4	5.9	-6.3	0.379
Brown								
Unbanded	27.0	4.0	-8.7	0.110	59.9	11.1	-13.2	0.152
Mid-banded	5.2	1.3	1.5	0.327	2.6	1.8	-2.1	0.059
Banded	67.8	4.1	8.5	0.140	37.5	10.6	15.4	0.094
Past (1962/1969)								
Yellow	70.5	3.8			81.3	5.6		
Pink	29.3	3.7			18.7	5.6		
Brown								
Unbanded	35.7	5.7			73.2	11.3		
Mid-banded	3.7	0.9			4.7	2.6		
Banded	59.3	5.7			22.1	9.8		
	Riba				Tort			
	Mean	S.E.	Mean % change	P-value	Mean	S.E.	Mean % change	P-value
Present (2017/2018)								
Yellow	75.9	5.4	10.4	0.061	94.6	1.5	1.5	0.541
Pink	9.0	3.2	-1.0	0.752	3.9	1.1	-2.3	0.204
Brown	15.4	5.2	-8.8*	0.049	1.4	1.0	0.6	0.570
Unbanded	85.7**	4.2	-9.6**	0.008	42.9	5.9	-6.6	0.239
Mid-banded	0.4	0.4	-1.2	0.328	8.4	1.5	2.5	0.141
Banded	13.9**	3.9	10.8**	0.007	48.7	6.3	4.1	0.499
Past (1962/1969)								
Yellow	65.5	5.7			93.0	1.4		
Pink	10.0	2.5			6.1	1.4		
Brown	24.2	5.8			0.8	0.0		
Unbanded	95.3**	1.7			49.4	5.4		
Mid-banded	1.5	1.2			6.0	1.1		
Banded	3.2**	0.7			44.6	5.6		

*p < 0.05. **p < 0.01. ***p < 0.001

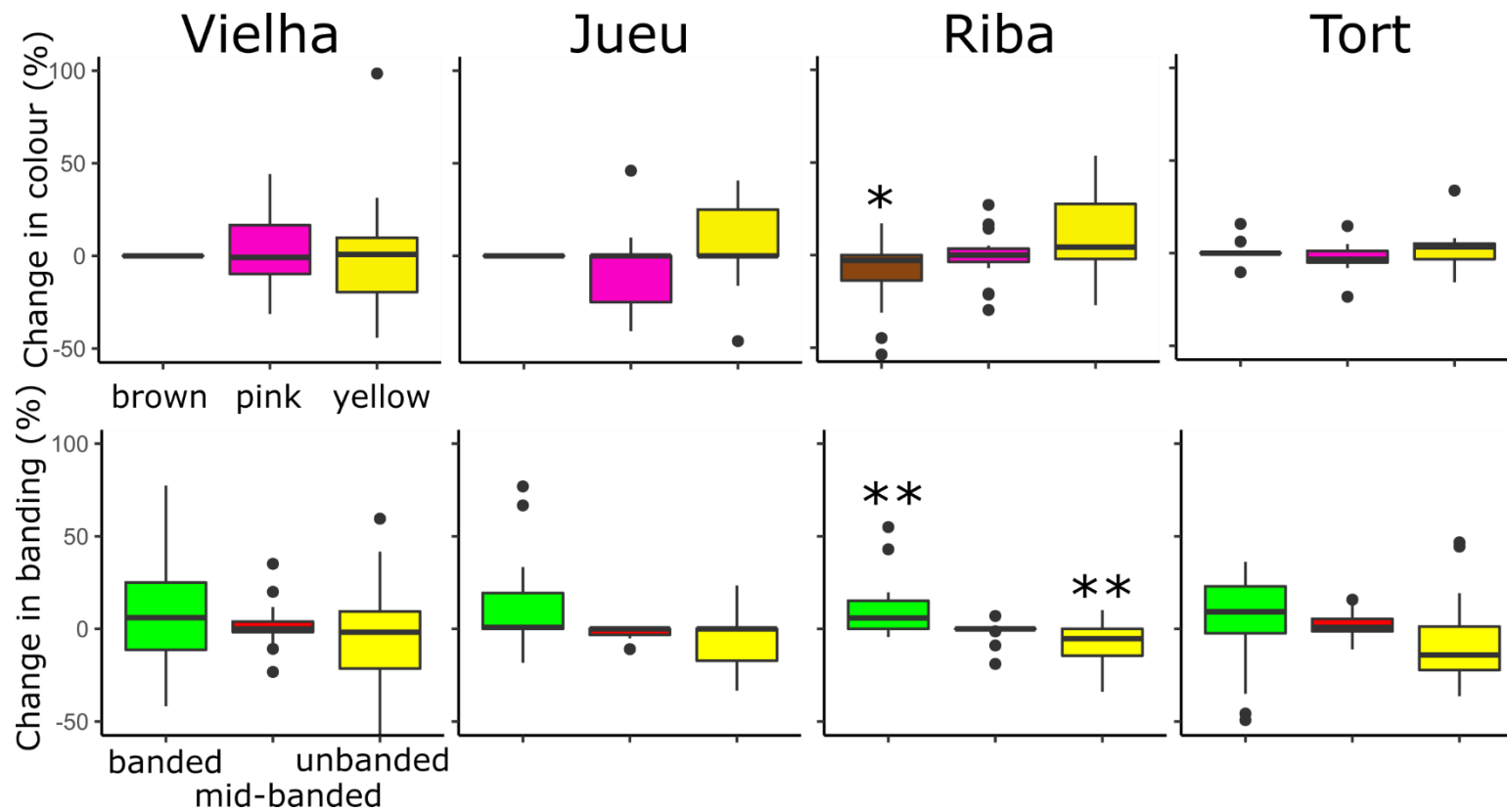


Figure 4.4. Comparison of changes in frequency of colour and banding types between paired sites (same location, or within 50 m) in four Pyrenean valleys over five decades, tested using paired T-test or Wilcoxon signed-rank test. Ribagorzana is the only valley that showed significant changes in colour and banding distribution, with the frequency of brown ($p < 0.05$) and unbanded ($p < 0.01$) shells decreasing, and with the proportion of banded shells increasing ($p < 0.01$).

The present-day relationship between altitude and frequency of colour and banding morphs was plotted (Figure 4.5). Jueu and Tort valleys showed a significant positive correlation between altitude and the frequency of yellows, with the former also showing a positive significant altitude-unbanded association (Figure 4.5; Table S4). As expected, pink and banded shells showed the reverse trend, but with non-significant altitudinal correlations; mid-banded shells did not show any correlation with altitudes. Tort showed a significant positive (but shallow) relationship between yellow-altitude and banded-altitude (Table S4.4, Figure 4.5, $r = 0.27, 0.34$ respectively and $p < 0.05$). There was also significant positive association of the white-lip morph with altitude in three valleys (Figure S4.2), in addition to associations of higher altitude with larger shell size ($H + W$), and relatively tall spires (H/W) (Figure S4.3).

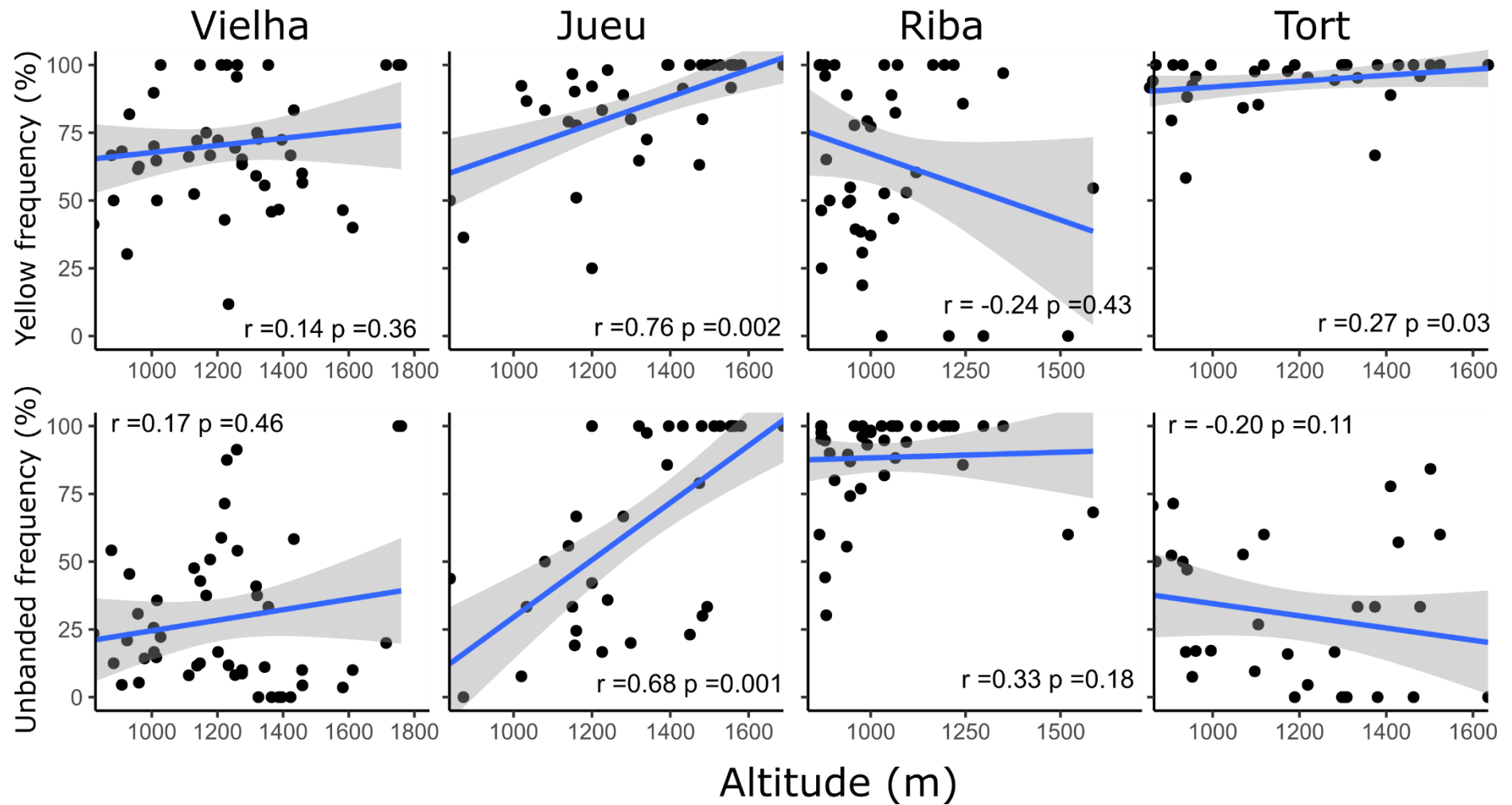


Figure 4.5. Scatterplots showing the present-day relationship between altitude and frequency of yellow and unbanded morphs in four Pyrenean valleys. Points represent collections of shells from the same location ($n \geq 10$). Only samples from Jueu show a significant strong positive relationship between altitude and frequency of yellow and unbanded shells; samples from Tort showed a shallow but significant association for altitude and yellow. Regression line and confidence intervals are shown, alongside the Pearson coefficient and p value.

Fishers' Z-transformation was used to test the significance of the difference between the past and present altitudinal correlation coefficients. There were no significant changes in Jueu, Ribagorzana and Tort (Table 4.3). In comparison, in the past sample from Vielha valley, both colour (Table S4.4, yellow shells $r = 0.48$, $p < 0.001$) and banding (Table S4.4, unbanded shells, $r = 0.51$ and banded shells, $r = -0.48$, $p < 0.001$) showed a moderate association with altitude. In the present-day, colour and banding did not show a significant correlation with altitude.

Table 4.3. Fisher r-to-z transformation, significance of the difference between two correlation coefficients

Past vs Present	Vielha		Jueu		Riba		Tort	
	Z-Value	P-Value	Z-Value	P-Value	Z-Value	P-Value	Z-Value	P-Value
Yellow	2.120*	0.017	-1.460	0.072	-0.310	0.378	0.270	0.394
Unbanded	2.210*	0.014	1.510	0.066	-0.310	0.378	0.140	0.444
Banded	-3.16***	0.001	-1.180	0.119	1.120	0.131	-0.590	0.278
Yellow sets								
Yellow subset	3.31***	0.001	-0.740	0.230				
Yellow dataset-subset	0.980	0.164	0.420	0.337				

* $p < 0.05$. ** $p < 0.01$. *** $p < 0.001$

Unfortunately, it was not possible to make the same comparisons with lip-colour and shell measurements, because the former data was not uploaded to the Evolution Megalab database, and the size measures were not recorded in the original studies.

4.3.2. Quantitative measures of shell colour and banding and associations with altitude

The reflectance spectra of 813 shells from Vielha and Jueu valleys was measured, a subset of the total collected (2633; Table 4.1), because some shells were too damaged to record quantitative colour. Colour spectra were transformed into human visual coordinates (CIE 1931 human colour standards) and principal component analysis was performed to linearize the uncorrelated values of the visual coordinates. A PCA on the xyz coordinates showed three axes which together explained 99% of the chromatic variation, PC1 51%, PC2 44%, and PC3 4%. As previously reported (Davison et al., 2019a), the third axis, PC3, tended to separate pink and yellow shells (Figure S4.4). Therefore, to visualize the present-day relationship between altitude and quantitative chromatic variation, PC3 was used because all the individuals in

Vielha and Jueu were yellow or pink (Figure 4.6). The graph shows PC3 results of each shell distributed in Vielha and Jueu altitudinal range. Each individual is coloured by its observed colour scored by myself. In Vielha, there was weak negative association of altitude and PC3, whereas Jueu showed a moderate positive correlation. These indicates that in Vielha there was no association of shell colour with altitude, whereas in Jueu yellow shells were more common at high altitude.

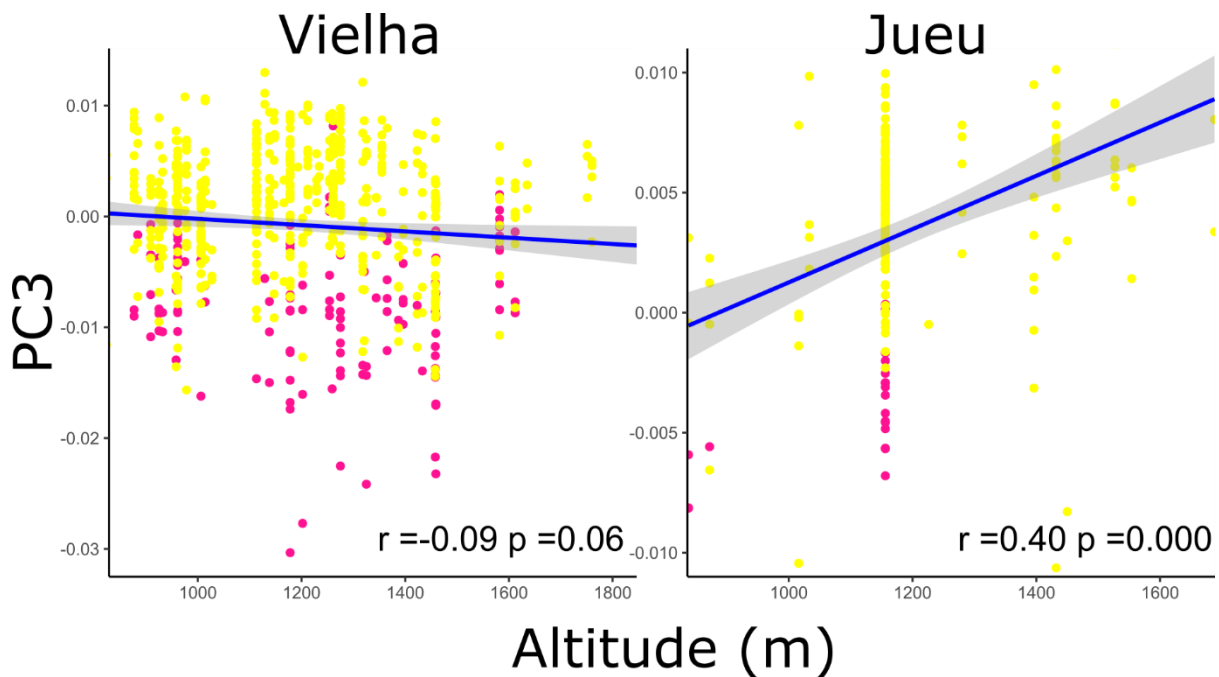


Figure 4.6. Scatterplots showing the relationship between altitude and chromatic variation (PC3) for individual shells from Vielha and Jueu valleys. Points represent individual shells, colour coded according to human-scored colours. There is a strong positive association of PC3 with altitude in shells from Jueu, and a weak but non-significant negative association in shells from Vielha. Regression line and confidence intervals are shown, alongside the Pearson coefficient and p value.

4.3.3. Past and present-day associations, using qualitative and quantitative methods

We compared altitude-colour associations between historical and present-day samples from Vielha and Jueu. While the past data was analysed using just the qualitative method, the present data was analysed following both methods above mentioned.

For Jueu valley (Figure 4.7), the same significant altitudinal associations were recovered whether using historical data ($n = 1862$), the present-day data with human-scoring of colour ($n = 637$), or quantitative measures of colour or pattern as manual scoring ($n = 206$; Figure 4.7). Fishers' Z-transformation test showed no significant changes among the altitudinal correlations for each of these four graphs (Table 4.3).

For Vielha valley (Figure 4.7), there was a significant altitudinal association with colour only in the historical dataset ($n = 4756$, $r = 0.48$, $p = 0.0001$), compared with a non-significant positive relationship using the present-day data with human-scored colour ($n = 942$, $r = 0.14$, $p = 0.355$), and a non-significant negative relationship using quantitative measures of colour ($n = 607$, $r = -0.09$, $p = 0.056$). To further explore these differences, we also tested for a correlation using the present-day data with human-scored colour, but just using the subset of shells, which were considered sufficiently undamaged for spectrophotometry (Figure 4.7 inset graph). This showed a negative relationship ($r = -0.08$, $p = 0.588$), likely indicating that some (old) pink shells were mistakenly scored as yellow in the qualitative analysis.

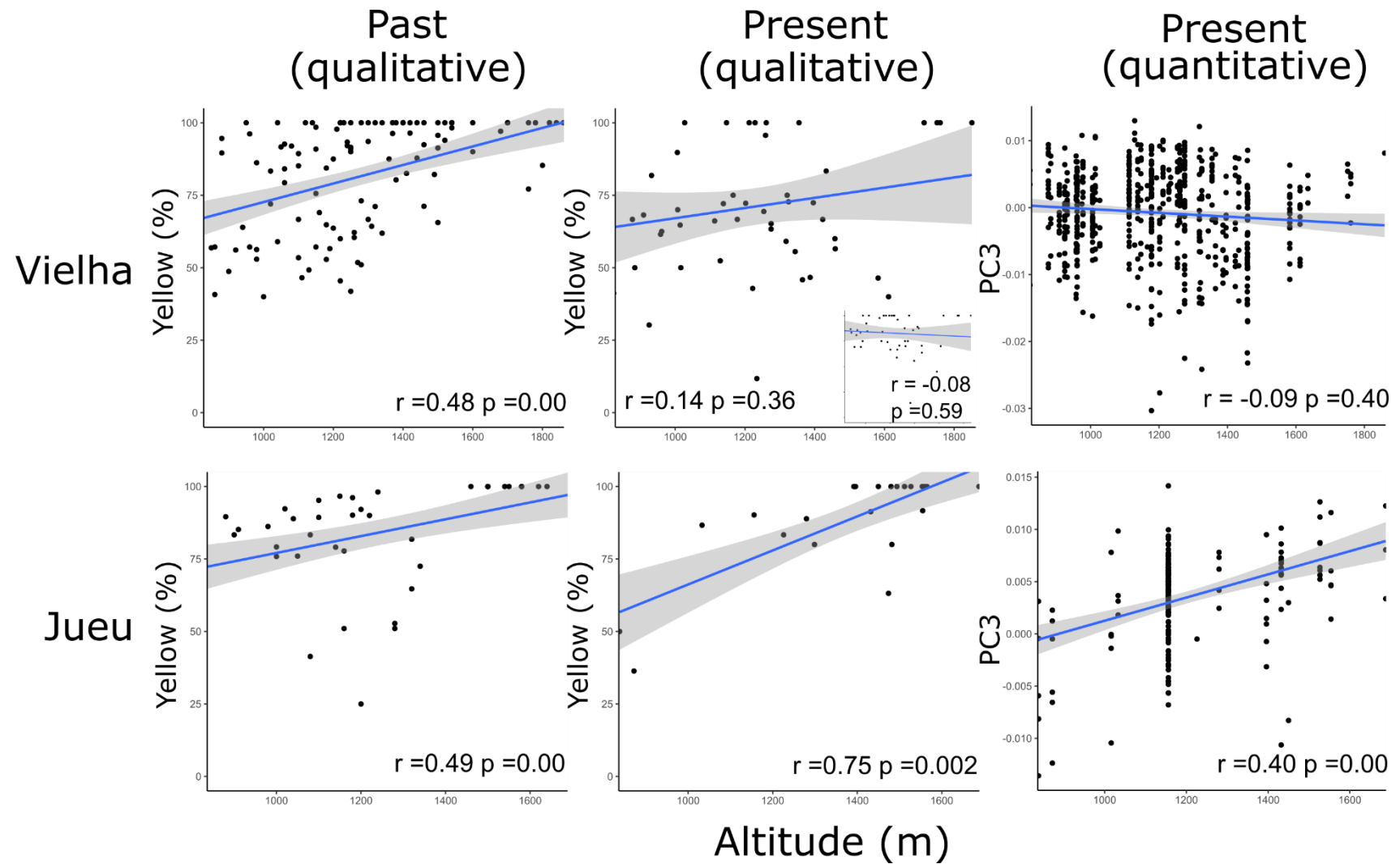


Figure 4.7. Summary figure showing the relationship between altitude and colour variation for shells from Vielha and Jueu valleys, comparing past and present-day collections, and using qualitative or quantitative methods to score colour. The small inset graph shows the same data, but only using the subset of shells that were considered sufficiently undamaged for spectrophotometry.

4.4. Discussion

4.4.1. Quantitative versus qualitative methods to score shell phenotype

In prior studies, the shell ground colour was scored by eye, sorting individuals into three discrete categories, either yellow, pink or brown. In this study, in addition to the human-scoring of shell colour, we evaluated a quantitative method, based on spectrophotometry in the laboratory, by comparing patterns of *C. nemoralis* shell colour polymorphism from the past and the present day. The main finding was that while spectrophotometry of shell colour has the benefit of being quantitative and is objective, the same trends were recovered. In fact, there was a remarkable stability in the local shell patterns in most valleys over five decades.

Both qualitative and quantitative methods have benefits and also disadvantages. Spectrophotometry produces a quantitative output for an individual shell, which better reflects the non-discrete nature of variation in snail shell colour, and is reproducible. However, it is only accessible to a few persons, requires expensive equipment, and ideally, that the reflectance measures are taken in the laboratory. All of these latter factors together reduce throughput. In comparison, field-based methods do not require the snails to be taken to a laboratory, are rapid and accessible to a wide range of persons, including citizen scientists. The disadvantage is that the shell colour phenotype must be binned into one of three subjective categories, with the snails from a sometimes ill-defined single location making a single data point. Moreover, the data that is collected must be carefully filtered (Silvertown et al., 2011) to remove misidentified species (especially confusion with *C. hortensis*, juvenile *Cornu aspersum* and *Arianta arbustorum*), a difficult task because the specimen is not preserved. Nonetheless, human-scoring of snail colour data remains valuable, especially with appropriate training.

In the future, we anticipate that a model that takes the best of both methods may be used instead. Websites and apps such as SnailSnap, iNaturalist and iRecord (Harvey, 2018; Horn et al., 2018; Kerstes et al., 2019) are already being used extensively by the general public to capture records and images of snails, which are

then identified using a combination of machine-learning methods and input from persons with various degrees of expertise. For example, iNaturalist has over 9000 observations, including photos, of *C. nemoralis* at “research grade” quality (including >1000 in the UK, but only 29 in the Pyrenean region). One suggestion is that it would be relatively straightforward to extend the use of a machine-learning based method to inspect individual images, and then record the colour and the band category. A more sophisticated (but difficult to implement) alternative would be to extract quantitative colour data from the images, but this would have to be robust to the wide variety of circumstances under which the photos were taken; likely including some sort of colour control (e.g. a card; van den Berg et al., 2020) would limit the number of participants.

4.4.2. Past and present-day geographic distribution of colour and banding morphs

By analysing the geographical and altitudinal distribution of colour and banding attributes in the Central Pyrenees and comparing with previous studies, we aimed to understand how local factors, human impact and rapid climate change acted upon the variation of *C. nemoralis* shell polymorphism.

Broadly, we found a remarkable stability in the local shell patterns in most valleys over five decades, despite large changes in habitat, human impact and rapid climate changes over five decades. Most valleys still showed visibly similar patterns of shell types, whether colour, banding, lip colour or shell-shape (Figures 4.2, 4.3, S4.1), concordant with another study over the wider Pyrenean region (Ellis, 2004). One possible explanation on the maintenance of the Pyrenean patterns may be predation, which can be significantly important in the maintenance of the differences of neighbouring morph frequencies under both, positive and negative frequency-dependent selection (Holmes et al., 2017).

There were just a few exceptions to the general pattern. For instance, the altitudinal cline in the frequency of yellows that was present in both Vielha and Jueu valleys is now only present in the latter valley (Figure 4.7). The present-day absence of a clinal relationship is striking, and contrasts with the paired comparisons at each location, which did not show any overall change in the frequency of yellow or pink in

Vielha over the decades (Figure 4.4). The explanation for the discrepancy (Table S4.3) is that while pinks have increased in frequency at higher altitudes in Vielha, they have also decreased in frequency at lower altitudes. Vielha is interesting because the establishment of Baqueira-Beret ski resort (now the largest in Spain) has led to an increase of human activity and the construction of infrastructure such as dams, tunnels or mines, with a corresponding growth of urban areas in the adjoining tributary valleys. In comparison, the Jueu valley has remained largely intact, perhaps because it is a protected reserve. The loss of altitudinal-colour variation in this valley is therefore likely explained by the accidental movement of individuals and changing local habitat.

The only other location that showed change was in the Ribagorzana valley, where the proportion of banded shells has risen from ~3% to 14%, with substantially fewer brown shells recorded and more yellow shells. The explanation for changes in this valley are less clear. One possibility is that we were more likely to score an intermediate shell as pink rather than brown compared with previous workers. However, this can probably be discounted because an increased proportion of yellow rather than pink shells matches the lower proportion of recorded brown shells in our samples from Ribagorzana. The general finding of reduced browns is perhaps in line with other studies. Cowie and Jones (1998) and Cook et al. (1999) documented an overall decrease in the frequency of the brown shells, Özgo and Schilthuizen (2012) identified that brown shells decreased at the expenses of yellow shells, Cameron et al. (2013) reported a general increase of yellows and Cook (2014) found an increase of yellows in woodland habitats. All this findings probably agreed with the increase of temperatures due to climate change (Cameron et al., 2013).

4.4.3. From phenotype to genotype

One limitation of comparative studies on *Cepaea* is that there is a risk that we ascribe “just-so” explanations to changes in the frequencies of a particular phenotype over time. This is particularly the case when changes are relatively local, rather than at European scale or on how well documented selection or other mechanisms can be. For example, in this study, we have concluded that the changes that we observed in Vielha valley are due to immigration of new individuals (because of construction), but of course it is not possible to discount natural selection, especially because of changed

habitat associated with the construction industry. The corollary is that we also lack understanding or explanation for circumstances when phenotype frequencies remain stable. This may be solved with manipulative experiments.

Recent progress in genomic technologies will certainly offer a solution, including the availability of a first draft of *C. nemoralis* genome (Saenko et al., 2020). For example, it should be possible to use genomics to understand the relative roles of migration/founder effect and selection in determining the population structure of *Cepaea* populations. In particular, genomics may be used to understand the history of a population e.g. is there evidence for recent immigration to the high altitude regions of the Vielha valley, from snails that perhaps originate from elsewhere? Alternatively, is there evidence for a selective sweep at the loci that control the shell phenotype, perhaps indicative of a local response to a change in the selective regime?

Some of the other remaining issues, that we have only touched upon here, are the correlations between altitude and multiple phenotypic traits (banding, colour, lip colour, size, shape), as well as both linkage and linkage disequilibrium between the genes involved (Cook, 2013; Gonzalez et al., 2019). Given that lip colour is ordinarily a dark colour in *C. nemoralis* across most of Europe (with some exceptions), and that this is the main character that distinguishes this species from *C. hortensis*, the wide variation in this character in the Pyrenees is particularly mysterious. In the future, we hope to understand the genetic basis for these characters; it is hoped that this will bring forth an era in which we are better able to understand the impact of the multiple factors (Jones et al., 1977), including natural selection and random genetic drift, that determine the patterns of shell types that we see in nature.

4.4.4. Conclusions

The main finding was that while quantitative measures of shell colour reduced the possibility of error, and standardised the procedure, the same altitudinal trends were recovered, irrespective of the method. There was a remarkable stability in the local shell patterns over five decades with not enough evidences to give an explanation. Furthermore, little changes in the phenotype frequencies were found and possible conclusions were made rising the risk of giving “just-so” assumptions, which may not

cover the entire picture. Overall, while there are key benefits in taking quantitative measures of colour in the laboratory, there are also several practical disadvantages. In the future, with the increasing use of digital cameras to capture and record species presence, there is the potential that colour and banding data may be extracted from the images uploaded to public databases and apps such as iRecord, iNaturalist and SnailSnap (Harvey, 2018; Horn et al., 2018; Kerstes et al., 2019). For the moment, the fact remains that human-scoring of snail colour data is valuable, especially with appropriate training.

4.5. Acknowledgments

This work was supported by the University of Nottingham; the Biotechnology and Biological Sciences Research Council [grant number BB/M008770/1], via a studentship to Daniel Ramos Gonzalez. Thanks to Hannah Jackson and Alejandro Garcia Alvarez for helping in the sampling collection in the Pyrenees; to Jonathan Silvertown and the Evolution Megalab team who provided the historical data used in this research, and to Sophie Poole who helped with some of the shell colour measurements.

Chapter 5:

A new *C. nemoralis* recognition and shell morph classification system using deep learning

Abstract

The classification of colour is a subjective matter when it comes to the perception of the human eye. Colour is continuous and the description of discrete colours may differ depending on the viewer. Thus, an objective and standardised method is needed. In this work, we used *Cepaea nemoralis* shell colour polymorphism, spectrophotometry and deep neural networks to generate a visual recognition system. Firstly, colour was quantified by extracting the spectra of 94 shells. Then, 1408 pictures were taken to train the Region-based Fully Convolutional Networks (R-FCN), 101 pictures collected from the iNaturalist database (<https://www.inaturalist.org/>; Horn et al., 2018) to validate the algorithm, and an extra 1400 images to test it. The results illustrate that this method can achieve high levels of detection of snail shells, and further, classify the individuals into the right colour and banding morph. However, this method needs to be improved and challenge artificial intelligence of finding visual hidden patterns to differentiate close related species with no clear phenotype differences for the human eye. This work may facilitate future colour polymorphism studies and it shows potential room for development.

5.1. Introduction

Throughout the past century, the need of a new visual recognition system to aid studies of colour polymorphism and investigate the maintenance of colour polymorphism has grown in the field of evolutionary biology (Cameron et al., 2012; Cook, 2017; Silvertown et al., 2011). There are issues in the identification of colour polymorphism such as recognising the discrete colour in phenotypes at the boundary of two different discrete colours, complex backgrounds or lighting and the challenges of human perception (Davison et al., 2019a). Thus, the generation of a system, which classifies colour morphs may help researchers to speed up accurately the ongoing and long term studies. Thus, the application of deep neural network models of detection and classification may facilitate, cheapen and optimise ecological studies.

Easy morph scoring, collection, and diverse habitats and locations made the siblings *Cepaea nemoralis* and *Cepaea hortensis* an important model to study the colour polymorphism (Cain et al., 1950, 1952, 1954; Jones et al., 1977; Lamotte, 1952). Shell polymorphism in those named species illustrated a simple Mendelian inheritance at one major locus (Cook, 1967; Jones et al., 1977). Shell colour and banding were recorded by observation. Whereas, banding, in more of the case is straightforward (although in some individuals can be difficult due to banding pigmentation, etc.), simply counting band presence, colour is a subjective and variable aspect. *C. nemoralis* shell ground-colour polymorphism is classified, traditionally, in one of the three more discrete colours (Cain et al., 1954), yellow, pink or brown. Past research found that when crossing *C. nemoralis* snails, its offspring followed the Mendelian laws, generally describing the three main discrete colours (Cain et al., 1960; Cain Arthur James 1968; Jones et al., 1977).

In the past, research on colour polymorphism and generation of databases was undertaken by using the human perception, found for example, in projects using citizen science such as “Evolution Megalab” or the phone app in Kerstes et al. 2019 (Kerstes et al., 2019; Silvertown et al., 2011). On one hand, Evolution Megalab digitised a large set of 20th century samples with the objective to help to survey shell polymorphism in *C. nemoralis* and *C. hortensis*. In this case, users reported their personal collections

summary in its website (Cameron et al., 2012; Silvertown et al., 2011). On the other hand, Kerstes et al. (2019) used citizen science to monitor colour shell phenotype changes in the “urban heat island”, which refer to human settlements. Citizens were asked to take and upload of a single snail picture each time into an app. The phone app recorded the location, and sent the photograph to a database where 10 specialists recognised and scored snails in each picture (Kerstes et al., 2019). Even though, human criteria can be trained, it is still subjective and not quantitative.

Colour standardization by using quantitative analyses of pigmentation has started to be applied in research (Corl et al., 2018; Davison et al., 2019a; Huber et al., 2015; Jones et al., 2012). For example, *C. nemoralis* shell colour morphs were determined from a few snails to test crypsis in different heterogeneous backgrounds (Surmacki et al., 2013). Moreover, in Davison et al. (2019a), a psychophysical model of bird perception of colour vision was used to characterise chromatic variation from spectrophotometry measurements into 1172 shells all collected across Europe. Avian visual perception was used due to its relationship with *C. nemoralis* as one of the main predators. Further, Davison et al. (2019a) opened the possibility of clustering shells into the three traditional colours using Gaussian finite mixture modelling (Davison et al., 2019a; Scrucca et al., 2016).

As an alternative to the large-scale surveys, scientists may apply deep learning algorithms to combine quantitative methods with a quick and cheap collection and classification (Angermueller et al., 2016; Webb, 2018). Deep learning is a branch of computer science in which its algorithms takes a huge amount of annotated raw data such as images or genomes to find hidden patterns (Webb, 2018). Thereafter, the trained algorithms can be used to analyse and make predictions to other data. Deep learning is preferred in biology over machine learning algorithms because it does not need to use human intervention. This is due to the use of multilevel layers in deep neural networks avoiding the need of structured and tagged data (Angermueller et al., 2016; Webb, 2018).

Deep learning algorithms are used in biology mainly to analyse remarkably large datasets of images or genomes (Webb, 2018). Once the deep neural network is trained, new data can be analysed automatically from a broad range of sources. For

example, deep learning is used in medicine image recognition, which can identify, quantify and localise trained targets from photographic datasets (Ren et al., 2015; Schneider et al., 2018). In particular, deep-learning can be found in research such as microscopy image processing to detect variations in the cell density, colour and shape in sample preparations allowing the recognition of particular cells or organism like parasites in blood or cancer cells (Du et al., 2019; Zhang et al., 2016). In another example, artificial intelligence can be used in mass spectrometry to approach challenges like off-sample products caused by sample preparation (Ovchinnikova et al., 2020).

Artificial intelligence is also introduced and used in the field of evolutionary biology and ecology. As an illustration, in evolutionary biology, deep learning can help to solve population genetic problems. For example, it can reconstruct effective population size histories by creating deep neural networks using single nucleotide polymorphic sites (SNPs), like in the case of cattle breed populations (Sanchez et al., 2020), or applying deep learning algorithms such as convolutional neural networks into the detection, identification and evaluation of natural selection in population genomic data (Torada et al., 2019). On the other hand, in recent evolutionary ecology research, deep learning algorithms were generally used to recognise and classify species from footage or picture datasets. For example, in the creation of an Android phone application using deep learning to recognise and classify species like *Paphiopedilum* Orchid (Arwatchananukul et al., 2020). Besides, it was also used to accelerate and enhance the process of extracting information from extremely large datasets by using computer visual models in the identification and recognition of European wild mammal species (Carl et al., 2020). In addition, this technology was employed in the ambitious and promising citizen science project, “iNaturalist Species Classification and Detection Dataset” which utilised pictures from across the world to observe, collect and classify species into categories by applying deep neural networks (Horn et al., 2018). For example, a recent study targeted three spatial scales enhance long-term and geographical range of surveys in the Great Lakes area of North America using records of iNaturalist (Lehtinen et al., 2020).

In this instance, this research examines the emerging role of deep learning to detect *C. nemoralis* from pictures, and classify them according to their shell colour

(standardised colour by spectrophotometry) and banding. With this method, I avoid factors that appear to influence the spatiotemporal variability in *C. nemoralis* shell colour such as human individual perception or lighting. Moreover, I aimed to create a deep neural network based on *C. nemoralis* dataset that will reduce time-consuming in the manual scoring. Furthermore, the records can be stored automatically and the colour can be quantified at any time for further long-term research. Finally, it is quick, accessible to the public and cheap to use. The novel method should make an important contribution to the field of understanding the maintenance of the colour phenotype of *C. nemoralis* and the natural factors acting upon it, as the strategy followed by this method is to classify by their respective phenotype and not just the species.

5.2. Materials and methods

5.2.1. Image datasets

C. nemoralis shell photos were taken by myself between 2019 and 2020. Three different datasets were generated, training, validation and test (Table 5.1). The training dataset was used to train the deep neural network. Consequently, the algorithm will examine all the training dataset pictures acquiring parameters and labelling each type. Then, the validation dataset will evaluate the model after the training and tuning the hyper-parameters and data preparation to re-do the process. This procedure will go repeatedly until the evaluation with the validation dataset reach high accuracy values. Therefore, the model will be in contact with the validation dataset during the training procedure, but not be trained from it. Finally, the test dataset is an unbiased assessment of a final model fit on the training dataset. Therefore, the shells selected for the test dataset were not employed in the training procedure.

Shells were first classified by colour and banding, as described previously (Davison et al., 2019a) in Chapter 4. Briefly, colour was measured by spectrophotometry in shells used in training and test dataset. Ocean Optics spectrometer (model USB2000+UV-VIS-ES) and a Xenon light source (DT-MINI-2-GS UV-VIS-NIR) were used to extract the spectra and human trichromatic colour coordinates x, y and z (2-CIE, International Commission on Illumination) were generated using Pavo R package 2.2.0 (Davison et al., 2019a; Maia et al., 2018; Smith et al., 1931).

Shells were first categorised in yellow unbanded (YO), yellow mid-banded (YM), yellow banded (all banding options excluding mid-banded, YB), pink unbanded (PO), pink mid-banded (PM), pink banded (all banding options excluding mid-banded, PB), brown unbanded (BO) and brown mid-banded (BM) (Table 5.1 and Figure S5.1). All the images of the training and test dataset were taken by myself. In total 59 shells were chosen for the training dataset (10 YO, 6 YM, 15 YB, 8 PO, 4 PM, 6 PB, and 10 BO). Validation dataset included 101 pictures, which were extracted from the iNaturalist database (<https://www.inaturalist.org/>; Horn et al., 2018). Only no copyright

photos were used. iNaturalist dataset were assess by DRG, after training and discussing with AD. A total of 35 shells from the datasets used in chapter 3 and 4 were selected randomly. 5 different shells for each class except brown mid-banded due to lack of individuals, were used in the test dataset (Table 5.1).

The training and validation datasets showed multiple shells per picture. To calculate accuracy (precision and sensitivity statistics), individual shell pictures were required. Therefore, the test dataset illustrated only one shell per photo. In addition, seven different *C. nemoralis* common habitats (grassland, woodland, scree, stone wall, hedgerow area, sand-mud land and road) and blank background were selected as a picture background. Some samples of the snail dataset are illustrated in the additional information (Figure S5.1).

Table 5.1. Summary of the picture datasets (training, validation and test), bounding box (morph classification) and background

Training (1408 pictures)	General	Blank	Grassland	Hedgerow	Road	Sandland	Scree	Woodland	Wall
Yellow unbanded	312	36	53	27	18	90	6	37	45
Yellow mid-banded	192	19	58	6	4	38	9	36	22
Yellow Banded	517	79	115	49	18	148	15	30	63
Pink unbanded	272	10	62	23	14	65	18	26	54
Pink mid-banded	210	16	44	13	17	40	12	48	20
Pink Banded	157	21	26	31	4	45	0	15	15
Brown unbanded	402	37	92	47	20	83	14	35	74
Brown mid-banded	6	0	0	0	1	0	0	5	0
Total	2068	218	450	196	96	509	74	232	293

Validation (101 pictures)	General	Blank	Grassland	Hedgerow	Road	Sandland	Scree	Woodland	Wall
Yellow unbanded	24	0	7	0	3	4	0	6	4
Yellow mid-banded	12	0	2	1	4	2	0	2	1
Yellow Banded	38	0	7	2	13	1	2	6	7
Pink unbanded	12	0	3	1	2	0	0	2	4
Pink mid-banded	9	0	1	0	3	0	0	5	0
Pink Banded	7	0	1	0	1	3	0	2	0
Brown unbanded	7	0	3	0	2	0	0	2	0
Brown mid-banded	5	0	0	0	0	0	0	5	0
Total	114	0	24	4	28	10	2	30	16

Test (1400 pictures)	General	Blank	Grassland	Hedgerow	Road	Sandland	Scree	Woodland	Wall
Yellow unbanded	200	25	25	25	25	25	25	25	25
Yellow mid-banded	200	25	25	25	25	25	25	25	25
Yellow Banded	200	25	25	25	25	25	25	25	25
Pink unbanded	200	25	25	25	25	25	25	25	25
Pink mid-banded	200	25	25	25	25	25	25	25	25
Pink Banded	200	25	25	25	25	25	25	25	25
Brown unbanded	200	25	25	25	25	25	25	25	25
Total	1400	175							

5.2.2. Training inputs

Pictures were taken randomly in all size ranges. All image sizes were resized by python-resize-image version 1.1.19 (<https://pypi.org/project/python-resize-image/>), in which the script was used to standardise and stretched all input images into the size 800x600 pixels (ratio 4:3). Even though, deep neural networks can obtain inputs from a wide range of size, resizing pictures is a crucial pre-processing step in deep learning due to hardware limitations. The Tensorflow framework trains the deep learning model by batches (Dai et al., 2016), each batch being a sample of the images, and each batch needs to fit in memory. Thus, the resizing step was necessary to make sure that the batches fit in the memory. Moreover, resizing the images also decreases the time needed to train the model, which allowed for testing different parameters and different sets of images. Finally, given the quantity of images used in the training, having distorted or blurred images in the dataset can actually help improve the detection.

To identify the object in a picture to further show it to the deep learning network, imaginary boxes called 'Bounding boxes' were created. Bounding boxes in the semantic segmentation processing were generated by using python package Open CV (Open Source Computer Vision Library) 4.1.2 version (Bradski et al., 2013). Bounding boxes were selected in each image with a total of 8 classes; yellow unbanded, yellow mid-banded, yellow banded, pink unbanded, pink mid-banded, pink banded, brown unbanded and brown mid-banded.

Each snail shell was tightly surrounded by a drawn bounding box. If the shell were occluded, the box was drawn around the visible part (Figure 5.1). Manual filtering after input image processing were made, and deleterious images were removed from the dataset. For image with multiple shells on with multiple class, all of them were boxed up to a limit of 10 (Figure 5.1). Pictures were taken in several backgrounds randomly and from all possible angles and distances. Therefore, small, medium and big bounding boxes were generated.

Bounding box pictures

Entire shell picture

Occluded-blurry picture

Matching background

Multiple bounding box



Figure 5.1. Bounding boxes are shown in the following pictures. First column shows standard picture with the entire shell and lip. Second column illustrates blurry and occluded snail picture with its bounding box. Third column shows matching background picture. Last column display multiple shells in the same picture with its respective bounding boxes.

5.2.3. System overview

Region-based Fully Convolutional Networks (R-FCN) was selected to detect and cluster snail images into its respective morph (Dai et al., 2016) after try other methods like the Fast-CNN (Girshick, 2015). The deep neural network R-FCN is an efficient method to process pictures and to recognise objects. This model was chosen due to its precision identifying objects, the normalization of colour (it converts human colour scales such as RGB or HSI scale into Gray-scale) and because its fully linked-layer net avoids network insensitivity to the target position in the detection and classification. Gray-scale is a shade scale, which gives different values giving 256 possibilities. In artificial intelligence, Gray-scale is used instead of visual colour spaces due to the reduction of dimensions, therefore, less information in each pixel, to avoid complexities and harder-to-process colour images.

The object detection model was based on the Alejandro Garcia Alvarez code source (https://github.com/Raikao/shell_recognition). The image detection framework contained two stages: (i) the proposal stage, which consisted into extracting candidate regions of interest (RoI) from pictures using residual nets, a fully convolutional architecture backbone, and (ii) the classification stage, which the R-FCN model classifies the proposal regions into its class (Dai et al., 2016).

The procedure of the deep neural network (R-FCN) is structured as follows (Dai et al., 2016). Firstly, an input image is presented to the model allowing it to generate a fully convolutional architecture backbone (Figure 5.2). A fully convolutional architecture backbone is referred to the approach where the neural network produces pixel-wise maps in the input images. Secondly, the Region Proposal Network (RPN) proposes RoI candidates classifying these regions by their class and sharing with R-FCN (Figure 5.2). Thirdly, proposed Rols are classified into object categories by the R-FCN architecture. In the last stage, the final convolutional layer generates a deposit of position-sensitive scores (k^2) produced by a spatial grid ($k \times k = 3 \times 3$), which it describes relative positions in the image, encoding the first the top-left, then to top-centre, etc... Finally, the positive position-sensitive Rols were combined producing a final convolutional layer output with each selected Rols (Figure 5.2).

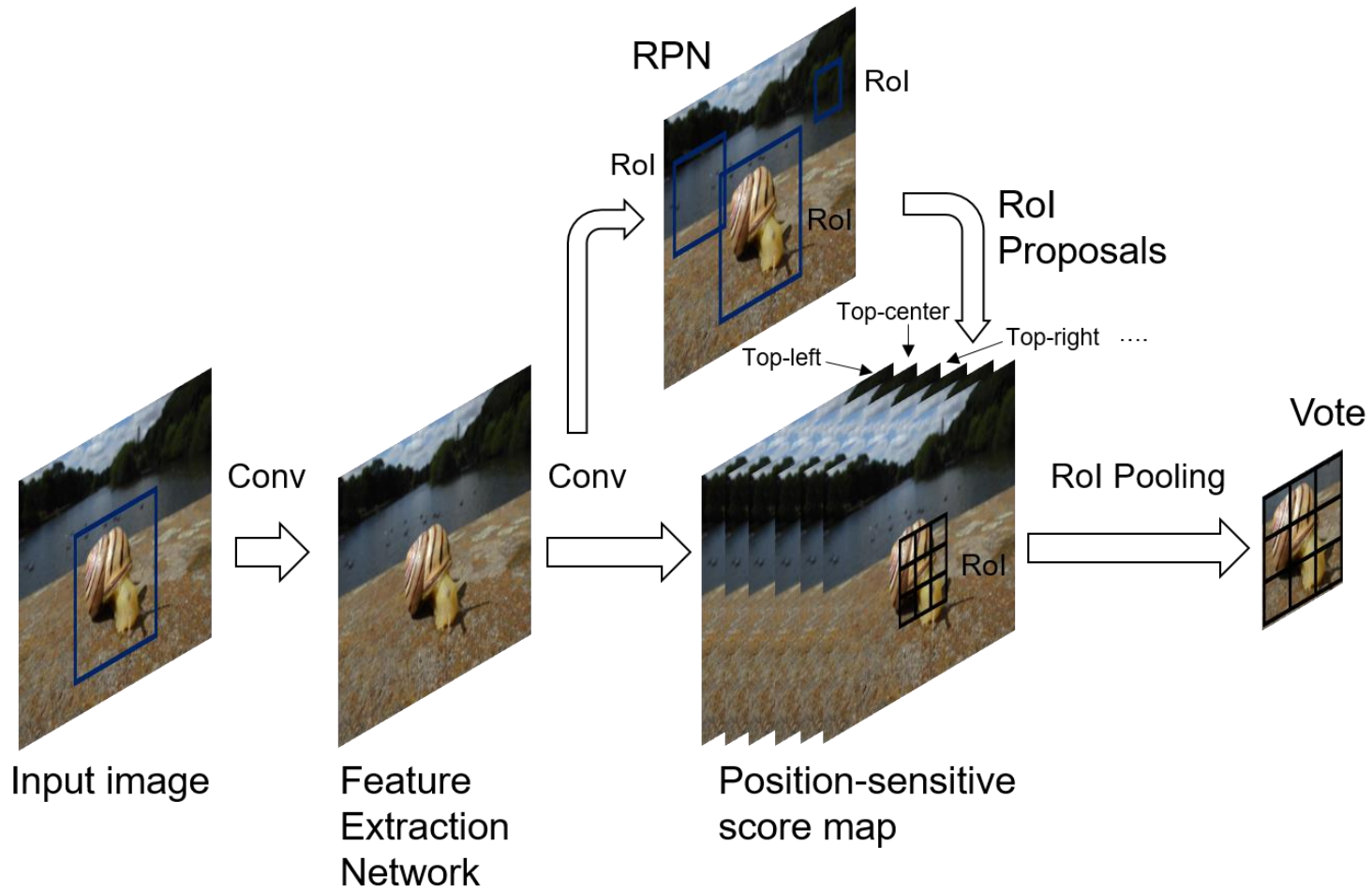


Figure 5.2. General organization of R-FCN. An input image is presented to the model allowing it to generate a fully convolutional architecture backbone. A Region Proposal Network (RPN) (Dai et al., 2016) proposes RoI candidates, which are then used on the position-sensitive score maps. All learnable weight layers are convolutional and are estimated on the whole picture. Finally, the positive position-sensitive Rols were combined producing a final convolutional layer output with each selected Rols.

The deep neural network model was pre-trained with the COCO dataset (a large-scale object detection dataset) to speed up the training process (<https://cocodataset.org/>). The network was trained for 10000 epochs spending 4 hours to train. The training metrics (quantifiable measurements used to track and assess the results of the model) used are illustrated in the additional supporting information (Supporting information S5.1). The convolution network training process used pre-set image inputs (weights and parameters) to optimise and generate the output likelihood for each type. Thus, when a new picture is used as input, the network goes through all the weights and parameters optimised based on the training dataset to detect the object (*C. nemoralis* shell) and output the class probability.

To calculate accuracy; precision, sensitivity (recall) and F1-score were applied (Goutte et al., 2005). Precision ratio showed the correct true positive from all observations in a morph group. Recall statistic illustrated the right observation in each class. Finally, F1 score statistic is a weighted average of both, precision and recall ratios. The three statistic were calculated for validation and test datasets.

5.3 Results

A total of 2909 *C. nemoralis* shell pictures were taken by myself for the training and test datasets. The extra 101 belonging to the validation dataset were extracted from iNaturalist database (<https://www.inaturalist.org/>; Horn et al., 2018). A total of 1408 belong to the training dataset, 101 to the validation dataset and 1400 to the test dataset. The training dataset had 2068 bounding boxes (individuals presence) within all the pictures, which they were divided into 312 yellow unbanded, 192 yellow mid-banded, 517 yellow banded, 272 pink unbanded, 210 pink mid-banded, 157 pink banded, 402 brown unbanded and 6 brown mid-banded (Table 5.1). The validation dataset had 114 bounding boxes split into 24 yellow unbanded, 12 yellow mid-banded, 38 yellow banded, 12 pink unbanded, 9 pink mid-banded, 7 pink banded, 7 brown unbanded and 5 brown mid-banded (Table 5.1). The test dataset had one bounding box for each picture. 25 pictures of each class and each background were taken. Brown mid-banded were not used in the test dataset due to the low number of individuals collected. Thus, 200 photos of each cluster were captured (Table 5.1).

Region-based Fully Convolutional Networks (R-FCN) were used to identify and classify pictures from the validation and test datasets. Predictions are presented in graphs, in which each axis represented pixels. The deep neural network detected, surrounded the object, evaluated and clustered the object using the positive sensitive score mapping illustrating the predicted percentage (Figure 5.3).



Figure 5.3. Prediction result examples of all morphs in different backgrounds with its respective prediction and score. Yellow unbanded (top-left and bottom-middle), yellow mid-banded (middle-top), yellow banded (top-right), pink unbanded (second row–left and bottom-right), pink mid-banded (second row–middle), pink banded (second row–right) and brown unbanded (bottom–left).

C. nemoralis can be found in a wide range of environments, conditions and scenarios. Thus, The deep neural network (R-FCN) was tested in various lighting, shell angles, distances and poses allowing the detection of the shells from blurry pictures, as well as enclosed shells and occluded shells (Figure S5.2). R-FCN also was challenged to characterise shell colour, as it can differ and can be difficult to identify in different backgrounds. Even though, the R-FCN was robust to detect, label and classify, there were three different kinds of prediction failures; (i) shells were classified in the wrong class (ii) shells were predicted in two different groups and (iii) other objects, which were not shells, were labelled as shells and classified in a morph class (Figure 5.4). I reported in the test a total of 8/1400 (0.6%) errors by labelling objects which were not shells, 17/1400 (1.2%) of double classification and 58/1400 (4.1%) of wrong colour and banding prediction (Figure 5.4).

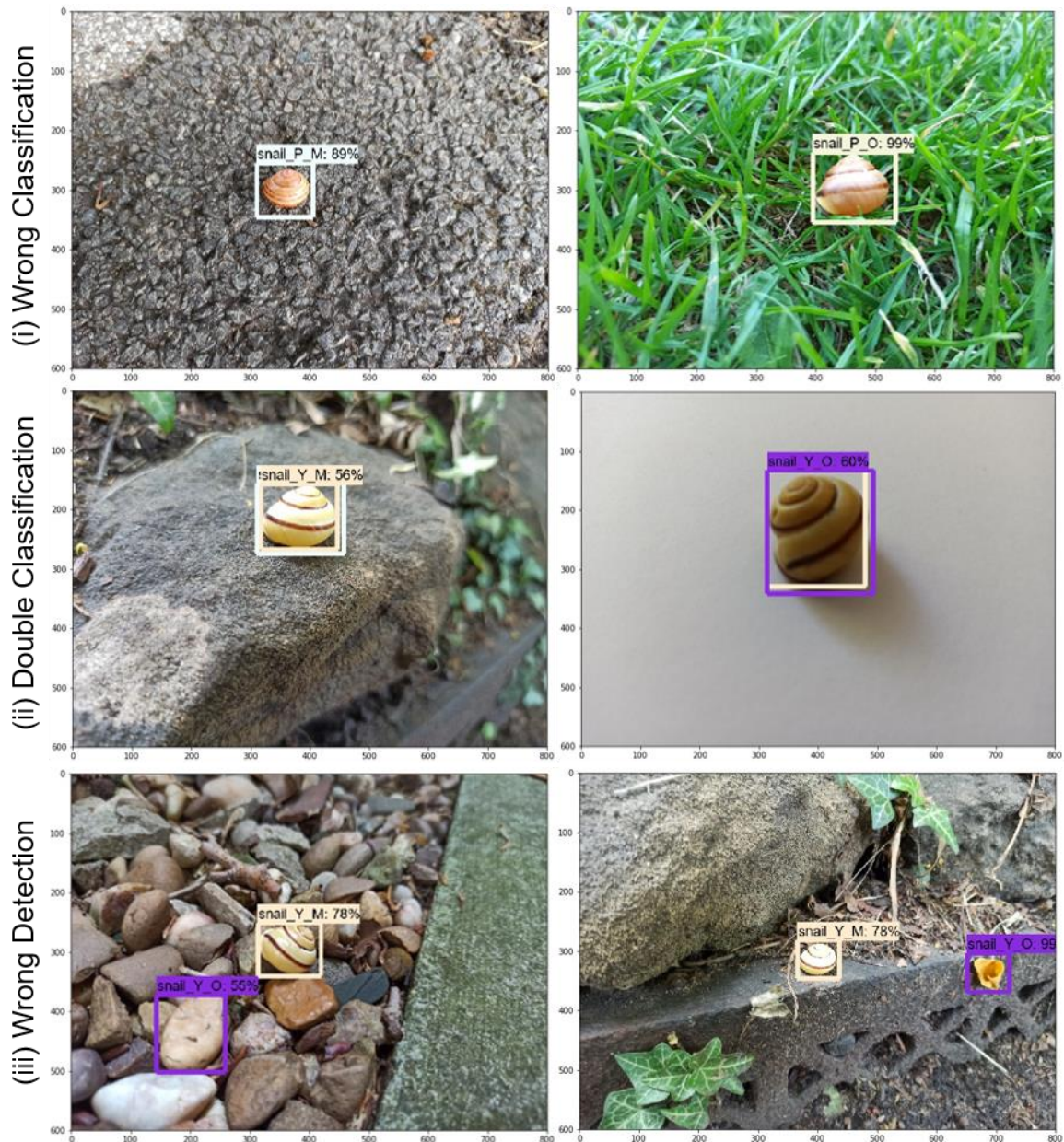


Figure 5.4. Examples of prediction failure. (i) Show wrong classifications; top-left image is classified as pink mid-banded and top-right as pink un-banded whereas top-left is pink banded and top-right pink mid-banded. (ii) Illustrate double labels for each shell; middle-left is marked as pink and yellow mid-banded and middle-right as yellow un-banded and mid-banded. (iii) Exemplify wrong shell detections.

To evaluate the accuracy of detection and classification difficulty of *C. nemoralis* shells colour and banding phenotype, a validation test and an unbiased test was performed in 8 different backgrounds. Precision, recall and F1-score showed 94%, 93% and 93% respectively in the validation test (Table 5.2). The unbiased test illustrated 96% in all three statistics (Table 5.2). Focusing in each background, precision, recall and F1-score range from 94% to 98%. Hedgerow, grassland and

blank backgrounds showed lower accuracy compared to the others, whereas woodland and road illustrated 98% accuracy (Table 5.2). However, when interpreting the accuracy results, we must be careful because the statistic also used the double-labelled shells (prediction failure ii) as right classification, when one of the options is the right one. This explains why 96% accuracy is shown in the test when 83/1400 (5.9%) errors are found.

Table 5.2. Summary of precision, recall and F1-score results

Backgrounds	Precision	Recall	F1-score
Validation	0.94	0.93	0.93
Test	0.96	0.96	0.96
Blank	0.95	0.94	0.94
Grassland	0.95	0.94	0.94
Hedgerow	0.94	0.94	0.94
Road	0.98	0.98	0.98
Sandland	0.97	0.97	0.97
Scree	0.97	0.96	0.96
Woodland	0.98	0.98	0.98
Wall	0.96	0.95	0.95
Morph Class Test average			
Yellow unbanded	0.97	1	0.99
Yellow mid-banded	0.94	0.94	0.94
Yellow banded	0.97	0.99	0.98
Pink unbanded	0.9	1	0.95
Pink mid-banded	0.95	0.88	0.91
Pink banded	0.99	0.92	0.95
Brown unbanded	0.99	0.97	0.98

Morph class displayed divergence in accuracy and varies depending on the background. Yellow banded and brown unbanded clusters exhibited the higher precision showing 99% true positives in each cluster. However, yellow mid-banded and pink unbanded had the lowest precision displaying 94% and 90% true positives respectively (Table 5.2 and Figure 5.5). In contrast, yellow and pink unbanded were classified in the right cluster in all the pictures. However, the R-FCN struggled clustering pink mid-banded and banded with a recall of 88% and 92% respectively (Table 5.2 and Figure 5.5).

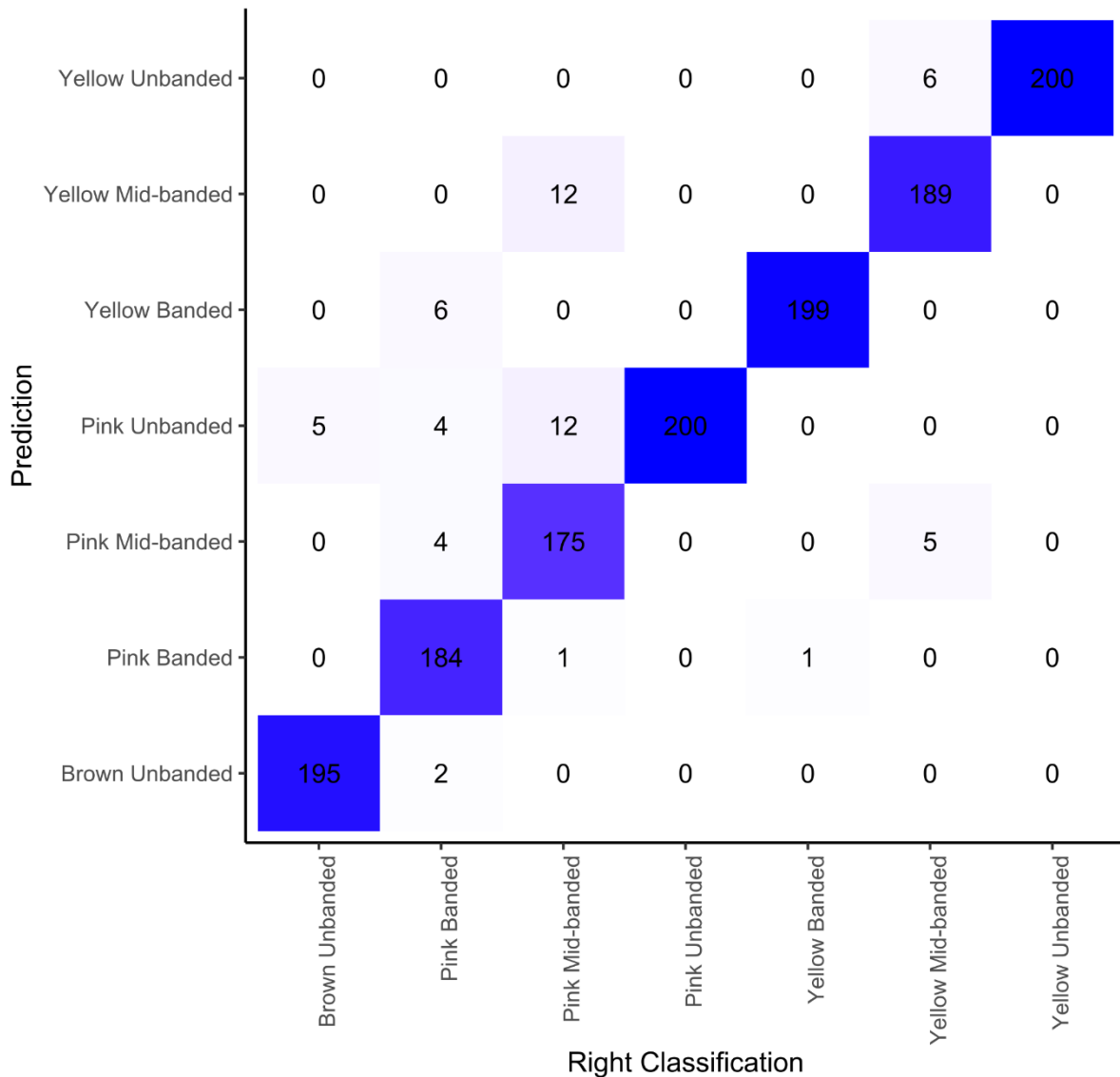


Figure 5.5. Prediction accuracy results in the test dataset. This heat-map shows each morph predicted (rows) with its respective right classification (columns).

Overall, similar results were found in all kind of backgrounds. Yellow and pink unbanded together with yellow banded are well recognised and clustered in all backgrounds (Figure 5.6, recall ratio = 100%). However, in their clusters, other morphs such as pink and yellow mid-banded are found due to the lower precision of those classes. The lowest precision ratios are found in blank and scree background where pink mid-banded and pink unbanded groups showed 79% and 81% precision (Figure 5.6). On the other hand, pink mid-banded illustrated 76% recalls in woodlands and hedgerow backgrounds (Figure 5.6).

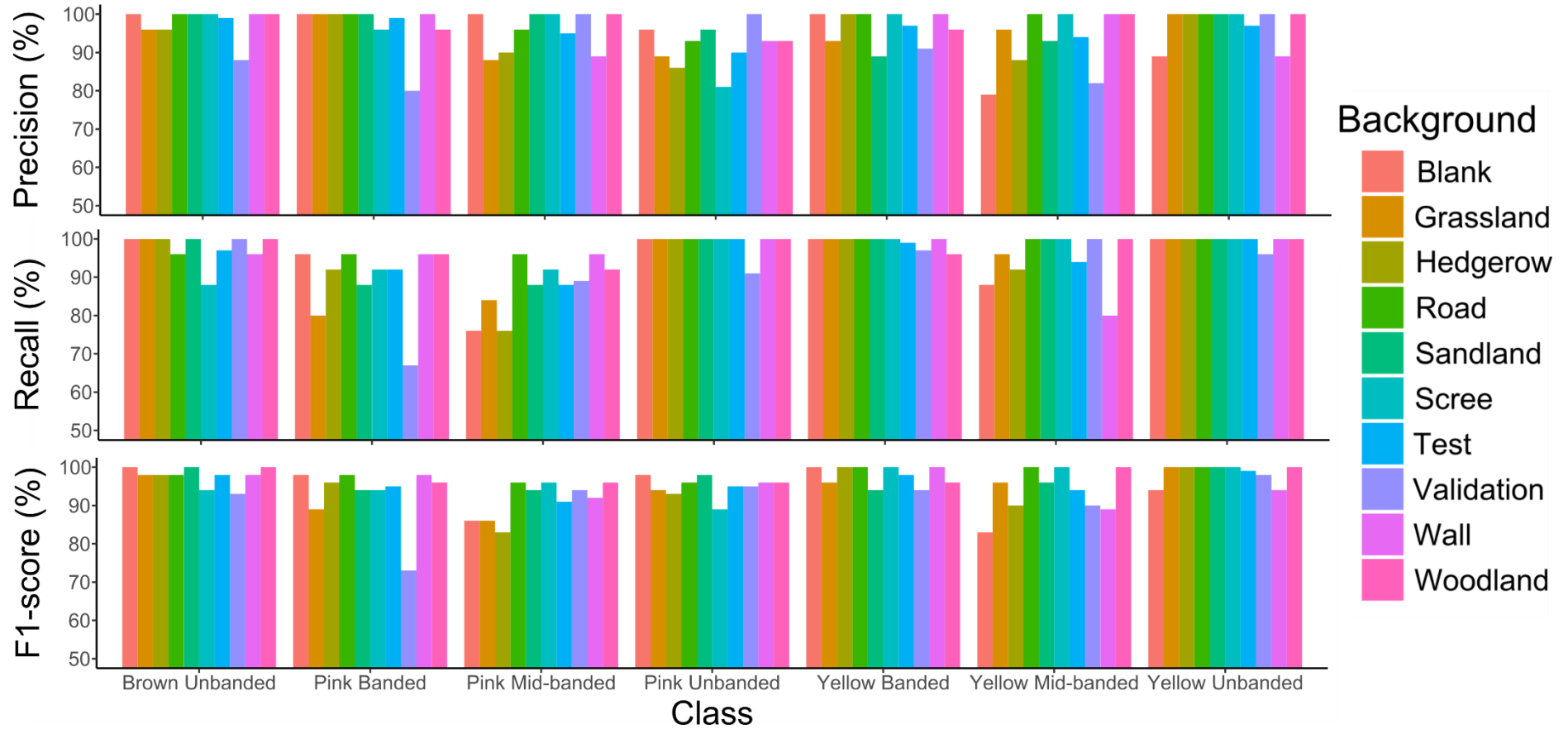


Figure 5.6. The bar-charts exhibit the results of the accuracy statistics of each class in the validation and test datasets in the particular different backgrounds. First row illustrates prediction ratios, second row the recall ratios and the third row the F1-score. General outcome from validation and test sets and specific backgrounds are coloured.

5.4. Discussion

In this research, I explored the use of deep learning tools, using *C. nemoralis* shells, with the objective to reduce and facilitate surveys, which colour detection is needed. For example, in studies such as the understanding of the maintenance of polymorphism, natural population variation, habitat switch or the fundamental role of natural selection (Cameron et al., 2012; Cameron et al., 2013; Cook, 2014; Davison et al., 2019a; Kerstes et al., 2019; Orstan et al., 2011; Ozgo et al., 2011; Silvertown et al., 2011; Worthington et al., 2012). The proposed classification system automatically recorded and standardised the colour efficiently in the sampling collection. The results opened a new field to consider in citizen science making the data collection cheaper, easier and more accessible to everyone. For example, this strategy extend the work done elsewhere by creating a common citizen-science project integrating the phenotype classification.

Overall, I found that the deep neural network can detect *C. nemoralis* from pictures where snails were located in the eight different habitats. Once the snail were spotted, the algorithm classified them into the trained different groups according to their shell colour background and banding. The recognition and classification, using the Region-based Fully Convolutional Networks (R-FCN) (Dai et al., 2016), of *C. nemoralis* morphs achieved a stable accuracy of 93% in the validation test and 96% in the test (Table 2 and Figure 6).

Using the deep learning tool, R-FCN (Dai et al., 2016), I achieved a classification system which; i) the technology opens the science to everyone since only a photo from a camera-smart phone is needed. ii) the deep neural network is trained by shells where colour was quantified by spectrometry and banding recorded by experts. iii) The detection and classification is unbiased. Even though people will take the pictures, the deep neural network will be responsible for detecting snails and classifying them into colour and banding groups. iv) It is trained and tested in eight different backgrounds, which exhibit real world challenges. v) Finally, it shows a tool that can be used in many fields such as biology, ecology and evolutionary genetics.

Moreover, adding deep neural networks to projects such as Evolution Megalab or Kertes phone application can facilitate, standardise and generate a more objective dataset (Cameron et al., 2012; Kerstes et al., 2019; Silvertown et al., 2011). Meanwhile kertes app and Evolution Megalab lack of this technology, the iNaturalist project used the algorithm to detect in the wild data individuals and classified them into the main fauna categories (Horn et al., 2018). Clearly, this strategy is really challenging due to the ambition of classifying all animal and plant kingdoms, but it becomes uncertain when classifying specific species. Thus, the strengths of this work using deep neural network compared to other methodologies is that, firstly, targets an specific identification of just one species and further morph classification within this species. And secondly, that the trained and test dataset colour classification was made by extracting the colour spectra using a spectrophotometer and transforming the spectra into human visual coordinates (Davison et al., 2019a). In previous similar studies, specialists such as in the Butterfly or Orchid databases (Arwatchananukul et al., 2020; Zhao et al., 2019) trained personally, the training datasets models.

However, the results found weaknesses in this procedure. One of the main challenges I found is that the identification of the *C. nemoralis* species over other *Cepaea* genus species *C. hortensis*. The deep neural network can distinguish snail species from other animal species. However, to differentiate between the *Cepaea* siblings becomes an issue. Pictures require visually different phenotypes to categorise one class from another. *C. nemoralis* are usually bigger than *C. hortensis*, like warmer climates and its lip colour generally is dark (Jones et al., 1977). Nonetheless, *C. hortensis* also shows sometimes populations with similar size, and even though usually lives in cooler areas, both species can be found in the same global zones and habitats (Jones et al., 1977).

Traditionally, the *Cepaea* siblings were recognised based on the lip colour (Jones et al., 1977). *C. hortensis* usually exhibits white lip colour whereas *C. nemoralis* shows dark lip colour. The deep neural network could be trained to recognise shells based on the lip colour. However, *C. nemoralis* coming from certain areas such as the Pyrenees valleys may present white lip colour due to its high frequencies of white-lipped shells (Chapter 4; Arnold, 1968; Cameron et al., 1973; Jones et al., 1975). Thus, the best method to differentiate between both species is by comparing the genital

structure, which requires dissection and cannot be illustrated in a picture to support the species classification (Jones et al., 1977).

There may be two hypothetical procedures using deep learning to fix these problems. One possible approach would be to build a huge training dataset for both species, hoping that the algorithm will find hidden patterns, which the human eye cannot detect. The other possible approach would be to use geographical filters, by taking GPS coordinates into account, and use population frequencies to infer in the outcome result when the pictures are taken in areas with presence of snails showing opposed lip colour. However, the second option will also have lower accuracy and be uncertain in those regions.

Furthermore, mistakes such as wrong detection, wrong classification and labelling the snail with two possible groups are encountered. Interestingly, the types, which had low presence in the training dataset, such as yellow and pink mid-banded and pink banded, are the ones with a higher ratio of mistakes. Furthermore, shells with different colour shades, not found in the training dataset, also showed a greater ratio of misleading classification (Figure 5.7). This results support the idea of creating a big and balanced training dataset. According to Horn et al. (2018), the deep neural network accuracy can improve when the training dataset is bigger and the number of classes are balanced. Thus, it is important to have a training dataset with a similar number of images of all the classes, ranging all the shell spectra, in all kinds of backgrounds (Horn et al., 2018).

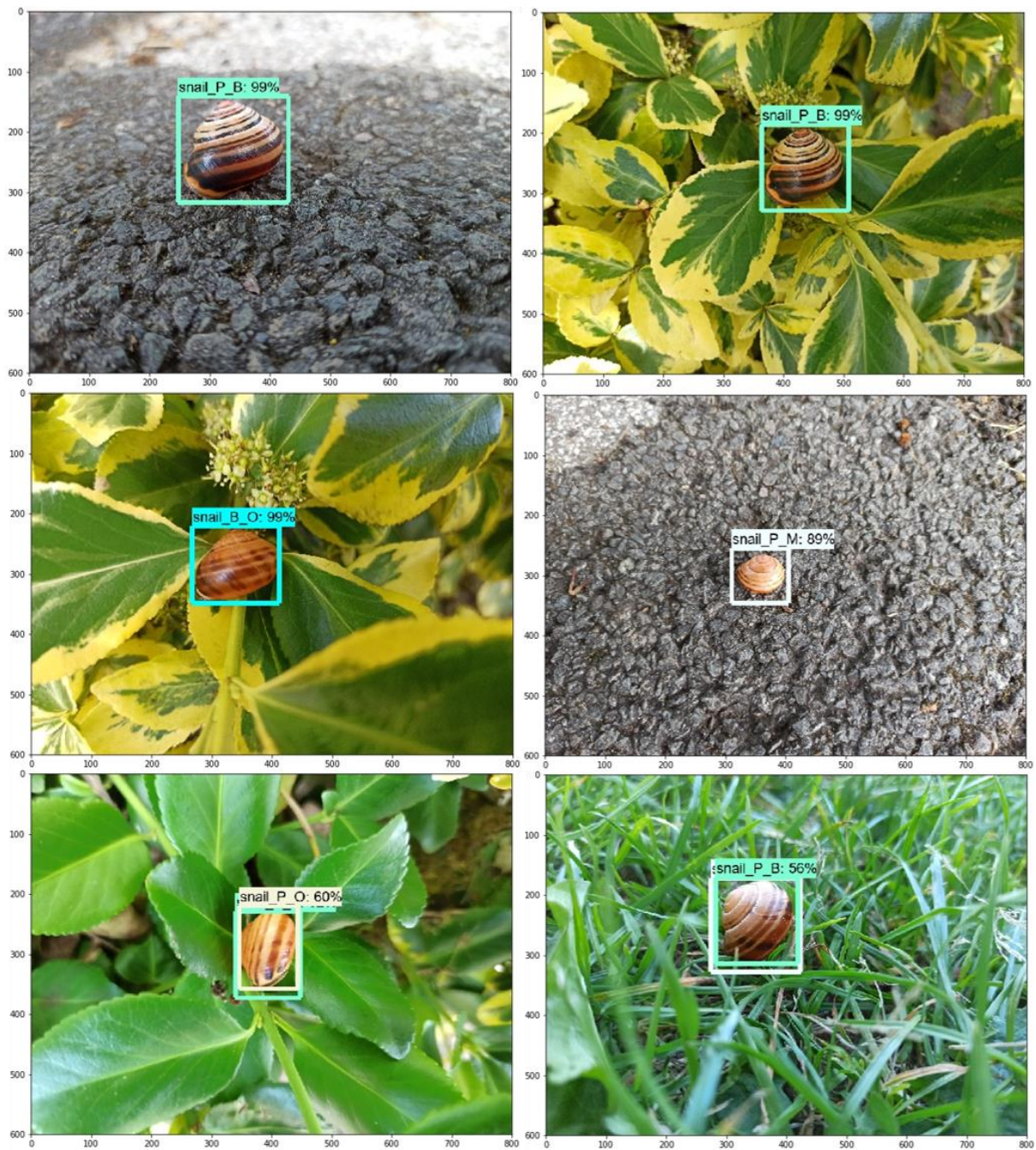


Figure 5.7. This image show pink banded snails. First row shows the type of pink banded shells found in the training dataset. The deep neural network identifies them correctly. Second and third row pictures shows pink banded shells with a banding colour shade not present in the training dataset. In this case, the deep neural network struggles to classify this morph. Second row represented wrong prediction where the pink banded is labelled as pink mid-banded or brown unbanded. Third row illustrates the algorithm double marking the shell due to its confusion.

5.5. Conclusion

In conclusion, I explored successfully the resolution of applying deep neural network models of detection and classification of *C. nemoralis* phenotypes based on colour quantitative methods. This method is intended for citizen science with the objective to facilitate, cheapen and reach globally ecological studies. In contrast to other approaches, this system standardised colour shade variation and clustered it into different morph types with high accuracy. Furthermore, the experiments also shown how important is to create a balanced large number of training dataset to ensure good prediction. This work also raised the question of finding a way to differentiate closely related species with no clear phenotype differences for human perception, and may facilitate the way of colour polymorphism studies were performed showing more room for development.

5.6. Acknowledgments

This work was supported by the University of Nottingham; the Biotechnology and Biological Sciences Research Council [grant number BB/M008770/1], via a studentship to Daniel Ramos Gonzalez. Thanks to Alejandro Garcia Alvarez to develop the deep learning algorithm and help in all IT issues; to all citizen scientist, which freely published non-copy right snail pictures in iNaturalist and to iNaturalist team who created this database.

Chapter 6:

General discussion and conclusions

6.1. *Cepaea nemoralis* colour polymorphism, a multidisciplinary challenge

Comparable to Jones et al. (1977) title “a problem with too many solutions”, the case study of colour polymorphism will only be solved by the comprehension and combination of multiple factors involving this topic, including for example, genetic, ecological, and evolutionary arguments. Therefore, to understand how *C. nemoralis* colour polymorphism existed and is maintained, the most suitable strategy is to approach these varieties of causes that generated it. In this multifaceted thesis, I have focussed on addressing the subject from the genetic mechanisms and its evolutionary history to the implementation of new quantitative technologies in the colour scoring step.

The contributions of this thesis to the research of the maintenance of the polymorphism are fourfold: Firstly, it shows that the apparent putative “recombination events” found in between both colour/banding, and colour/pigmentation loci in past studies were perhaps mistaken. A better explanation, to those phenotypes found, are an incomplete penetrance or epistasis, or both together (Gonzalez et al., 2019). Secondly, a population genomics study using ddRad-sequencing in European populations generated several outcomes. I found the genomic European structure accordance with the mitochondrial DNA phylogeny. Thirdly, I evaluated the limitations of colour manual scoring using spectrophotometry in a local altitudinal comparative survey in the Central Pyrenees. The results show that both methods have advantages and disadvantages, and both describe an overall remarkable stasis in *C. nemoralis* populations during the past 50 years in the area. Finally, I explored the use of deep learning to generate a new system, which recognises snails from pictures, and further classifies the individuals in their respective type.

In chapter 2 of this thesis (Gonzalez et al., 2019), using a new set of crosses segregating colour, banding, and pigmentation and genotyping them, I was able to explain rare phenotypic frequencies results found in *C. nemoralis* offsprings. Prior researchers attributed these results to mere “recombination events” since testing those individuals were not easy to verify. Currently, I found that the phenotypes, which were classified as putative “recombinants”, are better explained as the product of a possible epistasis event or incomplete penetrance or both at the same time. Overall, this work, therefore, shows that the architecture of the supergene may not be as previously supposed. Furthermore, it provides a resource for fine mapping of the supergene and other major shell phenotype loci.

In chapter 3 of this thesis, using ddRad sequencing, I mapped Western Europe to search for evolutionary answers. The results increased the understanding of the current geographic variation in *C. nemoralis* populations. On the one hand, the comparison of colour and genomic diversity across populations showed a striking difference. Colour variation occurred before the Pleistocene, as the present geographical genomic distribution does not match with its supergene variation in concordance with Ochman et al. (1983) and Ellis (2004) studies. The genomic variation, nonetheless, corresponded to the geographical distribution. Some gene candidates were described as likely responsible for that geographic genomic variation, but further analyses are needed to corroborate it. On the other hand, this study helped to reconstruct the expansion of *C. nemoralis* from the Pyrenees towards Europe probably helped by human migration using fluvial and ancient inland roads. This conclusion is in line with Grindon et al. (2013a) mitochondrial results.

In chapter 4 of this thesis, a comparative study in the Central Pyrenees was conducted using two colour-scoring techniques. When comparing techniques, results illustrated similar outcomes. However, the main finding was that while spectrophotometry of shell colour has the benefit of being quantitative and it is objective, the same trends were found, rising that both qualitative and quantitative methods have benefits and disadvantages. I concluded that a model that takes the best of both methods may be used in the future. Moreover, I aimed at understanding, through local altitudinal and geographic surveys, how local factors, human impact and the rapid climate change acted upon the variation of *C. nemoralis* shell polymorphism.

A remarkable overall stability of frequencies was found through the valleys, but some exceptions showed possible human disruptions in the area. We must consider, however, that these results can lead to risks of ascribing changes in the frequencies of a particular phenotype over time to 'just-so' explanations; and bringing the lack of understanding or explanations to circumstances when phenotype frequencies remain stable.

In chapter 5 of this thesis, I examined the use of deep learning tools given the increase of citizen science demand. Through the use of the quantitative spectra of *C. nemoralis* shells, I aimed at reducing time spent and facilitating the recognition of individuals and classification within their respective types. Overall, I found that a deep neural network can detect *C. nemoralis* from pictures in different backgrounds with high accuracy. Moreover, the algorithm correctly classified the individuals into the trained groups according to their shell colour background and banding. This work opens the door to use citizen science data to all researchers with greater reliability as the algorithm was trained with the results of spectrophotometric readings of *C. nemoralis* shells. Nonetheless, the project revealed a challenge regarding the detection of sibling species, *C. nemoralis* and *C. hortensis*. This research may bring context to a new era where ecological and evolutionary genetic studies will be much faster and cheaper with quantitative records.

Overall, these studies will help in future projects focused on understanding *C. nemoralis* colour polymorphism. On the one hand, thanks to genetic work, future research will be able to recognise real recombinant events, which will help to map the genome and specifically the supergene. Besides, the population study showed that in two thirds of all loci represented in our genomic data, the development of the shell polymorphism was not due to recent natural selection, facilitating the findings of when and how this variation was originated. I also contributed in the description of the European expansion of *C. nemoralis* after the Pleistocene. In addition, I evaluated how local factors act upon its local distribution and how the geographic genomic expansion happened. Finally, the development of a new colour scoring techniques will contribute to obtaining more reliable quantitative results, which will cover globally a greater number of *C. nemoralis* populations quicker and with a reduced cost.

6.2. Future steps towards understanding *Cepaea nemoralis* shell polymorphism

6.2.1. Mapping *Cepaea nemoralis* genome

In this thesis, the four studies generated some attractive and new insights; they also produced new challenges and rose questions, which need to be addressed in future research.

Perhaps, one of the greatest difficulties found in this thesis was the proportion of missing data generated by ddRAD sequencing in chapter 3. Even though, the outcomes are still valuable, a reduction of the dataset was necessary to obtain reliable results (Huang et al., 2014). It is likely that the reduction of a large part of the ddRAD-seq data limited number of markers, so that many genome contigs did not contain any variability, which decreased the broader picture of the genome. It is clear that the next step in understanding both, the supergene controlling shell polymorphism and the evolutionary history of *C. nemoralis*, would be to perform a fine mapping using new generation sequencing methods and applying the availability of a first draft of *C. nemoralis* genome (Saenko et al., 2020). For example, GWAS methodology could genotype the genome, and further it could compare all sequenced genomes to search for the genetic variations influencing phenotypic traits (Manolio et al., 2009). This procedure could also help to order the contigs of the existing genome and the creation of a linkage map to associate phenotypes to genotypes.

This methodology may help in the understanding of factors affecting changes or stasis of phenotypic frequencies. In the case of chapter 4, I tried to study the possible factors acting upon the shell phenotypes in the Pyrenees. Even though, using a comparative frequency study helped to explain the frequency changes, this method did not produce enough evidences to explain the remarkable stability of shell phenotypes found across valleys after 17 generations of *C. nemoralis*. The lack of evident selective forces maintaining the shell polymorphism, however, does not mean that there are none. Maybe the best answer lies on the time-scale of the study. Time is relative and, even though this comparative study is based on 50 years, the effects

of selective forces or random drift may need more time to show evidences at frequency level. Therefore, comparative studies using morph frequency have shown limitations since the interpretation of the results are subjected to the time-scale (Cook, 2014), environment and population size. For example, the rapid modification of habitats in the area and connectivity among them occurring before the sampling may cause deviations in morph frequencies influencing the results. Probably, the use of population genomic techniques and the wealth of bioinformatics would, offer a solution these limitations and also bring evidences forth an era. In the future, we will have a better understanding of the impact of the multiple factors (Jones et al., 1977), including gene flow, natural selection and random genetic drift, which determine the patterns of shell types that we see in nature. For example, in the Pyrenean study, I concluded that in Vielha valley, a probable explanation of the drop in the relationship between attitude and shell colour is a possible immigration helped by human activity. In this case, it should be possible to use genomics to understand and to corroborate the mentioned explanation by describing the relative roles of migration, founder effect and selection in determining the population structure of *Cepaea* populations. These outcomes will definitely help scientist steer clear of “just-so” explanations about found stability or changes in the frequencies of a particular phenotype over time. In addition, in chapter 2 the genotyping of the crosses shows that phenocopies may be problematic in using the shell phenotype alone to detect recombination events within the supergene. This could also lead to an issue when calculating shell morph frequencies. Recombination frequencies are used in gene mapping to create linkage maps showing the relative distance between genes and the order. Ergo, false recombinant may lead to wrong interpretation of the supergene mapping. Thus, this chapter highlight the importance of detecting the real putative recombinant events and reviews more accurate techniques. For example, fine mapping by genomic studies can identify exposures that are causally associated with the genotype (Gage et al., 2016) and unmask the “false-positive” phenotypes.

A further suggestion to study the factors acting upon shell polymorphism of *C. nemoralis* is to use manipulative experiments. The alteration of factor levels in controlled snail populations may help to understand the causes and effects of each factor in the shell polymorphism. Furthermore, the combination manipulative experiments together with epigenetics may bring the link between environmental and

phenotypic variation (Herrel et al., 2020). In particular, contemporary studies have enhanced the revision of processes of phenotypic adaptation and plasticity by evaluating epigenetic variation due to controlled environmental manipulation (Ledón-Rettig et al., 2013). This can contribute in the understanding of relatively local changes of frequencies or stability found over time. However, this must be taken carefully as many standard experimental designs are simply unwieldy for realistic field experiments and we still do not know how many generations are required to expose evidence of selection or genetic drift. Perhaps, these studies may be used just to assist or validate particular cases.

Another general issue is to determine candidate genes under selections leading the genomic variation. In chapter 3, I identify possible genomic regions, which can be confirmed or help to find the genomic geographical signals and the selective factors acting upon those populations. Even though, genome scan (Fst and Mantel test) can be used to search for genetic divergence associated to geographical distances, the outcomes must be taken cautiously. The results brings context to the future understanding of the genomic variation found by showing possible spatial mechanism affecting genomic regions leading to a geographical population structure. Fst and specially Mantel test are powerful tools to approach ecological and evolutionary challenges, but their results may be a biased definition of the spatial variation in the data (Diniz-Filho et al., 2013; Hoban et al., 2016). There are many genomic techniques in the scientific knowledge to approach and detect genomic regions under selection apart of the genome scan. To verify the results found, methods such as gene expression, linkage mapping or quantitative trait locus (QTL) mapping (West et al., 2007) may be used. Each methodology requires different information, resulting in an increasing capability to bind specific genomic regions to specific features. Similar to the genome scan, gene expression, like the genome scan, also maps the genome searching for potential high differentiation among genes. Then, linkage mapping and gene order (synteny) can be performed together with quantitative trait locus (QTL) mapping, adding phenotypic data, to link the candidate genes with its respective phenotypes (Rice et al., 2011).

Moreover, a larger sampling collection can also contribute to the big picture of the evolutionary history of *C. nemoralis*. Locally, thanks to new smartphones and

accurate GPS capabilities, sampling individuals can be precise. A possible new approach for future comparative studies may use individual data-points instead of population sites. Currently, in the study of environmental factors, all researchers are focused on comparing populations avoiding intrinsic events or interactions. In theory, using just individuals may lead to a generation of density or interactive maps having an increased data ending with more power in future statistic models. The reason for this is that this way of collecting data brings new perspective to associate external interactions such as predation, habitat, human disruption or interaction with frequency changes due to habitat changes and climatic events being live-time recorded, which can track specific and localise occurrence.

In the broad picture, the European phylogeny built in chapter 3, revealed a limitation that must be considered. All samples were taken from Western Europe, which helped to describe the expansion of *C. nemoralis* populations from the Pyrenees to Europe after the Pleistocene. However, the survey may not properly show the general genetic diversity in Europe as it did not map properly the other Pleistocene refuges. *Cepaea* populations in the Alps and Balkans may have also undergone differentiation and could have found other routes to colonise Europe pushed by humans intervention such as transportation of snails through river or land routes (Gutiérrez-Zugasti, 2011; Lubell, 2004; Richards et al., 2013). For example, mapping the other mountain enclaves and river routes such the Danube, Rhine, Loire, Vistula and Elbe may change the genomic distribution of *C. nemoralis*. A fine mapping of the entire European continent may help to understand, possible differentiation in the other refuges, and its further interactions in the expansion after the Pleistocene. Moreover, it can help to find variation that occurred before the mentioned epoch, as shared or conserved genes in samples coming from all refugees may indicate past genetic origination.

6.2.2. Citizen science, the future of ecological and evolutionary genetics

As mentioned in chapters 1, 4 and 5, there has been a growth of citizen science in ecological projects with the application of more reliable approaches such as SnailSnap, iNaturalist and iRecord (Harvey, 2018; Horn et al., 2018; Kerstes et al., 2019), and thanks to the availability of new technologies recently developed and

available to the general public like smartphones with cameras and GPS capabilities. Moreover, artificial intelligence developed deep learning algorithms, which are capable to detect objects in images, and generate further analysis such as colour extraction. Both improvements combined enable and ask for new perspectives and applications of abovementioned high-tech into the study of colour polymorphism in ecological and evolutionary studies in the coming era. This methodology may help in the future to generate surveys at various spatial scales to enhance the temporal and spatial range of studies.

Current citizen science projects are already being used extensively by the public to capture records and images of snails. However, they lack reliable standardised methods, and automated phenotype scorings. Particularly in *C. nemoralis*, I found several excellent project ideas, which collected a huge amount of data. In the case of iNaturalist (Horn et al., 2018), it has over 9000 observations, including photos, at “research grade” quality (including >1000 in the UK, but only 29 in the Pyrenean region). Although, this citizen project uses already its own artificial intelligence to classify species, the training system showed some limitations. Firstly, the artificial intelligence algorithms were trained by limited pictures of each species scored by biologist. Secondly, the algorithms self-update using other pictures scored by the public criteria. Consequently, the system illustrates high accuracy in the detection of species. However, due to the ambition of the project aiming at classifying all the species found on this planet, the current accuracy of classification of similar species is quite low. Especially, when comparing sister species such as *C. nemoralis* and *hortensis*. On the other hand, in the particular case of the targeted species of study, SnailSnap (Kerstes et al., 2019) is worth mentioning. It is an app created by a Dutch research group specifically to find and score *C. nemoralis* aiming to contribute in its evolutionary research. However, the mentioned app only stored the pictures to further manual-scoring of the researchers. Even though, this system generates a large amount of data, it also has limitations in the scoring time and in the viability of usage of results since the photos are taken by different cameras in different environments, and the scoring criteria still depends on human perception. Moreover, it would be interesting to have a common project instead of separate system, like a collaborative project among the different citizen-science projects, integrating the different mechanism in, for example, iNaturalist.

One suggestion is to extend the use of a deep learning based method to inspect individual images, and then record the colour and band category. This is a straightforward method, which could easily be employed in current citizen science projects. Furthermore, a more sophisticated (but difficult to implement) alternative would be to extract quantitative colour data from the images. Nonetheless, these algorithms need to be based on reliable training datasets to avoid misclassifications. Hence, like in the prototype produced in chapter 5, the use of quantitative methods like spectrophotometry, to score individuals and a controlled set up of conditions may be the solution to teach the algorithm. This system can be implemented in projects like iNaturalist (Horn et al., 2018) or especially in SnailSnap (Kerstes et al., 2019). In the second suggested case, it would be very simple. Once the photo is uploaded to the application, the deep neural network can scan the photo in search of snails and once they are found, classify them in their respective morphs, as previously trained. However, a possible disadvantage of the method would be that it must be robust to the wide variety of circumstances under which the photos would be taken; which the application of some sort of colour control (e.g. a card; van den Berg et al., 2020). However, the application of these controls may limit the number of participants.

The interesting part of this project is that it can be applied to all kinds of species showing colour polymorphism, from other species of land or aquatic snails to other species of animals or plants having a diverse colour variation. Certainly, what this study presents is a training strategy for deep learning algorithms whose objective is the identification of individuals of a specific species and their subsequent classification in their various colour morphs. Therefore, this tactic applied to citizen-science projects could give a breadth of data whose individuals will be selected as a part of an species and classified in their respective types saving valuable time. This possible large studies of morph frequencies will contribute to discover factors acting on large-scale on those individuals helping to answer questions about their ecological, evolutionary and genetic procedures in the wild.

In addition, the detection of species can be complicated when similar species are present in the same areas and habitats. It is the case of the sibling *C. hortensis* with *C. nemoralis* and also the confusion of juvenile snails of *Cornu aspersum* and

Arianta arbustorum with juveniles of *C. nemoralis* (Jones et al., 1977). Particularly in the case of *C. hortensis*, which only a dissection can properly clarify its species. The image dataset must be carefully filtered to avoid misidentification of species. In chapter 5, I recommend a plausible approach. The generation of a huge training datasets for both species can lead the algorithm to find hidden patterns, which human eye cannot detect. Then an exhaustive evaluation of the species classifications will be needed, as we, as a humans, may not be able to understand the mechanism to categorise the species. In the case of juvenile snails, a simple warning to citizen scientists can be done to avoid the use of spotted juveniles since they have not yet fully developed the shell and its polymorphic traits in its whole.

6.3. Final conclusion

The abovementioned suggestions should provide new perspectives towards a better procedure in the understanding of the pulmonate *Cepaea nemoralis* in its ecological and evolutionary genetics and genomics over the next few years. Shell colour polymorphism is shown in this thesis as a complex subject. I argued, notably in chapters 2 and 3, for a proper explanation and understanding of genetics and genomes. The use of new generation sequencing and further analysis such as linkage mapping or quantitative trait locus (QTL) mapping (Rice et al., 2011; West et al., 2007) will contribute in the generation of appropriate associations between genotype and phenotype. We should see more studies focused in the whole genome sequencing, avoiding the generation of missing data (Huang et al., 2014), and further appropriate linkage mapping of phenotype and genotype. This should finally help in finding the hidden patterns underlying the genetics and genomic mechanisms.

However, genome scans and linkage mapping itself will not be enough. I hope to see in future research also population genomic approaches (Rajora, 2019), interpreting evolutionary processes and factors such as gene flow, mutations, random drift or natural selection affecting the genome. Additionally, an appropriate sampling collection all over Europe is needed to decode the underlying evolution occurred before and after the Pleistocene. The other Pleistocene refugees are poorly described in *C. nemoralis* population. I expect to observe new surveys and research describing properly the geographical expansion of *C. nemoralis* over Europe from other Pleistocene settlements. Similarly with the Irish case, this screening may expose new associations with other species bringing to light exciting events (Grindon et al., 2013a). A final combination of all three expansions may contribute to understand further evolution occurred in the ancestry of the *Cepaea* genus. Perhaps, even describe the events causing the differentiation of the *Cepaea* siblings.

Another fascinating point that this thesis emphasised, is the key role of the use of comparative studies in the understanding of the evolution of the polymorphic shell in pulmonate taxa and specially in *C. nemoralis*. With the growth of new technologies available to researchers and citizen science (Harvey, 2018; Horn et al., 2018; Kerstes

et al., 2019; Silvertown et al., 2011), the data collection worldwide increased massively aiming specially at taxonomic efforts. As indicated in chapters 4 and 5, this can also be used for the purpose of shell scoring, either colour, banding or pigmentation, in pulmonate species. I hope to see studies comparing the evolution of these phenotypes over time to understand, for example, the effect of present climatic changes and other disruptions and whether there is a shared ecological process with other similar species. This would definitely help in the understanding of how the colour polymorphism evolved and how it is maintained. Therefore, procedures using a combination of spectrophotometry, deep learning algorithms and citizen science may facilitate and provide extensive insights.

Ultimately, I would like to state that the understanding of colour polymorphism in pulmonate taxa is far from just the intense research of one scientific field. A combination of all fields involving this topic is necessary. I would like, that this multidisciplinary thesis, guide future research towards a novel conclusion and perhaps the proper understanding of colour polymorphism evolution and maintenance, both from the genetic and genomic point of view, up to the required reliable extraction of the colour acquired in the shells.

References

- Adema, C. M. (2021). Sticky problems; extraction of nucleic acids from molluscs. *Philosophical Transactions of the Royal Society of London B Biological Sciences* *in press*.
- Affenzeller, S., Cerveau, N., & Jackson, D. J. (2018). Identification and validation of reference genes for qPCR in the terrestrial gastropod *Cepaea nemoralis*. *Plos One*, *13*(8), e0201396.
- Affenzeller, S., Wolkenstein, K., Frauendorf, H., & Jackson, D. J. (2020). Challenging the concept that eumelanin is the polymorphic brown banded pigment in *Cepaea nemoralis*. *Scientific reports*, *10*(1), 1-7.
- Akey, J. M., Zhang, G., Zhang, K., Jin, L., & Shriver, M. D. (2002). Interrogating a high-density SNP map for signatures of natural selection. *Genome research*, *12*(12), 1805-1814.
- Alexander, D. H., & Lange, K. (2011). Enhancements to the ADMIXTURE algorithm for individual ancestry estimation. *BMC Bioinformatics*, *12*(1), 246. doi:10.1186/1471-2105-12-246
- Angermueller, C., Pärnamaa, T., Parts, L., & Stegle, O. (2016). Deep learning for computational biology. *Molecular systems biology*, *12*(7), 878.
- Arnold, R. (1969). The effects of selection by climate on the land-snail *Cepaea nemoralis* (L.). *Evolution*, *23*(3), 370-378. doi:10.2307/2406693
- Arnold, R. W. (1968). Studies on *Cepaea* VII. Climatic selection in *Cepaea nemoralis* (L) in Pyrenees. *Philosophical Transactions of the Royal Society of London Series B-Biological Sciences*, *253*(789), 549-593. doi:10.1098/rstb.1968.0011
- Arwatchananukul, S., Kirimasthong, K., & Aunsri, N. (2020). A New *Paphiopedilum* orchid database and its recognition using Convolutional Neural Network. *Wireless Personal Communications*. doi:10.1007/s11277-020-07463-3
- Ayala, F. J., & Campbell, C. A. (1974). Frequency-dependent selection. *Annual Review of Ecology and Systematics*, *5*, 115-138.
- Baker, R. R., & Parker, G. A. (1979). The evolution of bird coloration. *Philosophical Transactions of the Royal Society of London. B, Biological Sciences*, *287*(1018), 63-130.
- Bay, R. A., Rose, N., Barrett, R., Bernatchez, L., Ghalambor, C. K., Lasky, J. R., . . . Ralph, P. (2017). Predicting responses to contemporary environmental change using evolutionary response architectures. *The American Naturalist*, *189*(5), 463-473.
- Beadle, G. W., & Tatum, E. L. (1941). Genetic control of biochemical reactions in *Neurospora*. *National academy of sciences of the USA*, *27*(11), 499.
- Berjano, R., Gauthier, P., Parisi, C., Vaudey, V., Pons, V., Renaux, A., . . . Thompson, J. D. (2015). Variation of a floral polymorphism at different spatial scales in the Mediterranean geophyte *Narcissus assoanus*. *Journal of Plant Ecology*, *9*(3), 333-345. doi:10.1093/jpe/rtv057
- Bolger, A. M., Lohse, M., & Usadel, B. (2014). Trimmomatic: a flexible trimmer for Illumina sequence data. *Bioinformatics*, *30*(15), 2114-2120.
- Brace, S., Ruddy, M., Miller, R., Schreve, D. C., Stewart, J. R., & Barnes, I. (2016). The colonization history of British water vole (*Arvicola amphibius* (Linnaeus, 1758)): Origins and development of the Celtic fringe. *Proceedings of the Royal Society B: Biological Sciences*, *283*(1829), 20160130.
- Bradshaw, R. A., & Dennis, E. A. (2009). *Handbook of cell signaling*: Academic press.

- Bradski, G., & Kaehler, A. (2013). *Learning OpenCV: Computer Vision in C++ with the OpenCV Library*: O'Reilly Media, Inc.
- Byers, J. A. (2006). Analysis of insect and plant colors in digital images using Java software on the Internet. *Annals of the Entomological Society of America*, 99(5), 865-874.
- Cain, A. (1984). Genetics of some morphs in the land snail *Theba pisana*. *Malacologia*, 25(2), 381-411.
- Cain, A. J., & Currey, J. D. (1963). Area effects in *Cepaea*. *Philosophical Transactions of the Royal Society of London Series B-Biological Sciences*, 246(726), 1-&. doi:10.1098/rstb.1963.0001
- Cain, A. J., & Currey, J. D. (1968). Studies on *Cepaea* .3. Ecogenetics of a population of *Cepaea nemoralis* (L) subject to strong area effects. *Philosophical Transactions of the Royal Society of London Series B-Biological Sciences*, 253(789), 447-&. doi:10.1098/rstb.1968.0007
- Cain, A. J., King, J. M., & Sheppard, P. M. (1960). New data on the genetics of polymorphism in the snail *Cepaea nemoralis* L. *Genetics*, 45(4), 393-411.
- Cain, A. J., & Sheppard, P. M. (1950). Selection in the polymorphic land snail *Cepaea nemoralis*. *Heredity*, 4(3), 275-294. doi:10.1038/hdy.1950.22
- Cain, A. J., & Sheppard, P. M. (1952). The effects of natural selection on body colour in the land snail *Cepaea-nemoralis*. *Heredity*, 6(2), 217-231. doi:10.1038/hdy.1952.22
- Cain, A. J., & Sheppard, P. M. (1954). Natural selection in *Cepaea*. *Genetics*, 39(1), 89-116.
- Cain Arthur James , S. P. M. a. K. J. M. B. (1968). Studies on *Cepaea* I. The genetics of some morphs and varieties of *Cepaea nemoralis* (L.). *Phil. Trans. R. Soc. Lond. B*, 253(789). doi:rstb.1968.0005
- Cameron, R. (1998). *Cepaea* research 1900–1950; too many problems for a solution? *Archives of Natural History*, 25(3), 401-412.
- Cameron, R. A., & von Proschwitz, T. (2020). *Cepaea nemoralis* (L.) on Öland, Sweden: recent invasion and unexpected variation. *Folia Malacologica*, 28(4), 303-310.
- Cameron, R. A. D., Carter, M. A., & Haynes, F. N. (1973). The variation of *Cepaea nemoralis* in three Pyrenean valleys. *Heredity*, 31(AUG), 43-74. doi:10.1038/hdy.1973.58
- Cameron, R. A. D., & Cook, L. M. (2012). Habitat and the shell polymorphism of *Cepaea nemoralis* (L.): interrogating the Evolution Megalab database. *Journal of Molluscan Studies*, 78, 179-184. doi:10.1093/mollus/eyr052
- Cameron, R. A. D., Cook, L. M., & Greenwood, J. J. D. (2013). Change and stability in a steep morph-frequency cline in the snail *Cepaea nemoralis* (L.) over 43 years. *Biological Journal of the Linnean Society*, 108(3), 473-483. doi:10.1111/j.1095-8312.2012.02033.x
- Campbell, C. R., Poelstra, J. W., & Yoder, A. D. (2018). What is Speciation Genomics? The roles of ecology, gene flow, and genomic architecture in the formation of species. *Biological Journal of the Linnean Society*, 124(4), 561-583. doi:10.1093/biolinnean/bly063
- Carl, C., Schönfeld, F., Profft, I., Klamm, A., & Landgraf, D. (2020). Automated detection of European wild mammal species in camera trap images with an existing and pre-trained computer vision model. *European Journal of Wildlife Research*, 66(4), 62. doi:10.1007/s10344-020-01404-y

- Cassey, P., Honza, M., Grim, T., & Hauber, M. E. (2008). The modelling of avian visual perception predicts behavioural rejection responses to foreign egg colours. *Biology Letters*, *4*(5), 515-517. doi:10.1098/rsbl.2008.0279
- Caugant, D., Selander, R. K., & Jones, J. S. (1982). Geographic structuring of molecular and morphological polymorphism in Pyrenean populations of the snail *Cepaea nemoralis*. *Genetica*, *57*(3), 177-191. doi:10.1007/bf00056481
- Chen, Z., Farrell, A. P., Matala, A., Hoffman, N., & Narum, S. R. (2018). Physiological and genomic signatures of evolutionary thermal adaptation in redband trout from extreme climates. *Evolutionary Applications*, *11*(9), 1686-1699.
- Chiba, S. (1999). Accelerated evolution of land snails *Mandarina* in the oceanic Bonin Islands: evidence from mitochondrial DNA sequences. *Evolution*, *53*(2), 460-471.
- Chueca, L., Schell, T. & Pfenninger, M. (2020). Whole genome re-sequencing data to infer historical demography and speciation processes in land snails: the study of two *Candidula* sister species. *Philosophical Transactions of the Royal Society of London B Biological Sciences* in press. doi:doi: <https://doi.org/10.1098/rstb.2020.0156>
- Clarke, B. (1969). The evidence for apostatic selection. *Heredity*, *24*(3), 347-352.
- Clarke, B., & Murray, J. (1971). Polymorphism in a Polynesian land snail *Partula suturalis vexillum*. In *Ecological genetics and evolution* (pp. 51-64): Springer.
- Cook, L. (1967). The genetics of *Cepaea nemoralis*. *Heredity*, *22*(3), 397.
- Cook, L. (2003). A colony of pale-lipped *Cepaea nemoralis*. *J Conchol*, *38*, 73–78.
- Cook, L., & Jones, D. (1996). The medionigra gene in the moth *panaxia dominulcr*: the case for selection. *Philosophical Transactions of the Royal Society of London. Series B: Biological Sciences*, *351*(1347), 1623-1634.
- Cook, L. M. (2013). Selection and disequilibrium in *Cepaea nemoralis*. *Biological Journal of the Linnean Society*, *108*(3), 484-493. doi:10.1111/j.1095-8312.2012.02027.x
- Cook, L. M. (2014). Morph frequency in British *Cepaea nemoralis*: what has changed in half a century? *Journal of Molluscan Studies*, *80*, 43-46. doi:10.1093/mollus/eyt040
- Cook, L. M. (2017). Reflections on molluscan shell polymorphisms. *Biological Journal of the Linnean Society*, *121*(4), 717-730. doi:10.1093/biolinnean/blx033
- Cook, L. M., Cowie, R. H., & Jones, J. S. (1999). Change in morph frequency in the snail *Cepaea nemoralis* on the Marlborough Downs. *Heredity*, *82*, 336-342.
- Cook, L. M., & King, J. M. (1966). Some data on the genetics of shell-character polymorphism in the snail *Arianta arbustorum*. *Genetics*, *53*(3), 415-425.
- Corl, A., Bi, K., Luke, C., Challa, A. S., Stern, A. J., Sinervo, B., & Nielsen, R. (2018). The genetic basis of adaptation following plastic changes in coloration in a novel environment. *Curr Biol*, *28*(18), 2970-2977.e2977. doi:10.1016/j.cub.2018.06.075
- Cowie, R. H. (1990). Climatic selection on body colour in the land snail *Theba pisana* (Pulmonata: Helicidae). *Heredity*, *65*(1), 123-126. doi:10.1038/hdy.1990.78
- Cowie, R. H., & Jones, J. S. (1998). Gene frequency changes in *Cepaea* snails on the Marlborough Downs over 25 years. *Biological Journal of the Linnean Society*, *65*(3), 233-255. doi:10.1006/bijl.1998.0250
- Cuthill, I. C., Allen, W. L., Arbuckle, K., Caspers, B., Chaplin, G., Hauber, M. E., . . . Kelber, A. (2017). The biology of color. *Science*, *357*(6350).

- Dai, J., Li, Y., He, K., & Sun, J. (2016). R-fcn: Object detection via region-based fully convolutional networks. *Advances in neural information processing systems*, 379-387.
- Dallinger, R., Berger, B., Hunziger, P., & Kgi, J. H. (1997). Metallothionein in snail Cd and Cu metabolism. *Nature*, 388(6639), 237-238.
- Danecek, P., Auton, A., Abecasis, G., Albers, C. A., Banks, E., DePristo, M. A., . . . Group, G. P. A. (2011). The variant call format and VCFtools. *Bioinformatics*, 27(15), 2156-2158. doi:10.1093/bioinformatics/btr330
- Danecek, P., & McCarthy, S. A. (2017). BCFtools/csq: haplotype-aware variant consequences. *Bioinformatics*, 33(13), 2037-2039.
- Darwin, C. (1859). *On the Origin of Species by Means of Natural Selection Or the Preservation of Favoured Races in the Struggle for Life*: H. Milford; Oxford University Press.
- Davison. (1999). Isolation and characterization of long compound microsatellite repeat loci in the land snail, *Cepaea nemoralis* L-(Mollusca, Gastropoda, Pulmonata). *Molecular Ecology*, 8(10), 1760-1761. doi:10.1046/j.1365-294x.1999.00723-4.x
- Davison. (2000a). An East-West distribution of divergent mitochondrial haplotypes in British populations of the land snail, *Cepaea nemoralis* (Pulmonata). *Biological Journal of the Linnean Society*, 70(4), 697-706. doi:10.1006/bijl.1999.0426
- Davison. (2000b). The inheritance of divergent mitochondria in the land snail, *Cepaea nemoralis*. *Journal of Molluscan Studies*, 66, 143-147. doi:10.1093/mollus/66.2.143
- Davison. (2006). The ovotestis: an underdeveloped organ of evolution. *BioEssays*, 28(6), 642-650. doi:<https://doi.org/10.1002/bies.20424>
- Davison, & Clarke, B. (2000). History or current selection? A molecular analysis of 'area effects' in the land snail *Cepaea nemoralis*. *Proceedings of the Royal Society B-Biological Sciences*, 267(1451), 1399-1405. doi:10.1098/rspb.2000.1156
- Davison, Jackson, H. J., Murphy, E. W., & Reader, T. (2019a). Discrete or indiscrete? Redefining the colour polymorphism of the land snail *Cepaea nemoralis*. *Heredity*, 123, 162-175. doi:10.1038/s41437-019-0189-z
- Davison, A. (2002). Land snails as a model to understand the role of history and selection in the origins of biodiversity. *Population Ecology*, 44(3), 129-136. doi:10.1007/s101440200016
- Davison, A., Jackson, H. J., Murphy, E. W., & Reader, T. (2019b). Discrete or indiscrete? Redefining the colour polymorphism of the land snail *Cepaea nemoralis*. *Heredity*, 123, 162-175. doi:10.1038/s41437-019-0189-z
- Davison, A., & Neiman, M. (2020). Mobilising molluscan models and genomes in biology.
- de Andrade Martins, R., & Silva, C. C. (2001). Newton and colour: the complex interplay of theory and experiment. In *Science Education and Culture* (pp. 273-291): Springer.
- Delhey, K., Delhey, V., Kempenaers, B., & Peters, A. (2015). A practical framework to analyze variation in animal colors using visual models. *Behavioral Ecology*, 26(2), 367-375. doi:10.1093/beheco/aru198
- Delhey, K., & Peters, A. (2017). Conservation implications of anthropogenic impacts on visual communication and camouflage. *Conservation Biology*, 31(1), 30-39.

- Diniz-Filho, J. A., Soares, T. N., Lima, J. S., Dobrovolski, R., Landeiro, V. L., de Campos Telles, M. P., . . . Bini, L. M. (2013). Mantel test in population genetics. *Genet Mol Biol*, 36(4), 475-485. doi:10.1590/s1415-47572013000400002
- Dobzhansky, T., & Dobzhansky, T. G. (1970). *Genetics of the evolutionary process* (Vol. 139): Columbia University Press.
- Du, X., Liu, L., Wang, X., Ni, G., Zhang, J., Hao, R., . . . Liu, Y. (2019). Automatic classification of cells in microscopic fecal images using convolutional neural networks. *Bioscience reports*, 39(4), BSR20182100. doi:10.1042/BSR20182100
- Dussex, N., Alberti, F., Heino, M. T., Olsen, R.-A., van der Valk, T., Ryman, N., . . . Askeyev, O. V. (2020). Moose genomes reveal past glacial demography and the origin of modern lineages. *Bmc Genomics*, 21(1), 1-13.
- Egorov, R., & Sverlova, N. G. (2021). Shell colour and banding polymorphism in *Cepaea nemoralis* (Gastropoda, Pulmonata, Helicidae) from the Moscow region. *Ruthenica*, 31, 27-38.
- Ellis, D. (2004). *Evolutionary genetics of the land snail Cepaea nemoralis in the Central Pyrenees*: University of London, University College London (United Kingdom).
- Endler, J. A. (1987). Predation, light intensity and courtship behaviour in *Poecilia reticulata* (Pisces: Poeciliidae). *Animal Behaviour*, 35(5), 1376-1385.
- Endler, J. A. (1990). On the measurement and classification of colour in studies of animal colour patterns. *Biological Journal of the Linnean Society*, 41(4), 315-352.
- Erlichman, J. S., Coates, E., & Leiter, J. (1994). Carbonic anhydrase and CO₂ chemoreception in the pulmonate snail *Helix aspersa*. *Respiration physiology*, 98(1), 27-41.
- Ernst, A. (1936). Further investigations on the phenological analysis, the fertility problem and the genetics of *Heterostylyc Primroses. Primula hortensis. Wettst. Arch. J. K.-Stift. Ver. Sozialanthropol. Ras.* 11, 1-280.
- Fisher, R. A. (1921). On the "Probable Error" of a coefficient of correlation deduced from a small sample. *Metron*, 1, 3-32.
- Fisher, R. A. (1930). *The genetical theory of natural selection. Clarendon Press, Oxford.*
- Fisher, R. A., & Diver, C. (1934). Crossing-over in the Land Snail *Cepaea nemoralis*, L. *Nature*, 133(3370), 834-835. doi:10.1038/133834b0
- Fisher, R. A., Ford, E. B. (1947). The Spread of a Gene in Natural Conditions in a Colony of the Moth *Panaxia Dominula L.*
- Ford, E. (1971). Captain Cyril Diver (1892-1969). A Memoir. In: JSTOR.
- Ford, E. B. (1975). *Ecological Genetics. Chapman and Hall, London, 4th ed, Chap. 7.*
- Franks, D. W., & Oxford, G. S. (2009). The evolution of exuberant visible polymorphisms. *Evolution*, 63(10), 2697-2706. doi:10.1111/j.1558-5646.2009.00748.x
- Funk, D. J., & Omland, K. E. (2003). Species-level paraphyly and polyphyly: frequency, causes, and consequences, with insights from animal mitochondrial DNA. *Annual Review of Ecology, Evolution, and Systematics*, 34(1), 397-423.
- Gage, S. H., Davey Smith, G., Ware, J. J., Flint, J., & Munafò, M. R. (2016). G = E: What GWAS Can Tell Us about the Environment. *PLoS Genet*, 12(2), e1005765. doi:10.1371/journal.pgen.1005765
- Galeotti, P., Rubolini, D., Dunn, P. O., & Fasola, M. (2003). Colour polymorphism in birds: causes and functions. *Journal of evolutionary biology*, 16(4), 635-646.

- García-Ruiz, J. M. (2015). Geo-ecological effects of Global Change in the Central Spanish Pyrenees: A review at different spatial and temporal scales. In T. L. M. J. I. López-Moreno, S. M. Vicente Serrano, P. González-Sampériz, B. L. Valero-Garcés, Y. Sanjuán, S. Beguería, E. Nadal-Romero, N. Lana-Renault, & A. (Ed.). CSIC - Instituto Pirenaico de Ecología (IPE): CSIC - Instituto Pirenaico de Ecología (IPE).
- Garrido-Ramos, M. A., Stewart, D. T., Sutherland, B. W., & Zouros, E. (1998). The distribution of male-transmitted and female-transmitted mitochondrial DNA types in somatic tissues of blue mussels: implications for the operation of doubly uniparental inheritance of mitochondrial DNA. *Genome*, 41(6), 818-824.
- Garvin, M. R., Thorgaard, G. H., & Narum, S. R. (2015). Differential expression of genes that control respiration contribute to thermal adaptation in redband trout (*Oncorhynchus mykiss gairdneri*). *Genome biology and evolution*, 7(6), 1404-1414.
- Germer, T. A., Zwinkels, J. C., & Tsai, B. K. (2014). *Spectrophotometry: Accurate measurement of optical properties of materials*: Elsevier.
- Girshick, R. (2015). *Fast r-cnn*. Paper presented at the Proceedings of the IEEE international conference on computer vision.
- Gonzalez, D. R., Aramendia, A. C., & Davison, A. (2019). Recombination within the *Cepaea nemoralis* supergene is confounded by incomplete penetrance and epistasis. *Heredity*. doi:10.1038/s41437-019-0190-6
- Goodhart, C. B. (1963). Area effect and non-adaptive variation between populations of *Cepaea (Mollusca)*. *Heredity*, 18(4), 459-&. doi:10.1038/hdy.1963.51
- Goutte, C., & Gaussier, E. (2005). *A probabilistic interpretation of precision, recall and F-score, with implication for evaluation*. Paper presented at the European conference on information retrieval.
- Grace, P. B., & Teale, P. (2006). Purification of the crude solution from *Helix pomatia* for use as β -glucuronidase and aryl sulfatase in phytoestrogen assays. *Journal of Chromatography B*, 832(1), 158-161.
- Grindon, A. J., & Davison, A. (2013a). Irish *Cepaea nemoralis* land snails have a cryptic Franco-Iberian origin that is most easily explained by the movements of Mesolithic humans. *Plos One*, 8(6). doi:10.1371/journal.pone.0065792
- Grindon, A. J., & Davison, A. (2013b). Irish *Cepaea nemoralis* land snails have a cryptic Franco-Iberian origin that is most easily explained by the movements of Mesolithic humans. *PloS One*, 8(6), e65792. doi:10.1371/journal.pone.0065792
- Guiller, A., & Madec, L. (1993). A contribution to the study of morphological and biochemical differentiation in French and Iberian populations of *Cepaea-nemoralis*. *Biochemical Systematics and Ecology*, 21(3), 323-339. doi:10.1016/0305-1978(93)90024-l
- Guo, Y., Zhang, Y., Liu, Q., Huang, Y., Mao, G., Yue, Z., . . . Li, S. (2019). A chromosomal-level genome assembly for the giant African snail *Achatina fulica*. *GigaScience*, 8(10), giz124.
- Gutiérrez-Zugasti, I. (2011). *Early Holocene land snail exploitation in northern Spain: the case of La Fragua cave (Cantabria, Spain)* (Vol. 16).
- Harvey, M. (2018). Using iRecord to support site-based recording. *Conservation Land Management*, 16(4), 25-29.
- Heller, J. (1981). Visual versus climatic selection of shell banding in the landsnail *Theba pisana* in Israel. *Journal of Zoology*, 194(1), 85-101.

- Hendricks, S., Anderson, E. C., Antao, T., Bernatchez, L., Forester, B. R., Garner, B., . . . Koop, B. (2018). Recent advances in conservation and population genomics data analysis. *Evolutionary Applications*, 11(8), 1197-1211.
- Herrel, A., Joly, D., & Danchin, E. (2020). Epigenetics in ecology and evolution. *Functional Ecology*, 34(2), 381-384.
- Hirano, T., Saito, T., Tsunamoto, Y., Koseki, J., Ye, B., Miura, O., . . . Chiba, S. (2019). Enigmatic incongruence between mtDNA and nDNA revealed by multi-locus phylogenomic analyses in freshwater snails. *Scientific reports*, 9(1), 1-13.
- Hoban, S., Kelley, J. L., Lotterhos, K. E., Antolin, M. F., Bradburd, G., Lowry, D. B., . . . Whitlock, M. C. (2016). Finding the genomic basis of local adaptation: pitfalls, practical solutions, and future directions. *The American Naturalist*, 188(4), 379-397.
- Hohenlohe, P. A., Hand, B. K., Andrews, K. R., & Luikart, G. (2018). Population genomics provides key insights in ecology and evolution. In *Population Genomics* (pp. 483-510): Springer.
- Holmes, I. A., Grundler, M. R., & Rabosky, A. R. D. (2017). Predator Perspective Drives Geographic Variation in Frequency-Dependent Polymorphism. *The American Naturalist*, 190(4), E78-E93. doi:10.1086/693159
- Horn, G., Aodha, O., Song, Y., Cui, Y., Sun, C., Shepard, A., . . . Belongie, S. (2018). The iNaturalist species classification and detection dataset. In (pp. pp. 8769-8778): Proceedings of the IEEE Conference on Computer Vision and Pattern Recognition (CVPR).
- Huang, H., & Knowles, L. L. (2014). Unforeseen consequences of excluding missing data from Next-generation sequences: Simulation study of RAD sequences. *Systematic Biology*, 65(3), 357-365. doi:10.1093/sysbio/syu046
- Huber, B., Whibley, A., Poul, Y. L., Navarro, N., Martin, A., Baxter, S., . . . Joron, M. (2015). Conservatism and novelty in the genetic architecture of adaptation in *Heliconius* butterflies. *Heredity (Edinb)*, 114(5), 515-524. doi:10.1038/hdy.2015.22
- Hunt, R. W. G. (2004). *The reproduction of color* (Vol. 6th Edition). Chichester UK: Wiley-*IS&T Series in Imaging Science and Technology*.
- Jari Oksanen, F., Friendly, M., Kindt, R., Legendre, P., McGlinn, D., Minchin, P. R., . . . Stevens, M. H. H. (2018). Vegan: community ecology package. *R package version*, 2(6).
- Johnson, C. W. (1906). On the distribution of *Helix hortensis* Mueller, in North America. *The Nautilus*, 20(7), 73-80.
- Johnson, M. S. (1976). Allozymes and area effects in *Cepaea-nemoralis* on Western Berkshire Downs. *Heredity*, 36(FEB), 105-121. doi:10.1038/hdy.1976.11
- Johnson, M. S. (2011). Thirty-four years of climatic selection in the land snail *Theba pisana*. *Heredity*, 106(5), 741-748. doi:10.1038/hdy.2010.114
- Jones, E. P., Eager, H. M., Gabriel, S. I., Jóhannesdóttir, F., & Searle, J. B. (2013). Genetic tracking of mice and other bioproxies to infer human history. *Trends in Genetics*, 29(5), 298-308.
- Jones, J. S., & Irving, A. J. (1975). Gene frequencies, genetic background and environment in Pyrenean populations of *Cepaea nemoralis* (L.). *Biological Journal of the Linnean Society*, 7(4), 249-259. doi:10.1111/j.1095-8312.1975.tb00228.x
- Jones, J. S., Leith, B. H., & Rawlings, P. (1977). Polymorphism in *Cepaea* - A problem with too many solutions. *Annual Review of Ecology and Systematics*, 8, 109-143. doi:10.1146/annurev.es.08.110177.000545

- Jones, R. T., Salazar, P. A., French-Constant, R. H., Jiggins, C. D., & Joron, M. (2012). Evolution of a mimicry supergene from a multilocus architecture. *Proc Biol Sci*, 279(1727), 316-325. doi:10.1098/rspb.2011.0882
- Jordaens, K., De Wolf, H., Van Houtte, N., Vandecasteele, B., & Backeljau, T. (2006). Genetic variation in two land snails, *Cepaea nemoralis* and *Succinea putris* (Gastropoda, Pulmonata), from sites differing in heavy metal content. *Genetica*, 128(1-3), 227-239. doi:10.1007/s10709-005-5705-9
- Jordaens, K., De Wolf, H., Vandecasteele, B., Blust, R., & Backeljau, T. (2006). Associations between shell strength, shell morphology and heavy metals in the land snail *Cepaea nemoralis* (Gastropoda, Helicidae). *Science of the Total Environment*, 363(1-3), 285-293. doi:10.1016/j.scitotenv.2005.12.002
- Joron, M., & Mallet, J. L. (1998). Diversity in mimicry: paradox or paradigm? *Trends in Ecology & Evolution*, 13(11), 461-466.
- Kajtoch, Ł., Davison, A., Grindon, A., Deli, T., Sramkó, G., Gwardjan, M., . . . Fehér, Z. (2017). Reconstructed historical distribution and phylogeography unravels non-steppic origin of *Caucasotachea vindobonensis* (Gastropoda: Helicidae). *Organisms Diversity & Evolution*. doi:10.1007/s13127-017-0337-3
- Kerkvliet, J., de Boer, T., Schilthuizen, M., & Kraaijeveld, K. (2017). Candidate genes for shell colour polymorphism in *Cepaea nemoralis*. *PeerJ*, 5. doi:10.7717/peerj.3715
- Kerstes, N. A. G., Breeschoten, T., Kalkman, V. J., & Schilthuizen, M. (2019). Snail shell colour evolution in urban heat islands detected via citizen science. *Communications Biology*, 2(1), 264. doi:10.1038/s42003-019-0511-6
- Kocot, K. M., Aguilera, F., McDougall, C., Jackson, D. J., & Degnan, B. M. (2016). Sea shell diversity and rapidly evolving secretomes: insights into the evolution of biomineralization. *Frontiers in Zoology*, 13(1), 23.
- Korf, I., Yandell, M., & Bedell, J. (2003). *Blast*. " O'Reilly Media, Inc."
- Kotlík, P., Marková, S., Konczal, M., Babik, W., & Searle, J. B. (2018). Genomics of end-Pleistocene population replacement in a small mammal. *Proceedings of the Royal Society B: Biological Sciences*, 285(1872), 20172624.
- Lamotte, M. (1951). Recherches sur la structure génétique des populations naturelles de *Cepaea nemoralis* (L.). *Bull Biol Fr Belg (Suppl)*, 35, 1-239.
- Lamotte, M. (1952). Influence de l'effectif des populations sur la diversité des fréquences du gène absence de bandes chez *Cepaea-nemoralis* L. *Comptes Rendus Hebdomadaires Des Seances De L Academie Des Sciences*, 235(15), 826-828.
- Lamotte, M. (1954). Sur le déterminisme génétique du polymorphisme, chez *Cepaea nemoralis*-L. *Comptes Rendus Hebdomadaires Des Seances De L Academie Des Sciences*, 239(4), 365-367.
- Lamotte, M. (1959). *Polymorphism of natural populations of Cepaea nemoralis*. Paper presented at the Cold Spring Harbor Symposia on Quantitative Biology.
- Le Luyer, J., Laporte, M., Beacham, T. D., Kaukinen, K. H., Withler, R. E., Leong, J. S., . . . Bernatchez, L. (2017). Parallel epigenetic modifications induced by hatchery rearing in a Pacific salmon. *Proceedings of the National Academy of Sciences*, 114(49), 12964-12969.
- Ledón-Rettig, C. C., Richards, C. L., & Martin, L. B. (2013). Epigenetics for behavioral ecologists. *Behavioral Ecology*, 24(2), 311-324.
- Lehtinen, R. M., Carlson, B. M., Hamm, A. R., Riley, A. G., Mullin, M. M., & Gray, W. J. (2020). Dispatches from the neighborhood watch: Using citizen science and field survey data to document color morph frequency in space and time.

- Leighton, G. R., Hugo, P. S., Roulin, A., & Amar, A. (2016). Just Google it: assessing the use of Google Images to describe geographical variation in visible traits of organisms. *Methods in Ecology and Evolution*, 7(9), 1060-1070.
- Li, H. (2011). A statistical framework for SNP calling, mutation discovery, association mapping and population genetical parameter estimation from sequencing data. *Bioinformatics*, 27(21), 2987-2993. doi:10.1093/bioinformatics/btr509
- Lim, W. K., & Mathuru, A. S. (2020). Design, challenges, and the potential of transcriptomics to understand social behavior. *Current Zoology*, 66(3), 321-330. doi:10.1093/cz/zoaa007
- Liu, C., Ren, Y., Li, Z., Hu, Q., Yin, L., Wang, H., . . . Xi, Y. (2021). Giant African snail genomes provide insights into molluscan whole-genome duplication and aquatic–terrestrial transition. *Molecular Ecology Resources*, 21(2), 478-494.
- Lubell, D. (2004). Are land snail a signature for the Mesolithic-Neolithic transition. *Documenta Praehistorica*, 31, 1-24.
- Lucena-Perez, M., Marmesat, E., Kleinman-Ruiz, D., Martínez-Cruz, B., Węcek, K., Saveljev, A. P., . . . Ozolins, J. (2020). Genomic patterns in the widespread Eurasian lynx shaped by Late Quaternary climatic fluctuations and anthropogenic impacts. *Molecular Ecology*, 29(4), 812-828.
- Maia, Eliason, C. M., Bitton, P. P., Doucet, S. M., & Shawkey, M. D. (2013). pavo: an R package for the analysis, visualization and organization of spectral data. *Methods in Ecology and Evolution*, 4(10), 906-913. doi:10.1111/2041-210x.12069
- Maia, Gruson, H., Endler, J. A., & White, T. E. (2018). pavo 2.0: new tools for the spectral and spatial analysis of colour in R. *bioRxiv*, 427658. doi:10.1101/427658
- Mann, K., & Jackson, D. J. (2014). Characterization of the pigmented shell-forming proteome of the common grove snail *Cepaea nemoralis*. *Bmc Genomics*, 15. doi:10.1186/1471-2164-15-249
- Manolio, T. A., Collins, F. S., Cox, N. J., Goldstein, D. B., Hindorff, L. A., Hunter, D. J., . . . Chakravarti, A. (2009). Finding the missing heritability of complex diseases. *Nature*, 461(7265), 747-753.
- Martin, S. H., Dasmahapatra, K. K., Nadeau, N. J., Salazar, C., Walters, J. R., Simpson, F., . . . Jiggins, C. D. (2013). Genome-wide evidence for speciation with gene flow in *Heliconius* butterflies. *Genome research*, 23(11), 1817-1828.
- Masel, J. (2011). Genetic drift. *Current Biology*, 21(20), R837-R838.
- Mazon, L. I., Depancorbo, M. A. M., Vicario, A., Aguirre, A. I., Estomba, A., & Lostao, C. M. (1987). Distribution of *Cepaea-nemoralis* according to climatic regions in Spain. *Heredity*, 58, 145-154. doi:10.1038/hdy.1987.19
- McDevitt, A., Vega, R., Rambau, R. V., Yannic, G., Herman, J. S., Hayden, T., & Searle, J. B. (2011). Colonization of Ireland: revisiting ‘the pygmy shrew syndrome’ using mitochondrial, Y chromosomal and microsatellite markers. *Heredity*, 107(6), 548-557.
- McDevitt, A. D., Coscia, I., Browett, S. S., Ruiz-González, A., Statham, M. J., Ruczyńska, I., . . . Norén, K. (2020). Next-generation phylogeography resolves post-glacial colonization patterns in a widespread carnivore, the red fox (*Vulpes vulpes*), in Europe. *bioRxiv*.

- McKinnon, J. S., & Pierotti, M. E. (2010). Colour polymorphism and correlated characters: genetic mechanisms and evolution. *Molecular Ecology*, *19*(23), 5101-5125.
- McLean, C. A., & Stuart-Fox, D. (2014). Geographic variation in animal colour polymorphisms and its role in speciation. *Biological Reviews*, *89*(4), 860-873.
- McMillen, D., & McMillen, M. D. (2013). Package 'McSpatial'. *Nonparametric Spatial Data Analysis*. August, 4.
- Miura, O., Urabe, M., Mori, H., & Chiba, S. (2020). Ancient drainage networks mediated a large-scale genetic introgression in the East Asian freshwater snails. *Ecology and Evolution*, *10*(15), 8186-8196.
- Müller, F. (1879). *Ituna* and *Thyridia*: a remarkable case of mimicry in butterflies. *Trans. Entomol. Soc. Lond*, 1879, 20-29.
- Murray, J., & Clarke, B. (1978). Changes of gene frequency in *Cepaea-nemoralis* over 50 years. *Malacologia*, *17*(2), 317-330.
- Narum, S. R., & Hess, J. E. (2011). Comparison of FST outlier tests for SNP loci under selection. *Molecular Ecology Resources*, *11*, 184-194.
- Neiber, M. T., & Hausdorf, B. (2015). Molecular phylogeny reveals the polyphyly of the snail genus *Cepaea* (Gastropoda: Helicidae). *Mol Phylogenet Evol*, *93*, 143-149.
- Neiber, M. T., Sagorny, C., & Hausdorf, B. (2016). Increasing the number of molecular markers resolves the phylogenetic relationship of 'Cepaea' vindobonensis (Pfeiffer 1828) with Caucasotachea Boettger 1909 (Gastropoda: Pulmonata: Helicidae). *Journal of Zoological Systematics and Evolutionary Research*, *54*(1), 40-45. doi:10.1111/jzs.12116
- Nichols, R. (2001). Gene trees and species trees are not the same. *Trends in Ecology & Evolution*, *16*(7), 358-364.
- Notten, M. J. M., Oosthoek, A., Rozema, J., & Aerts, R. (2006a). The landsnail *Cepaea nemoralis* regulates internal Cd levels when fed on Cd-enriched stinging nettle (*Urtica dioica*) leaves at low, field-relevant concentrations. *Environmental Pollution*, *139*(2), 296-305. doi:10.1016/j.envpol.2005.05.007
- Notten, M. J. M., Oosthoek, A. J. P., Rozema, J., & Aerts, R. (2006b). Heavy metal pollution affects consumption and reproduction of the landsnail *Cepaea nemoralis* fed on naturally polluted *Urtica dioica* leaves. *Ecotoxicology*, *15*(3), 295-304. doi:10.1007/s10646-006-0059-3
- Ochman, H., Jones, J. S., & Selander, R. K. (1983). Molecular area effects in *Cepaea*. *Proceedings of the National Academy of Sciences of the United States of America-Biological Sciences*, *80*(13), 4189-4193. doi:10.1073/pnas.80.13.4189
- Orstan, A., Sparks, J. L., & Pearce, T. A. (2011). Wayne Grimm's legacy: A 40-year experiment on the dispersal of *Cepaea nemoralis* in Frederick County, Maryland. *American Malacological Bulletin*, *29*(1-2), 139-142.
- Ott, J. (1999). *Analysis of human genetic linkage*: JHU Press.
- Ovchinnikova, K., Kovalev, V., Stuart, L., & Alexandrov, T. (2020). OffsampleAI: artificial intelligence approach to recognize off-sample mass spectrometry images. *BMC Bioinformatics*, *21*(1), 11. doi:10.1186/s12859-020-3425-x
- Ozgo, M., & Bogucki, Z. (2011). Colonization, stability, and adaptation in a transplant experiment of the polymorphic land snail *Cepaea nemoralis* (Gastropoda: Pulmonata) at the edge of its geographical range. *Biological Journal of the Linnean Society*, *104*(2), 462-470. doi:10.1111/j.1095-8312.2011.01732.x

- Ożgo, M., Cameron, R. A. D., Horsák, M., Pokryszko, B., Chudaś, M., Cichy, A., . . . Żołądek, J. (2019). *Cepaea nemoralis* (Gastropoda: Pulmonata) in Poland: patterns of variation in a range-expanding species. *Biological Journal of the Linnean Society*, 127(1), 1-11. doi:10.1093/biolinnean/blz029
- Ożgo, M., Liew, T. S., Webster, N. B., & Schilthuizen, M. (2017). Inferring microevolution from museum collections and resampling: lessons learned from *Cepaea*. *PeerJ*, 5, e3938-e3938. doi:10.7717/peerj.3938
- Ożgo, M., & Schilthuizen, M. (2012). Evolutionary change in *Cepaea nemoralis* shell colour over 43 years. *Global Change Biology*, 18(1), 74-81. doi:10.1111/j.1365-2486.2011.02514.x
- Pardo-Diaz, C., Salazar, C., Baxter, S. W., Merot, C., Figueiredo-Ready, W., Joron, M., . . . Jiggins, C. D. (2012). Adaptive introgression across species boundaries in *Heliconius* butterflies. *PLoS Genet*, 8(6), e1002752.
- Parmakelis, A., Kotsakiozi, P., & Rand, D. (2013). Animal mitochondria, positive selection and cyto-nuclear coevolution: insights from pulmonates. *Plos One*, 8(4), e61970.
- Patterson, N., Moorjani, P., Luo, Y., Mallick, S., Rohland, N., Zhan, Y., . . . Reich, D. (2012). Ancient admixture in human history. *Genetics*, 192(3), 1065-1093.
- Paulson, D. R. (1973). Predator polymorphism and apostatic selection. *Evolution*, 269-277.
- Pearce, T. A., & Olori, J. C. (2004). *Land snails from St. Elzéar Cave, Gaspé Peninsula, Quebec: antiquity of Cepaea hortensis in North America*. Paper presented at the American Malacological Society, Sannibel
- Petr, M., Vernot, B., & Kelso, J. (2019). admixr—R package for reproducible analyses using ADMIXTOOLS. *Bioinformatics*, 35(17), 3194-3195. doi:10.1093/bioinformatics/btz030
- Pocock, M. J., Newson, S. E., Henderson, I. G., Peyton, J., Sutherland, W. J., Noble, D. G., . . . Brereton, T. (2015). Developing and enhancing biodiversity monitoring programmes: a collaborative assessment of priorities. *Journal of Applied Ecology*, 52(3), 686-695.
- Poelstra, J. W., Vijay, N., Bossu, C. M., Lantz, H., Ryll, B., Müller, I., . . . Grabherr, M. G. (2014). The genomic landscape underlying phenotypic integrity in the face of gene flow in crows. *Science*, 344(6190), 1410-1414.
- Pratlong, M., Haguénauer, A., Chabrol, O., Klopp, C., Pontarotti, P., & Aurelle, D. (2015). The red coral (*Corallium rubrum*) transcriptome: a new resource for population genetics and local adaptation studies. *Molecular Ecology Resources*, 15(5), 1205-1215.
- Proćków, M., Proćków, J., Błażej, P., & Mackiewicz, P. (2018). The influence of habitat preferences on shell morphology in ecophenotypes of *Trochulus hispidus* complex. *Science of the Total Environment*, 630, 1036-1043.
- Purcell, S., Neale, B., Todd-Brown, K., Thomas, L., Ferreira, M. A., Bender, D., . . . Sham, P. C. (2007). PLINK: a tool set for whole-genome association and population-based linkage analyses. *Am J Hum Genet*, 81(3), 559-575. doi:10.1086/519795
- Rajora, O. P. (2019). *Population genomics: concepts, approaches and applications*: Springer.
- Ramos, M. A. (1984). Polymorphism of *Cepaea nemoralis* (Gastropoda, Helicidae) in the Spanish occidental Pyrenees. *Malacologia*, 25(2), 325-341.
- Ravinet, M., Elgvin, T. O., Trier, C., Aliabadian, M., Gavrillov, A., & Sætre, G.-P. (2018). Signatures of human-commensalism in the *house sparrow* genome.

- Proceedings of the Royal Society B: Biological Sciences*, 285(1884), 20181246.
- Ren, S., He, K., Girshick, R., & Sun, J. (2015). Faster R-CNN: Towards Real-Time Object Detection with Region Proposal Networks. *IEEE Transactions on Pattern Analysis and Machine Intelligence*, 39. doi:10.1109/TPAMI.2016.2577031
- Rice, A. M., Rudh, A., Ellegren, H., & Qvarnström, A. (2011). A guide to the genomics of ecological speciation in natural animal populations. *Ecology letters*, 14(1), 9-18.
- Richards, A. V., & Murray, J. (1975). Relation of phenotype to habitat in an introduced colony of *Cepaea-nemoralis*. *Heredity*, 34(FEB), 128-131. doi:10.1038/hdy.1975.13
- Richards, P. M., Liu, M. M., Lowe, N., Davey, J. W., Blaxter, M. L., & Davison, A. (2013). RAD-Seq derived markers flank the shell colour and banding loci of the *Cepaea nemoralis* supergene. *Molecular Ecology*, 22(11), 3077-3089. doi:10.1111/mec.12262
- Richardson, A. M. M. (1974). Differential climatic selection in natural population of land snail *Cepaea nemoralis*. *Nature*, 247(5442), 572-573. doi:10.1038/247572a0
- Riesch, H., & Potter, C. (2014). Citizen science as seen by scientists: Methodological, epistemological and ethical dimensions. *Public understanding of science*, 23(1), 107-120.
- Robinson, N. A., Johnsen, H., Moghadam, H., Andersen, Ø., & Tveiten, H. (2019). Early developmental stress affects subsequent gene expression response to an acute stress in Atlantic salmon: An approach for creating robust fish for aquaculture? *G3: Genes, Genomes, Genetics*, 9(5), 1597-1611.
- Rohwer, S. (1990). Foraging differences between white and dark morphs of the Pacific Reef Heron *Egretta sacra*. *Ibis*, 132(1), 21-26.
- Roodi, M., Lak, Z., & Moshovos, A. (2019). *BWA-MEM performance: Suffix array storage size*. Paper presented at the 2019 IEEE EMBS International Conference on Biomedical & Health Informatics (BHI).
- Rubin, B. E., Ree, R. H., & Moreau, C. S. (2012). Inferring phylogenies from RAD sequence data. *Plos One*, 7(4), e33394.
- Russello, M. A., Waterhouse, M. D., Etter, P. D., & Johnson, E. A. (2015). From promise to practice: pairing non-invasive sampling with genomics in conservation. *Peerj*, 3, e1106. doi:10.7717/peerj.1106
- Saenko, S. V., Groenenberg, D. S. J., Davison, A., & Schilthuizen, M. (2020). The draft genome sequence of the grove snail *Cepaea nemoralis*. *in review*.
- San-Jose, L. M., & Roulin, A. (2017). Genomics of coloration in natural animal populations. *Philosophical Transactions of the Royal Society B: Biological Sciences*, 372(1724), 20160337.
- Sanchez, T., Cury, J., Charpiat, G., & Jay, F. (2020). Deep learning for population size history inference: Design, comparison and combination with approximate Bayesian computation. *Molecular Ecology Resources*, 16. doi:10.1111/1755-0998.13224
- Scheil, Gärtner, U., & Köhler, H.-R. (2012a). Colour polymorphism and thermal capacities in *Theba pisana* (O.F. Müller 1774). *Journal of Thermal Biology*, 37(6), 462-467. doi:<https://doi.org/10.1016/j.jtherbio.2012.03.006>
- Scheil, A. E., Gärtner, U., & Köhler, H.-R. (2012b). Colour polymorphism and thermal capacities in *Theba pisana* (Müller 1774). *Journal of Thermal Biology*, 37(6), 462-467.

- Schneider, S., Taylor, G., & Kremer, S. (2018). *Deep Learning object detection methods for ecological camera trap data*.
- Scrucca, L., Fop, M., Murphy, T. B., & Raftery, A. E. (2016). mclust 5: Clustering, classification and density estimation using Gaussian Finite Mixture models. *R Journal*, 8(1), 289-317.
- Searle, J. B., Kotlik, P., Rambau, R. V., Markova, S., Herman, J. S., & McDevitt, A. D. (2009). The Celtic fringe of Britain: insights from small mammal phylogeography. *Proceedings of the Royal Society B: Biological Sciences*, 276(1677), 4287-4294.
- Silvertown, J., Cook, L., Cameron, R., Dodd, M., McConway, K., Worthington, J., . . . Juan, X. (2011). Citizen science reveals unexpected continental-scale evolutionary change in a model organism. *Plos One*, 6(4). doi:10.1371/journal.pone.0018927
- Smith, T., & Guild, J. (1931). The C.I.E. colorimetric standards and their use. *Transactions of the Optical Society*, 33(3), 73-134. doi:10.1088/1475-4878/33/3/301
- Stahlke, A., Bell, D., Dhendup, T., Kern, B., Pannoni, S., Robinson, Z., . . . Hohenlohe, P. A. (2020). Population Genomics Training for the Next Generation of Conservation Geneticists: ConGen 2018 Workshop. *Journal of Heredity*, 111(2), 227-236.
- Stamatakis, A. (2014). RAxML version 8: a tool for phylogenetic analysis and post-analysis of large phylogenies. *Bioinformatics*, 30(9), 1312-1313. doi:10.1093/bioinformatics/btu033
- Stange, M., Barrett, R. D. H., & Hendry, A. P. (2020). The importance of genomic variation for biodiversity, ecosystems and people. *Nature reviews genetics*. doi:10.1038/s41576-020-00288-7
- Staples-Browne, R. (1908). *On the inheritance of colour in domestic pigeons, with special reference to reversion*. Paper presented at the Proceedings of the Zoological Society of London.
- Star, B., & Spencer, H. G. (2013). Effects of genetic drift and gene flow on the selective maintenance of genetic variation. *Genetics*, 194(1), 235-244. doi:10.1534/genetics.113.149781
- Stuart-Fox, D., Newton, E., Mulder, R. A., D'Alba, L., Shawkey, M. D., & Iqic, B. (2018). The microstructure of white feathers predicts their visible and near-infrared reflectance properties. *Plos One*, 13(7). doi:10.1371/journal.pone.0199129
- Surmacki, A., Ozarowska-Nowicka, A., & Rosin, Z. M. (2013). Color polymorphism in a land snail *Cepaea nemoralis* (Pulmonata: Helicidae) as viewed by potential avian predators. *Naturwissenschaften*, 100(6), 533-540. doi:10.1007/s00114-013-1049-y
- Svensson, E. I. (2017). Back to basics: using colour polymorphisms to study evolutionary processes. *Molecular Ecology*, 26(8), 2204-2211.
- Terrett, J. A., Miles, S., & Thomas, R. H. (1996). Complete DNA sequence of the mitochondrial genome of *Cepaea nemoralis* (Gastropoda: Pulmonata). *Journal of Molecular Evolution*, 42(2), 160-168. doi:10.1007/BF02198842
- Thomaz, D., Guiller, A., & Clarke, B. C. (1996). Extreme divergence of mitochondrial DNA within species of pulmonate land snails. *Proceedings of the Royal Society of London. Series B: Biological Sciences*, 263(1368), 363-368.
- Torada, L., Lorenzon, L., Beddis, A., Isildak, U., Pattini, L., Mathieson, S., & Fumagalli, M. (2019). ImaGene: a convolutional neural network to quantify natural

- selection from genomic data. *BMC Bioinformatics*, 20, 12. doi:10.1186/s12859-019-2927-x
- Valdez, M., Kassem, I., & Lamotte, M. (1988). Geographic-variation of enzyme polymorphism in populations of *Cepaea-nemoralis* from the French Pyrenees. *Genetics Selection Evolution*, 20(4), 441-459. doi:10.1051/gse:19880405
- van den Berg, C. P., Troscianko, J., Endler, J. A., Marshall, N. J., & Cheney, K. L. (2020). Quantitative Colour Pattern Analysis (QCPA): A comprehensive framework for the analysis of colour patterns in nature. *Methods in Ecology and Evolution*, 11(2), 316-332.
- Wade, M. (2008). Evolutionary genetics. *The Stanford Encyclopedia of Philosophy (Fall 2008 Edition)*, Edward N. Zalta (ed.).
- Wagner, C. E., Keller, I., Wittwer, S., Selz, O. M., Mwaiko, S., Greuter, L., . . . Seehausen, O. (2013). Genome-wide RAD sequence data provide unprecedented resolution of species boundaries and relationships in the Lake Victoria cichlid adaptive radiation. *Molecular Ecology*, 22(3), 787-798.
- Walker, D. (2003). JMASM9: Converting Kendall's Tau for correlational or meta-analytic analyses. *Journal of Modern Applied Statistical Methods*, 2, 525-530. doi:10.22237/jmasm/1067646360
- Wang, X., Liu, Z., & Wu, W. (2017). Transcriptome analysis of the freshwater pearl mussel (*Cristaria plicata*) mantle unravels genes involved in the formation of shell and pearl. *Molecular genetics and genomics*, 292(2), 343-352.
- Webb, S. (2018). Deep learning for biology. *Nature*, 554(7693).
- Wellenreuther, M., Svensson, E. I., & Hansson, B. (2014). Sexual selection and genetic colour polymorphisms in animals. *Molecular Ecology*, 23(22), 5398-5414. doi:10.1111/mec.12935
- West, M. A., Kim, K., Kliebenstein, D. J., Van Leeuwen, H., Michelmore, R. W., Doerge, R., & Clair, D. A. S. (2007). Global eQTL mapping reveals the complex genetic architecture of transcript-level variation in Arabidopsis. *Genetics*, 175(3), 1441-1450.
- Westland, W., Ripamonti, C., & Cheung, V. (2012). Computing CIE Tristimulus Values. In *Computational Colour Science using MATLAB* (pp. 27-47): Wiley.
- Westram, A. M., Rafajlović, M., Chaube, P., Faria, R., Larsson, T., Panova, M., . . . Johannesson, K. (2018). Clines on the seashore: The genomic architecture underlying rapid divergence in the face of gene flow. *Evolution letters*, 2(4), 297-309.
- Wheldale, M. (1907). The inheritance of flower colour in *Antirrhinum majus*. *Proceedings of the Royal Society of London. Series B, Containing Papers of a Biological Character*, 79(532), 288-305.
- Williams, S. T. (2017). Molluscan shell colour. *Biological Reviews*, 92(2), 1039-1058.
- Wilson, I. F. (1996). Application of ecological genetics techniques to test for selection by habitat on allozymes in *Cepaea nemoralis* (L). *Heredity*, 77, 324-335.
- Wolda, H. (1969). Genetics of polymorphism in the land snail, *Cepaea nemoralis*. *Genetica*, 40(1), 475-502. doi:10.1007/bf01787373
- Worthington, J. P., Silvertown, J., Cook, L., Cameron, R., Dodd, M., Greenwood, R. M., . . . Skelton, P. (2012). Evolution MegaLab: a case study in citizen science methods. *Methods in Ecology and Evolution*, 3(2), 303-309. doi:10.1111/j.2041-210X.2011.00164.x
- Wright, S. (1937). The distribution of gene frequencies in populations. *Proc Natl Acad Sci U S A*, 23(6), 307-320. doi:10.1073/pnas.23.6.307

- Wright, S. (1948). On the roles of directed and random changes in gene frequency in the genetics of populations. *Evolution*, 279-294.
- Yamazaki, N., Ueshima, R., Terrett, J. A., Yokobori, S.-i., Kaifu, M., Segawa, R., . . . Thomas, R. H. (1997). Evolution of Pulmonate Gastropod Mitochondrial Genomes: Comparisons of Gene Organizations of *Euhadra*, *Cepaea* and *Albinaria* and Implications of Unusual tRNA Secondary Structures. *Genetics*, 145(3), 749.
- Zeuss, D., Brandl, R., Brändle, M., Rahbek, C., & Brunzel, S. (2014). Global warming favours light-coloured insects in Europe. *Nature Communications*, 5(1), 1-9.
- Zhang, J. K., Hu, H. G., Chen, S. Y., Huang, Y. J., Guan, Q., & Ieee. (2016). Cancer cells detection in phase-contrast microscopy images based on Faster R-CNN. In *Proceedings of 2016 9th International Symposium on Computational Intelligence and Design* (pp. 363-367).
- Zhao, R., Li, C., Ye, S., & Fang, X. (2019). Butterfly recognition based on Faster R-CNN. *Journal of Physics: Conference Series*, 1176, 032048. doi:10.1088/1742-6596/1176/3/032048

Supporting information

Chapter 2:

Table S2.1: Summary of the parental information of *C. nemoralis* crosses used in this chapter. Location and phenotypes of colour, banding and pigmentation are specified.

Table S2.2: Summary of the *C. nemoralis* crosses offspring. The offspring is classified by their shell colour, banding and pigmentation phenotype.

Table S2.3: Summary of the genotyping results for each cross. Each cross contains the restriction enzyme used and the genotype outcome of each individual in the restriction enzymatic assay.

Table S2.4: A comparison of the genotype and phenotype results in each cross. Shells with a phenotype that may be due to a potential recombination event in parent are shown in bold.

Supplementary Material: Copies of letters between Fisher and Diver in the archive of Bryan Clarke can be found in the supplementary information of Gonzalez, D.R., Aramendia, A.C. & Davison, A. Recombination within the *Cepaea nemoralis* supergene is confounded by incomplete penetrance and epistasis. *Heredity* 123, 153–161 (2019). <https://doi.org/10.1038/s41437-019-0190-6>.

Table S2.1. Summary of parent phenotypes and location from *C. nemoralis* crosses

Cross	Parent			Source
	phenotype			
1	P O	Y M	Wye Valley, Derbyshire	Marlborough Downs, Wiltshire/ Slieve Carron, Ireland
	C100	C101		
2	P O	Y M	Marlborough Downs, Wiltshire/ Slieve Carron, Ireland	Marlborough Downs, Wiltshire/ Slieve Carron, Ireland
	C102	C103		
3	P O	Y M	Marlborough Downs, Wiltshire/ Slieve Carron, Ireland	Marlborough Downs, Wiltshire/ Slieve Carron, Ireland
	C104	C105		
4	P O	Y B	Nottingham	Esles, Spain
	C110	C111		
5	P O	Y B (12345)	Nottingham	Esles, Spain
	C112	C113		
6	P O	Y B	San Roque, Spain	Esles, Spain
	C114	C115		
7	P M	Y M	Offspring of C101 × C102	Offspring of C104 × C105
	C119	C118		
8	P O L	Y M L	San Roque, Spain	San Roque, Spain
	C108	C109		
9	P M N	Y B H	Offspring of C108 × C109	Nottingham
	C116	C120		
10	Inbreeding	P M N	Y B N	Offspring of C116 × C120
		C450	C449	
11	Inbreeding	P M N	Y B N	Offspring of C116 × C120
		C451	C452	
12	Inbreeding	P M N	Y B N	Offspring of C116 × C120
		C662	C665	
13	Inbreeding	P M N	Y B H	Offspring of C451 × C452
		C825	C841	
14		Y B S	Y O	UK
		C568	C569	

Table S2.2. Summary of offspring phenotypes from *C. nemoralis* crosses

Cross	number	Offspring						
		phenotype						
1		P M	Y O					
	103	56	47					
2		P O	Y M	Y O				
	43	20	20	3				
3		P O	Y M					
	46	27	19					
4		P B	Y O					
	27	17	10					
5		P B (00345)	P B (12345)	P B (02345)	Y O	P M		
	109	27	12	16	53	1		
6		P O	Y B	Y M				
	34	18	8	8				
7		P M	Y M					
	75	37	38					
8		P M L	Y O L	Y O A	P O L			
	50	26	11	12	1			
9		P M N	P B N	Y M N	Y B N			
	16	4	4	3	5			
10		P M N	P B N	Y M N	Y B N	Y M H	Y B H	
	12	5	2	2	1	2	0	
11		P M N	P B N	Y M N	Y B N	Y M H	Y B H	P M H
	116	34	28	12	22	10	6	4
12		P M N	P B N	Y M N	Y B N	Y M H	Y B H	P M H
	146	39	46	7	19	15	12	8
13		P M N	P B N	Y M N	Y B N	Y M H	Y B H	P M H
	63	14	18	0	0	20	9	2
14		Y B S	Y O					
	44	28	16					
Total	884							

Phenotypes that may be due to a recombination event in a parent are highlighted in bold. Inferred genotypes of offspring are detailed in Supplementary Table 1. Key: P pink, Y yellow, O unbanded, M mid-banded, B all other banding patterns; N normal band pigmentation; H hyalozonate banding (nearly always with white lip—see text); S spread-banding; L normal lip pigmentation; A albolabiate (white lip). Cross 5 also showed segregation for another one or two band-suppressing loci, T and X, so the detailed banding notation is also shown.

Table 2.3. Results of genotyping for each cross, including details of restriction enzyme assay.

Cross 100x101 used Rad11 (BstUI), Ra06(Ddel) and Rad09(BstUI).

Cross:	100x101 Phenotype Genotype				Recombination	100x101 Phenotype Genotype				Recombination	100x101 Phenotype Genotype				Recombination
	ID	RAD11	RAD06	RAD09		ID	RAD11	RAD06	RAD09		ID	RAD11	RAD06	RAD09	
Parent 1	100 P O	Aa	Aa	Aa		169 P M	Aa	Aa	aa		233 P M	Aa	Aa	aa	
Parent 2	101 Y M	aa	aa	aa		142 P M	Aa	Aa	aa		234 P M	Aa	Aa	aa	
Offspring	148 P M	Aa	Aa	aa		146 P M	aa	aa	aa	RAD06/supergene	239 P M	Aa	Aa	aa	
	149 P M	Aa	Aa	aa		214 P M	aa	aa	aa	RAD06/supergene	243 P M	Aa	Aa	aa	
	150 P M	Aa	Aa	aa		215 P M	aa	aa	aa	RAD06/supergene	244 P M	Aa	Aa	aa	
	151 P M	Aa	Aa	aa		216 P M	0 0	Aa	aa		132 P M	aa	aa	aa	RAD06/supergene
	152 P M	Aa	Aa	aa		230 P M	aa	aa	aa	RAD06/supergene	135 P M	Aa	Aa	aa	
	153 P M	Aa	Aa	aa		136 P M	Aa	Aa	aa		145 P M	Aa	Aa	aa	
	154 P M	aa	Aa	aa	RAD11/RAD06	147 P M	Aa	Aa	aa		232 P M	Aa	Aa	aa	
	155 P M	Aa	Aa	aa		217 P M	Aa	Aa	aa		237 P M	Aa	Aa	aa	
	156 P M	Aa	Aa	aa		235 P M	Aa	Aa	aa		245 P M	Aa	Aa	aa	
	157 P M	Aa	Aa	aa		236 P M	Aa	Aa	aa		170 Y O	Aa	aa	Aa	RAD11/supergene
	158 P M	Aa	Aa	aa		238 P M	Aa	Aa	aa		171 Y O	aa	aa	Aa	
	159 P M	Aa	Aa	aa		240 P M	Aa	Aa	aa		172 Y O	aa	aa	Aa	
	160 P M	aa	aa	aa	RAD06/supergene	241 P M	Aa	Aa	aa		173 Y O	aa	aa	aa	supergene/RAD09
	161 P M	aa	aa	aa	RAD06/supergene	247 P M	Aa	Aa	aa		174 Y O		aa	Aa	
	162 P M	Aa	Aa	aa		246 P M	Aa	Aa	aa		175 Y O	aa	aa	Aa	
	163 P M	Aa	Aa	aa		134 P M	Aa	Aa	aa		176 Y O	aa	aa	Aa	
	164 P M	Aa	Aa	aa		138 P M	Aa	Aa	aa		177 Y O	aa	aa	Aa	
	165 P M	aa	aa	aa	RAD06/supergene	141 P M	Aa	Aa	aa		131 Y O	Aa	Aa	Aa	RAD06/supergene
	166 P M	Aa	Aa	aa		143 P M	Aa	Aa	aa		211 Y O	Aa	Aa	Aa	RAD06/supergene
	167 P M	Aa	Aa	aa		144 P M	Aa	Aa	aa		218 Y O	aa	aa	Aa	
	168 P M	Aa	Aa	aa		231 P M	Aa	Aa	aa		220 Y O	aa	aa	Aa	

121 Y O aa aa Aa
122 Y O aa aa Aa
125 Y O aa aa Aa
127 Y O aa aa Aa
129 Y O aa aa Aa
207 Y O aa aa Aa
221 Y O aa aa Aa
224 Y O aa aa Aa
225 Y O aa aa Aa
228 Y O aa aa Aa
229 Y O aa aa Aa
242 Y O aa aa Aa

123 Y O aa aa Aa
130 Y O aa aa Aa
140 Y O aa aa Aa
208 Y O aa aa Aa
213 Y O aa aa Aa
226 Y O aa aa Aa
124 Y O aa aa Aa
126 Y O aa aa Aa
128 Y O aa aa Aa
133 Y O aa aa Aa
137 Y O aa aa Aa
139 Y O aa aa Aa

204 Y O aa aa Aa
205 Y O aa aa Aa
206 Y O aa aa Aa
209 Y O aa aa Aa
210 Y O aa aa Aa
212 Y O aa aa Aa
219 Y O aa aa Aa
222 Y O aa aa Aa
223 Y O aa aa Aa
227 Y O aa aa Aa
248 Y O aa aa Aa

Cross 102x103 used RAD11 (BtgI) and RAD09 (BstUI).

Cross:	102x103 Phenotype Genotype				Recombination	ID	RAD11	RAD09	Recombination	
	ID		RAD11	RAD09						
Parent 1	102	P O	<i>aa</i>	<i>Aa</i>		183	Y M	<i>Aa</i>	<i>aa</i>	
Parent 2	103	Y M	<i>Aa</i>	<i>aa</i>		184	Y M	<i>aa</i>	<i>aa</i>	
Offspring	117	P O	<i>aa</i>	<i>Aa</i>		185	Y M	<i>aa</i>	<i>aa</i>	
	186	P O	<i>Aa</i>	<i>Aa</i>		258	Y M	<i>Aa</i>	<i>aa</i>	
	187	P O	<i>aa</i>	<i>Aa</i>		259	Y M	<i>aa</i>	<i>aa</i>	
	188	P O	<i>Aa</i>	<i>Aa</i>		260	Y M	<i>Aa</i>	<i>aa</i>	
	189	P O	<i>Aa</i>	<i>Aa</i>		263	Y M		<i>aa</i>	
	190	P O	<i>Aa</i>	<i>aa</i>	supergene/RAD09	264	Y M	<i>Aa</i>	<i>aa</i>	
	191	P O	<i>Aa</i>	<i>Aa</i>		265	Y M	<i>aa</i>	<i>aa</i>	
	261	P O	<i>Aa</i>	<i>Aa</i>		266	Y M	<i>Aa</i>	<i>aa</i>	
	262	P O	<i>aa</i>	<i>aa</i>		267	Y M	<i>aa</i>	<i>aa</i>	
	268	P O	<i>aa</i>	<i>Aa</i>		363	Y M		<i>aa</i>	
	372	P O	<i>aa</i>	<i>Aa</i>		364	Y M	<i>Aa</i>	<i>aa</i>	
	373	P O	<i>aa</i>	<i>Aa</i>		365	Y M	<i>aa</i>	<i>aa</i>	
	374	P O		<i>Aa</i>		366	Y O	<i>Aa</i>	<i>aa</i>	colour/banding
	375	P O	<i>aa</i>	<i>Aa</i>		367	Y M	<i>Aa</i>	<i>aa</i>	
	376	P O		<i>Aa</i>		368	Y O	<i>Aa</i>	<i>aa</i>	colour/banding
	377	P O	<i>aa</i>	<i>Aa</i>		369	Y M	<i>aa</i>	<i>Aa</i>	supergene/RAD09
	378	P O		<i>Aa</i>		370	Y O	<i>Aa</i>	<i>aa</i>	colour/banding
	379	P O	<i>Aa</i>	<i>Aa</i>		371	Y M	<i>Aa</i>	<i>aa</i>	
	380	P O	<i>Aa</i>	<i>Aa</i>		478	Y M	<i>aa</i>	<i>aa</i>	
	381	P O	<i>Aa</i>	<i>Aa</i>		479	Y M	<i>Aa</i>	<i>aa</i>	
	182	Y M	<i>Aa</i>	<i>aa</i>						

Cross 116x120 and 450x449 RAD06 (MspI) RAD09 (HaeIII).

Cross:	116x120 Phenotype Genotype					450x449 Phenotype Genotype				
	ID		RAD06	RAD09	Recombination	ID		RAD06	RAD09	Recombination
Parent 1	116	P M N	<i>Aa</i>	<i>Aa</i>		450	P M N	<i>Aa</i>	<i>Aa</i>	
Parent 2	120	Y B H	<i>aa</i>	<i>aa</i>		449	Y B N	<i>aa</i>	<i>aa</i>	
Offspring	382	P M N juv	<i>aa</i>	<i>Aa</i>	RAD06/supergene	673	P M N	<i>Aa</i>	<i>Aa</i>	
	383	P B N	<i>Aa</i>	<i>Aa</i>		675	P M N	<i>Aa</i>	<i>Aa</i>	
	384	P B N	<i>Aa</i>	<i>Aa</i>		676	P M N	<i>Aa</i>	<i>Aa</i>	
	448	P B N	<i>aa</i>	<i>Aa</i>	RAD06/supergene	679	P M N	<i>Aa</i>	<i>Aa</i>	
	450	P M N	<i>Aa</i>	<i>Aa</i>		684	P M N	<i>Aa</i>	<i>aa</i>	supergene/RAD09
	451	P M N	<i>Aa</i>	<i>Aa</i>		694	P B N	<i>Aa</i>	<i>Aa</i>	
	662	P M N	<i>Aa</i>	<i>Aa</i>		738	P B N	<i>aa</i>	<i>Aa</i>	RAD06/supergene
	663	P B N	<i>Aa</i>	<i>Aa</i>		678	Y M N	<i>Aa</i>	<i>aa</i>	RAD06/supergene
	447	Y M N	<i>aa</i>	<i>aa</i>		683	Y M N	<i>aa</i>	<i>aa</i>	
	449	Y B N	<i>aa</i>	<i>aa</i>		685	Y M H	<i>aa</i>	<i>aa</i>	
	452	Y B N	<i>aa</i>	<i>aa</i>		693	Y M H	<i>aa</i>	<i>aa</i>	
	570	Y M N	<i>aa</i>	<i>aa</i>		739	Y B N	<i>aa</i>	<i>aa</i>	
	571	Y B N	<i>aa</i>	<i>aa</i>						
	664	Y M N	<i>aa</i>	<i>aa</i>						
	665	Y B N	<i>aa</i>	<i>aa</i>						
	669	Y B N	<i>aa</i>	<i>aa</i>						

Cross 108x109 RAD11 (HinfI) and RAD09 (HaeIII).

Cross	108x109 Phenotype Genotype												
	ID	RAD11	RAD09	Recombination	ID	RAD11	RAD09	Recombination	ID	RAD11	RAD09	Recombination	
Parent 1	108	P O L	Aa	Aa	536	P O L	Aa	Aa	colour/banding	281	Y O L		aa
Parent 2	109	Y M L	aa	aa	537	P M L	Aa	Aa		299	Y O L	aa	aa
Offspring	116	P M L	Aa	Aa	561	P M L	aa	Aa	RAD11/supergene	300	Y O A		aa
	275	P M L	Aa	Aa	562	P M L	Aa	Aa		482	Y O L	aa	aa
	276	P M L	Aa	Aa	563	P M L	Aa	Aa		483	Y O L	aa	aa
	487	P M L		Aa	564	P M L	Aa	Aa		484	Y O L	aa	aa
	488	P M L	aa	Aa	RAD11/supergene	565	P M L	Aa	Aa	485	Y O A	aa	aa
	489	P M L	Aa	Aa	566	P M L	Aa	Aa		486	Y O A		aa
	490	P M L	Aa	Aa	567	P M L	Aa	Aa		530	Y O A		aa
	491	P M L	Aa	Aa	573	P M L	Aa	Aa		531	Y O A	aa	aa
	492	P M L	Aa	Aa	574	P M L	Aa	Aa		532	Y O L	aa	aa
	493	P M L	Aa	Aa	575	P M L		aa	supergene/RAD09	533	Y O A	aa	aa
	494	P M L	Aa	Aa	269	Y O L	aa	aa		534	Y O L	aa	aa
	495	P M L	Aa		270	Y O A	aa	aa		535	Y O L	aa	aa
	496	P M L	Aa	Aa	277	Y O A		aa		559	Y O A	aa	aa
	497	P M L	Aa	Aa	278	Y O A	aa	aa		560	Y O A	aa	aa
	498	P M L	Aa	Aa	279	Y O L	aa	aa		572	Y O A	aa	aa
	499	P M L	Aa	Aa	280	Y O L	aa	aa					

Cross 451x452 RAD06 (Ddel) and RAD09 (BstUI).

Cross: 451x452 Phenotype Genotype												
	ID	RAD06	RAD09	Recombination	ID	RAD06	RAD09	Recombination	ID	RAD06	RAD09	Recombination
Parent 1	451	P M N	Aa	Aa	750	Y M N	aa	aa	800	P M juv	aa	
Parent 2	452	Y B N	aa	aa	751	Y B N	aa	aa	804	P M H	aa	Aa RAD06/super/hyaloz
Offspring	691	P B N	Aa	Aa	752	Y B N	aa	aa	805	Y M H	aa	aa
	692	P M N	Aa	Aa	753	P B N	Aa	Aa	806	P M N	Aa	Aa
	695	Y B N	aa	aa	754	P B N	Aa	Aa	807	Y B N	aa	aa
	697	P M N	Aa	Aa	755	Y M N	aa	aa	808	Y B N	aa	aa
	698	P M N	Aa	Aa	756	Y M H	aa	aa	809	P M N	Aa	Aa
	699	P B N	Aa	Aa	757	P M N	Aa	Aa	810	P M N	Aa	Aa
	700	P B N	Aa	Aa	758	P B N	Aa	Aa	811	P M N	Aa	Aa
	701	P B N	Aa	Aa	767	Y M N	aa	aa	812	P M N	Aa	Aa
	702	P B N	Aa	Aa	768	Y B N	aa	aa	813	P B N	Aa	Aa
	703	P B N	Aa	Aa	769	Y M H	aa	aa	814	P B N	Aa	Aa
	704	P B N	Aa	Aa	770	P B N	Aa	Aa	815	P B N	Aa	Aa
	705	P M N		Aa	771	P M N	Aa	Aa	816	P B N	Aa	Aa
	706	P B N	Aa	Aa	772	P B N	aa	Aa RAD06/supergene	825	P M N	Aa	Aa
	707	Y M N	aa	aa	773	P B N	Aa	Aa	826	Y B N	aa	aa
	708	Y M H	aa	aa	774	P M N	Aa	Aa	827	Y B N	aa	aa
	709	Y B H	aa	aa	775	P M N	Aa	Aa	828	Y B N	aa	aa
	714	Y B H	aa	aa	785	P M N	aa	Aa RAD06/supergene	830	Y M N		aa
	715	P M N	Aa	Aa	786	Y B N	aa	aa	833	P M N	Aa	aa supergene/RAD09
	716	P M N	Aa	Aa	787	Y M H	aa	aa	834	Y M N	aa	aa
	724	Y B N	aa	aa	788	P M H	Aa	Aa colour/hyalozonate	835	Y B N	aa	aa
	725	Y B N	aa	aa	795	P M N	Aa	Aa	836	Y B N	aa	aa
	726	Y M N	aa	Aa supergene/RAD09	796	P M N	Aa	Aa	837	P M N	Aa	Aa

727	P M N	<i>Aa</i>	<i>Aa</i>		797	P M N	<i>Aa</i>	<i>Aa</i>		838	P M N	<i>Aa</i>	<i>Aa</i>	
728	Y B N	<i>aa</i>	<i>aa</i>		799	Y M N	<i>aa</i>	<i>aa</i>		839	Y B H	<i>aa</i>	<i>aa</i>	
849	Y B N	<i>aa</i>	<i>aa</i>		883	Y M H	<i>aa</i>	<i>aa</i>		915	P M N juv	<i>Aa</i>	<i>Aa</i>	
850	P B N	<i>Aa</i>	<i>Aa</i>		885	P M N	<i>Aa</i>	<i>Aa</i>		916	P B N juv	<i>Aa</i>	<i>Aa</i>	
852	Y B N	<i>aa</i>	<i>aa</i>		886	P M N	<i>Aa</i>	<i>Aa</i>		917	P B N juv	<i>Aa</i>	<i>Aa</i>	
854	Y B N	<i>aa</i>	<i>aa</i>		887	Y M N	<i>aa</i>	<i>aa</i>		918	Y B N juv	<i>aa</i>	<i>aa</i>	
855	Y M N	<i>aa</i>	<i>aa</i>		888	Y B H	<i>aa</i>	<i>aa</i>		919	Y B N juv	<i>aa</i>	<i>aa</i>	
856	Y M N	<i>aa</i>	<i>aa</i>		889	Y M H	<i>Aa</i>	<i>aa</i>		920	Y M H juv	<i>aa</i>	<i>aa</i>	
857	Y M H	<i>aa</i>	<i>aa</i>		890a	P M H	<i>Aa</i>		colour/hyalozonate	925	P N M		<i>aa</i>	
858	Y M H	<i>aa</i>	<i>aa</i>		890b	P M N	<i>Aa</i>	<i>Aa</i>		926	P M H	<i>Aa</i>	<i>Aa</i>	colour/hyalozonate
859	Y B N	<i>Aa</i>	<i>aa</i>	RAD06/supergene	893a	P B N	<i>Aa</i>	<i>Aa</i>						
860	P B N	<i>Aa</i>	<i>Aa</i>		895a	P M N	<i>Aa</i>	<i>Aa</i>						
861	P B N	<i>Aa</i>	<i>Aa</i>		914	P M N juv	<i>Aa</i>	<i>Aa</i>						

Cross 662x665 RAD06 (MspI) and RAD09 (HaeIII).

Cross: 662x665 Phenotype Genotype														
	ID	RAD06	RAD09	Recombination	ID	RAD06	RAD09	Recombination	ID	RAD06	RAD09	Recombination		
Parent 1	662	P M N	Aa	Aa	789	Y B N	aa	aa	851	P B N	Aa	Aa		
Parent 2	665	Y B N	aa	aa	794	Y M H	Aa	aa	RAD06/supergene	853	P B N	Aa	Aa	
Offspring	717	P M N	Aa	Aa	798	Y B H	aa	aa	862	Y B H	aa	aa		
	718	Y B H	aa	aa	801	P B N	Aa	Aa	863	Y M H	aa	aa		
	719	P B N	Aa	Aa	802	P B N	Aa	Aa	864	Y B N	aa	aa		
	720	P B N	Aa	Aa	803	Y M H	aa	aa	865	Y B H	aa	aa		
	721	P B N	Aa	Aa	817	P M N	Aa	Aa	866	Y M N	aa	aa		
	722	P M N	Aa	Aa	818	P B N	Aa	Aa	867	Y M H	aa	aa		
	723	Y B N	aa	aa	819	P B N	Aa	Aa	868	Y M N	aa	aa		
	740	P M N	Aa	Aa	820	Y B N	aa	aa	869	Y B N	aa	aa		
	741	P B N	Aa	Aa	821	P M H	Aa	Aa	hyalozonate/colour	870	P M N	Aa	Aa	
	743	P B N	Aa	Aa	822	P M H	Aa	Aa	hyalozonate/colour	871	P M N	Aa	aa	supergene/RAD09
	744	P B N	Aa	Aa	829	P M N	aa	Aa	RAD06/supergene	872	P B N	Aa	Aa	
	745	Y M N	aa	aa	831	P M N	Aa	Aa	873	Y B N juv	aa	aa		
	746	Y B N	aa	aa	832	P M N	Aa	Aa	874	P B N	Aa	Aa		
	747	Y B N	aa	aa	840	Y M N	aa	aa	875	P B N	Aa	Aa		
	748	Y B N	aa	aa	841	Y B H		aa	876	P B N	Aa	Aa		
	759	Y M H	aa	aa	842	Y M H	aa	aa	877	Y B N	aa	aa		
	760	Y B H	aa	aa	843	P B N	Aa	Aa	878	P B N	Aa	Aa		
	761	Y B H	aa	aa	844	P M N	Aa	Aa	879	P M N	Aa	Aa		
	762	Y M N	aa	aa	845	P M N	Aa	Aa	880	Y M N	aa	aa		
	763	P B N	Aa	Aa	846	P B N	Aa	Aa	881	Y M N	Aa	aa	RAD06/supergene	
764	P B N	Aa	Aa	847	Y M H	aa	aa	882	Y M H	aa	aa			
765	P M N	Aa	Aa	848	Y M H	aa	aa	900	P M N juv	Aa	Aa			

901	Y M H	aa	aa		935	P M N juv	Aa	aa	supergene/RAD09	958	Y M H juv	aa	aa	
902	Y B H juv	aa	aa		936	P M N juv	Aa	Aa		959	Y B H juv	aa	aa	
903	Y B N juv	aa	aa		937	P M N juv	Aa	Aa		960	Y M H juv	aa	aa	
904	Y B H juv	aa	aa		939	P M N juv	Aa	Aa		961	Y B H juv	aa	aa	
905	Y B N juv	aa	aa		940	P M N juv		aa	supergene/RAD09	962	Y B H juv	aa	aa	
906	P B N juv	Aa	Aa		941	P M N juv		Aa		963	Y M H juv	aa	aa	
907	P B N juv	Aa	Aa		942	P M N juv	Aa	Aa		964	Y B H juv	aa	aa	
908	P B N juv	Aa	Aa		943	P M N juv	Aa	Aa		966	P M H juv	Aa	Aa	hyalozonate/colour
909	P B N juv	aa	Aa		944	P M N juv	Aa	Aa		967	P B N juv	Aa	Aa	
911	Y B N	aa	aa		945	P M H juv	Aa	Aa	colour/hyalozonate	968	P M H juv	Aa	Aa	hyalozonate/colour
912	Y M H	aa	aa		946	P M H juv	Aa	Aa	colour/hyalozonate	891a	P M N	Aa	Aa	
923	P B N	Aa	Aa		947	P B N juv		Aa		892a	P M H	Aa	Aa	
924	P M N	Aa	Aa		948	P B N juv	Aa	Aa		895b	P M N juv	Aa	Aa	
927	P M N	Aa	Aa		949	P B N juv	Aa	aa	supergene/RAD09	896a	P M N	Aa	Aa	
928	P M N		aa	supergene/RAD09	950	P B N juv	Aa	Aa		896b	P M N juv	Aa	Aa	
929	Y B N juv	aa	aa		951	P B N juv	Aa	Aa		897b	P M N juv	Aa	Aa	
930	Y B N	aa	aa		952	P B N juv	Aa	Aa		898a	P M N juv	Aa	Aa	
931	Y B N juv	aa	aa		953	P B N juv	Aa	Aa		898b	P M N juv	Aa	Aa	
932	Y B N juv	aa	aa		955	P B N juv	Aa	Aa		899a	P B N juv	aa	Aa	
933	Y B N juv	aa	aa		956	P B N juv	Aa	Aa		899b	P M N juv	Aa	Aa	
934	P M N juv	Aa	aa	supergene/RAD09	957	P B N juv	Aa	Aa						

Cross 825x841 RAD06 (Mspl) and RAD09 (HaeIII).

Cross: 825x841 Phenotype Genotype															
	ID	P	M	N	RAD06	RAD09	Recombination	ID	P	B	N	RAD06	RAD09	Recombination	
Parent 1	825	P	M	N	<i>Aa</i>	<i>Aa</i>		1004	P	B	N	<i>Aa</i>	<i>Aa</i>		
Parent 2	841	Y	B	H	<i>aa</i>	<i>aa</i>		1005	P	B	N	<i>Aa</i>	<i>Aa</i>		
Offspring	969	P	M	N	<i>Aa</i>	<i>Aa</i>		1006	Y	B	H	<i>aa</i>	<i>aa</i>		
	970	P	M	N	<i>Aa</i>	<i>Aa</i>		1007	Y	B	H	<i>aa</i>	<i>aa</i>		
	971	Y	M	H		<i>aa</i>		1008	P	B	N		<i>Aa</i>		
	972	P	B	N		<i>Aa</i>		1009	P	M	N	juv	<i>Aa</i>	<i>Aa</i>	
	973	P	M	N	<i>Aa</i>			1010	P	M	N	juv	<i>Aa</i>	<i>Aa</i>	
	974	P	M	N	<i>Aa</i>			1011	P	M	N		<i>aa</i>	supergene/RAD09	
	975	Y	M	H	juv	<i>Aa</i>	<i>aa</i>	RAD06/supergene	1012	P	M	N	juv	<i>Aa</i>	<i>Aa</i>
	976	Y	M	H			<i>aa</i>		1013	P	B	N	juv		<i>Aa</i>
	978	Y	M	H	<i>Aa</i>	<i>aa</i>	RAD06/supergene	1014	P	M	N	juv	<i>Aa</i>	<i>Aa</i>	
	979	Y	M	H	<i>aa</i>	<i>aa</i>		1015	Y	B	N	juv	<i>aa</i>		
	980	Y	M	H		<i>aa</i>		1016	P	M	H	juv	<i>Aa</i>	<i>Aa</i>	colour/hyalozonate
	981	Y	M	H	<i>aa</i>	<i>aa</i>		1017	P	B	N		<i>Aa</i>	<i>Aa</i>	
	984	P	B	N	<i>Aa</i>	<i>Aa</i>		1018	P	M	N	juv	<i>Aa</i>	<i>Aa</i>	
	987	P	B	N	<i>Aa</i>	<i>Aa</i>		1019	P	M	H	juv	<i>Aa</i>	<i>Aa</i>	colour/hyalozonate
	989	P	B	N	<i>Aa</i>	<i>Aa</i>		1020	P	M	N	juv	<i>Aa</i>	<i>Aa</i>	
	990	P	B	N	juv	<i>Aa</i>	<i>Aa</i>		1021	P	M	N	juv	<i>Aa</i>	<i>Aa</i>
	995	Y	M	H		<i>aa</i>		1022	P	M	N	juv	<i>Aa</i>	<i>Aa</i>	
	998	Y	B	H	<i>aa</i>	<i>aa</i>		1023	P	B	N	juv	<i>Aa</i>	<i>Aa</i>	
	999	P	B	N	<i>Aa</i>			1024	P	B	N	juv	<i>aa</i>	<i>Aa</i>	RAD06/supergene
	1000	Y	M	H		<i>aa</i>		1025	Y	M	H	juv	<i>aa</i>	<i>aa</i>	
	1001	P	M	N	<i>Aa</i>	<i>Aa</i>		1026	Y	M	H	juv	<i>aa</i>	<i>aa</i>	
	1002	Y	B	H	<i>aa</i>	<i>aa</i>		1027	Y	B	H	juv	<i>aa</i>	<i>aa</i>	

Cross 118x119 RAD8 (Hinfl) and RAD10 (DpnII).

Cross:		118x119 Phenotype Genotype								118x119 Phenotype Genotype			
	ID	RAD8	RAD10	Recombination	ID	RAD8	RAD10	Recombination	ID	RAD8	RAD10	Recombination	
Parent 1	118	Y M	aa	aa	462	Y M	Aa	Aa	398	P M	aa	aa	
Parent 2	119	P M	Aa	Aa	463	Y M	Aa	Aa	399	P M	aa	aa	
Offspring	353	Y M	Aa	Aa	465	Y M	Aa	Aa	410	P M	aa	aa	
	354	Y M	Aa	Aa	466	Y M	Aa	Aa	411	P M	aa	aa	
	355	Y M	Aa	Aa	468	Y M	Aa	Aa	415	P M	aa	aa	
	356	Y M	Aa	Aa	538	Y M	Aa	Aa	417	P M	aa	aa	
	391	Y M	Aa	Aa	539	Y M	Aa	Aa	419	P M	aa	aa	
	392	Y M	Aa	Aa	540	Y M	Aa	Aa	420	P M	aa	aa	
	393	Y M	Aa	Aa	469	Y M	Aa	Aa	453	P M	aa	aa	
	400	Y M	Aa	Aa	470	Y M	Aa	Aa	454	P M	aa	aa	
	412	Y M	Aa	Aa	471	Y M	Aa	Aa	455	P M	aa	aa	
	413	Y M	Aa	Aa	472	Y M	Aa	Aa	456	P M	aa	aa	
	414	Y M	Aa	Aa	473	Y M	Aa	Aa	457	P M	aa	aa	
	418	Y M	Aa	Aa	474	Y M	Aa	Aa	458	P M	aa	aa	
	421	Y M	Aa	Aa	357	P M	aa	aa	459	P M	aa	aa	
	432	Y M	Aa	Aa	358	P M	aa	aa	460	P M	aa	aa	
	433	Y M	Aa	Aa	359	P M	aa	aa	541	P M	aa	aa	
	434	Y M	Aa	Aa	360	P M	aa	aa	542	P M	aa	aa	
	435	Y M	Aa	Aa	361	P M	aa	aa	543	P M	aa	aa	
	436	Y M	Aa	Aa	362	P M	aa	aa	416	P M	aa	aa	
	437	Y M	Aa	Aa	394	P M	aa	aa					
	438	Y M	Aa	Aa	395	P M	aa	aa					
	439	Y M	Aa	Aa	396	P M	aa	aa					
	461	Y M	Aa	Aa	397	P M	aa	aa					

Cross 104x105 all markers were homozygous. Thus, not informative results came out of this offspring.

Cross:	104x105	Phenotype	Genotype	ID	ID
Parent 1	104	P O	All markers homozygous - not informative	329	P O
Parent 2	105	Y M		330	P O
Offspring	192	P O		331	P O
	193	P O		332	P O
	194	P O		333	P O
	197	P O		118	Y M
	198	P O		178	Y M
	199	P O		179	Y M
	200	P O		180	Y M
	256	P O		181	Y M
	257	P O		201	Y M
	321	P O		202	Y M
	322	P O		249	Y M
	323	P O		250	Y M
	324	P O		251	Y M
	327	P O		252	Y M
	328	P O		254	Y M
	334	P O		317	Y M
	401	P O		402	Y M
	195	P O		203	Y M
	196	P O		253	Y M
	255	P O		318	Y M
325	P O		319	Y M	
326	P O		320	Y M	

Table S2.4. Inferred genotypes of all individuals. Shells with a phenotype that may be due to a potential recombination event in parent are shown in **bold**.

Locus		Parent 1		Parent 2		Offspring					
Cross #1		C100		C101							
Phenotype		P O		x	Y M	Sum	P M		Y O		
						103	56		47		
Genotype	Colour	C^P	C^Y	C^Y	C^Y	C^P	C^Y	C^Y	C^Y		
	Banding	B^B	B^O	B^B	B^B	B^B	B^B	B^O	B^B		
	Mid-band	U^3	U^3	U^3	$U^{3/-}$	U^3	$U^{3/-}$	U^3	$U^{3/-}$		
Cross #2		C102		C103							
Phenotype		P O		x	Y M	Sum	P O		Y M	Y O	
						43	20		20	3	
Genotype	Colour	C^P	C^Y	C^Y	C^Y	C^P	C^Y	C^Y	C^Y	C^P	C^Y
	Banding	B^O	B^B	B^B	B^B	B^O	B^B	B^B	B^B	B^B	B^B
	Mid-band	U^3	U^3	$U^{3/-}$	$U^{3/-}$	U^3	$U^{3/-}$	U^3	$U^{3/-}$	U^3	$U^{3/-}$
Cross #3		C104		C105							
Phenotype		P O		x	Y M	Sum	P O		Y M		
						46	27		19		
Genotype	Colour	C^P	C^Y	C^Y	C^Y	C^P	C^Y	C^Y	C^Y		
	Banding	B^O	B^B	B^B	B^B	B^O	B^B	B^B	B^B		
	Mid-band	U^3	U^3	$U^{3/-}$	$U^{3/-}$	U^3	$U^{3/-}$	U^3	$U^{3/-}$		
Cross #4		C110		C111							
Phenotype		P O		x	Y B	Sum	P B		Y O		
						27	17		10		
Genotype	Colour	C^P	C^Y	C^Y	C^Y	C^P	C^Y	C^Y	C^Y		
	Banding	B^B	B^O	B^B	B^B	B^B	B^B	B^O	B^B		
	Mid-band	U^-	U^-	U^-	U^-	U^-	U^-	U^-	U^-		

Cross #5		C112		C113												
Phenotype		P O		x	Y B (12345)	Sum	P B (00345)	P B (12345)	P B (02345)	Y O				P M		
						109	27	12	16	53				1		
Genotype	Colour	C^P	C^Y		C^Y	C^Y	C^P	C^Y	C^P	C^Y	C^P	C^Y	C^Y	C^Y	C^P	C^Y
	Banding	B^B	B^O		B^B	B^b	B^B	B^B	B^B	B^B	B^B	B^O	B^B	B^B	B^B	B^B
	Mid-band	U^-	U^-		U^-	U^-	U^-	U^-	U^-	U^-	U^-	U^-	U^-	U^-	U^-	U^-
	00345-band	T^{345}	T^-		T^-	T^-	T^{345}	T^-	T^-	T^-	T^-	$T^{345/-}$	T^-			
	02345-band	X^{2345}	X^-		X^-	X^-	$X^{2345/-}$	X^-	X^-	X^-	X^{2345}	X^-	X^{2345}	X^-		
Cross #6		C114		C115												
Phenotype		P O		x	Y B	Sum	P O		Y B		Y M					
						34	18		8		8					
Genotype	Colour	C^P	C^Y		C^Y	C^Y	C^P	C^Y	C^Y	C^Y	C^Y	C^Y	C^Y	C^Y	C^Y	
	Banding	B^O	B^B		B^B	B^B	B^O	B^B	B^B	B^B	B^B	B^B	B^B	B^B	B^B	
	Mid-band	U^3	U^-		U^-	U^-	U^3	U^-	U^-	U^-	U^3	U^-	U^-			
Cross #7		C118		C119												
Phenotype		P M		x	Y M	Sum	P M		Y M							
						75	37		38							
Genotype	Colour	C^P	C^Y		C^Y	C^Y	C^P	C^Y	C^Y	C^Y						
	Mid-band	U^3	$U^{3/-}$		U^3	$U^{3/-}$	U^3	$U^{3/-}$	U^3	$U^{3/-}$						
Cross #8		C108		C109												
Phenotype		P O L		x	Y M L	Sum	P M L		Y O L		Y O A		P O L			
						50	26		11		12		1			
Genotype	Colour	C^P	C^Y		C^Y	C^Y	C^P	C^Y	C^Y	C^Y	C^Y	C^P	C^Y	C^Y	C^Y	
	Banding	B^B	B^O		B^B	B^B	B^B	B^B	B^O	B^B	B^O	B^B	B^O	B^B	B^B	
	Lip	L^L	L^A		L^L	L^A	L^L	$L^{L/A}$	L^A	L^L	L^A	L^A	L^L	L^A	L^A	
	Mid-band	U^3	U^3		U^3	U^-	U^3	$U^{3/-}$	U^3	$U^{3/-}$	U^3	$U^{3/-}$	U^3	$U^{3/-}$	$U^{3/-}$	

Cross #9		C116		C120															
Phenotype		P MN		x Y B H		Sum P MN		P B N		Y MN		Y B N							
						16 4		4		3		5							
Genotype	Colour	C^P	C^Y	C^Y	C^Y	C^P	C^Y	C^P	C^Y	C^Y	C^Y	C^Y	C^Y	C^Y	C^Y	C^Y	C^Y	C^Y	C^Y
	Banding	B^B	B^B	B^B	B^B	B^B	B^B	B^B	B^B	B^B	B^B	B^B	B^B	B^B	B^B	B^B	B^B	B^B	B^B
	Band pigmentation	P^N	P^N	P^H	P^H	P^N	P^H	P^N	P^H	P^N	P^H	P^N	P^H	P^N	P^H	P^N	P^H	P^H	P^H
	Mid-band	U^3	U^-	U^-	U^-	U^3	U^-	U^-	U^-	U^-	U^3	U^-	U^-						
Cross #10		C450		C449															
Phenotype		P MN		x Y B N		Sum P MN		P B N		Y MN		Y B N		Y MH		Y B H			
						12 5		2		2		1		2		0			
Genotype	Colour	C^P	C^Y	C^Y	C^Y	C^P	C^Y	C^P	C^Y	C^Y	C^Y	C^Y	C^Y	C^Y	C^Y	C^Y	C^Y	C^Y	C^Y
	Banding	B^B	B^B	B^B	B^B	B^B	B^B	B^B	B^B	B^B	B^B	B^B	B^B	B^B	B^B	B^B	B^B	B^B	B^B
	Band pigmentation	P^N	P^H	P^N	P^H	P^N	$P^{N/H}$	P^N	$P^{N/H}$	P^N	P^H	P^N	P^H	P^H	P^H	P^H	P^H	P^H	P^H
	Mid-band	U^3	U^-	U^-	U^-	U^3	U^-	U^-	U^-	U^3	U^-	U^-	U^-	U^3	U^-	U^-	U^-	U^-	U^-
Cross #11		C451		C452															
Phenotype		P MN		x Y B N		Sum P MN		P B N		Y MN		Y B N		Y MH		Y B H		P M H	
						116 34		28		12		22		10		6		4	
Genotype	Colour	C^P	C^Y	C^Y	C^Y	C^P	C^Y	C^P	C^Y	C^Y	C^Y	C^Y	C^Y	C^Y	C^Y	C^Y	C^Y	C^P	C^Y
	Banding	B^B	B^B	B^B	B^B	B^B	B^B	B^B	B^B	B^B	B^B	B^B	B^B	B^B	B^B	B^B	B^B	B^B	B^B
	Band pigmentation	P^N	P^H	P^N	P^H	P^N	$P^{N/H}$	P^N	P^N	P^H	P^N	P^H	P^H						
	Mid-band	U^3	U^-	U^-	U^-	U^3	U^-	U^-	U^-	U^3	U^-	U^-	U^-	U^3	U^-	U^-	U^-	U^3	U^-
Cross #12		C662		C665															
Phenotype		P MN		x Y B N		Sum P MN		P B N		Y MN		Y B N		Y MH		Y B H		P M H	
						146 39		46		7		19		15		12		8	
Genotype	Colour	C^P	C^Y	C^Y	C^Y	C^P	C^Y	C^P	C^Y	C^Y	C^Y	C^Y	C^Y	C^Y	C^Y	C^Y	C^P	C^Y	C^Y
	Banding	B^B	B^B	B^B	B^B	B^B	B^B	B^B	B^B	B^B	B^B	B^B	B^B	B^B	B^B	B^B	B^B	B^B	B^B
	Band pigmentation	P^N	P^H	P^N	P^H	P^N	P^H	P^N	P^N	P^H	P^N	P^H	P^H						
	Mid-band	U^3	U^-	U^-	U^-	U^3	U^-	U^-	U^-	U^3	U^-	U^-	U^-	U^3	U^-	U^-	U^-	U^3	U^-

Cross #13		C825		C841		Sum		P MN		P B N		Y M N		Y B N		Y M H		Y B H		P M H	
Phenotype		P M N		x Y B H		63	14	18	0	0	20	9	2								
Genotype	Colour	C^P	C^Y	C^Y	C^Y	C^P	C^Y	C^P	C^Y	C^P	C^Y										
	Banding	B^B	B^B	B^B	B^B	B^B	B^B	B^B	B^B	B^B	B^B	B^B	B^B	B^B	B^B	B^B	B^B	B^B	B^B	B^B	B^B
	Band pigmentation	P^N	P^H	P^H	P^H	P^N	P^H	P^N	P^H	P^N	P^H	P^N	P^H	P^H							
	Mid-band	U^3	U^-	U^-	U^-	U^3	U^-	U^-	U^-	U^3	U^-	U^-	U^-	U^3	U^-	U^-	U^-	U^3	U^-	U^-	U^-
Cross #14		C568		C569		Sum		Y B (12345)		Y O											
Phenotype		Y B (12345) x		Y O		44	28	16													
Genotype	Colour	C^Y	C^Y	C^Y	C^Y	C^Y	C^Y	C^Y	C^Y												
	Banding	B^B	B^B	B^O	B^B	B^B	B^B	B^O	B^B												
	Spread-banding	S^S	S^S	S^-	S^-	S^S	S^-	S^-	S^S												
	Mid-band	U^-	U^-	U^-	U^-	U^-	U^-	U^-	U^-												

Chapter 3:

Figure S3.1. The following density graphs illustrate the quality of the vcf file. Phred quality score (top-left), the variant mean depth (top-right), individual missing data (centre-left) and the variant missing data (centre-right) for each loci were plotted. Minor allele frequency density graphs of the entire variant calling data (bottom-left) and the filtered file (bottom-right) are illustrated. Filtering removed all the loci with minor allele frequency lower or equal to 10% ruling out possible genotyping error rates and invariant loci.

Figure S3.2. Correlation between contig length and the number of SNPs present in the whole-genome dataset.

Figure S3.3. The proportion of the variation explained by each axis returned by the principal components analysis.

Figure S3.4. Cross validation error results for each admixture group (K).

Table S3.1. Illumina reads sequenced per individual and allelic coverage of the double restriction site–associated DNA (RAD) loci dataset.

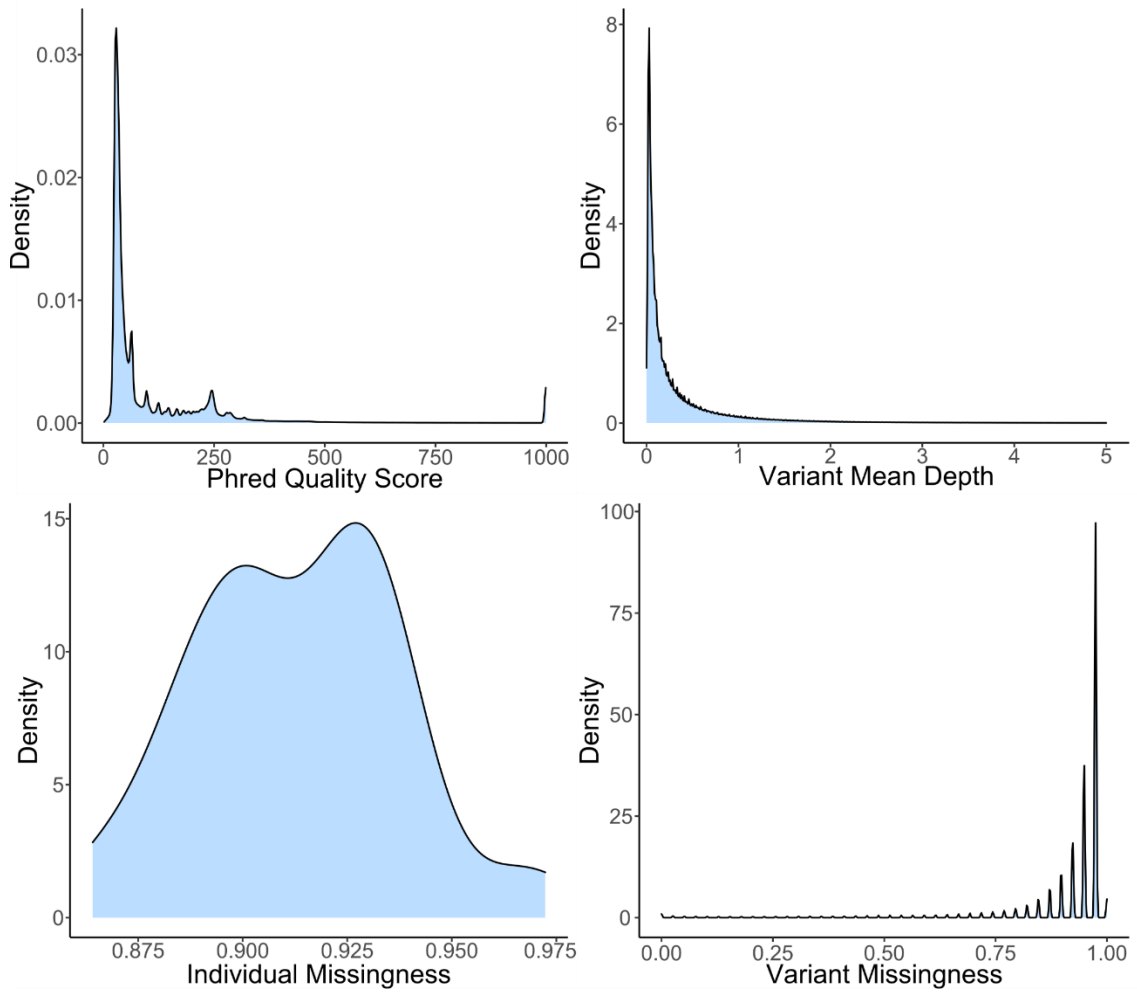
Table S3.2. Contigs surrounding the supergene described by Dr. Suzanne Saenko, RAD-seq loci mapping supergene-linked contigs and supergene-linked contigs (with their RAD-seq loci started position) presenting SNP's in the filtered dataset and their SNP's position.

Table S3.3. PCA data for the whole-genome dataset.

Table S3.4. All contigs present in the final dataset showing their length and number of SNPs. Moreover, Mantel test results between genetic distance of each RAD genomic regions and the geographical distance.

Supplementary Material: The allelic balance at heterozygotes to detect contamination for each sample can be access by request.

Variant Calling quality test



Minor allele frequency

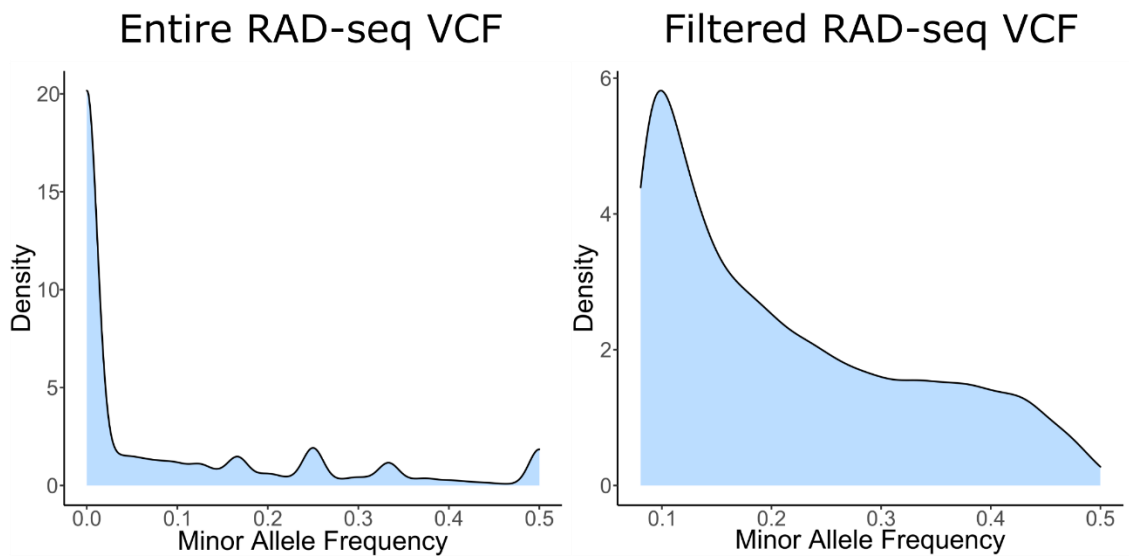


Figure S3.1. Quality checks of the variant calling dataset and filtering.

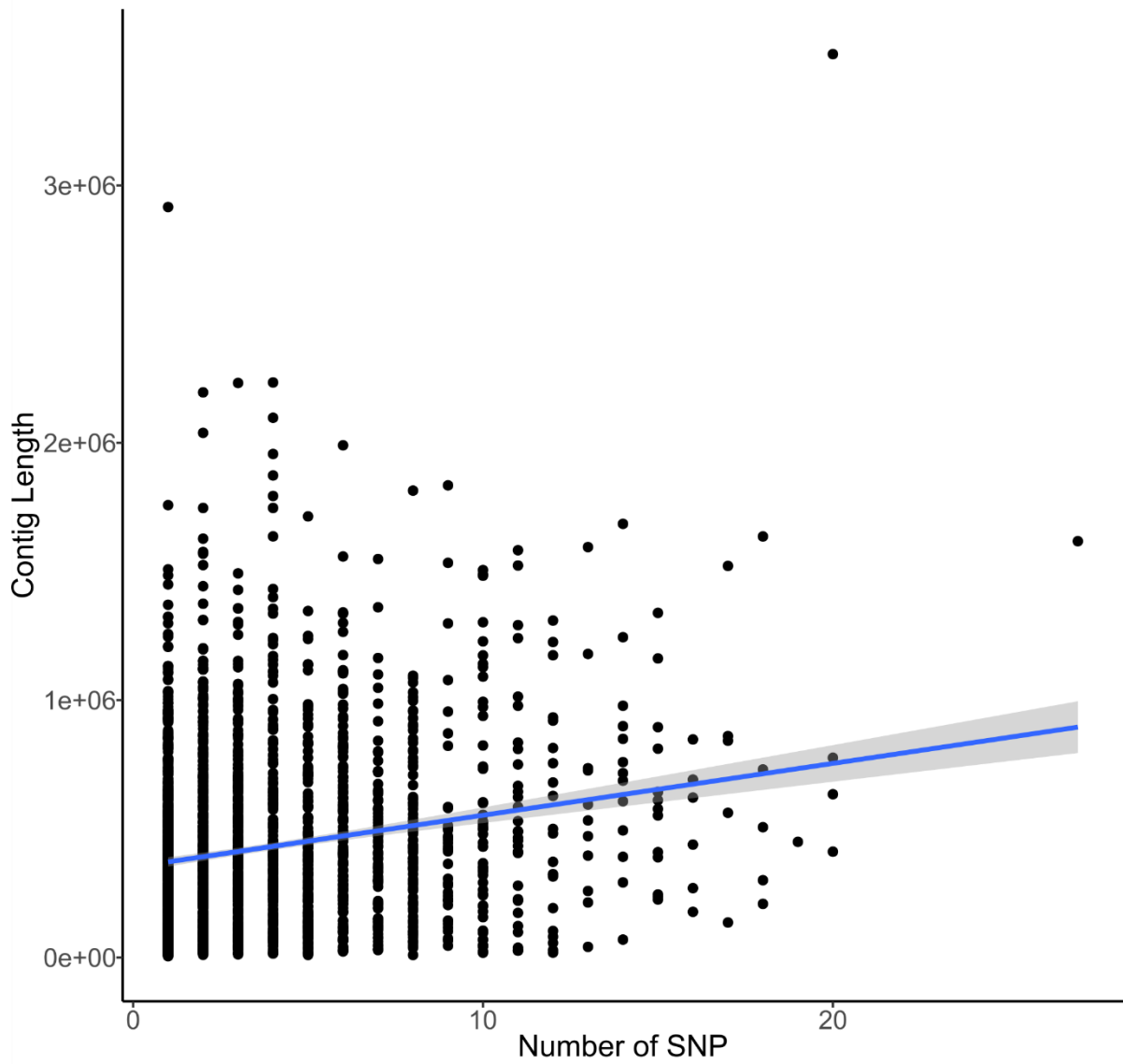


Figure S3.2. Correlation between contig length and the number of SNPs present in the whole-genome dataset.

Principal component variance explained

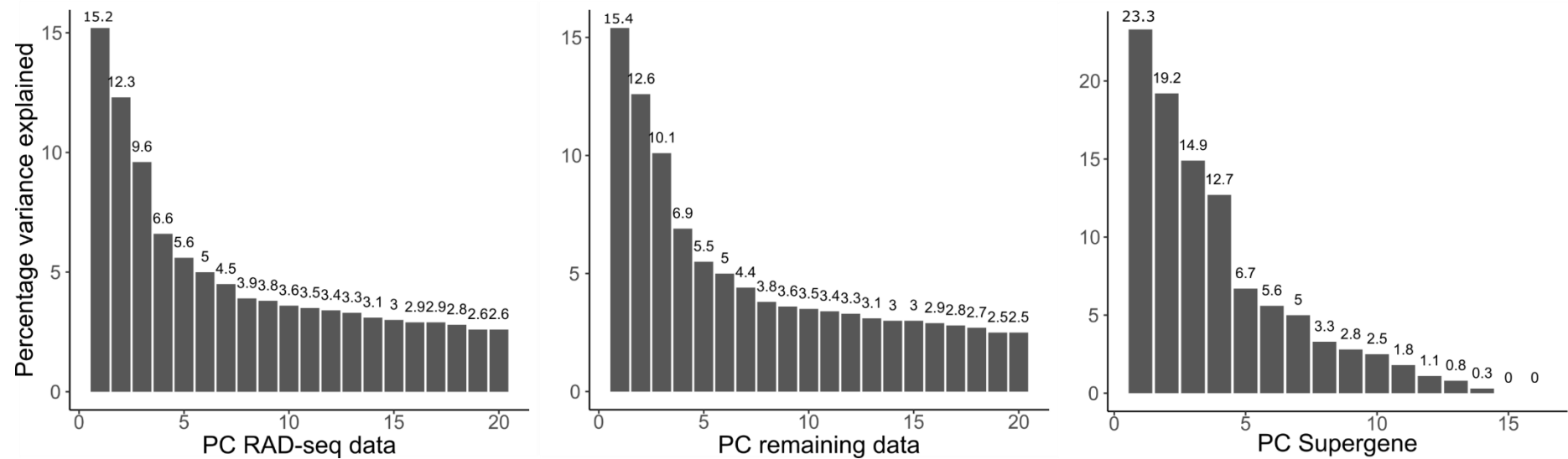


Figure S3.3. The proportion of the variation explained by each axis returned by the principal components analysis.

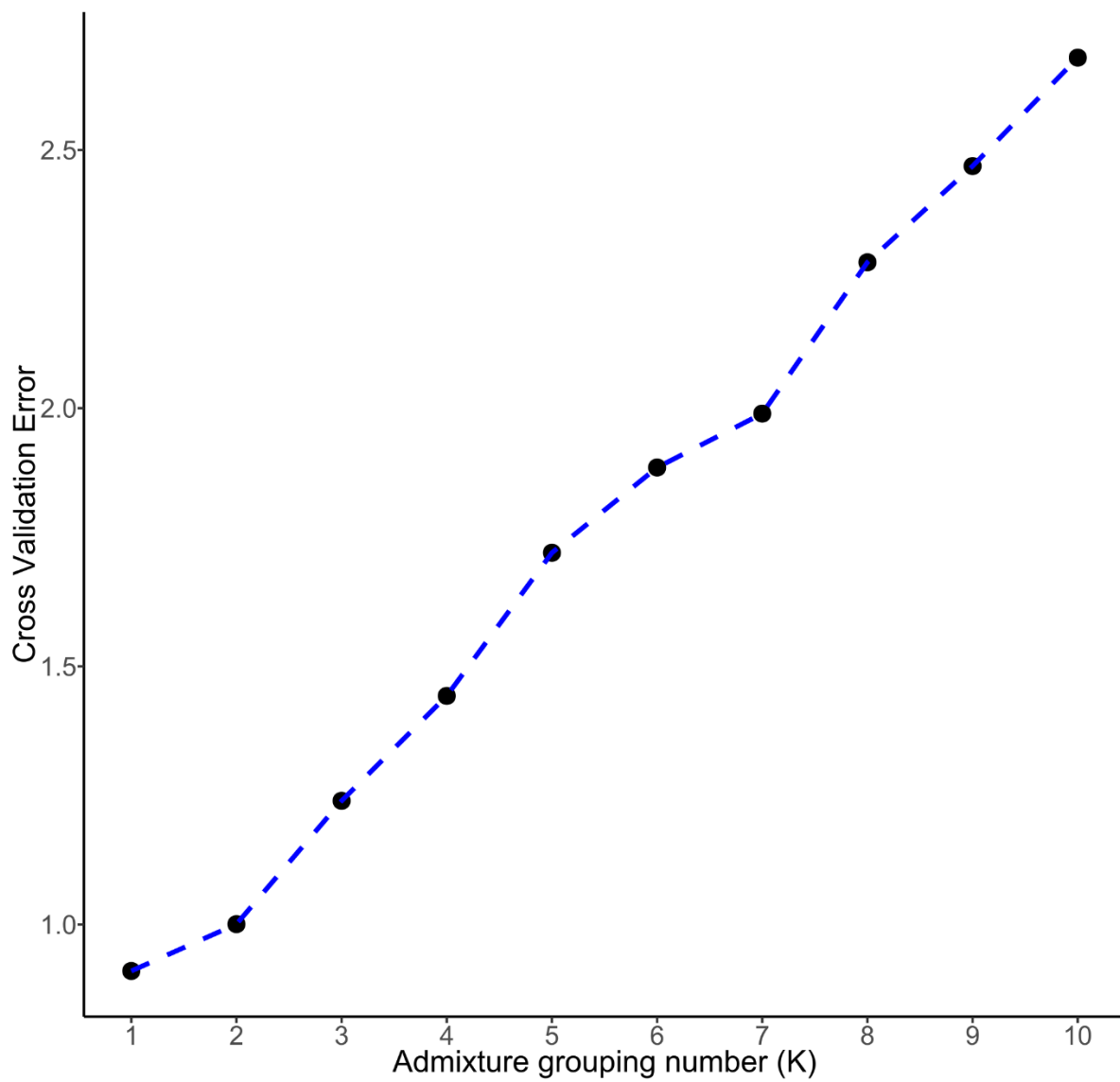


Figure S3.4. Cross validation error results for each admixture group (K).

Table S3.1. Illumina reads sequenced per individual and allelic coverage of the double restriction site–associated DNA (RAD) loci dataset.

ID samples	HQ reads	HQ reads mapped to reference	% reads mapped to reference	Genotype count final dataset			
				./.	0/0	0/1	1/1
26	8849929	8441460	0.95	1861	3835	1231	1755
27	7719430	7382608	0.96	1709	4054	1097	1816
28	5375147	5133507	0.96	1864	4080	1198	1531
29	8984822	8611299	0.96	1216	4414	1367	1679
30	6930986	6530062	0.94	1954	3268	1017	2436
31	7148020	6868309	0.96	983	4200	1375	2114
32	8108195	7679710	0.95	1518	3699	1250	2207
33	8484716	8049748	0.95	1364	3907	1258	2141
34	8893638	8449811	0.95	1476	3883	1057	2259
35	10029342	9499300	0.95	1821	3281	1142	2427
36	8517263	8160706	0.96	1708	3776	1099	2098
37	6564917	6220633	0.95	1714	3786	1095	2084
38	4831810	4617760	0.96	3284	2966	804	1630
39	4246532	3982228	0.94	2999	3144	870	1666
40	9898068	9440156	0.95	1591	3886	1202	2000
41	7803244	7436938	0.95	1685	3648	1075	2267
42	8559966	7946228	0.93	2153	3398	647	2478
43	4244115	3909122	0.92	3093	2904	799	1881
44	8127575	7458672	0.92	1862	3528	909	2374
45	10456078	9967158	0.95	1194	4028	1483	1973
46	6833045	6582555	0.96	1395	4348	1061	1873
47	6327893	6097916	0.96	1699	4181	989	1812
48	9159767	8690192	0.95	1121	4647	1281	1630
49	7681527	7369040	0.96	1062	4537	1310	1768
50	7770439	7427688	0.96	1242	4230	1195	2008

51	1896319	1824665	0.96	3113	3302	959	1304
52	8045555	7750617	0.96	1257	4520	1128	1771
53	7050933	6767607	0.96	1649	4187	1044	1800
54	7992130	7683529	0.96	900	4537	1314	1929
55	9381678	8877341	0.95	1374	3562	1230	2507
56	5344676	5068577	0.95	1105	3944	1463	2159
57	188180	-	-	-	-	-	-
58	58766	-	-	-	-	-	-
59	6123971	5874845	0.96	1166	4008	1260	2241
60	7544753	7211956	0.96	892	3586	1601	2587
61	6842140	6583604	0.96	1262	4027	1102	2282
62	2008007	1912867	0.95	3894	2597	707	1480
63	8119802	7688658	0.95	1667	3751	1239	2019
64	6463278	6129393	0.95	1945	3679	1131	1923
65	6384347	6050609	0.95	2428	3079	1077	2096
66	7585286	7232495	0.95	1519	4080	1165	1915

Table S3.2. Contigs surrounding the supergene described by Dr. Suzanne Saenko, RAD-seq loci mapping supergene-linked contigs and supergene-linked contigs (with their RAD-seq loci started position) presenting SNP's in the filtered dataset and their SNP's position.

Supergene Contigs	RAD-seq Supergene contigs	RAD-seq supergene variant (Starting-pos)	RAD-seq supergene SNPs
ctg61795	ctg61795	ctg18101-31427	ctg18101-31462
ctg57160	ctg57160	ctg7799-57269	ctg18101-31485
ctg57388	ctg57388	ctg6465-72273	ctg18101-31487
ctg52372	ctg52372	ctg10711-128872	ctg18101-31497
ctg46636	ctg46636	tig00001874-209300/209316	ctg18101-31568
ctg45378	ctg45378	tig02170041 (RAD8/10)-201334	ctg7799-57301
ctg41688	ctg41688	tig00045252-71	ctg7799-57375
ctg40857	ctg40857		ctg6465-72280
ctg38937	ctg38937		ctg6465-72292
ctg33047	ctg33047		ctg6465-72313
ctg33079	ctg33079		ctg6465-72337
ctg31172	ctg31172		ctg6465-72351
ctg30377	ctg30377		ctg6465-72417
ctg29158	ctg29158		ctg10711-128947
ctg26173	ctg26173		ctg10711-128949
ctg22062	ctg22062		ctg10711-128990
ctg29028	ctg29028		ctg10711-129013
ctg23215	ctg23215		tig00001874-209360
ctg19577	ctg19577		tig00001874-209405
ctg26823 (RAD06)	ctg26823 (RAD06)		tig00001874-209411
ctg18462	ctg18462		tig00001874-209414
ctg18261	ctg18261		tig00001874-209423
ctg27326	ctg27326		tig00001874-209432
ctg31541	ctg31541		tig02170041-203393
ctg14665	ctg14665		tig02170041-203394

ctg15079
ctg14676
ctg10733
ctg15298
ctg9575
ctg8491
ctg4892
ctg12182
ctg39989
ctg23821
ctg18101
ctg15973
ctg29354
ctg14244
ctg15341
ctg16135
ctg7799
ctg6901
ctg12782
ctg5603 (RAD06)
ctg6465
ctg20315
ctg7855
ctg7898
ctg10711
contig_18515
tig02169229
ctg5701 (RAD9)
ctg8479

ctg15079
ctg14676
ctg10733
ctg15298
ctg9575
ctg8491
ctg4892
ctg12182

tig02170041-203482
tig00045252-132
tig00045252-137
tig00045252-141
tig00045252-207
tig00045252-209

ctg6294
tig00001874
tig02170041 (RAD8/10)
tig00398893
tig00012620
tig00045252

Table S3.3. PCA data for the whole-genome dataset.

ID	PC1	PC2	PC3	PC4	PC5	PC6	PC7	PC8	PC9	PC10	PC11	PC12	PC13	PC14	PC15	PC16
26	0.155	0.080	0.041	-0.040	0.529	-0.196	0.297	-0.139	-0.170	-0.053	0.023	0.037	0.013	-0.037	0.040	0.017
27	0.136	0.076	0.054	0.082	0.072	-0.018	-0.175	0.200	0.088	0.055	0.780	-0.237	-0.005	-0.288	-0.017	0.153
28	0.154	0.074	0.032	-0.062	0.095	-0.076	-0.210	0.125	0.192	0.267	-0.197	-0.132	0.038	-0.008	-0.043	-0.459
29	0.166	0.109	0.057	-0.122	0.087	-0.128	-0.209	0.062	0.134	0.223	-0.078	-0.153	0.049	-0.044	-0.017	-0.281
30	-0.279	0.149	-0.221	-0.050	0.050	-0.156	-0.042	0.000	0.030	-0.072	0.013	-0.040	-0.062	0.026	0.037	-0.035
31	0.073	0.034	0.002	0.095	-0.035	-0.116	-0.050	0.091	-0.088	0.347	-0.338	-0.317	0.213	-0.311	-0.180	0.318
32	0.026	-0.321	-0.096	-0.059	0.004	0.031	0.057	-0.020	0.043	-0.136	0.137	-0.033	0.011	-0.006	-0.204	-0.333
33	0.013	-0.308	-0.082	-0.010	0.022	0.017	0.049	-0.099	0.015	-0.082	0.021	-0.011	0.118	0.068	-0.267	-0.254
34	0.026	-0.324	-0.129	-0.085	-0.033	0.003	0.021	0.098	0.024	-0.142	-0.104	-0.133	0.057	-0.110	-0.021	0.115
35	-0.270	0.144	-0.244	-0.022	-0.020	-0.142	-0.068	-0.025	0.054	-0.022	0.004	0.013	-0.020	-0.006	0.055	0.011
36	0.040	-0.001	-0.020	0.500	0.024	0.113	-0.057	-0.207	0.125	-0.020	-0.118	-0.175	-0.159	0.045	0.174	0.005
37	0.039	-0.013	-0.015	0.527	0.072	0.122	-0.082	-0.157	0.050	-0.068	-0.044	-0.207	-0.204	0.100	0.154	0.017
38	0.070	0.066	0.007	0.280	0.045	0.072	-0.079	0.515	-0.089	-0.154	-0.142	0.345	0.089	-0.096	0.029	-0.027
39	0.061	0.049	0.041	0.268	0.060	0.072	-0.035	0.390	-0.191	-0.095	0.008	0.288	0.162	0.192	-0.137	-0.078
40	-0.033	0.137	-0.018	-0.167	-0.004	0.570	0.144	-0.030	-0.011	0.060	0.019	0.038	-0.125	-0.118	0.029	-0.046
41	-0.188	0.111	-0.069	0.039	-0.046	0.195	0.193	-0.047	-0.213	0.117	-0.045	-0.114	0.067	-0.100	-0.348	0.013
42	-0.325	-0.096	0.467	-0.032	-0.004	-0.061	0.015	0.033	0.031	-0.015	-0.020	-0.022	-0.025	-0.006	0.015	0.045
43	-0.277	-0.073	0.436	-0.029	-0.012	-0.030	-0.003	0.003	-0.021	-0.054	-0.012	-0.020	0.025	0.002	0.068	-0.050
44	-0.301	-0.078	0.447	-0.023	0.009	-0.049	-0.032	0.029	0.016	-0.014	0.002	-0.040	-0.036	0.009	0.005	-0.012
45	-0.031	0.144	-0.013	-0.134	-0.017	0.484	0.156	0.008	-0.133	0.043	-0.038	-0.036	-0.083	-0.247	0.186	-0.165
46	0.169	0.099	0.066	-0.070	-0.205	-0.097	-0.241	-0.296	-0.379	-0.091	-0.028	0.070	0.041	-0.028	-0.004	-0.133
47	0.162	0.105	0.080	-0.033	-0.219	-0.038	-0.286	-0.279	-0.458	-0.141	0.081	0.039	0.176	-0.014	0.086	0.056
48	0.180	0.071	0.064	-0.210	0.072	0.071	-0.219	-0.040	0.268	-0.132	0.043	0.131	-0.161	0.061	0.224	-0.056
49	0.161	0.084	0.037	-0.198	0.015	0.111	-0.131	-0.031	0.261	-0.163	-0.167	0.102	0.045	-0.052	-0.173	0.198
50	0.077	0.130	0.026	-0.097	-0.088	0.190	0.105	0.068	0.026	0.155	0.104	-0.285	0.277	0.750	-0.015	0.129
51	0.114	0.101	0.050	-0.182	-0.005	0.037	-0.055	-0.010	0.264	-0.185	-0.153	0.120	0.089	-0.003	0.016	0.376
52	0.170	0.102	0.063	-0.038	-0.133	-0.147	0.064	0.075	-0.084	-0.072	-0.034	-0.017	-0.713	0.158	-0.477	0.107
53	0.135	0.111	0.036	0.079	-0.377	-0.203	0.417	0.019	0.155	-0.035	0.015	0.036	0.074	-0.088	0.134	-0.123
54	0.130	0.102	0.026	0.070	-0.390	-0.209	0.395	-0.019	0.171	0.007	0.060	0.081	0.076	-0.071	0.151	-0.071
55	-0.271	0.166	-0.226	-0.028	0.023	-0.097	-0.042	-0.015	0.012	-0.028	0.031	0.033	-0.069	0.039	0.014	0.025

56	0.024	-0.305	-0.116	-0.063	-0.056	0.021	0.061	0.024	-0.019	-0.150	0.036	-0.111	0.015	-0.130	-0.059	0.043
59	-0.048	-0.133	-0.019	0.214	0.044	0.107	-0.069	-0.401	0.310	-0.004	0.059	0.273	0.253	-0.028	-0.270	0.075
60	-0.261	0.161	-0.240	-0.022	0.012	-0.105	-0.038	0.002	0.049	0.025	-0.006	0.056	-0.008	-0.020	-0.024	0.025
61	0.034	-0.327	-0.126	-0.099	-0.011	-0.034	-0.028	0.096	-0.128	-0.070	-0.094	-0.117	-0.103	0.115	0.274	-0.040
62	0.034	-0.269	-0.122	-0.104	-0.020	-0.016	-0.010	0.149	-0.082	-0.050	-0.100	-0.119	-0.039	0.019	0.269	0.244
63	0.009	-0.204	-0.075	-0.035	-0.041	0.011	0.003	0.041	-0.064	0.331	0.240	0.259	-0.012	0.097	-0.005	0.134
64	-0.013	-0.196	-0.037	-0.006	-0.015	-0.044	-0.043	-0.110	-0.043	0.589	-0.013	0.402	-0.196	0.033	0.156	0.082
65	-0.249	0.147	-0.215	-0.048	0.016	-0.103	-0.100	0.038	-0.033	-0.120	0.046	-0.011	0.097	0.067	0.038	-0.079
66	0.145	0.073	0.054	-0.044	0.506	-0.141	0.317	-0.123	-0.115	-0.029	-0.003	0.030	0.061	0.029	0.065	0.046

Table S3.4. All contigs present in the final dataset showing their length and number of SNPs. Moreover, Mantel test results between genetic distance of each RAD genomic regions and the geographical distance.

scaffold	Contig Length	SNPs	Fst mean	Mantel r	P-value
ctg10711	214766	4	0.299	0.010	0.274
ctg18101	41596	5	0.403	-0.003	0.529
ctg6465	130785	6	0.108	0.102	0.000
ctg7799	89027	2	0.281	0.002	0.454
tig00001874	347208	6	0.192	0.040	0.010
tig00045252	1171230	5	0.173	-0.009	0.621
tig02170041	440716	3	0.255	0.004	0.406
ctg5276	175985	1	0.135	-0.170	1.000
tig00041043	748783	1	0.137	-0.137	1.000
ctg7924	404164	1	0.066	-0.125	1.000
ctg6606	147718	1	0.112	-0.123	1.000
contig_23319	289200	3	0.205	-0.122	1.000
tig02186502	521409	1	0.170	-0.110	1.000
tig00054407	676461	1	0.125	-0.106	1.000
ctg18483	39850	1	0.189	-0.106	1.000
tig00401724	386201	2	0.220	-0.102	1.000
ctg6765	98076	1	0.131	-0.102	1.000
ctg291	466624	2	0.170	-0.101	1.000
ctg6031	104614	3	0.155	-0.101	1.000
tig00402053	412341	1	0.132	-0.101	1.000
ctg13598	116761	3	0.174	-0.100	1.000
ctg44666	12839	1	0.148	-0.100	1.000
ctg12314	121369	8	0.190	-0.099	1.000
contig_53782	638023	3	0.248	-0.097	1.000
ctg1015	337978	1	0.082	-0.096	1.000
tig00405312	546268	1	0.150	-0.096	1.000
ctg20106	104214	10	0.170	-0.089	1.000
tig00397172	347118	2	0.209	-0.088	1.000
ctg7192	240187	2	0.074	-0.084	1.000
contig_689	476457	2	0.227	-0.084	1.000
tig00050418	273796	4	0.163	-0.082	1.000
tig00396244	1834507	9	0.207	-0.080	1.000
tig00040990	955367	2	0.174	-0.079	1.000
tig00005194	612128	1	0.261	-0.078	1.000
tig00024280	522037	3	0.341	-0.061	1.000
tig00008071	418812	2	0.235	-0.058	1.000
tig00021475	252673	1	0.090	-0.112	1.000
tig00407665	258132	1	0.067	-0.097	1.000
ctg6557	190769	1	0.206	-0.085	1.000
ctg145	513807	1	0.171	-0.084	1.000
tig00015817	424690	2	0.125	-0.079	1.000
ctg6752	174357	1	0.233	-0.078	1.000
ctg3436	146131	2	0.243	-0.073	1.000
ctg4188	293217	5	0.197	-0.068	1.000
ctg1258	369546	1	0.270	-0.068	1.000
ctg6325	141808	6	0.310	-0.061	1.000
tig00398538	452927	1	0.174	-0.078	1.000
contig_431	589511	2	0.231	-0.068	1.000
tig00009358	809549	4	0.278	-0.055	1.000
scaffold_32099	454066	1	0.130	-0.090	1.000
tig02186388	759101	14	0.260	-0.070	1.000
ctg1210	716347	4	0.211	-0.063	1.000
tig00006570	592824	3	0.291	-0.063	1.000
contig_4695	367886	6	0.348	-0.055	1.000
ctg5838	108313	2	0.373	-0.044	1.000
ctg1474	382591	1	0.172	-0.082	1.000
contig_52177	222994	2	0.212	-0.066	1.000
tig00396812	424463	5	0.276	-0.059	1.000
ctg4789	236449	3	0.206	-0.052	1.000
tig00403009	398319	1	0.105	-0.099	1.000
ctg2428	334772	1	0.127	-0.088	1.000

ctg6981	161642	5	0.283	-0.064	1.000
tig00036448	352128	2	0.272	-0.051	1.000
ctg46545	13873	5	0.196	-0.071	0.999
tig00399345	573471	7	0.189	-0.068	0.999
ctg1969	249935	3	0.257	-0.057	0.999
tig00397759	417826	1	0.260	-0.057	0.999
ctg1729	227373	5	0.271	-0.045	0.999
ctg1327	304415	8	0.205	-0.034	0.999
scaffold_56103	419285	1	0.251	-0.055	0.998
tig02186840	468967	1	0.169	-0.075	0.998
tig00119532	356718	1	0.228	-0.064	0.998
tig00006926	902723	2	0.292	-0.054	0.998
ctg6571	149310	4	0.143	-0.075	0.998
tig00002546	437028	4	0.251	-0.048	0.998
tig00057919	436433	8	0.210	-0.047	0.998
ctg11117	106448	7	0.265	-0.056	0.997
ctg2051	206267	6	0.204	-0.051	0.997
tig02171594	616023	3	0.238	-0.044	0.997
ctg30048	105587	3	0.223	-0.034	0.997
tig00010953	659108	6	0.158	-0.060	0.997
ctg1262	473267	1	0.315	-0.043	0.997
ctg778	822759	6	0.222	-0.043	0.997
ctg40795	15483	3	0.184	-0.055	0.997
contig_27674	345663	2	0.208	-0.059	0.997
ctg1130	244509	3	0.217	-0.048	0.997
ctg2231	323080	4	0.180	-0.047	0.997
ctg3672	177353	16	0.360	-0.043	0.997
ctg3589	135977	17	0.198	-0.061	0.997
tig00406272	924428	1	0.259	-0.050	0.996
ctg3197	425979	1	0.316	-0.043	0.996
contig_27294	397769	4	0.445	-0.032	0.996
tig00005735	943713	5	0.177	-0.056	0.996
tig00006949	1521481	17	0.297	-0.045	0.996
contig_1838	281150	1	0.112	-0.074	0.995
ctg52391	9703	8	0.327	-0.041	0.995
ctg7429	139935	8	0.201	-0.042	0.995
ctg5571	143972	6	0.265	-0.051	0.995
tig00004394	1026468	3	0.146	-0.051	0.995
ctg4160	417727	2	0.288	-0.047	0.995
tig00046703	666969	3	0.256	-0.045	0.995
ctg6030	288957	2	0.219	-0.033	0.995
tig00053952	273129	1	0.338	-0.031	0.995
ctg7750	138288	2	0.195	-0.049	0.995
tig02170482	275430	1	0.236	-0.055	0.995
tig00038242	363803	2	0.118	-0.073	0.994
contig_18474	427180	3	0.183	-0.064	0.994
ctg34037	20530	4	0.111	-0.068	0.994
ctg518	409262	4	0.262	-0.042	0.994
ctg15951	66240	5	0.172	-0.057	0.994
ctg13923	53982	5	0.322	-0.050	0.994
tig02170140	733074	5	0.165	-0.048	0.993
tig02187252	680965	5	0.294	-0.047	0.993
contig_40511	233997	3	0.198	-0.058	0.993
ctg4236	198866	10	0.260	-0.043	0.993
ctg32976	35090	1	0.230	-0.053	0.992
ctg8508	149018	2	0.196	-0.047	0.992
tig02176378	1070279	2	0.124	-0.054	0.992
ctg1705	399091	5	0.385	-0.030	0.992
contig_4524	340071	4	0.342	-0.045	0.992
contig_15272	814290	2	0.252	-0.052	0.992
scaffold_46834	290133	2	0.100	-0.047	0.992
tig02171663	620512	1	0.210	-0.051	0.991
ctg125	701017	6	0.320	-0.040	0.991
contig_25791	989377	1	0.113	-0.069	0.991

ctg11116	222084	1	0.276	-0.048	0.991
tig00093181	974712	5	0.283	-0.040	0.990
ctg14575	51019	3	0.264	-0.047	0.990
ctg2370	427969	1	0.096	-0.062	0.990
tig00399423	661880	1	0.234	-0.054	0.990
ctg1840	356731	1	0.330	-0.037	0.989
ctg317	865042	2	0.365	-0.037	0.989
ctg22032	68149	1	0.254	-0.046	0.988
tig02171538	366358	10	0.233	-0.045	0.988
ctg16248	47162	3	0.269	-0.044	0.988
ctg498	528509	1	0.044	-0.067	0.988
ctg1811	477430	7	0.194	-0.043	0.988
ctg6639	160573	4	0.422	-0.026	0.988
ctg13069	99907	1	0.150	-0.064	0.988
tig00007057	1324150	1	0.249	-0.047	0.988
ctg39323	17110	1	0.238	-0.049	0.987
tig00028358	406162	4	0.314	-0.039	0.987
tig00032819	433670	1	0.141	-0.056	0.987
ctg28552	29826	1	0.165	-0.055	0.987
tig00399328	437189	2	0.221	-0.049	0.987
ctg6944	433447	5	0.438	-0.012	0.986
contig_26754	357624	1	0.277	-0.041	0.986
contig_19330	830498	6	0.183	-0.033	0.986
ctg7749	108123	6	0.255	-0.043	0.985
tig00009350	799186	1	0.343	-0.031	0.985
tig00064007	342934	1	0.144	-0.058	0.985
ctg4207	284892	2	0.250	-0.045	0.985
ctg4983	330389	1	0.058	-0.067	0.985
ctg51856	10423	2	0.261	-0.046	0.985
contig_61810	613156	3	0.302	-0.033	0.984
ctg5129	119983	2	0.276	-0.042	0.984
tig00397802	696041	2	0.136	-0.059	0.984
tig00031716	616509	4	0.298	-0.039	0.984
tig00016167	1008196	2	0.239	-0.047	0.984
ctg8197	97348	1	0.183	-0.056	0.984
ctg2160	487772	1	0.181	-0.056	0.983
tig00399075	411201	20	0.254	-0.042	0.983
ctg8810	115513	2	0.106	-0.056	0.983
tig00398828	850437	8	0.208	-0.039	0.982
tig00041084	252056	1	0.125	-0.060	0.982
ctg10194	72179	2	0.264	-0.043	0.982
contig_8740	463624	3	0.390	-0.026	0.981
tig00397755	229364	2	0.255	-0.040	0.981
contig_6833	679942	12	0.321	-0.042	0.981
scaffold_59590	510281	2	0.336	-0.030	0.981
tig00396865	961683	4	0.395	-0.026	0.981
contig_53681	1302649	10	0.233	-0.031	0.980
ctg4944	223218	2	0.175	-0.047	0.980
contig_1774	895011	15	0.387	-0.036	0.980
ctg1861	247159	1	0.156	-0.048	0.979
tig00024223	665328	2	0.183	-0.051	0.978
tig02169800	615581	1	0.110	-0.044	0.978
contig_17623	686403	2	0.221	-0.035	0.977
contig_35656	409111	7	0.233	-0.041	0.977
ctg8224	340785	8	0.299	-0.036	0.976
contig_7543	649077	3	0.204	-0.035	0.976
tig00066007	320286	10	0.184	-0.038	0.976
tig00005910	857596	1	0.226	-0.045	0.976
ctg2887	255917	1	0.159	-0.052	0.975
tig00398326	606047	2	0.340	-0.032	0.975
ctg14959	117517	2	0.066	-0.058	0.975
tig02187655	457626	9	0.378	-0.029	0.975
tig00398865	1094907	8	0.146	-0.038	0.974
tig00001599	1569036	2	0.203	-0.039	0.973

contig_16749	805603	8	0.194	-0.041	0.972
ctg14055	107045	5	0.317	-0.037	0.972
contig_39644	403775	1	0.305	-0.030	0.971
ctg203	781417	6	0.100	-0.043	0.971
scaffold_51892	755035	12	0.194	-0.035	0.970
ctg3693	460654	2	0.243	-0.041	0.970
ctg8392	84527	2	0.234	-0.029	0.970
tig00001835	686990	14	0.227	-0.038	0.969
ctg6	975128	3	0.317	-0.033	0.969
tig00396497	398212	3	0.178	-0.052	0.969
ctg3041	418962	1	0.104	-0.053	0.969
contig_4414	1442777	2	0.223	-0.040	0.968
ctg29297	24059	10	0.311	-0.036	0.968
tig00026631	323405	5	0.320	-0.034	0.968
tig02187047	470317	9	0.242	-0.042	0.968
ctg3050	401065	2	0.211	-0.034	0.967
tig00406281	515387	3	0.300	-0.034	0.967
ctg17341	39936	2	0.248	-0.038	0.967
tig00027297	324241	8	0.301	-0.030	0.967
tig00404294	599785	10	0.282	-0.037	0.966
tig00018155	445275	9	0.175	-0.038	0.966
contig_53018	203854	9	0.403	-0.028	0.965
tig00399885	213888	13	0.217	-0.039	0.965
tig02174516	1072428	2	0.217	-0.042	0.965
tig00395542	2232371	3	0.111	-0.039	0.964
tig00020656	553015	2	0.129	-0.051	0.964
tig00058006	235682	1	0.152	-0.049	0.964
ctg6971	330115	5	0.168	-0.043	0.964
tig00004485	423464	3	0.423	-0.020	0.964
tig00003704	707496	2	0.293	-0.035	0.964
ctg323	556690	2	0.094	-0.043	0.963
tig00400506	531125	8	0.229	-0.039	0.962
ctg8531	129756	1	0.133	-0.051	0.962
ctg11896	162155	1	0.121	-0.053	0.961
ctg6817	101147	5	0.403	-0.031	0.961
tig00400180	345951	8	0.330	-0.029	0.960
contig_4203	988606	1	0.071	-0.051	0.960
contig_28150	387256	1	0.109	-0.052	0.959
ctg8786	342317	1	0.170	-0.043	0.959
ctg9798	97912	2	0.189	-0.033	0.957
tig00005085	491010	2	0.213	-0.043	0.957
tig00399336	946996	1	0.246	-0.036	0.957
tig00011204	1249680	5	0.158	-0.032	0.957
tig00012568	574126	3	0.248	-0.039	0.956
tig02172097	365299	3	0.130	-0.040	0.955
tig00031696	266044	3	0.168	-0.038	0.955
ctg7033	151741	3	0.220	-0.036	0.955
tig00006733	1043551	6	0.185	-0.030	0.954
ctg26482	26678	6	0.282	-0.030	0.954
tig00005903	1009578	2	0.112	-0.039	0.953
ctg10623	69524	9	0.156	-0.040	0.953
ctg15842	69704	10	0.292	-0.036	0.953
contig_26080	861962	2	0.273	-0.035	0.953
contig_5925	420925	6	0.296	-0.033	0.952
tig00060711	208514	1	0.142	-0.042	0.952
tig00009400	615519	4	0.072	-0.040	0.951
ctg11556	83898	4	0.169	-0.044	0.951
tig00010342	723569	7	0.283	-0.036	0.950
ctg2900	156611	1	0.330	-0.027	0.950
contig_29041	433395	11	0.331	-0.029	0.950
tig00009539	643777	3	0.259	-0.036	0.949
ctg12971	127733	1	0.125	-0.049	0.949
tig02186518	472047	3	0.318	-0.029	0.948
contig_28867	848974	1	0.310	-0.030	0.947

ctg15832	75114	2	0.372	-0.022	0.947
contig_336	614953	3	0.304	-0.030	0.946
ctg6688	149816	7	0.259	-0.032	0.943
contig_15758	302168	3	0.116	-0.041	0.943
tig00028915	915042	2	0.299	-0.031	0.943
contig_3778	1355989	3	0.208	-0.028	0.942
scaffold_14843	501512	3	0.259	-0.032	0.941
ctg480	498185	2	0.121	-0.047	0.941
ctg3096	152478	1	0.168	-0.041	0.941
ctg1534	296282	5	0.202	-0.031	0.939
ctg7447	196381	2	0.223	-0.035	0.938
ctg331	405717	7	0.193	-0.031	0.938
ctg3000	166404	2	0.173	-0.037	0.938
tig00396206	951799	1	0.086	-0.044	0.937
tig00010978	557111	1	0.255	-0.033	0.937
ctg1925	242318	2	0.248	-0.030	0.937
tig00398143	1217370	4	0.263	-0.029	0.937
tig00007243	1873026	4	0.227	-0.027	0.937
ctg6740	378241	4	0.423	-0.015	0.937
tig00020837	324132	1	0.303	-0.029	0.935
ctg2972	280949	9	0.222	-0.025	0.935
contig_42854	440649	5	0.272	-0.032	0.933
ctg3920	102920	2	0.340	-0.024	0.933
ctg37731	24574	4	0.228	-0.034	0.933
ctg264	345035	1	0.158	-0.041	0.933
tig00008648	297928	7	0.249	-0.031	0.933
contig_15590	779967	2	0.210	-0.031	0.932
tig02188856	247997	2	0.285	-0.030	0.932
ctg1879	186375	1	0.280	-0.031	0.931
ctg3176	654005	3	0.198	-0.030	0.930
ctg18720	68624	1	0.244	-0.033	0.930
tig00007421	1013623	11	0.184	-0.033	0.930
ctg3687	140394	4	0.233	-0.030	0.930
tig00065518	218465	5	0.345	-0.027	0.929
ctg2422	255259	4	0.280	-0.031	0.929
tig00021369	590619	8	0.114	-0.032	0.928
tig00009506	391926	3	0.149	-0.030	0.928
tig00029220	269394	2	0.298	-0.026	0.926
tig00402298	335061	4	0.213	-0.035	0.925
tig00396387	764312	7	0.176	-0.034	0.924
contig_22179	1575906	2	0.221	-0.036	0.924
tig00015280	588197	4	0.194	-0.033	0.921
ctg25874	27740	2	0.337	-0.022	0.921
ctg5943	325961	2	0.206	-0.023	0.921
tig00049501	272678	1	0.457	-0.008	0.921
ctg7468	139581	2	0.231	-0.029	0.920
tig00396058	432337	2	0.205	-0.027	0.920
ctg6404	175970	6	0.331	-0.022	0.920
ctg5476	300032	1	0.331	-0.023	0.920
tig00396104	1357250	3	0.184	-0.038	0.920
ctg24552	26781	2	0.398	-0.018	0.918
ctg2867	204261	3	0.244	-0.028	0.918
contig_19943	454974	5	0.324	-0.026	0.915
ctg7084	95810	2	0.104	-0.036	0.915
tig00007145	637534	5	0.273	-0.029	0.914
ctg32603	21718	1	0.217	-0.034	0.913
ctg5302	126064	3	0.161	-0.031	0.913
ctg30189	51404	1	0.304	-0.024	0.912
tig00006721	772939	1	0.136	-0.040	0.912
ctg2126	335223	3	0.292	-0.027	0.912
ctg2832	239015	5	0.189	-0.027	0.911
tig00396607	437599	2	0.252	-0.024	0.911
ctg19536	370151	1	0.126	-0.039	0.910
ctg10461	123894	5	0.173	-0.035	0.910

tig00014626	450713	6	0.418	-0.019	0.909
ctg2153	418519	3	0.200	-0.031	0.908
contig_42867	313187	1	0.195	-0.034	0.908
ctg1045	289974	2	0.080	-0.039	0.907
ctg11214	160364	1	0.329	-0.024	0.907
contig_66136	394579	3	0.257	-0.024	0.906
contig_8179	371295	2	0.215	-0.029	0.906
ctg828	395305	5	0.354	-0.027	0.905
tig00396437	1110687	6	0.264	-0.028	0.905
ctg2756	574959	4	0.292	-0.027	0.903
ctg8444	86154	1	0.225	-0.033	0.903
tig02169070	933255	2	0.369	-0.019	0.902
tig00021366	508188	8	0.190	-0.024	0.900
tig00017162	433066	3	0.195	-0.026	0.900
ctg5914	367944	2	0.181	-0.026	0.897
ctg9723	181896	8	0.378	-0.021	0.897
tig00026115	768126	4	0.195	-0.025	0.896
ctg20	636299	7	0.224	-0.025	0.896
ctg2825	159545	3	0.274	-0.019	0.895
tig00395824	471337	1	0.315	-0.021	0.895
tig00061405	200533	1	0.207	-0.033	0.895
ctg35065	19620	1	0.149	-0.037	0.894
ctg4659	237480	1	0.242	-0.030	0.894
contig_15994	1138584	4	0.193	-0.024	0.893
ctg2772	267361	3	0.155	-0.033	0.892
ctg11399	143120	4	0.104	-0.024	0.892
ctg376	1005629	3	0.289	-0.025	0.891
ctg5354	142662	9	0.265	-0.025	0.891
ctg17592	71530	4	0.148	-0.034	0.890
ctg1919	226599	1	0.377	-0.016	0.890
ctg15550	48275	1	0.210	-0.030	0.890
tig00000469	885151	4	0.321	-0.021	0.889
contig_13806	582359	2	0.209	-0.031	0.888
contig_21667	383255	3	0.169	-0.023	0.884
contig_11478	694499	5	0.229	-0.021	0.883
tig00397752	484912	5	0.177	-0.027	0.882
contig_41137	821796	1	0.119	-0.035	0.881
ctg513	294026	2	0.291	-0.019	0.881
tig00398012	450310	3	0.343	-0.021	0.880
tig00397729	700475	3	0.347	-0.019	0.880
contig_6272	456004	5	0.360	-0.021	0.878
tig00000373	623218	3	0.208	-0.027	0.876
contig_12923	1127836	3	0.157	-0.023	0.876
tig00401621	453680	11	0.132	-0.027	0.875
ctg14482	73888	1	0.239	-0.027	0.875
tig00396995	801080	7	0.341	-0.026	0.875
contig_2411	359992	3	0.418	-0.013	0.875
ctg9857	137557	1	0.358	-0.017	0.874
tig00004487	993603	10	0.290	-0.024	0.874
contig_11432	447392	7	0.217	-0.022	0.872
ctg22586	30770	1	0.173	-0.032	0.871
ctg12942	220129	1	0.097	-0.036	0.871
ctg12083	173781	3	0.174	-0.025	0.870
tig00010284	641476	4	0.194	-0.029	0.869
ctg1685	286088	2	0.207	-0.019	0.869
ctg18591	119419	2	0.334	-0.022	0.868
tig00018143	333515	10	0.278	-0.023	0.866
tig00006862	822413	9	0.280	-0.019	0.866
ctg868	376583	4	0.148	-0.029	0.866
contig_19797	905007	8	0.213	-0.021	0.865
tig00042400	328831	4	0.328	-0.022	0.864
tig00399924	745335	8	0.204	-0.020	0.863
ctg21874	87731	2	0.222	-0.026	0.862
ctg2508	503754	9	0.372	-0.017	0.860

ctg4501	323693	1	0.104	-0.031	0.859
tig00071454	302856	3	0.310	-0.022	0.859
tig00016676	577223	15	0.188	-0.019	0.859
ctg3401	196760	5	0.297	-0.023	0.858
tig02186571	405257	6	0.247	-0.019	0.856
tig00043155	690817	3	0.158	-0.026	0.855
ctg320	359004	2	0.315	-0.020	0.853
ctg2355	168242	3	0.169	-0.027	0.851
tig00009262	640215	1	0.340	-0.018	0.850
ctg972	331155	2	0.142	-0.022	0.849
tig00014641	600358	1	0.170	-0.022	0.848
tig00053395	255810	2	0.167	-0.023	0.848
ctg1804	188773	1	0.341	-0.016	0.847
tig00404812	420122	2	0.178	-0.028	0.846
tig00119373	254233	1	0.208	-0.027	0.845
ctg53790	9456	1	0.237	-0.025	0.845
tig00107002	695308	1	0.387	-0.013	0.841
contig_34695	361553	2	0.260	-0.024	0.840
ctg6552	221404	5	0.182	-0.024	0.840
ctg10579	127802	3	0.081	-0.031	0.837
contig_38800	584394	3	0.115	-0.027	0.835
ctg4700	122142	11	0.396	-0.017	0.835
ctg21	770111	1	0.332	-0.016	0.834
contig_49782	506649	6	0.173	-0.017	0.834
tig00395793	652341	1	0.112	-0.024	0.832
ctg3476	191175	3	0.232	-0.024	0.831
ctg2349	288377	9	0.348	-0.016	0.829
tig00001443	534525	6	0.246	-0.017	0.828
ctg11916	60490	4	0.187	-0.025	0.827
ctg43	734717	1	0.143	-0.028	0.826
ctg2260	278184	5	0.278	-0.020	0.825
tig00396873	456457	8	0.233	-0.023	0.825
ctg8957	120884	1	0.096	-0.030	0.824
ctg6985	176142	6	0.232	-0.021	0.822
tig02186482	686166	6	0.289	-0.018	0.822
ctg5425	540309	5	0.213	-0.014	0.818
ctg9560	77795	4	0.157	-0.021	0.816
tig02169355	936654	6	0.226	-0.017	0.814
ctg855	246009	1	0.211	-0.024	0.813
ctg47	624958	1	0.098	-0.028	0.812
contig_3405	962480	3	0.240	-0.014	0.811
tig00397350	237877	6	0.270	-0.016	0.811
ctg113	448522	5	0.220	-0.019	0.810
tig00002843	507905	1	0.302	-0.018	0.810
ctg15667	77389	1	0.166	-0.022	0.809
ctg9368	140361	2	0.291	-0.018	0.808
ctg1607	381967	1	0.332	-0.015	0.805
ctg26054	53731	2	0.193	-0.019	0.805
tig00086880	365570	2	0.179	-0.018	0.804
contig_17063	386425	8	0.318	-0.018	0.802
tig00028821	241823	4	0.162	-0.021	0.802
tig00398075	810072	11	0.185	-0.016	0.800
ctg6948	136897	5	0.389	-0.011	0.798
ctg893	591911	1	0.166	-0.023	0.797
ctg7615	202002	2	0.257	-0.019	0.795
ctg10661	121186	1	0.077	-0.026	0.793
tig00016413	430220	9	0.249	-0.020	0.792
tig00009368	611554	1	0.249	-0.019	0.791
ctg6122	146735	1	0.247	-0.019	0.791
ctg3010	285174	1	0.088	-0.023	0.790
ctg26702	27159	1	0.126	-0.025	0.789
contig_4080	959621	1	0.191	-0.023	0.788
ctg10736	116861	1	0.202	-0.020	0.788
ctg13002	87428	2	0.264	-0.019	0.788

tig00059861	627643	12	0.262	-0.016	0.788
ctg1189	223704	1	0.253	-0.019	0.786
ctg6643	116228	9	0.402	-0.014	0.784
ctg16873	61982	7	0.406	-0.014	0.783
contig_23935	405199	1	0.140	-0.023	0.783
scaffold_944	983878	5	0.280	-0.016	0.782
contig_24216	646077	1	0.303	-0.016	0.781
ctg666	461153	5	0.234	-0.016	0.777
tig02169060	484131	1	0.158	-0.023	0.777
ctg41660	15405	4	0.186	-0.019	0.777
tig02172068	929912	8	0.216	-0.016	0.776
contig_21672	317146	3	0.273	-0.018	0.773
ctg162	383129	3	0.242	-0.010	0.773
ctg3018	593326	6	0.265	-0.017	0.772
tig00401106	535082	4	0.301	-0.016	0.770
ctg3026	235553	3	0.243	-0.019	0.770
contig_12348	554702	1	0.268	-0.017	0.769
ctg17401	82555	2	0.172	-0.020	0.769
tig00399457	348368	10	0.310	-0.015	0.769
ctg12180	62582	8	0.260	-0.015	0.767
contig_8143	362708	8	0.261	-0.015	0.765
ctg9036	187932	1	0.230	-0.018	0.764
tig00026478	509051	10	0.215	-0.016	0.764
tig00396301	327657	1	0.181	-0.020	0.762
contig_27554	896793	5	0.232	-0.018	0.762
contig_23941	225916	3	0.233	-0.016	0.761
tig00395668	570316	1	0.164	-0.021	0.760
contig_1897	611172	5	0.456	-0.009	0.759
ctg55	494795	2	0.227	-0.012	0.757
tig00020570	411200	1	0.179	-0.020	0.756
ctg13348	99632	4	0.236	-0.016	0.755
contig_25226	268350	6	0.331	-0.014	0.755
ctg5331	116510	1	0.180	-0.019	0.755
ctg5245	116128	7	0.389	-0.012	0.755
tig00002219	811392	1	0.308	-0.014	0.753
tig00010983	525514	2	0.278	-0.010	0.753
ctg40423	16488	4	0.176	-0.015	0.753
ctg8715	79747	5	0.218	-0.018	0.752
ctg15909	121615	2	0.202	-0.017	0.752
ctg15398	48685	1	0.231	-0.017	0.751
ctg14134	53369	1	0.075	-0.016	0.751
ctg13926	124705	5	0.246	-0.017	0.750
tig02169085	314262	6	0.236	-0.016	0.749
ctg1101	225191	15	0.190	-0.015	0.749
tig02169753	492903	6	0.434	-0.008	0.745
ctg6079	104669	1	0.045	-0.023	0.744
tig00053246	529663	1	0.187	-0.018	0.744
contig_12366	351532	8	0.219	-0.013	0.741
ctg1496	443367	4	0.201	-0.015	0.741
ctg5337	192064	6	0.177	-0.018	0.740
ctg41	652889	4	0.391	-0.010	0.740
ctg19863	38670	1	0.139	-0.016	0.740
contig_46838	334555	7	0.302	-0.014	0.739
tig00023964	334911	1	0.123	-0.020	0.738
ctg14451	143494	3	0.222	-0.015	0.738
tig00020520	382633	1	0.136	-0.020	0.735
ctg1612	584733	9	0.308	-0.014	0.735
ctg137	546492	7	0.274	-0.014	0.735
tig00398152	581694	5	0.412	-0.009	0.733
tig00403695	556649	3	0.296	-0.013	0.733
ctg7444	91689	1	0.114	-0.021	0.731
contig_13693	1713974	5	0.178	-0.014	0.730
ctg20882	36235	5	0.365	-0.012	0.730
tig00404874	594238	1	0.337	-0.011	0.730

tig00396249	218342	4	0.327	-0.012	0.729
ctg126	608767	2	0.321	-0.012	0.728
ctg46793	12551	1	0.294	-0.013	0.727
tig02169302	611393	4	0.300	-0.013	0.727
tig00094389	335517	1	0.206	-0.017	0.727
ctg15640	59951	1	0.114	-0.017	0.726
tig00091870	717535	1	0.268	-0.014	0.726
contig_24646	285580	3	0.200	-0.013	0.726
contig_13429	1627540	2	0.295	-0.013	0.725
tig00003166	2916146	1	0.260	-0.013	0.725
contig_17367	313943	1	0.321	-0.012	0.723
contig_52794	588399	5	0.229	-0.015	0.722
ctg4434	124676	2	0.226	-0.015	0.722
tig00400896	322104	1	0.215	-0.014	0.721
contig_841	490440	3	0.312	-0.012	0.721
ctg5473	145183	2	0.196	-0.016	0.720
ctg8675	92129	2	0.329	-0.011	0.720
tig00396777	446511	3	0.177	-0.014	0.719
ctg7445	89986	8	0.283	-0.013	0.718
tig00066970	235126	2	0.237	-0.014	0.718
tig00046167	222597	2	0.355	-0.013	0.713
contig_13130	385754	2	0.191	-0.010	0.713
ctg9905	74857	5	0.278	-0.013	0.711
tig02173580	325920	5	0.426	-0.010	0.710
contig_7573	220342	5	0.397	-0.009	0.709
ctg11504	108138	3	0.283	-0.011	0.708
tig00004441	1175210	6	0.279	-0.010	0.707
ctg15821	262696	10	0.296	-0.011	0.705
ctg10240	72657	4	0.232	-0.014	0.705
ctg4903	204066	1	0.251	-0.013	0.705
contig_10092	1119842	2	0.226	-0.009	0.704
ctg5756	218058	2	0.379	-0.009	0.704
ctg1490	490974	8	0.359	-0.010	0.704
contig_21119	661486	3	0.157	-0.014	0.703
tig00006792	266482	4	0.242	-0.014	0.703
tig00043771	1360784	7	0.187	-0.008	0.703
ctg7316	223284	6	0.400	-0.008	0.702
tig00403580	1746765	4	0.406	-0.008	0.700
contig_18859	1197349	2	0.216	-0.014	0.700
ctg63536	4982	1	0.111	-0.014	0.700
ctg26069	27437	11	0.157	-0.012	0.699
tig00030047	269674	3	0.268	-0.011	0.699
ctg8412	84657	4	0.300	-0.012	0.698
ctg33226	42254	1	0.202	-0.014	0.695
tig00036500	465936	9	0.284	-0.010	0.695
tig02170401	297736	8	0.315	-0.011	0.694
tig00009173	539588	1	0.148	-0.014	0.694
contig_48038	281645	5	0.103	-0.013	0.693
tig00043883	220572	1	0.359	-0.008	0.692
ctg2865	273214	1	0.089	-0.017	0.692
tig00073367	813981	12	0.262	-0.010	0.692
ctg16876	43751	7	0.242	-0.012	0.691
ctg5630	133340	1	0.174	-0.013	0.688
tig00397346	502732	2	0.251	-0.013	0.688
tig00055575	1103812	6	0.160	-0.009	0.688
tig00041928	973234	10	0.263	-0.011	0.687
ctg930	522006	4	0.364	-0.009	0.687
scaffold_16094	302431	4	0.205	-0.009	0.686
ctg16917	108112	1	0.255	-0.011	0.685
ctg13904	101038	2	0.271	-0.011	0.682
tig00396056	789257	2	0.337	-0.009	0.680
ctg325	760294	2	0.186	-0.012	0.677
ctg1202	623912	2	0.273	-0.009	0.677
tig00027453	527258	2	0.200	-0.010	0.674

ctg10529	216459	1	0.229	-0.012	0.673
tig00395581	211649	1	0.166	-0.013	0.671
ctg698	290216	7	0.342	-0.009	0.670
tig00397222	228681	1	0.184	-0.012	0.667
ctg7267	91819	2	0.105	-0.012	0.667
tig00396525	704356	2	0.113	-0.012	0.666
ctg10284	71050	1	0.379	-0.007	0.665
ctg3968	268251	1	0.195	-0.013	0.664
ctg9253	78260	4	0.081	-0.012	0.662
ctg6432	103239	1	0.192	-0.012	0.658
tig00083019	730520	18	0.268	-0.009	0.657
ctg570	385748	4	0.237	-0.011	0.656
ctg919	692053	3	0.327	-0.008	0.656
ctg6764	164637	1	0.174	-0.012	0.655
contig_3490	322447	3	0.319	-0.009	0.654
ctg3438	403988	1	0.110	-0.011	0.652
ctg21369	35982	3	0.382	-0.006	0.652
contig_8493	511816	7	0.235	-0.009	0.651
ctg24876	28312	2	0.124	-0.011	0.648
ctg500	345663	2	0.355	-0.008	0.646
tig00000780	278461	1	0.256	-0.009	0.646
ctg5116	168283	4	0.367	-0.008	0.646
contig_16273	663146	1	0.064	-0.012	0.645
tig02172889	252454	9	0.199	-0.008	0.645
ctg18922	75457	1	0.247	-0.009	0.644
ctg1530	577320	1	0.288	-0.009	0.644
ctg1387	514557	1	0.208	-0.010	0.643
ctg4567	191649	2	0.420	-0.005	0.643
contig_5195	843944	4	0.232	-0.009	0.641
contig_897	455080	2	0.276	-0.009	0.640
ctg805	604068	5	0.307	-0.008	0.639
tig00010893	1338994	15	0.302	-0.007	0.636
tig02171490	1030388	8	0.229	-0.008	0.636
ctg31238	34468	5	0.377	-0.006	0.635
ctg35899	19864	1	0.362	-0.006	0.634
tig00395320	1033643	6	0.367	-0.007	0.632
tig00028901	551257	2	0.236	-0.009	0.631
ctg8565	121928	5	0.283	-0.008	0.631
ctg3267	370137	8	0.317	-0.007	0.630
tig00399725	355106	1	0.314	-0.007	0.630
ctg8991	210350	8	0.441	-0.005	0.629
ctg8008	104172	2	0.250	-0.008	0.628
ctg43878	14345	2	0.304	-0.007	0.628
tig00400853	386323	3	0.119	-0.008	0.627
contig_33969	263993	8	0.292	-0.008	0.627
ctg2908	226314	9	0.266	-0.007	0.627
tig00014977	370639	1	0.271	-0.008	0.626
tig00017255	471635	1	0.086	-0.009	0.626
scaffold_41143	467631	2	0.144	-0.008	0.624
ctg25649	57345	2	0.226	-0.007	0.623
ctg4797	224255	2	0.247	-0.008	0.620
contig_31783	244048	2	0.076	-0.007	0.618
ctg19669	82762	1	0.345	-0.007	0.615
contig_43563	439607	4	0.228	-0.007	0.614
ctg1059	573554	1	0.215	-0.008	0.614
ctg12213	62309	1	0.335	-0.005	0.613
ctg182	397717	6	0.454	-0.004	0.613
tig00040415	1244426	14	0.242	-0.005	0.611
ctg1497	260225	3	0.318	-0.007	0.611
tig00038427	437035	2	0.176	-0.009	0.611
ctg6661	141709	4	0.255	-0.007	0.611
ctg2241	250175	2	0.194	-0.008	0.610
contig_40725	709630	1	0.148	-0.008	0.608
ctg4266	119268	7	0.411	-0.004	0.608

ctg1381	234532	1	0.197	-0.009	0.607
contig_5714	681477	1	0.275	-0.007	0.607
ctg8256	87012	1	0.072	-0.008	0.606
tig00395532	669779	8	0.253	-0.006	0.606
tig00042780	306102	9	0.357	-0.005	0.604
ctg6808	258490	13	0.180	-0.005	0.600
contig_6104	500458	10	0.219	-0.007	0.599
ctg2529	433038	7	0.279	-0.005	0.597
tig00001967	1524795	2	0.285	-0.006	0.595
contig_17921	524413	2	0.244	-0.007	0.594
ctg16252	45673	9	0.317	-0.006	0.592
ctg3934	547533	1	0.167	-0.006	0.591
tig00395527	1034874	1	0.322	-0.006	0.591
tig00035074	512272	9	0.329	-0.005	0.590
contig_13836	783511	2	0.228	-0.007	0.590
tig02188898	666550	3	0.137	-0.006	0.589
ctg5527	184576	4	0.253	-0.006	0.588
tig00399081	1078544	1	0.184	-0.007	0.587
ctg1912	487146	6	0.236	-0.004	0.587
tig00400810	487621	1	0.202	-0.007	0.586
tig00053577	244843	1	0.141	-0.007	0.585
ctg4235	910052	3	0.257	-0.006	0.585
tig00027697	488684	11	0.337	-0.005	0.583
ctg15102	165018	4	0.162	-0.005	0.582
contig_46319	441250	4	0.271	-0.006	0.581
tig00401160	431609	3	0.271	-0.006	0.579
ctg11032	228265	2	0.185	-0.007	0.578
ctg1334	216750	1	0.215	-0.006	0.576
tig02169171	1137723	5	0.243	-0.005	0.575
ctg8648	245069	2	0.246	-0.006	0.575
tig00007716	1298565	1	0.053	-0.007	0.574
tig00397782	1052995	2	0.437	-0.003	0.573
tig00047187	221709	9	0.318	-0.005	0.571
ctg1936	284549	1	0.109	-0.006	0.570
tig00400104	303083	1	0.053	-0.007	0.570
ctg35355	18397	2	0.178	-0.004	0.569
ctg8024	110807	4	0.218	-0.005	0.568
tig00398510	391527	5	0.295	-0.005	0.568
contig_1845	734391	3	0.239	-0.004	0.567
tig02170273	603096	10	0.231	-0.004	0.566
ctg11810	63609	2	0.207	-0.004	0.564
contig_12211	409191	6	0.171	-0.004	0.562
tig00004124	1011600	8	0.259	-0.003	0.561
ctg6956	277633	1	0.202	-0.005	0.561
tig00041919	508276	1	0.284	-0.004	0.557
ctg1263	425904	3	0.193	-0.004	0.556
tig02170092	629326	1	0.088	-0.005	0.556
tig00036475	647372	4	0.235	-0.004	0.555
ctg2119	189271	4	0.256	-0.004	0.555
ctg831	389348	15	0.229	-0.004	0.555
tig00018277	587778	1	0.287	-0.004	0.555
tig00399333	496237	9	0.267	-0.004	0.555
tig02171434	533159	2	0.188	-0.005	0.555
contig_34639	546659	2	0.155	-0.004	0.549
ctg17345	42194	3	0.250	-0.004	0.547
ctg1748	263778	6	0.305	-0.004	0.547
ctg1061	359285	2	0.212	-0.004	0.546
ctg2655	399946	2	0.239	-0.004	0.545
ctg5625	210968	2	0.217	-0.003	0.545
tig00076252	521038	1	0.216	-0.004	0.543
tig00006648	777613	6	0.278	-0.003	0.542
tig00023974	948520	1	0.107	-0.004	0.542
contig_1864	239348	9	0.237	-0.004	0.540
ctg838	507887	1	0.117	-0.004	0.540

ctg313	401801	4	0.297	-0.003	0.538
tig00015391	506855	1	0.303	-0.003	0.537
tig00102205	1311232	2	0.389	-0.003	0.537
tig00400191	279898	2	0.187	-0.002	0.533
tig00019828	437531	1	0.225	-0.003	0.533
tig00396412	1132115	1	0.351	-0.003	0.533
tig02172912	349288	1	0.216	-0.003	0.531
contig_50564	508870	2	0.046	-0.004	0.530
tig00402541	1116159	6	0.208	-0.003	0.529
ctg3507	799998	3	0.156	-0.003	0.529
tig00014687	531722	3	0.269	-0.002	0.529
ctg2158	928513	5	0.375	-0.002	0.528
ctg19070	39069	1	0.193	-0.003	0.525
ctg14829	102996	5	0.285	-0.002	0.525
scaffold_62778	301450	1	0.309	-0.003	0.524
ctg111	550433	3	0.425	-0.002	0.523
tig00001521	1814178	8	0.209	-0.002	0.523
tig00397854	1340822	6	0.257	-0.002	0.523
ctg16812	52416	1	0.293	-0.002	0.520
tig00040162	655590	2	0.130	-0.003	0.520
contig_38988	427185	4	0.295	-0.002	0.519
tig00397426	224590	4	0.295	-0.002	0.518
ctg16789	81665	5	0.155	-0.002	0.516
ctg27966	26012	6	0.257	-0.002	0.516
tig00399224	274976	7	0.180	-0.002	0.514
contig_167	379846	5	0.229	-0.002	0.513
tig00402753	297647	7	0.205	-0.002	0.512
ctg18611	40214	3	0.204	-0.001	0.512
tig00009696	621637	1	0.163	-0.002	0.511
tig00020401	361343	1	0.237	-0.002	0.510
ctg6939	264968	1	0.206	-0.002	0.510
tig00008084	992601	3	0.391	-0.002	0.509
tig00008190	629190	1	0.092	-0.002	0.508
tig02171222	219427	7	0.304	-0.001	0.508
ctg2366	480735	7	0.337	-0.001	0.506
tig00399004	340133	1	0.210	-0.001	0.506
contig_30102	390755	1	0.062	-0.002	0.506
ctg51138	10694	1	0.165	-0.001	0.505
tig00014974	549881	1	0.310	-0.002	0.505
ctg5389	240228	1	0.337	-0.002	0.503
tig00398942	533835	6	0.239	-0.001	0.503
contig_34666	642048	2	0.305	-0.002	0.502
tig00396028	570496	1	0.241	-0.002	0.502
ctg11215	66374	1	0.077	-0.001	0.502
contig_24015	410659	1	0.188	-0.001	0.501
contig_38459	326343	1	0.184	-0.001	0.500
ctg1899	309002	4	0.226	-0.001	0.500
ctg17228	43623	1	0.247	-0.001	0.498
ctg32	723123	1	0.285	-0.002	0.498
ctg53500	9450	1	0.267	-0.001	0.494
tig00003469	331209	1	0.292	-0.001	0.493
ctg7102	96382	1	0.275	-0.001	0.493
scaffold_34793	251364	3	0.210	-0.001	0.492
contig_24247	834838	2	0.283	-0.001	0.490
tig00014020	484590	1	0.119	0.000	0.490
ctg8146	216194	1	0.200	0.000	0.489
contig_10102	552091	1	0.194	0.000	0.489
ctg26463	27064	1	0.144	0.000	0.488
tig00031805	320586	1	0.275	-0.001	0.487
tig00006081	1034151	3	0.178	0.000	0.486
tig00016527	794251	2	0.249	0.000	0.482
tig02168946	650385	2	0.336	0.000	0.482
tig02186709	609292	3	0.269	0.000	0.482
tig00077938	256834	1	0.269	0.000	0.481

ctg9566	314685	7	0.200	0.000	0.479
ctg5785	214093	1	0.252	0.000	0.475
tig00044630	922835	3	0.315	0.000	0.474
tig00399904	430432	10	0.270	0.001	0.474
tig00019804	373618	6	0.331	0.001	0.473
ctg3152	733178	10	0.306	0.001	0.471
tig02170015	398876	4	0.236	0.000	0.469
tig00032843	353947	2	0.298	0.000	0.468
ctg5867	219649	1	0.244	0.001	0.468
contig_9662	1228451	10	0.280	0.001	0.467
tig02169631	837755	5	0.200	0.001	0.465
ctg616	527122	5	0.203	0.001	0.464
ctg1791	298529	4	0.275	0.000	0.464
tig00034802	480886	8	0.327	0.001	0.462
ctg2400	344491	1	0.098	0.002	0.462
ctg10561	117120	6	0.141	0.001	0.462
tig00030658	331077	7	0.224	0.001	0.459
tig00023902	543692	3	0.196	0.001	0.457
contig_9558	882490	1	0.118	0.002	0.457
ctg18061	41478	2	0.313	0.001	0.456
tig00396080	408416	8	0.272	0.001	0.455
ctg3832	337311	2	0.161	0.002	0.454
tig00061516	328044	4	0.260	0.001	0.454
ctg19368	37938	8	0.257	0.001	0.454
ctg7556	83281	1	0.059	0.002	0.453
tig00399854	715880	5	0.131	0.001	0.453
contig_9324	1484920	1	0.281	0.001	0.453
ctg1080	345086	3	0.318	0.002	0.453
tig00399158	566761	3	0.275	0.001	0.452
tig00399063	297754	6	0.239	0.002	0.452
ctg2267	287725	3	0.196	0.002	0.452
tig00038898	203416	1	0.057	0.003	0.452
contig_35763	924599	4	0.161	0.002	0.451
contig_55226	469688	2	0.184	0.002	0.451
ctg1391	542348	3	0.382	0.001	0.450
contig_5364	441384	2	0.143	0.001	0.449
contig_11399	872055	6	0.213	0.002	0.449
ctg3925	129008	7	0.274	0.002	0.446
ctg4594	121809	2	0.240	0.002	0.445
scaffold_68823	749868	3	0.227	0.002	0.443
ctg22063	44424	3	0.083	0.003	0.443
ctg25088	60155	1	0.135	0.003	0.443
ctg3847	140969	1	0.037	0.004	0.443
ctg4936	118375	2	0.150	0.002	0.441
ctg2463	300679	2	0.327	0.002	0.440
contig_18092	623818	2	0.258	0.002	0.440
ctg16750	92128	4	0.182	0.002	0.440
tig02186728	403509	3	0.155	0.003	0.439
contig_405	661065	3	0.209	0.002	0.438
tig00027581	444229	4	0.294	0.002	0.437
scaffold_6949	368580	3	0.342	0.002	0.437
tig00402141	287753	1	0.197	0.003	0.435
contig_17666	849625	14	0.292	0.002	0.435
tig00027224	341833	1	0.207	0.003	0.434
contig_4310	359971	3	0.184	0.003	0.434
contig_70356	503602	1	0.313	0.002	0.434
ctg3294	391014	3	0.321	0.002	0.434
ctg2316	208433	1	0.257	0.003	0.433
tig00399036	399234	1	0.187	0.004	0.433
tig00397290	1137711	2	0.115	0.003	0.432
ctg6707	98833	2	0.234	0.003	0.431
ctg19766	36126	3	0.189	0.003	0.430
tig00003060	473357	4	0.171	0.003	0.429
contig_16508	284442	2	0.159	0.004	0.428

contig_1664	360730	5	0.375	0.003	0.428
ctg4071	383765	1	0.394	0.001	0.428
ctg3996	138028	5	0.321	0.003	0.427
ctg11442	65828	1	0.305	0.002	0.427
ctg26023	28036	12	0.342	0.002	0.426
tig00409871	202717	1	0.115	0.003	0.425
ctg8856	124036	1	0.109	0.005	0.423
tig00085471	646292	6	0.306	0.003	0.423
ctg8695	83338	1	0.249	0.004	0.423
contig_27873	199960	5	0.270	0.003	0.422
ctg2286	329912	5	0.180	0.003	0.421
contig_48726	493185	3	0.199	0.002	0.421
ctg11764	63857	8	0.186	0.002	0.420
ctg1397	396155	1	0.317	0.003	0.420
ctg5410	128609	1	0.111	0.004	0.420
ctg6133	147616	2	0.205	0.003	0.419
ctg28915	23102	1	0.167	0.005	0.419
ctg5922	107431	1	0.233	0.003	0.418
tig00042959	303547	1	0.339	0.002	0.417
ctg9169	139841	2	0.319	0.003	0.416
tig00045243	465416	11	0.253	0.005	0.415
ctg7079	95697	6	0.303	0.004	0.411
ctg174	431346	4	0.190	0.004	0.409
tig02170991	444866	5	0.229	0.004	0.409
contig_52009	666542	2	0.333	0.003	0.409
contig_55590	388109	1	0.210	0.005	0.407
ctg2627	297983	2	0.155	0.006	0.407
tig00024900	301345	5	0.253	0.004	0.407
contig_16859	753330	4	0.329	0.004	0.407
ctg479	1027179	1	0.285	0.004	0.405
tig00039289	422826	4	0.327	0.003	0.405
ctg3397	135310	3	0.216	0.003	0.405
tig00038294	302025	6	0.114	0.004	0.405
contig_8775	285451	1	0.137	0.006	0.403
contig_27594	1956444	4	0.214	0.004	0.403
ctg11895	92023	3	0.153	0.005	0.403
tig00002241	860234	2	0.220	0.006	0.403
ctg238	498939	2	0.200	0.005	0.402
contig_29523	221790	1	0.334	0.004	0.402
tig00043906	1233451	4	0.253	0.004	0.401
tig00395980	590998	6	0.346	0.003	0.401
tig02169307	295274	3	0.129	0.006	0.401
tig00026057	346620	1	0.116	0.007	0.399
ctg11792	80376	2	0.261	0.004	0.398
ctg11173	389268	1	0.287	0.004	0.398
contig_10636	230810	2	0.379	0.003	0.397
ctg1333	1139614	5	0.173	0.005	0.396
contig_1486	1077882	9	0.179	0.004	0.395
tig00397833	1018425	2	0.270	0.005	0.394
tig02186434	524742	1	0.168	0.006	0.393
tig00402945	237922	3	0.318	0.004	0.391
scaffold_45183	233345	8	0.266	0.005	0.390
contig_49703	241010	1	0.275	0.005	0.389
ctg11542	64574	1	0.247	0.005	0.389
scaffold_64729	624955	1	0.252	0.005	0.388
tig00399346	1028168	3	0.194	0.006	0.387
ctg2938	352946	3	0.363	0.003	0.387
ctg35727	18729	2	0.227	0.005	0.385
contig_16955	522175	3	0.167	0.007	0.385
ctg6821	98412	5	0.285	0.005	0.385
ctg30127	23394	6	0.270	0.006	0.384
ctg23252	88985	2	0.411	0.002	0.382
ctg23626	51948	3	0.277	0.005	0.381
tig00403819	607026	14	0.238	0.005	0.381

ctg11033	68333	1	0.244	0.006	0.381
tig00031425	691299	16	0.325	0.005	0.380
tig00064960	478952	5	0.304	0.005	0.379
ctg39807	16525	4	0.218	0.006	0.378
ctg16510	45327	1	0.130	0.007	0.378
ctg366	614486	3	0.159	0.006	0.376
ctg9334	264644	1	0.054	0.009	0.375
ctg388	517509	4	0.181	0.006	0.374
ctg17374	72477	2	0.077	0.007	0.372
ctg1518	300125	1	0.177	0.009	0.370
contig_28127	464494	1	0.366	0.004	0.368
tig00399293	499527	12	0.266	0.006	0.365
ctg4364	313481	2	0.265	0.007	0.363
contig_7963	283313	6	0.186	0.008	0.363
ctg7839	326469	3	0.281	0.007	0.361
tig00011099	903735	4	0.356	0.006	0.361
ctg11226	406031	2	0.228	0.008	0.361
contig_11332	693295	1	0.120	0.009	0.359
ctg1241	556466	2	0.454	0.001	0.359
ctg10413	74261	3	0.236	0.007	0.358
contig_3519	723942	7	0.311	0.005	0.358
ctg10371	221668	9	0.368	0.006	0.357
tig00049519	502421	5	0.270	0.007	0.357
ctg3647	334639	4	0.208	0.008	0.357
contig_16291	215563	3	0.230	0.007	0.356
tig00396472	1300381	6	0.221	0.006	0.355
ctg792	256016	2	0.280	0.006	0.355
contig_11612	514562	1	0.123	0.011	0.354
ctg50750	26482	11	0.164	0.006	0.353
tig00000220	1112024	4	0.284	0.006	0.351
contig_26538	225584	5	0.273	0.006	0.349
ctg3241	433825	2	0.109	0.009	0.349
tig00008767	823990	10	0.291	0.006	0.348
ctg21642	31698	4	0.309	0.007	0.346
ctg3161	562706	1	0.122	0.009	0.346
ctg2376	405901	11	0.216	0.007	0.345
ctg3232	583900	3	0.226	0.008	0.344
tig00397077	323985	12	0.190	0.006	0.344
tig00061909	406925	1	0.196	0.010	0.342
tig00042694	313962	2	0.184	0.010	0.342
tig00017426	722482	5	0.293	0.007	0.341
ctg713	278249	4	0.162	0.008	0.341
contig_24117	377481	1	0.176	0.010	0.341
tig00004882	305917	7	0.271	0.008	0.340
ctg24806	28923	3	0.082	0.011	0.339
tig00045603	1505374	10	0.227	0.009	0.339
ctg4373	128964	3	0.287	0.008	0.338
tig00011884	1225809	12	0.201	0.007	0.338
ctg2395	404071	2	0.265	0.009	0.337
tig00002394	2038556	2	0.153	0.012	0.337
ctg2044	489276	1	0.246	0.009	0.337
ctg2809	187657	1	0.146	0.011	0.337
ctg450	299471	7	0.401	0.006	0.337
ctg2273	177579	2	0.127	0.010	0.336
contig_8265	226666	5	0.366	0.006	0.334
ctg11118	100228	2	0.080	0.010	0.334
tig00397604	528125	6	0.297	0.009	0.333
tig00398120	245272	3	0.267	0.006	0.333
ctg5105	307454	2	0.049	0.011	0.332
tig00045694	580614	4	0.321	0.007	0.330
tig00029766	895646	4	0.246	0.008	0.330
ctg883	647412	3	0.102	0.011	0.329
ctg712	302024	4	0.322	0.008	0.329
ctg183	759955	8	0.275	0.009	0.329

ctg1920	666823	11	0.306	0.008	0.329
tig00011506	783833	3	0.128	0.012	0.328
ctg6988	97337	4	0.211	0.010	0.328
contig_47429	246707	2	0.123	0.008	0.327
tig00099272	527006	3	0.332	0.007	0.326
tig00011771	645681	2	0.246	0.010	0.325
ctg1529	420124	8	0.359	0.006	0.325
ctg5497	203990	1	0.109	0.014	0.324
ctg21508	62935	3	0.129	0.012	0.323
tig00003558	705364	3	0.252	0.006	0.323
tig02169097	318812	1	0.234	0.009	0.323
contig_3679	252125	1	0.111	0.014	0.322
contig_34045	1449546	1	0.141	0.013	0.322
ctg3846	305419	2	0.276	0.008	0.321
ctg11944	114540	6	0.335	0.009	0.320
ctg5397	111370	1	0.292	0.009	0.319
ctg21811	69469	14	0.271	0.009	0.318
ctg5832	158175	2	0.084	0.013	0.316
tig00008230	1400285	4	0.259	0.010	0.316
contig_12673	479480	10	0.369	0.007	0.316
ctg17209	43325	3	0.249	0.009	0.315
contig_26028	448753	1	0.217	0.012	0.315
tig00030298	243623	6	0.110	0.010	0.315
tig02170901	829001	5	0.237	0.009	0.313
ctg19165	47385	2	0.354	0.006	0.311
ctg12719	60178	3	0.286	0.010	0.309
tig00027603	286992	4	0.435	0.005	0.308
ctg54	641522	2	0.260	0.008	0.308
tig00082947	362372	4	0.213	0.012	0.308
contig_5161	1115787	5	0.243	0.009	0.307
ctg1371	344290	1	0.172	0.013	0.307
tig00395483	847536	2	0.152	0.011	0.307
tig00050415	277569	6	0.123	0.009	0.306
contig_10263	505274	3	0.236	0.008	0.306
tig00003355	271986	1	0.152	0.013	0.304
ctg9546	81194	5	0.266	0.011	0.304
tig00403306	291777	2	0.403	0.005	0.302
ctg15403	67458	2	0.225	0.011	0.302
tig02171032	898652	8	0.154	0.010	0.301
tig00398109	263642	5	0.313	0.009	0.301
tig00397477	419834	4	0.152	0.012	0.300
tig00396306	735482	12	0.166	0.012	0.299
tig00405137	269972	5	0.382	0.007	0.298
contig_69386	378855	1	0.359	0.007	0.297
ctg5375	200329	3	0.192	0.012	0.297
scaffold_26714	221214	1	0.327	0.010	0.296
tig02173403	539115	3	0.401	0.007	0.295
ctg2179	338079	2	0.193	0.011	0.295
tig00002471	718824	3	0.230	0.013	0.294
contig_1209	476419	2	0.330	0.009	0.293
ctg1668	321688	12	0.335	0.009	0.293
ctg1967	178723	10	0.218	0.010	0.292
contig_26950	996727	3	0.344	0.008	0.292
ctg1809	1047252	2	0.163	0.014	0.291
ctg2274	195032	2	0.309	0.010	0.290
tig00402136	368560	3	0.295	0.010	0.290
tig00060131	617991	6	0.325	0.010	0.290
tig00396701	410243	4	0.243	0.011	0.290
ctg8567	83098	3	0.184	0.011	0.287
ctg4670	199821	1	0.169	0.015	0.286
ctg16687	60298	1	0.136	0.017	0.285
ctg386	578986	3	0.296	0.011	0.284
tig00005188	869273	2	0.182	0.014	0.282
contig_50820	223879	2	0.308	0.011	0.281

tig00011756	1256973	1	0.308	0.011	0.281
tig00022871	832104	4	0.160	0.016	0.280
contig_26333	3510238	20	0.234	0.011	0.280
ctg59	461472	1	0.175	0.015	0.279
ctg48563	12119	3	0.328	0.010	0.279
scaffold_5606	863916	1	0.165	0.014	0.278
tig00031524	621365	16	0.369	0.010	0.276
ctg8119	176077	2	0.196	0.014	0.276
tig02186286	784776	3	0.109	0.012	0.276
contig_29836	269249	3	0.206	0.015	0.276
ctg22323	60152	1	0.365	0.008	0.275
ctg2509	192930	7	0.139	0.013	0.273
tig02186979	276463	3	0.355	0.007	0.272
ctg755	377340	5	0.336	0.010	0.272
ctg3033	172190	5	0.238	0.013	0.271
ctg1023	251366	2	0.190	0.012	0.270
tig00021227	391113	14	0.201	0.013	0.269
ctg9372	140531	2	0.217	0.015	0.269
ctg946	261740	1	0.334	0.010	0.268
tig00060048	455239	3	0.164	0.016	0.268
ctg9658	429156	1	0.162	0.015	0.266
tig00034225	431080	1	0.281	0.012	0.266
ctg1143	269436	16	0.374	0.011	0.265
ctg13353	64487	2	0.219	0.015	0.263
ctg4676	655169	1	0.168	0.017	0.263
ctg1175	1488075	10	0.223	0.012	0.263
tig00396252	2234354	4	0.212	0.011	0.263
contig_16422	412391	9	0.271	0.012	0.262
ctg12304	99606	1	0.394	0.006	0.262
ctg41048	16536	1	0.367	0.008	0.262
ctg1950	226520	2	0.104	0.018	0.260
contig_8502	659955	3	0.311	0.012	0.259
tig00104814	1793396	4	0.232	0.014	0.259
tig00025127	537042	4	0.321	0.012	0.259
ctg194	600697	4	0.199	0.013	0.258
ctg6063	225047	2	0.293	0.007	0.258
tig00044057	466073	1	0.247	0.015	0.257
tig00395942	338607	1	0.315	0.012	0.257
ctg752	602464	4	0.404	0.006	0.255
ctg34789	17479	3	0.258	0.015	0.254
tig02170971	414449	6	0.338	0.008	0.254
ctg3	1179550	12	0.201	0.014	0.254
tig00001022	1086513	8	0.200	0.015	0.253
ctg415	311524	1	0.216	0.016	0.253
ctg8985	210385	1	0.088	0.020	0.252
contig_2258	313162	3	0.321	0.011	0.252
ctg4939	265483	1	0.133	0.020	0.252
tig00004411	978213	11	0.348	0.014	0.252
ctg23705	43644	4	0.159	0.014	0.252
contig_59892	425997	4	0.162	0.017	0.251
tig00399998	282483	1	0.121	0.018	0.251
ctg15020	55150	1	0.179	0.015	0.250
ctg50003	20875	2	0.149	0.015	0.249
contig_27618	278105	2	0.146	0.017	0.249
tig00053685	529554	8	0.240	0.013	0.249
ctg177	471256	2	0.272	0.015	0.249
tig00397775	602392	6	0.181	0.012	0.248
ctg3365	406722	5	0.239	0.016	0.248
ctg9125	76434	2	0.130	0.013	0.247
ctg4715	460241	6	0.229	0.015	0.246
tig00395493	735867	3	0.196	0.016	0.246
tig00397358	211492	2	0.182	0.013	0.246
ctg1157	328581	1	0.196	0.016	0.245
ctg17303	40441	1	0.343	0.011	0.245

ctg6668	100423	4	0.137	0.020	0.245
ctg7718	88837	3	0.248	0.015	0.244
ctg6837	427499	5	0.275	0.016	0.244
tig00052855	768200	1	0.237	0.016	0.244
ctg38	1002682	1	0.231	0.016	0.243
tig02186981	429664	1	0.253	0.014	0.242
contig_11800	293398	4	0.279	0.011	0.242
ctg26085	41784	2	0.226	0.018	0.241
tig00398125	242286	3	0.286	0.015	0.239
scaffold_4683	835377	8	0.299	0.014	0.239
tig00019413	834945	1	0.305	0.014	0.238
tig00395664	739937	1	0.374	0.009	0.237
ctg4981	238808	5	0.323	0.014	0.236
ctg10095	116421	1	0.106	0.022	0.235
ctg6562	100056	6	0.441	0.011	0.235
contig_700	528404	10	0.220	0.015	0.234
ctg4863	119947	3	0.127	0.018	0.234
ctg1475	293470	1	0.355	0.009	0.233
contig_28122	981579	3	0.305	0.016	0.233
ctg18773	38018	11	0.086	0.016	0.232
tig02170329	932701	1	0.173	0.019	0.232
contig_9938	210024	2	0.325	0.013	0.230
contig_28334	417081	3	0.190	0.020	0.230
ctg6202	106203	1	0.257	0.016	0.229
ctg7818	171048	5	0.270	0.012	0.228
ctg22944	32023	2	0.196	0.019	0.228
tig00027088	326734	1	0.214	0.019	0.227
ctg3204	256046	3	0.276	0.018	0.227
ctg13400	51769	2	0.339	0.013	0.226
ctg607	520191	2	0.349	0.012	0.226
tig00396649	1110334	6	0.248	0.015	0.226
ctg19555	38077	6	0.248	0.016	0.226
ctg10144	130904	9	0.188	0.018	0.225
ctg13430	177202	1	0.350	0.012	0.224
ctg2815	148288	3	0.232	0.015	0.223
ctg46	597493	4	0.274	0.015	0.222
ctg505	732007	2	0.316	0.014	0.222
tig00032134	632509	1	0.225	0.018	0.221
tig00034708	906525	5	0.273	0.014	0.220
tig00083023	456639	1	0.185	0.021	0.219
tig00014463	384586	8	0.313	0.015	0.219
ctg812	258346	3	0.392	0.011	0.218
contig_30589	301511	3	0.190	0.018	0.218
ctg2384	234273	2	0.216	0.019	0.218
ctg4951	130550	1	0.313	0.013	0.216
ctg501	324510	1	0.242	0.018	0.215
contig_49819	327541	2	0.140	0.023	0.214
tig00395565	484104	2	0.103	0.021	0.214
ctg791	410033	2	0.311	0.015	0.214
tig00398853	541814	2	0.219	0.019	0.214
contig_4852	367073	1	0.320	0.012	0.214
ctg5333	174133	2	0.407	0.010	0.214
ctg24568	81426	1	0.266	0.017	0.213
ctg1298	491818	3	0.221	0.020	0.213
ctg5899	178746	6	0.192	0.018	0.213
ctg5912	109367	3	0.149	0.022	0.213
ctg10292	137413	7	0.371	0.013	0.213
tig00396717	1067560	2	0.256	0.012	0.212
ctg22309	32068	1	0.261	0.018	0.212
contig_27424	766992	2	0.191	0.022	0.212
ctg9604	129815	2	0.304	0.013	0.212
contig_6376	506229	18	0.311	0.016	0.209
ctg7623	319599	2	0.183	0.015	0.209
tig00031330	337571	4	0.267	0.018	0.208

tig00395829	939538	1	0.085	0.025	0.207
ctg4442	128076	1	0.199	0.022	0.207
contig_14639	342501	1	0.237	0.020	0.206
ctg12753	107548	5	0.246	0.019	0.206
ctg4226	130450	2	0.319	0.014	0.205
tig00016242	349565	3	0.333	0.015	0.205
ctg19	1757703	1	0.279	0.010	0.205
contig_40126	220821	6	0.401	0.012	0.204
ctg5199	117210	5	0.311	0.016	0.204
ctg1363	310217	2	0.298	0.017	0.203
tig00009046	363448	4	0.288	0.017	0.203
contig_34921	726249	1	0.171	0.023	0.202
tig02173057	245732	10	0.274	0.017	0.202
ctg6384	157654	2	0.289	0.017	0.202
tig02171089	681003	4	0.153	0.018	0.202
ctg2486	168115	1	0.303	0.015	0.201
ctg8387	82843	1	0.171	0.024	0.201
scaffold_51090	201924	10	0.447	0.016	0.200
tig00068622	643852	15	0.294	0.015	0.199
ctg416	480940	6	0.188	0.017	0.199
tig02170072	566287	3	0.207	0.018	0.199
tig00403857	341728	4	0.200	0.021	0.199
ctg2064	174429	5	0.280	0.015	0.198
tig00018405	594493	12	0.300	0.017	0.198
ctg3955	136729	1	0.302	0.016	0.196
ctg13554	95815	4	0.174	0.023	0.196
ctg13445	113468	3	0.229	0.021	0.195
ctg24821	78194	2	0.168	0.022	0.195
tig02169569	900060	6	0.238	0.017	0.195
tig00400766	576764	2	0.206	0.016	0.193
tig00051059	252625	2	0.173	0.022	0.193
contig_28197	1091378	10	0.279	0.018	0.191
ctg197	369360	1	0.319	0.016	0.191
ctg23876	28747	7	0.356	0.014	0.190
contig_18424	335265	2	0.206	0.020	0.190
tig00403669	210366	6	0.253	0.021	0.190
ctg5130	114906	5	0.321	0.017	0.189
ctg128	835180	11	0.366	0.014	0.189
ctg11256	66331	6	0.372	0.014	0.189
tig00103826	512531	1	0.163	0.025	0.189
ctg641	644179	11	0.421	0.015	0.188
tig00002144	1990210	6	0.285	0.017	0.188
ctg16131	125915	2	0.092	0.025	0.187
tig00003427	642141	4	0.202	0.018	0.186
tig00395632	1118853	2	0.299	0.019	0.185
tig02172227	247409	1	0.245	0.022	0.185
ctg58	577410	8	0.433	0.010	0.185
contig_28094	304911	1	0.263	0.020	0.185
ctg31411	22800	1	0.312	0.016	0.185
tig00019692	1311592	2	0.223	0.020	0.185
contig_25682	247942	1	0.245	0.021	0.185
tig00018293	491220	3	0.103	0.026	0.185
ctg5996	183610	1	0.149	0.027	0.183
tig00047427	215122	1	0.101	0.027	0.183
tig00015418	430920	2	0.258	0.021	0.183
tig00013252	704132	3	0.254	0.017	0.182
ctg2024	241686	10	0.249	0.022	0.181
ctg1223	231197	1	0.159	0.027	0.181
ctg7940	870028	1	0.351	0.013	0.181
ctg136	393986	2	0.226	0.020	0.180
ctg28607	20096	2	0.230	0.022	0.180
tig00047747	520343	10	0.382	0.018	0.178
tig02170177	675280	4	0.341	0.017	0.178
ctg13748	93108	5	0.248	0.022	0.177

ctg12310	59610	1	0.186	0.025	0.177
ctg13393	56688	12	0.172	0.019	0.177
contig_9266	400374	7	0.237	0.018	0.176
tig00030293	499278	10	0.249	0.018	0.175
tig02169402	1346358	5	0.272	0.019	0.174
ctg2892	162450	1	0.051	0.029	0.174
ctg15865	262610	2	0.381	0.013	0.173
ctg1757	197352	1	0.325	0.015	0.173
ctg4368	156690	10	0.338	0.019	0.173
ctg4142	283712	3	0.167	0.020	0.173
tig00034901	542379	6	0.234	0.021	0.172
contig_27216	489124	1	0.187	0.026	0.171
contig_27767	324240	3	0.414	0.009	0.170
tig00004876	725133	1	0.377	0.011	0.170
scaffold_57123	698343	3	0.144	0.026	0.170
tig00017462	452237	1	0.178	0.027	0.170
contig_5207	409274	15	0.286	0.022	0.167
tig00067412	285212	1	0.126	0.029	0.166
ctg10934	69119	6	0.325	0.019	0.166
ctg956	442449	1	0.226	0.023	0.166
ctg14981	50209	1	0.238	0.021	0.165
tig00398726	672806	1	0.237	0.024	0.165
tig00022120	650579	1	0.148	0.029	0.164
ctg12458	144718	1	0.229	0.024	0.164
tig00000976	1174329	12	0.261	0.012	0.164
tig00400623	436297	1	0.321	0.017	0.163
ctg2246	235283	2	0.214	0.020	0.163
ctg21136	35148	1	0.193	0.025	0.163
tig00397303	1139691	3	0.122	0.025	0.161
ctg2176	240940	2	0.132	0.030	0.160
ctg2580	164974	1	0.280	0.022	0.159
contig_9526	719582	2	0.372	0.014	0.158
tig00006887	1374660	2	0.346	0.017	0.158
tig00067460	364697	3	0.352	0.015	0.158
contig_4005	268413	5	0.212	0.017	0.158
contig_48487	430468	7	0.176	0.020	0.157
ctg4086	130934	3	0.221	0.026	0.157
tig02169264	426178	1	0.323	0.019	0.156
ctg5319	137218	5	0.352	0.019	0.156
ctg36169	16644	3	0.169	0.023	0.156
tig02174016	236047	2	0.218	0.025	0.155
tig02170588	927838	3	0.182	0.014	0.155
ctg15722	48597	1	0.094	0.032	0.155
ctg28425	26067	1	0.167	0.028	0.155
ctg5955	149833	1	0.186	0.029	0.154
tig00014486	560161	7	0.209	0.025	0.153
tig00020255	2097197	4	0.201	0.016	0.153
tig00041114	938714	10	0.252	0.024	0.153
ctg12554	70604	1	0.384	0.012	0.152
ctg2336	293455	4	0.257	0.023	0.152
ctg14248	103089	12	0.166	0.024	0.152
ctg31901	21456	2	0.148	0.022	0.152
contig_18268	617667	2	0.161	0.024	0.151
tig00400633	450002	1	0.260	0.023	0.150
ctg6888	173630	5	0.252	0.024	0.149
ctg5094	350740	3	0.285	0.022	0.149
ctg50939	11056	1	0.219	0.026	0.149
tig00402293	311504	3	0.343	0.018	0.148
contig_12207	344708	4	0.184	0.030	0.147
ctg9447	115335	3	0.276	0.020	0.147
ctg8519	117111	1	0.263	0.024	0.147
tig02171455	959563	1	0.356	0.015	0.146
ctg14701	92059	2	0.310	0.022	0.145
ctg16374	46258	8	0.276	0.016	0.144

ctg2004	422001	9	0.233	0.024	0.144
contig_48697	299926	3	0.377	0.013	0.141
ctg5471	112247	5	0.206	0.027	0.141
ctg9753	69859	2	0.180	0.029	0.141
ctg2873	202807	1	0.115	0.034	0.141
tig00050794	595241	3	0.242	0.020	0.140
ctg2695	246890	5	0.306	0.023	0.140
ctg3133	204978	8	0.342	0.020	0.139
ctg8167	178131	1	0.160	0.019	0.139
ctg12352	144582	1	0.345	0.017	0.138
ctg3937	134666	2	0.108	0.031	0.137
tig00397735	344122	5	0.202	0.024	0.136
ctg22537	40060	3	0.067	0.033	0.136
ctg3348	307910	1	0.388	0.013	0.135
ctg9946	104536	1	0.326	0.020	0.135
ctg7736	138851	1	0.121	0.033	0.134
ctg4633	247280	1	0.114	0.033	0.134
contig_6879	842352	17	0.284	0.023	0.133
ctg7278	146418	2	0.298	0.023	0.133
tig00049172	244735	15	0.208	0.019	0.133
ctg10474	74107	1	0.203	0.030	0.133
ctg4765	248602	2	0.104	0.036	0.132
ctg9190	77655	2	0.310	0.021	0.132
ctg1228	217822	5	0.319	0.020	0.132
ctg3512	238290	6	0.202	0.028	0.132
ctg13885	86125	3	0.187	0.029	0.131
contig_53901	913944	2	0.288	0.023	0.131
tig00398102	347227	2	0.248	0.027	0.131
tig02170524	305717	3	0.138	0.025	0.131
tig02171876	556263	8	0.225	0.019	0.131
contig_17614	363950	2	0.280	0.025	0.131
ctg25379	64759	2	0.169	0.030	0.130
tig02186395	595854	2	0.200	0.023	0.130
contig_9160	324608	3	0.282	0.023	0.129
ctg5426	318738	6	0.231	0.024	0.129
tig00396849	528231	3	0.252	0.026	0.129
tig00038539	404378	3	0.187	0.026	0.129
tig02172089	485835	3	0.271	0.024	0.129
contig_13059	338872	1	0.254	0.025	0.128
tig00054655	279091	11	0.348	0.022	0.128
ctg11195	64099	2	0.242	0.026	0.127
tig00031334	488180	2	0.090	0.030	0.127
scaffold_23509	388149	3	0.095	0.033	0.126
contig_68927	593454	4	0.248	0.019	0.126
tig00095047	355461	2	0.289	0.024	0.125
ctg13486	64113	4	0.139	0.025	0.125
contig_14989	220416	1	0.239	0.028	0.125
tig00403837	472304	6	0.183	0.019	0.122
ctg1377	291711	14	0.263	0.026	0.122
tig00398415	431708	1	0.144	0.035	0.122
tig00010409	860270	17	0.253	0.028	0.122
tig02188414	611268	15	0.147	0.024	0.122
ctg1449	311382	5	0.164	0.027	0.121
ctg308	342101	4	0.243	0.024	0.121
ctg10573	66024	3	0.192	0.033	0.120
contig_27827	573841	2	0.178	0.032	0.119
ctg10839	105569	4	0.324	0.018	0.119
tig00031516	490907	11	0.347	0.010	0.118
ctg31486	22527	2	0.138	0.036	0.118
contig_34420	534918	7	0.449	0.013	0.117
ctg4088	151336	1	0.169	0.032	0.117
ctg200	686270	3	0.143	0.027	0.117
ctg3812	587781	5	0.153	0.022	0.115
tig00014319	771882	3	0.254	0.022	0.115

contig_1867	386438	7	0.213	0.031	0.115
contig_24200	284891	2	0.338	0.022	0.115
contig_19940	271251	1	0.242	0.029	0.115
ctg7729	90060	2	0.198	0.029	0.114
contig_39825	201903	2	0.102	0.035	0.114
tig00043743	477109	7	0.341	0.021	0.113
ctg4822	190782	7	0.078	0.038	0.113
ctg4972	260808	1	0.174	0.035	0.112
tig00396046	377165	1	0.091	0.037	0.112
ctg11946	61955	2	0.072	0.039	0.112
ctg10316	256538	1	0.095	0.031	0.112
tig00002140	824019	1	0.066	0.036	0.112
tig00396482	1492648	3	0.144	0.037	0.112
tig02187012	489260	5	0.112	0.038	0.112
tig00395592	338297	2	0.182	0.026	0.111
tig00040410	358271	4	0.245	0.029	0.111
ctg190	396973	4	0.423	0.018	0.111
tig00035554	547632	2	0.182	0.033	0.111
tig00397363	369024	2	0.307	0.026	0.110
tig00009735	831506	5	0.363	0.020	0.110
contig_42310	1685085	14	0.239	0.022	0.110
tig00401650	707187	5	0.416	0.016	0.109
ctg9969	72843	1	0.290	0.027	0.109
contig_42321	807301	2	0.200	0.030	0.109
tig00076432	494427	1	0.076	0.033	0.108
ctg2290	342104	5	0.271	0.027	0.108
tig00049835	345574	1	0.265	0.028	0.108
tig00397795	932899	12	0.279	0.026	0.107
ctg978	585390	11	0.188	0.026	0.106
ctg15042	49812	2	0.202	0.027	0.106
contig_28370	232401	3	0.371	0.017	0.105
ctg14714	49084	7	0.211	0.033	0.105
ctg922	1057594	3	0.178	0.033	0.105
ctg5042	213268	1	0.131	0.037	0.104
ctg7751	85816	1	0.214	0.032	0.104
tig00052769	266873	4	0.369	0.021	0.104
scaffold_94674	680024	2	0.256	0.029	0.104
tig00036920	628439	4	0.253	0.030	0.104
tig00396799	523015	4	0.250	0.026	0.103
ctg4443	120157	2	0.301	0.030	0.102
ctg19559	76023	1	0.106	0.033	0.102
tig00013870	715056	5	0.257	0.026	0.102
tig00398587	867860	3	0.195	0.025	0.101
tig02172578	541140	3	0.182	0.035	0.101
contig_25650	217746	1	0.132	0.040	0.100
tig00092050	598562	8	0.225	0.026	0.100
tig00398163	841317	2	0.085	0.032	0.100
tig00025802	371027	8	0.469	0.017	0.099
ctg17499	42256	10	0.242	0.029	0.099
contig_16550	324209	1	0.252	0.030	0.099
ctg2029	438676	16	0.214	0.025	0.099
contig_39781	655175	4	0.163	0.025	0.098
tig00397234	768625	3	0.111	0.035	0.097
ctg30912	29980	1	0.175	0.025	0.097
ctg1882	268473	3	0.307	0.028	0.097
ctg20376	35832	2	0.081	0.033	0.097
contig_9316	563718	1	0.286	0.027	0.096
tig02173306	339606	10	0.200	0.029	0.096
tig00025485	974134	1	0.249	0.031	0.096
ctg5754	111839	1	0.282	0.029	0.096
tig00019190	1004314	3	0.107	0.034	0.095
tig02168986	1298228	9	0.282	0.029	0.095
tig00400224	321049	5	0.342	0.023	0.094
tig00003533	1523134	11	0.162	0.030	0.094

ctg14642	50316	2	0.217	0.034	0.094
ctg9202	78296	8	0.208	0.033	0.093
ctg8845	128516	1	0.172	0.037	0.093
tig02170472	434111	3	0.219	0.025	0.092
ctg2294	174791	1	0.360	0.019	0.092
ctg40	674212	7	0.253	0.025	0.092
tig00065268	800706	8	0.313	0.025	0.091
ctg615	323150	5	0.333	0.026	0.091
ctg7333	248012	4	0.140	0.036	0.090
tig00055777	834326	4	0.351	0.026	0.089
tig00007377	562298	17	0.260	0.030	0.088
contig_52069	314819	12	0.221	0.023	0.088
tig00398731	381291	4	0.237	0.030	0.088
tig00012443	883435	8	0.509	0.011	0.088
tig00001218	1336257	4	0.176	0.030	0.087
tig00044101	368905	3	0.285	0.026	0.087
tig00011865	1265338	6	0.324	0.028	0.087
ctg31582	46656	2	0.296	0.030	0.087
ctg9502	116796	2	0.228	0.036	0.086
contig_37294	398132	4	0.140	0.034	0.085
ctg2397	191799	1	0.187	0.036	0.085
ctg7830	175838	1	0.217	0.035	0.085
ctg2055	186193	1	0.185	0.039	0.084
tig00395741	1163745	7	0.151	0.034	0.083
ctg1052	707240	5	0.249	0.030	0.083
ctg3135	633471	4	0.152	0.030	0.083
ctg5322	128455	1	0.197	0.038	0.083
tig00402372	249817	1	0.255	0.033	0.081
ctg1332	209734	8	0.179	0.028	0.081
tig00028491	815577	1	0.296	0.031	0.081
tig00401976	530010	11	0.237	0.032	0.080
contig_13197	455877	5	0.210	0.039	0.080
tig00396045	315602	1	0.204	0.039	0.080
tig00395851	811956	1	0.293	0.029	0.080
ctg2918	491192	4	0.263	0.034	0.080
tig00399136	311364	2	0.289	0.022	0.080
tig00017296	468995	7	0.172	0.038	0.080
tig02171858	251538	5	0.105	0.043	0.080
tig02172874	371406	3	0.186	0.033	0.079
ctg23170	44939	1	0.184	0.041	0.078
ctg22524	30860	1	0.291	0.030	0.078
contig_23659	1240781	11	0.214	0.036	0.078
tig00014637	265440	3	0.302	0.031	0.078
ctg4959	267811	3	0.200	0.035	0.078
tig00004287	748237	3	0.223	0.023	0.078
tig00395577	504154	4	0.105	0.028	0.077
ctg24297	29782	6	0.368	0.026	0.077
contig_18300	741972	5	0.441	0.014	0.077
tig02175514	409057	3	0.155	0.030	0.077
ctg6730	173209	2	0.196	0.027	0.076
ctg31731	73812	1	0.155	0.044	0.076
tig00399415	429662	6	0.412	0.025	0.075
ctg1981	391910	4	0.169	0.031	0.075
ctg3340	145592	2	0.227	0.038	0.073
ctg6099	103822	8	0.215	0.036	0.073
ctg1483	426845	1	0.100	0.041	0.073
contig_31380	682858	1	0.248	0.036	0.072
ctg5599	205566	3	0.250	0.033	0.072
contig_3763	926234	6	0.159	0.035	0.071
tig00397678	343430	2	0.153	0.042	0.071
tig00006320	1548266	7	0.298	0.026	0.070
tig02170292	406180	3	0.279	0.034	0.070
tig00399515	978291	14	0.344	0.030	0.070
tig00039376	596493	4	0.387	0.021	0.070

ctg10102	402089	1	0.309	0.031	0.070
ctg2393	207005	1	0.117	0.047	0.070
tig00403120	260950	8	0.439	0.022	0.069
tig00395718	564760	6	0.270	0.032	0.069
tig02188736	360770	6	0.296	0.032	0.069
ctg2288	543449	1	0.148	0.038	0.068
contig_21048	364039	9	0.231	0.038	0.067
tig00399629	518206	1	0.112	0.046	0.067
ctg1953	404025	6	0.308	0.030	0.067
tig00396454	341977	6	0.322	0.033	0.067
ctg6590	94434	1	0.097	0.046	0.067
ctg10358	88629	8	0.364	0.027	0.067
tig02173246	302649	1	0.247	0.037	0.067
ctg15148	64402	6	0.247	0.027	0.066
ctg12875	118304	5	0.411	0.017	0.065
ctg7121	96465	3	0.374	0.024	0.065
scaffold_63216	219384	1	0.195	0.041	0.065
tig00396772	615465	8	0.225	0.028	0.065
ctg629	375856	8	0.290	0.031	0.065
contig_1907	606618	3	0.306	0.029	0.065
ctg820	811518	6	0.273	0.024	0.065
ctg591	438264	4	0.173	0.032	0.064
contig_11056	828308	1	0.069	0.046	0.064
tig00094964	554302	10	0.266	0.031	0.064
ctg3960	219660	3	0.247	0.037	0.063
ctg40136	16287	2	0.251	0.038	0.063
contig_51102	459059	1	0.188	0.044	0.062
ctg1896	469057	2	0.239	0.026	0.062
tig02186551	485617	1	0.133	0.038	0.062
ctg1036	394758	1	0.347	0.026	0.062
ctg9020	80434	3	0.193	0.043	0.062
contig_53973	398156	1	0.356	0.027	0.061
ctg10931	162315	5	0.166	0.034	0.061
tig02169483	613103	7	0.219	0.039	0.061
tig00012863	435582	1	0.329	0.030	0.061
tig00026489	374319	1	0.339	0.031	0.061
ctg18166	109389	1	0.135	0.047	0.061
ctg971	541096	8	0.218	0.036	0.061
tig00012553	1156763	4	0.212	0.026	0.060
scaffold_15707	587030	2	0.197	0.040	0.060
ctg59383	6543	1	0.337	0.028	0.059
ctg6917	123434	4	0.307	0.034	0.059
scaffold_10725	716497	14	0.192	0.038	0.059
tig00402138	797966	2	0.433	0.017	0.058
tig00010398	706136	2	0.142	0.040	0.058
tig00402879	668623	6	0.162	0.028	0.058
ctg1380	576893	6	0.200	0.037	0.058
ctg13033	55628	2	0.118	0.042	0.058
ctg15895	44998	1	0.234	0.040	0.058
ctg81	453102	1	0.209	0.041	0.057
ctg11514	65566	6	0.177	0.044	0.057
scaffold_65312	307975	1	0.124	0.050	0.057
tig00095300	212648	1	0.141	0.037	0.057
tig00011294	435001	8	0.234	0.035	0.056
tig00020462	820660	6	0.235	0.041	0.056
tig00008647	556418	2	0.122	0.041	0.056
ctg5975	161718	5	0.358	0.027	0.056
tig00403395	786131	4	0.218	0.043	0.056
ctg5968	183496	3	0.248	0.039	0.055
tig00009944	967587	6	0.320	0.034	0.055
ctg16121	46856	4	0.221	0.043	0.055
ctg33402	18884	12	0.196	0.036	0.054
contig_36004	642631	15	0.325	0.034	0.054
ctg2696	236870	1	0.166	0.047	0.054

ctg447	469335	1	0.104	0.051	0.054
scaffold_4869	488840	2	0.240	0.037	0.053
tig00051157	754715	4	0.283	0.037	0.053
contig_14276	464119	3	0.361	0.029	0.053
tig00012074	455278	4	0.379	0.022	0.052
ctg3559	233024	3	0.225	0.034	0.052
ctg13230	56304	5	0.445	0.025	0.052
ctg20437	72760	2	0.147	0.051	0.052
tig00053279	858646	5	0.267	0.031	0.052
ctg3180	210723	1	0.104	0.047	0.052
tig02169873	368293	1	0.316	0.031	0.051
ctg122	536279	1	0.260	0.038	0.051
contig_7084	674387	2	0.079	0.043	0.051
ctg1505	251746	1	0.214	0.044	0.051
tig00060542	219432	3	0.204	0.040	0.051
contig_19519	364393	1	0.259	0.039	0.050
ctg6362	113516	1	0.130	0.053	0.050
tig00087718	454750	8	0.255	0.037	0.050
tig02169831	1370563	1	0.066	0.043	0.050
tig00396707	583320	1	0.130	0.051	0.050
contig_13875	400802	6	0.150	0.046	0.050
tig00022921	1617563	27	0.160	0.037	0.050
contig_24331	586665	2	0.279	0.038	0.049
tig00000226	1241487	4	0.194	0.037	0.049
tig00001955	741964	10	0.299	0.030	0.049
ctg1461	589194	3	0.268	0.034	0.049
tig00396415	419492	1	0.292	0.037	0.049
ctg5307	209734	1	0.203	0.048	0.048
tig00396591	1081309	1	0.033	0.056	0.048
ctg13176	74173	6	0.253	0.042	0.048
ctg6324	262359	4	0.272	0.034	0.048
tig00003249	854161	1	0.094	0.055	0.048
ctg16173	91888	1	0.354	0.029	0.048
tig00403985	917864	1	0.101	0.055	0.047
ctg29668	36919	1	0.260	0.040	0.047
ctg4966	236235	15	0.304	0.037	0.047
contig_15754	440990	1	0.117	0.054	0.047
ctg2209	258152	6	0.379	0.033	0.047
ctg335	445921	1	0.044	0.054	0.047
ctg15750	198890	2	0.295	0.032	0.047
ctg24635	28702	1	0.259	0.038	0.046
ctg5047	542881	1	0.265	0.039	0.046
tig00006917	607877	7	0.317	0.042	0.046
ctg35522	33765	1	0.144	0.048	0.046
ctg117	620042	6	0.293	0.034	0.046
ctg4024	494457	1	0.184	0.047	0.046
tig00075681	382639	7	0.325	0.035	0.044
tig00013160	523727	7	0.151	0.043	0.044
contig_1892	532185	1	0.272	0.038	0.044
ctg120	638507	1	0.208	0.044	0.044
tig02171123	271405	5	0.237	0.042	0.043
ctg21119	56462	1	0.133	0.054	0.043
tig00002426	314643	3	0.254	0.044	0.043
contig_26757	510540	2	0.391	0.027	0.042
scaffold_46359	378012	3	0.147	0.041	0.042
ctg7702	127480	1	0.164	0.044	0.042
contig_56399	458482	3	0.211	0.041	0.042
contig_9881	580440	7	0.261	0.034	0.042
ctg12246	63216	1	0.100	0.057	0.042
ctg11197	67551	2	0.176	0.039	0.041
ctg5256	116043	5	0.072	0.056	0.041
tig00397010	391401	6	0.337	0.034	0.040
tig02169480	411259	5	0.243	0.040	0.040
tig02172441	292959	3	0.061	0.057	0.040

ctg19902	37382	1	0.122	0.053	0.040
ctg23126	36608	1	0.162	0.055	0.039
tig02175078	351916	1	0.131	0.058	0.039
ctg3799	886088	4	0.371	0.032	0.039
ctg2331	284205	8	0.185	0.050	0.039
tig00396906	536846	3	0.332	0.035	0.039
tig02170558	450451	1	0.198	0.048	0.039
tig00012334	1483541	10	0.226	0.037	0.038
tig00056339	458927	3	0.228	0.032	0.038
tig00072605	1254308	3	0.256	0.039	0.038
ctg17359	88633	2	0.188	0.047	0.038
contig_52764	335237	1	0.237	0.046	0.038
tig00085574	221342	1	0.146	0.056	0.037
tig00397167	405286	4	0.206	0.042	0.037
ctg3408	297141	1	0.267	0.043	0.037
ctg22197	32559	2	0.170	0.053	0.037
contig_30393	848990	6	0.329	0.038	0.037
tig00396953	1025232	6	0.191	0.038	0.037
contig_23455	263809	4	0.253	0.047	0.037
ctg29282	24537	2	0.282	0.034	0.036
ctg8248	174537	4	0.129	0.053	0.036
contig_43517	412687	8	0.409	0.032	0.036
tig00397102	219678	1	0.246	0.040	0.036
tig00052878	266346	2	0.153	0.055	0.035
tig00401031	363138	7	0.271	0.038	0.035
tig00396308	1636357	4	0.232	0.045	0.035
ctg9632	133344	8	0.201	0.041	0.035
tig00396787	1151301	2	0.190	0.043	0.035
ctg33031	21499	1	0.255	0.046	0.035
ctg22966	31916	7	0.179	0.033	0.035
tig00396557	253842	2	0.216	0.046	0.035
ctg27540	25015	1	0.303	0.039	0.035
ctg16345	48437	1	0.072	0.057	0.034
tig00021640	847352	16	0.202	0.040	0.034
contig_6581	301220	4	0.227	0.047	0.034
ctg8456	68528	2	0.372	0.030	0.034
tig02186379	882378	3	0.241	0.037	0.034
ctg16715	45693	1	0.250	0.047	0.033
tig00396989	256575	3	0.125	0.060	0.033
ctg16404	46102	10	0.405	0.035	0.033
ctg7436	254757	1	0.184	0.045	0.033
ctg30757	22452	1	0.185	0.053	0.033
ctg2697	326095	1	0.125	0.059	0.033
contig_24034	400000	3	0.169	0.052	0.033
tig00010483	395357	3	0.232	0.042	0.033
ctg9644	230838	1	0.174	0.054	0.033
contig_18270	585435	1	0.223	0.036	0.032
tig00056019	525453	2	0.155	0.045	0.032
ctg7591	129623	1	0.423	0.020	0.032
ctg2749	157293	1	0.297	0.040	0.032
ctg26192	27689	5	0.099	0.045	0.032
ctg4129	130558	4	0.315	0.040	0.032
ctg7012	97782	5	0.298	0.042	0.031
tig00401853	799671	6	0.255	0.042	0.031
ctg23045	56086	1	0.222	0.050	0.031
ctg18194	41279	13	0.255	0.045	0.031
tig00001240	624434	5	0.130	0.056	0.031
tig00398309	675622	3	0.293	0.040	0.031
tig02187648	272234	2	0.160	0.055	0.031
ctg39019	16809	3	0.157	0.057	0.031
tig00009952	997434	8	0.295	0.045	0.030
tig00396193	349908	7	0.149	0.049	0.030
tig00005290	982722	6	0.141	0.034	0.030
ctg17358	84937	1	0.322	0.039	0.030

ctg5089	602227	8	0.106	0.057	0.030
tig00021095	706838	3	0.250	0.046	0.029
ctg3393	178810	3	0.294	0.039	0.029
ctg9832	74507	3	0.182	0.048	0.029
contig_33466	924322	1	0.249	0.047	0.029
ctg1998	380250	2	0.090	0.054	0.029
contig_18912	453046	5	0.183	0.051	0.029
ctg26890	27048	1	0.343	0.036	0.029
ctg2245	341913	2	0.091	0.060	0.029
ctg5652	210066	1	0.264	0.044	0.029
tig02169652	1201699	2	0.352	0.039	0.028
ctg11389	66082	9	0.372	0.037	0.028
ctg9626	76951	3	0.256	0.048	0.028
tig00395624	1428496	3	0.138	0.055	0.027
tig00398795	243475	1	0.148	0.058	0.027
ctg8693	144496	5	0.096	0.048	0.027
tig02169793	430736	1	0.155	0.059	0.027
contig_16699	336246	2	0.311	0.041	0.027
ctg2431	478108	1	0.283	0.043	0.026
ctg29730	23533	1	0.169	0.059	0.026
ctg11184	66172	3	0.357	0.035	0.026
contig_18881	477063	5	0.266	0.045	0.026
tig02169837	497673	1	0.059	0.067	0.026
contig_4609	481999	3	0.114	0.043	0.026
tig00034432	285275	6	0.333	0.036	0.026
tig00014480	370991	1	0.298	0.043	0.026
ctg6873	98417	11	0.325	0.045	0.026
ctg6554	232069	1	0.136	0.060	0.026
tig00038168	678826	1	0.246	0.048	0.026
tig02173502	236202	4	0.228	0.039	0.026
ctg441	371899	5	0.143	0.040	0.025
ctg4802	122455	7	0.415	0.036	0.025
tig00001819	750056	11	0.224	0.051	0.025
ctg886	422362	3	0.215	0.054	0.025
contig_41428	986481	7	0.282	0.042	0.025
ctg3995	134201	5	0.264	0.049	0.025
ctg938	495023	7	0.264	0.043	0.025
tig00009809	500401	7	0.303	0.042	0.024
contig_27486	583614	6	0.370	0.040	0.024
ctg5022	112713	1	0.085	0.063	0.024
ctg1927	300272	18	0.263	0.043	0.024
ctg1000	842217	7	0.225	0.047	0.024
tig00032820	222414	9	0.187	0.049	0.024
ctg1895	396209	5	0.183	0.047	0.024
tig00081624	713823	3	0.166	0.059	0.024
ctg13934	129182	6	0.350	0.035	0.023
ctg561	560353	2	0.175	0.054	0.023
tig00082713	221551	3	0.266	0.049	0.023
ctg1279	514016	4	0.234	0.050	0.023
contig_40939	209337	7	0.178	0.051	0.023
contig_11251	1040001	2	0.139	0.054	0.023
contig_98	1431894	4	0.208	0.054	0.023
tig00104614	228800	4	0.331	0.039	0.023
ctg16718	38053	2	0.248	0.041	0.022
tig00003879	1121621	2	0.151	0.050	0.022
contig_60781	565539	1	0.091	0.068	0.022
contig_50741	736334	3	0.080	0.056	0.022
ctg5948	116857	2	0.178	0.060	0.022
ctg2164	358456	5	0.241	0.049	0.021
tig00077143	449457	1	0.236	0.054	0.021
contig_37366	263246	1	0.055	0.068	0.021
ctg17049	152061	1	0.201	0.056	0.021
contig_30245	250958	1	0.234	0.052	0.021
tig00029045	775918	20	0.230	0.041	0.021

tig00062010	746043	2	0.173	0.058	0.021
contig_8945	1208804	1	0.178	0.061	0.021
scaffold_36687	1746710	2	0.208	0.043	0.021
ctg4653	132399	4	0.234	0.048	0.021
ctg1403	217423	2	0.174	0.061	0.021
ctg3457	312264	1	0.187	0.061	0.021
tig00025774	231739	2	0.203	0.051	0.020
ctg12880	59406	4	0.203	0.047	0.020
tig00008387	1206745	1	0.054	0.068	0.020
ctg11345	67118	2	0.170	0.051	0.020
ctg1744	488612	8	0.259	0.040	0.020
ctg11594	101235	2	0.295	0.046	0.020
ctg1227	254848	1	0.154	0.055	0.020
ctg4943	120815	1	0.185	0.045	0.019
ctg29278	24319	1	0.235	0.052	0.019
tig00395309	984356	2	0.427	0.027	0.019
tig00053376	481840	12	0.260	0.045	0.019
ctg17260	43454	2	0.174	0.051	0.019
ctg706	709138	5	0.401	0.037	0.019
ctg6864	190482	8	0.302	0.047	0.019
contig_13848	776025	5	0.324	0.045	0.019
ctg2836	363138	2	0.136	0.055	0.019
contig_10288	435980	1	0.148	0.065	0.019
ctg7143	154847	3	0.170	0.052	0.019
contig_35241	920474	12	0.321	0.043	0.019
tig00401008	734019	2	0.175	0.050	0.019
contig_16092	231821	1	0.118	0.066	0.019
tig00012906	465734	1	0.116	0.067	0.019
ctg15580	46249	1	0.302	0.042	0.019
ctg4645	175022	2	0.299	0.049	0.018
tig02186857	212821	7	0.277	0.043	0.018
tig00401048	1006707	2	0.168	0.051	0.018
tig00009101	550920	2	0.264	0.051	0.018
ctg4768	253436	3	0.273	0.052	0.018
ctg6722	99106	8	0.094	0.056	0.018
ctg13379	91079	7	0.358	0.037	0.018
ctg662	1122480	2	0.150	0.049	0.018
tig00401039	201987	1	0.116	0.068	0.018
ctg2937	161171	1	0.084	0.066	0.018
ctg8987	77918	2	0.244	0.038	0.017
ctg4430	244778	3	0.356	0.046	0.017
ctg2363	175673	1	0.249	0.049	0.017
ctg8641	81833	3	0.381	0.032	0.017
tig00041615	238995	1	0.273	0.050	0.017
tig00052588	395847	13	0.332	0.045	0.017
tig02186950	571650	6	0.236	0.046	0.017
ctg8868	174113	1	0.178	0.061	0.017
tig00010113	544917	2	0.118	0.053	0.016
tig00044442	1322741	1	0.194	0.062	0.016
tig00043964	472886	5	0.190	0.045	0.016
ctg20460	35400	1	0.418	0.026	0.016
ctg6518	217384	5	0.247	0.049	0.016
ctg5757	111496	4	0.269	0.050	0.016
tig00006727	561389	1	0.134	0.066	0.016
ctg5931	172571	2	0.106	0.061	0.016
ctg918	531109	1	0.144	0.066	0.016
contig_12766	335396	1	0.171	0.068	0.015
tig00064036	215676	8	0.127	0.053	0.015
tig00396519	695719	4	0.147	0.056	0.015
tig00003327	963361	5	0.167	0.051	0.015
ctg5114	180852	1	0.149	0.067	0.015
contig_24149	740605	8	0.156	0.051	0.015
ctg3045	153462	3	0.183	0.064	0.015
ctg6330	284254	4	0.128	0.073	0.015

ctg876	259010	3	0.116	0.046	0.015
tig02169053	775491	1	0.279	0.053	0.015
ctg1844	181985	1	0.278	0.053	0.015
tig02169099	801738	5	0.425	0.028	0.014
tig00022010	455476	1	0.122	0.067	0.014
tig00032807	898922	14	0.361	0.042	0.014
ctg305	380230	5	0.228	0.047	0.014
contig_51983	250726	2	0.317	0.048	0.014
ctg574	651584	1	0.174	0.065	0.014
ctg13113	154811	2	0.188	0.060	0.014
tig02177191	712921	1	0.203	0.065	0.014
ctg932	288213	1	0.146	0.067	0.014
contig_21039	429346	2	0.279	0.045	0.014
ctg2112	208492	2	0.268	0.052	0.014
tig00073763	439283	4	0.201	0.056	0.013
tig00029299	711128	2	0.202	0.045	0.013
tig02171851	622952	11	0.272	0.052	0.013
tig00399079	418017	1	0.244	0.059	0.013
ctg15885	47924	10	0.256	0.045	0.013
tig00057687	1109755	1	0.142	0.072	0.013
ctg10625	69426	2	0.208	0.056	0.013
tig00002260	634305	2	0.130	0.064	0.013
tig02172992	262449	1	0.138	0.070	0.013
contig_11907	731714	2	0.133	0.070	0.013
ctg18346	68544	2	0.138	0.071	0.013
ctg342	318049	2	0.260	0.056	0.013
tig02168959	709193	8	0.272	0.049	0.013
tig00398134	350876	1	0.074	0.074	0.013
tig00395608	811439	15	0.136	0.043	0.013
ctg5898	173878	1	0.283	0.054	0.013
ctg6773	100053	6	0.352	0.046	0.012
tig00012490	736866	1	0.250	0.060	0.012
ctg1062	384650	1	0.226	0.056	0.012
ctg21319	33605	2	0.317	0.050	0.012
contig_3901	1533463	9	0.129	0.055	0.012
tig02174455	594689	3	0.101	0.046	0.012
tig00036613	297434	4	0.189	0.050	0.012
contig_24776	953368	4	0.180	0.063	0.012
scaffold_56390	875467	1	0.079	0.071	0.012
ctg6885	161443	2	0.080	0.072	0.012
tig00397240	1309279	12	0.239	0.049	0.012
tig00399257	853184	3	0.345	0.039	0.012
contig_50490	587569	2	0.344	0.044	0.012
ctg3849	136426	1	0.255	0.053	0.012
ctg3605	193783	2	0.212	0.066	0.012
ctg3451	208450	18	0.226	0.044	0.012
tig00000132	1303810	3	0.325	0.046	0.012
tig00401611	533930	6	0.131	0.056	0.012
ctg3946	135996	3	0.216	0.064	0.011
ctg4528	155259	5	0.047	0.076	0.011
tig00035549	230244	6	0.194	0.053	0.011
ctg13106	56789	8	0.389	0.046	0.011
ctg9079	288632	5	0.323	0.048	0.011
ctg3130	151869	7	0.312	0.049	0.011
contig_25578	252329	1	0.054	0.085	0.011
tig00004291	1141289	10	0.302	0.050	0.010
tig00027007	580871	9	0.249	0.055	0.010
ctg38651	15997	2	0.267	0.056	0.010
ctg9091	82995	1	0.190	0.046	0.010
ctg9268	77721	3	0.259	0.049	0.010
ctg9918	75289	5	0.201	0.052	0.010
tig02175127	700198	2	0.228	0.054	0.010
ctg6182	323278	2	0.060	0.061	0.010
ctg5549	113086	3	0.055	0.077	0.010

ctg2516	431680	5	0.265	0.060	0.010
ctg15483	180865	2	0.166	0.066	0.010
tig02187896	290230	8	0.382	0.042	0.010
contig_14817	723262	6	0.254	0.058	0.010
tig00035722	370501	1	0.124	0.076	0.010
tig00059873	338295	1	0.079	0.078	0.010
contig_33834	349697	3	0.317	0.051	0.009
ctg9336	84247	3	0.183	0.074	0.009
contig_44179	1068800	8	0.317	0.048	0.009
ctg5121	273387	4	0.296	0.056	0.009
ctg16562	46615	5	0.162	0.064	0.009
ctg4504	125638	1	0.128	0.069	0.009
tig00399378	569838	6	0.185	0.056	0.009
ctg2076	471493	13	0.217	0.056	0.009
ctg9589	90739	5	0.149	0.067	0.009
ctg1835	204562	7	0.140	0.069	0.009
tig00002745	956161	8	0.283	0.045	0.009
contig_8185	390387	4	0.202	0.058	0.009
ctg9960	73514	9	0.314	0.053	0.009
contig_7948	250208	3	0.250	0.061	0.009
tig00396384	794700	3	0.172	0.056	0.009
ctg3854	186452	3	0.250	0.030	0.008
tig00007669	398995	3	0.488	0.033	0.008
tig02171830	509211	2	0.345	0.048	0.008
tig00399445	1355214	4	0.273	0.060	0.008
tig02170390	551687	15	0.263	0.045	0.008
ctg6543	144287	8	0.251	0.056	0.008
contig_17943	761653	1	0.118	0.078	0.008
tig02169642	217819	2	0.150	0.061	0.008
contig_54915	586664	1	0.272	0.061	0.008
ctg2235	431009	4	0.201	0.064	0.008
ctg1493	429882	1	0.203	0.070	0.008
tig00049313	510448	4	0.407	0.046	0.008
ctg304	428393	5	0.172	0.071	0.008
ctg2065	488593	1	0.177	0.074	0.008
ctg15235	77053	3	0.118	0.079	0.008
contig_19639	346525	8	0.159	0.058	0.008
tig00398650	701744	6	0.252	0.058	0.008
ctg13185	57542	1	0.243	0.061	0.008
ctg22551	32003	7	0.192	0.055	0.007
ctg11836	64306	2	0.105	0.070	0.007
contig_10109	662193	3	0.140	0.073	0.007
contig_40709	1152487	3	0.190	0.078	0.007
contig_7671	528083	1	0.111	0.082	0.007
contig_43003	828080	3	0.406	0.050	0.007
contig_38833	604027	2	0.215	0.061	0.007
tig02171079	533371	1	0.195	0.072	0.007
ctg35789	19613	1	0.109	0.082	0.007
tig00036171	2195921	2	0.302	0.050	0.007
tig00073033	363675	2	0.338	0.051	0.007
ctg1723	225672	2	0.324	0.052	0.007
tig00002418	1237577	5	0.234	0.056	0.007
contig_20729	865097	3	0.266	0.047	0.007
ctg3053	380384	5	0.144	0.061	0.007
tig00049286	218013	1	0.091	0.074	0.007
ctg958	239967	4	0.139	0.081	0.007
tig00005234	355003	7	0.158	0.055	0.007
ctg464	357866	3	0.218	0.050	0.007
contig_20357	756171	4	0.221	0.052	0.007
ctg4878	296449	1	0.101	0.072	0.007
contig_51952	416957	2	0.284	0.048	0.007
tig00048227	255982	2	0.257	0.062	0.007
ctg503	361361	2	0.162	0.066	0.007
tig00032605	332556	1	0.208	0.069	0.007

tig00011777	930573	1	0.290	0.055	0.006
tig00395658	796641	7	0.363	0.041	0.006
tig00009932	1047807	7	0.367	0.052	0.006
contig_2088	246692	1	0.260	0.067	0.006
ctg7088	240198	1	0.063	0.079	0.006
ctg15573	44675	1	0.045	0.091	0.006
ctg18830	40259	1	0.134	0.075	0.006
tig00001782	399619	2	0.191	0.077	0.006
contig_9485	207449	1	0.098	0.080	0.006
tig00010426	932016	2	0.240	0.067	0.006
contig_22381	756420	1	0.093	0.074	0.006
ctg35208	19926	5	0.353	0.047	0.006
tig00017610	299362	4	0.245	0.054	0.006
ctg8231	80920	12	0.315	0.054	0.006
tig00396435	870933	9	0.150	0.055	0.006
contig_7237	744510	6	0.248	0.068	0.006
tig02173845	774778	8	0.263	0.061	0.006
ctg2054	242868	4	0.308	0.066	0.006
contig_30818	371972	5	0.350	0.060	0.006
ctg3700	139634	2	0.130	0.079	0.006
tig00396970	864732	3	0.270	0.063	0.005
contig_21635	446265	10	0.248	0.068	0.005
contig_10934	379149	1	0.195	0.075	0.005
ctg14952	60034	3	0.241	0.053	0.005
tig00048408	1152938	2	0.278	0.062	0.005
contig_18274	615023	1	0.140	0.083	0.005
tig00008185	861467	3	0.335	0.050	0.005
ctg7371	183667	5	0.273	0.059	0.005
contig_25407	445815	1	0.232	0.069	0.005
contig_4262	585508	5	0.447	0.036	0.005
tig00398115	610845	7	0.331	0.043	0.005
ctg30809	64584	4	0.228	0.071	0.005
ctg8783	78486	5	0.298	0.058	0.005
contig_10059	978488	2	0.172	0.062	0.005
ctg1588	549819	1	0.220	0.077	0.005
ctg4536	123636	1	0.071	0.090	0.005
tig02186325	1062754	3	0.249	0.062	0.005
tig00404369	387001	1	0.201	0.072	0.005
ctg22439	32432	2	0.307	0.049	0.004
tig00409833	599385	1	0.254	0.065	0.004
ctg7967	88666	1	0.281	0.068	0.004
contig_22577	210263	1	0.231	0.069	0.004
ctg20480	50058	1	0.166	0.079	0.004
ctg1581	455164	1	0.091	0.089	0.004
tig00396826	235492	6	0.240	0.062	0.004
ctg3313	141113	4	0.183	0.063	0.004
ctg13535	89820	3	0.196	0.065	0.004
scaffold_4796	508383	2	0.089	0.067	0.004
ctg979	538727	6	0.215	0.069	0.004
tig00395711	406121	2	0.116	0.076	0.004
ctg16906	67950	4	0.271	0.053	0.004
tig00002644	1004164	4	0.241	0.068	0.004
ctg9077	99794	3	0.218	0.048	0.004
tig00006018	889293	2	0.347	0.053	0.004
ctg9434	75810	7	0.206	0.054	0.004
tig00012486	1161965	15	0.210	0.061	0.004
ctg25810	56923	1	0.200	0.078	0.004
tig00398299	1121549	1	0.117	0.089	0.004
contig_31543	243296	2	0.462	0.033	0.004
tig00053745	959500	8	0.201	0.063	0.004
ctg1303	276624	4	0.083	0.076	0.004
contig_8210	674378	3	0.115	0.080	0.004
ctg9027	80364	1	0.207	0.082	0.004
contig_1888	348863	1	0.172	0.084	0.004

ctg9017	394703	1	0.331	0.058	0.004
ctg2468	167128	4	0.234	0.073	0.004
ctg1034	511607	3	0.381	0.052	0.004
ctg15077	89959	4	0.221	0.053	0.004
contig_17744	208675	2	0.321	0.062	0.004
ctg2657	221561	3	0.267	0.069	0.004
ctg7181	173324	11	0.249	0.070	0.004
ctg5496	258052	2	0.163	0.070	0.004
ctg27712	38793	1	0.091	0.087	0.004
contig_43751	371606	12	0.236	0.064	0.004
ctg18137	41177	3	0.220	0.065	0.004
contig_16659	589510	1	0.277	0.066	0.004
ctg1787	462608	1	0.256	0.070	0.004
ctg44109	13436	1	0.261	0.073	0.004
ctg1420	314641	4	0.144	0.075	0.004
tig00400453	502313	9	0.245	0.072	0.003
tig00398384	507434	2	0.129	0.083	0.003
ctg7348	93251	1	0.367	0.047	0.003
tig00405585	447669	2	0.197	0.065	0.003
contig_11651	639743	1	0.283	0.066	0.003
ctg3914	147163	7	0.197	0.069	0.003
ctg11914	62325	3	0.277	0.067	0.003
tig00025801	378320	2	0.216	0.069	0.003
tig02171634	362300	3	0.102	0.074	0.003
ctg6466	103790	3	0.113	0.090	0.003
tig00012281	1095784	4	0.174	0.061	0.003
contig_12292	330830	1	0.293	0.066	0.003
ctg2777	421122	1	0.209	0.069	0.003
contig_26038	1128329	10	0.245	0.053	0.003
ctg32885	21337	1	0.308	0.059	0.003
ctg4073	265223	1	0.324	0.060	0.003
tig00397032	664490	1	0.050	0.099	0.003
tig00061215	331632	3	0.230	0.062	0.003
tig00031038	242167	5	0.289	0.066	0.003
contig_12812	484187	5	0.204	0.073	0.003
contig_29732	1109439	4	0.137	0.085	0.003
ctg19200	39208	1	0.084	0.086	0.003
tig00012179	394012	1	0.115	0.076	0.003
contig_21374	248563	1	0.055	0.095	0.003
ctg361	411299	11	0.147	0.053	0.003
ctg22269	58235	5	0.372	0.058	0.003
tig00001463	957974	2	0.189	0.082	0.003
ctg3316	140429	5	0.369	0.054	0.003
contig_41942	303149	2	0.202	0.078	0.003
ctg2830	160572	1	0.136	0.080	0.003
ctg10878	68089	3	0.194	0.067	0.003
ctg2298	174938	3	0.177	0.073	0.003
ctg3546	141388	5	0.280	0.073	0.003
ctg1734	388235	4	0.185	0.075	0.003
tig00395821	510214	3	0.192	0.077	0.003
tig00077193	457496	2	0.108	0.082	0.003
tig00401353	371848	1	0.191	0.084	0.003
ctg5385	110779	1	0.111	0.095	0.003
ctg14710	50655	1	0.053	0.095	0.003
ctg18184	40412	1	0.077	0.095	0.003
tig02188878	226859	1	0.123	0.096	0.003
ctg1418	415747	1	0.089	0.098	0.003
tig00395651	701058	6	0.211	0.052	0.002
ctg10073	200715	2	0.214	0.068	0.002
ctg4323	185232	3	0.243	0.069	0.002
ctg639	275266	1	0.190	0.085	0.002
tig02169111	518268	8	0.185	0.089	0.002
tig00056269	1105438	1	0.166	0.090	0.002
ctg3357	325326	1	0.115	0.101	0.002

tig00010830	362633	6	0.301	0.061	0.002
ctg18249	67394	3	0.311	0.064	0.002
tig00398065	1002344	2	0.117	0.064	0.002
ctg6787	207566	3	0.270	0.070	0.002
ctg4301	131532	2	0.109	0.088	0.002
tig00395688	396431	1	0.238	0.056	0.002
tig00403730	621907	6	0.176	0.073	0.002
ctg1471	202892	4	0.122	0.076	0.002
tig00405347	543473	5	0.157	0.079	0.002
tig02169458	962236	1	0.081	0.090	0.002
ctg2320	432401	4	0.340	0.062	0.002
tig00399539	282857	1	0.224	0.075	0.002
ctg33263	21223	1	0.142	0.082	0.002
ctg468	455220	7	0.161	0.071	0.002
tig02170431	955332	9	0.322	0.072	0.002
ctg13522	167494	2	0.148	0.092	0.002
tig00399738	453577	4	0.336	0.058	0.002
tig02169868	857412	6	0.390	0.061	0.002
ctg5666	344659	7	0.320	0.068	0.002
ctg7065	139213	7	0.251	0.072	0.002
ctg28120	96309	4	0.231	0.073	0.002
tig00399040	611393	2	0.174	0.075	0.002
ctg3157	183320	1	0.139	0.097	0.002
contig_28327	505316	1	0.088	0.100	0.002
tig00403292	917868	7	0.254	0.067	0.002
ctg5478	203258	2	0.305	0.069	0.002
ctg36424	18494	10	0.246	0.077	0.002
ctg3596	175065	5	0.203	0.084	0.002
contig_15985	614099	1	0.170	0.090	0.002
tig00003475	384296	8	0.091	0.094	0.002
tig00397067	1508104	1	0.113	0.095	0.002
tig00404052	254563	3	0.130	0.098	0.002
ctg278	700468	2	0.230	0.078	0.002
tig00015630	444711	3	0.181	0.082	0.002
tig00048729	291077	10	0.186	0.082	0.002
ctg1573	271466	1	0.082	0.100	0.002
contig_1219	625571	4	0.148	0.074	0.002
ctg1727	346568	1	0.128	0.097	0.002
ctg7275	217686	1	0.264	0.072	0.001
tig00395555	271328	8	0.147	0.079	0.001
ctg6355	105304	2	0.101	0.080	0.001
tig00032636	913796	1	0.178	0.082	0.001
tig00074206	384873	5	0.093	0.089	0.001
ctg4652	269717	1	0.150	0.093	0.001
contig_10547	335563	6	0.497	0.037	0.001
contig_8886	292449	3	0.384	0.055	0.001
tig00079487	951179	1	0.361	0.056	0.001
tig02188831	643395	7	0.193	0.060	0.001
tig00014655	351299	10	0.194	0.064	0.001
ctg18756	98018	8	0.309	0.065	0.001
ctg12448	165728	1	0.228	0.085	0.001
ctg20121	36987	1	0.179	0.086	0.001
ctg63201	9826	5	0.354	0.061	0.001
contig_19680	1173980	10	0.338	0.063	0.001
ctg3853	201225	1	0.318	0.070	0.001
tig00058991	244112	4	0.268	0.080	0.001
ctg6611	100866	6	0.160	0.082	0.001
tig00396149	623230	3	0.161	0.088	0.001
tig00397523	322509	3	0.219	0.092	0.001
tig00059977	206712	1	0.143	0.094	0.001
tig00065943	621099	3	0.145	0.101	0.001
ctg36792	18493	5	0.426	0.054	0.001
contig_27491	426366	5	0.267	0.071	0.001
ctg24	616767	8	0.262	0.077	0.001

ctg17515	42483	6	0.225	0.079	0.001
contig_2009	241801	1	0.204	0.090	0.001
ctg15643	47287	1	0.140	0.097	0.001
tig00018215	545841	5	0.388	0.057	0.001
ctg4689	205094	2	0.332	0.061	0.001
contig_32639	577279	7	0.228	0.067	0.001
tig02186583	453875	3	0.304	0.075	0.001
ctg1552	326042	1	0.251	0.080	0.001
contig_23904	445721	2	0.154	0.083	0.001
ctg16582	73716	4	0.195	0.086	0.001
ctg9736	109962	2	0.222	0.089	0.001
tig00399227	736035	6	0.195	0.094	0.001
ctg29432	23874	1	0.184	0.097	0.001
tig00399197	524909	1	0.176	0.099	0.001
ctg27879	25595	1	0.161	0.100	0.001
tig00093735	410540	2	0.075	0.108	0.001
ctg4406	125850	1	0.096	0.114	0.001
tig00028029	426442	8	0.385	0.055	0.001
tig00398278	361467	2	0.314	0.079	0.001
ctg4505	299987	3	0.238	0.088	0.001
tig00400420	264576	3	0.176	0.092	0.001
ctg8602	230135	2	0.097	0.122	0.001
ctg9542	77502	7	0.226	0.074	0.001
ctg5718	110930	7	0.264	0.080	0.001
tig00013101	268866	4	0.286	0.082	0.001
tig00027857	700320	2	0.186	0.097	0.001
ctg2079	413176	1	0.087	0.109	0.001
ctg2846	347791	2	0.092	0.113	0.001
tig00399901	811080	2	0.095	0.115	0.001
ctg2517	254880	1	0.098	0.118	0.001
contig_42809	351746	3	0.384	0.067	0.001
ctg1123	237209	3	0.269	0.074	0.001
ctg17685	45882	2	0.137	0.090	0.001
ctg9691	75105	6	0.216	0.090	0.001
ctg6339	334965	1	0.087	0.096	0.001
tig00059998	1068736	4	0.147	0.097	0.001
tig00017035	1132614	1	0.111	0.105	0.001
contig_13674	627862	1	0.077	0.106	0.001
tig02188748	571085	1	0.123	0.109	0.001
ctg3668	526163	2	0.132	0.117	0.001
tig00016009	623372	8	0.192	0.074	0.001
ctg10034	158959	8	0.381	0.075	0.001
tig00404038	641509	4	0.338	0.076	0.001
tig00137030	555776	1	0.305	0.080	0.001
ctg8899	80402	5	0.159	0.081	0.001
ctg9926	78349	4	0.283	0.084	0.001
tig00040441	397931	3	0.304	0.086	0.001
ctg36120	19521	1	0.179	0.093	0.001
tig00044954	583249	1	0.246	0.094	0.001
contig_5520	227618	1	0.245	0.097	0.001
tig00010587	1336264	6	0.193	0.098	0.001
tig00003873	791057	2	0.140	0.110	0.001
ctg27780	25018	1	0.174	0.110	0.001
ctg3120	269904	2	0.107	0.115	0.001
ctg7363	94642	1	0.106	0.116	0.001
contig_27828	686464	2	0.088	0.127	0.001
tig00013376	1099857	7	0.287	0.078	0.000
ctg5649	428367	8	0.167	0.080	0.000
ctg28671	22282	1	0.233	0.083	0.000
contig_37023	1291391	11	0.170	0.084	0.000
tig00001226	634311	20	0.235	0.084	0.000
ctg6281	218505	2	0.306	0.086	0.000
tig00398477	259891	2	0.138	0.086	0.000
tig02186361	536843	3	0.188	0.087	0.000

ctg29436	23631	1	0.226	0.091	0.000
ctg5058	134239	4	0.198	0.098	0.000
tig00049631	236709	3	0.185	0.112	0.000
ctg9955	81837	1	0.103	0.123	0.000
tig00034653	482718	1	0.072	0.123	0.000
tig00404607	513569	8	0.441	0.064	0.000
ctg25413	28004	3	0.424	0.068	0.000
ctg2742	317531	6	0.262	0.071	0.000
tig02169698	726794	13	0.232	0.073	0.000
tig02169510	472014	3	0.375	0.074	0.000
ctg7787	251517	3	0.296	0.078	0.000
tig00396258	746857	2	0.298	0.080	0.000
ctg14324	128536	1	0.203	0.085	0.000
ctg242	919531	2	0.182	0.086	0.000
contig_7359	400273	1	0.289	0.090	0.000
ctg2283	220690	11	0.261	0.090	0.000
tig00097609	300704	4	0.217	0.091	0.000
tig00088316	353022	4	0.199	0.091	0.000
ctg2930	323457	3	0.209	0.091	0.000
contig_26461	490084	2	0.292	0.091	0.000
ctg2491	168255	1	0.229	0.093	0.000
ctg442	403501	5	0.327	0.093	0.000
tig00001597	1594731	13	0.162	0.094	0.000
contig_28553	1558221	6	0.149	0.098	0.000
ctg7313	148101	5	0.151	0.100	0.000
ctg17866	41464	3	0.189	0.104	0.000
ctg7640	89382	3	0.083	0.111	0.000
ctg21292	34862	3	0.176	0.116	0.000
tig00010280	1014348	1	0.053	0.127	0.000
tig00396144	1246559	1	0.138	0.134	0.000
tig02186630	446353	5	0.281	0.067	0.000
tig02172233	477601	2	0.261	0.072	0.000
ctg8952	191809	12	0.448	0.073	0.000
ctg4754	226547	11	0.322	0.083	0.000
tig00020219	1582543	11	0.245	0.084	0.000
tig00020340	1636072	18	0.231	0.094	0.000
ctg6541	135355	5	0.258	0.095	0.000
ctg27332	26011	2	0.312	0.096	0.000
tig02169907	763412	2	0.304	0.097	0.000
ctg3368	235164	5	0.221	0.098	0.000
ctg1264	638142	6	0.119	0.101	0.000
ctg4898	121403	5	0.232	0.101	0.000
tig02170127	506055	4	0.346	0.104	0.000
contig_16551	552658	2	0.143	0.107	0.000
tig00013757	853991	1	0.173	0.112	0.000
tig00075283	491848	1	0.145	0.113	0.000
ctg10532	69894	4	0.236	0.118	0.000
ctg9146	121205	1	0.095	0.118	0.000
contig_51218	850550	1	0.142	0.118	0.000
ctg4165	205670	3	0.060	0.120	0.000
scaffold_46548	380348	3	0.172	0.123	0.000
ctg12024	104480	1	0.033	0.123	0.000
ctg15101	50662	1	0.132	0.125	0.000
ctg5822	424876	1	0.109	0.128	0.000
ctg10507	95448	10	0.102	0.129	0.000
tig02171260	684552	1	0.108	0.132	0.000
contig_25543	562659	1	0.050	0.136	0.000
ctg16452	198879	1	0.112	0.140	0.000
ctg357	533628	6	0.163	0.056	0.000
tig00000388	923617	3	0.293	0.077	0.000
contig_48617	1124269	2	0.224	0.081	0.000
ctg5775	214807	2	0.389	0.082	0.000
ctg13657	85231	5	0.369	0.084	0.000
contig_29750	831450	5	0.290	0.087	0.000

ctg13760	55398	4	0.370	0.089	0.000
contig_37992	158455	3	0.331	0.089	0.000
tig00398304	649387	7	0.309	0.090	0.000
tig00058741	449223	19	0.202	0.095	0.000
contig_4495	397920	4	0.324	0.095	0.000
tig00396753	694085	3	0.224	0.096	0.000
ctg10465	227629	4	0.139	0.097	0.000
tig00005901	1294013	3	0.209	0.097	0.000
tig00401456	1033341	1	0.271	0.098	0.000
contig_61276	243259	4	0.186	0.101	0.000
contig_8562	432781	2	0.216	0.103	0.000
ctg3025	155776	4	0.225	0.104	0.000
ctg4736	122597	2	0.077	0.105	0.000
ctg2490	469086	2	0.251	0.107	0.000
tig00395886	548602	3	0.264	0.107	0.000
tig02170574	313734	2	0.412	0.108	0.000
tig00396169	493748	14	0.220	0.110	0.000
ctg2000	251686	1	0.269	0.110	0.000
contig_29691	284461	4	0.271	0.111	0.000
tig00026233	282094	4	0.253	0.112	0.000
ctg14856	50818	1	0.291	0.113	0.000
ctg6510	102520	9	0.172	0.115	0.000
tig00396462	579784	3	0.265	0.116	0.000
tig00021261	419760	9	0.115	0.119	0.000
tig02169607	499162	8	0.152	0.119	0.000
tig02169928	928537	1	0.168	0.119	0.000
tig02169869	646305	1	0.166	0.122	0.000
tig00403326	206754	2	0.160	0.122	0.000
ctg6506	116431	8	0.127	0.123	0.000
ctg18711	39811	1	0.130	0.123	0.000
contig_22489	632453	1	0.190	0.128	0.000
ctg2589	368501	1	0.242	0.128	0.000
ctg4460	127493	3	0.181	0.129	0.000
ctg11469	84175	1	0.056	0.129	0.000
ctg1560	212380	1	0.120	0.131	0.000
ctg27349	22608	1	0.126	0.132	0.000
ctg8445	100647	1	0.037	0.133	0.000
contig_6378	651179	1	0.126	0.133	0.000
tig00400477	444752	4	0.131	0.133	0.000
contig_8232	217362	2	0.129	0.134	0.000
ctg852	248256	1	0.233	0.134	0.000
tig00058036	278178	3	0.038	0.135	0.000
contig_2548	273877	1	0.109	0.135	0.000
tig00402075	327274	3	0.203	0.136	0.000
ctg3372	143161	9	0.105	0.137	0.000
ctg12268	112660	3	0.269	0.137	0.000
ctg3169	476323	1	0.051	0.137	0.000
ctg4011	492880	1	0.052	0.137	0.000
ctg1519	240218	1	0.114	0.138	0.000
contig_4079	720163	7	0.229	0.138	0.000
tig00047947	229809	3	0.184	0.140	0.000
ctg8829	91237	2	0.191	0.142	0.000
tig00014963	470209	1	0.051	0.143	0.000
tig00047492	311084	1	0.086	0.144	0.000
tig00058221	370517	4	0.106	0.146	0.000
ctg2243	494601	1	0.304	0.146	0.000
ctg3407	229476	1	0.238	0.148	0.000
ctg287	682863	3	0.161	0.148	0.000
tig00395743	912175	3	0.339	0.149	0.000
ctg7939	119940	6	0.237	0.149	0.000
ctg6440	331778	1	0.211	0.149	0.000
ctg21626	68466	10	0.204	0.150	0.000
contig_37029	817425	6	0.192	0.150	0.000
ctg6609	154333	1	0.214	0.151	0.000

tig00395657	765970	1	0.129	0.154	0.000
ctg9541	75157	2	0.140	0.157	0.000
tig02175166	365575	1	0.129	0.157	0.000
tig00402739	313999	1	0.195	0.163	0.000
ctg3235	286464	1	0.121	0.166	0.000
ctg34396	20111	1	0.229	0.168	0.000
contig_17548	267555	1	0.104	0.168	0.000
ctg172	532540	13	0.169	0.168	0.000
ctg14352	72360	1	0.068	0.169	0.000
ctg9474	221587	2	0.033	0.174	0.000
contig_16540	228155	4	0.184	0.174	0.000
contig_3123	1138239	5	0.247	0.177	0.000
ctg12338	77367	1	0.189	0.179	0.000
ctg3990	216494	1	0.123	0.182	0.000
ctg11806	64035	1	0.195	0.184	0.000
ctg4256	486192	1	0.102	0.185	0.000
tig00006227	805723	3	0.259	0.192	0.000
ctg10925	67646	1	0.116	0.193	0.000
tig00028442	531138	1	0.040	0.200	0.000
ctg7090	171446	2	0.089	0.208	0.000
ctg17967	73963	1	0.119	0.242	0.000
tig00395900	652960	2	0.105	0.253	0.000

Chapter 4:

Figure S4.1: Present-day distribution of pale-lipped shell morphs in four Pyrenean valleys. Pie charts show frequencies of pale-lipped shells (white) versus other forms.

Figure S4.2: Scatterplots showing the present-day relationship between altitude and frequency of pale-lipped morphs in four Pyrenean valleys. Regression line and confidence intervals are shown, alongside the Pearson coefficient and p value.

Figure S4.3: Scatterplots showing the present-day relationship between altitude and size and shape of shells in four Pyrenean valleys. Regression line and confidence intervals are shown, alongside the Pearson coefficient and p value.

Figure S4.4: Scatterplot showing variation of visual space coordinates, xyz, on three principal component axes, using shells from Vielha and Jueu valleys in the Pyrenees. Units are in JNDs. Points are coloured according to human-scored classification of the shell, either yellow or pink.

Table S4.1: Summary of the Pyrenean sampling collection of 2017 and 2018. Geographical and habitat details are shown, further with the summary of shell phenotypes.

Table S4.2: Summary of the historical collections in the Pyrenees provided by the Evolution Megalab team. Geographical and habitat details are shown, further with the summary of shell phenotypes.

Table S4.3: Direction of change in shell morph frequencies, from 1960s to 2017/2018 in the Pyrenees.

Table S4.4: Statistical summary of shell altitudinal distribution in each valley; correlations (Pearson, parametric; Kendall, non-parametric).

Supplementary material: The qualitative phenotype and quantitative reflectance data for the samples used in this study can be access by request.

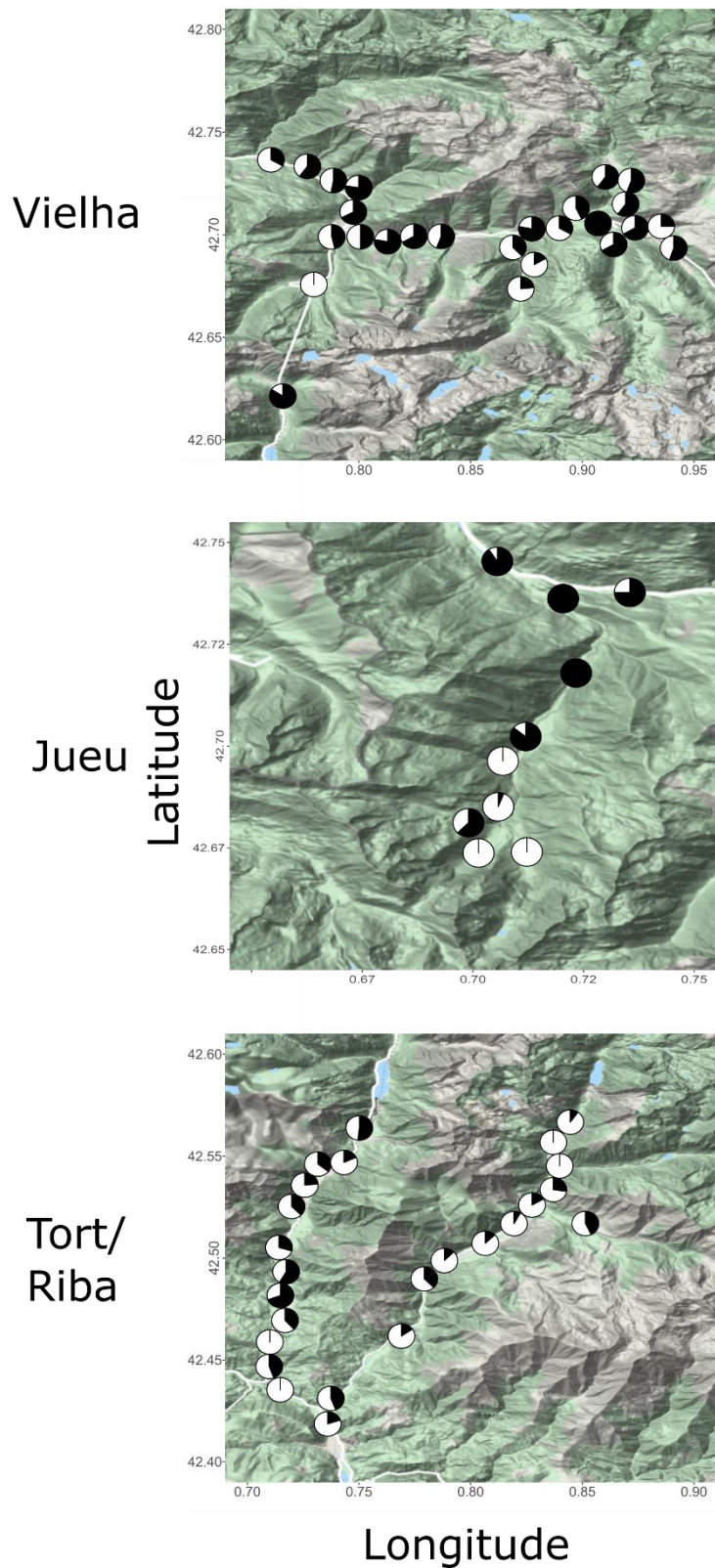


Figure S4.1. Present-day distribution of pale-lipped shell morphs in four Pyrenean valleys. Pie charts show frequencies of pale-lipped shells (white) versus other forms.

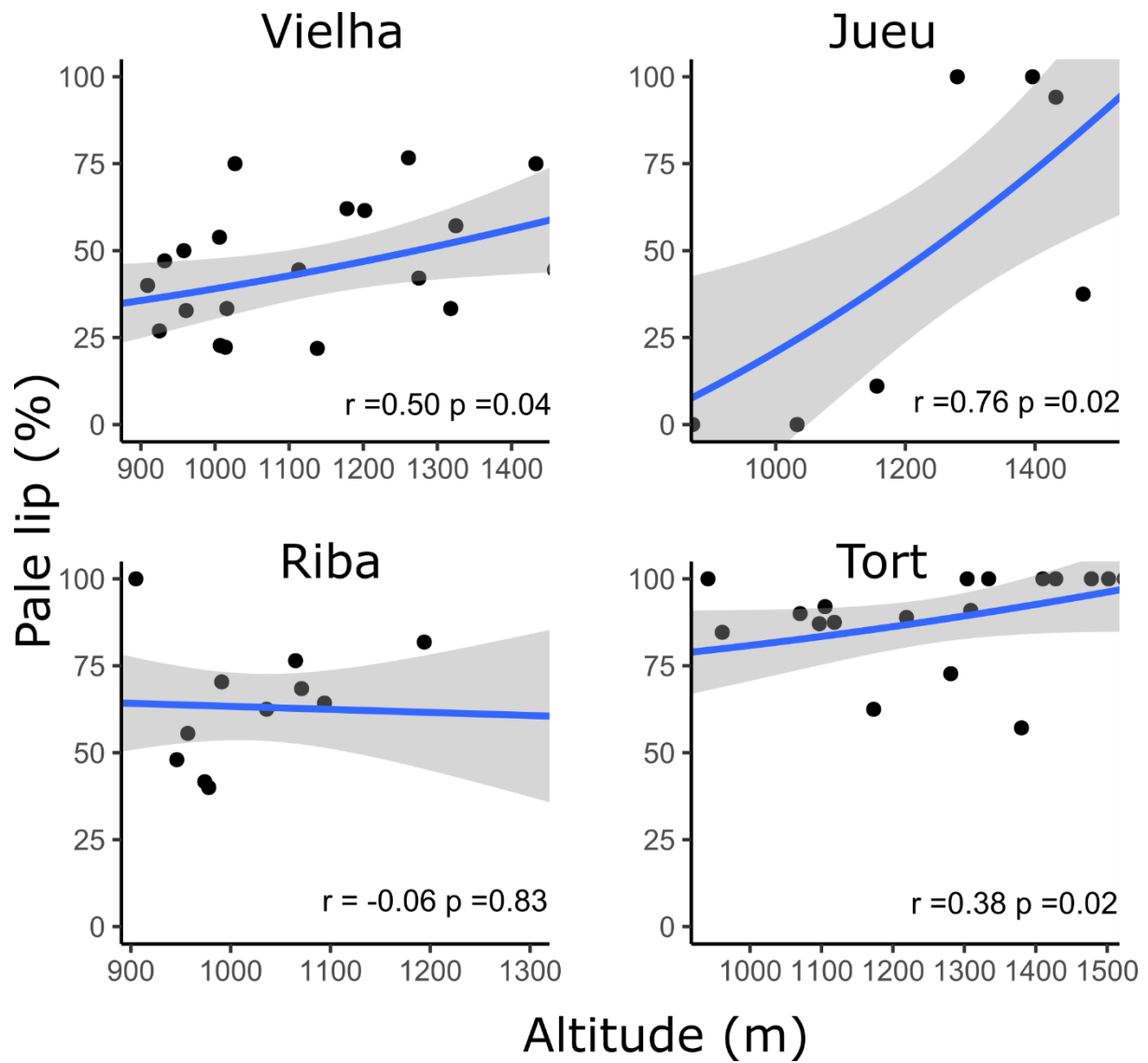


Figure S4.2. Scatterplots showing the present-day relationship between altitude and frequency of pale-lipped morphs in four Pyrenean valleys. Regression line and confidence intervals are shown, alongside the Pearson coefficient and p value.

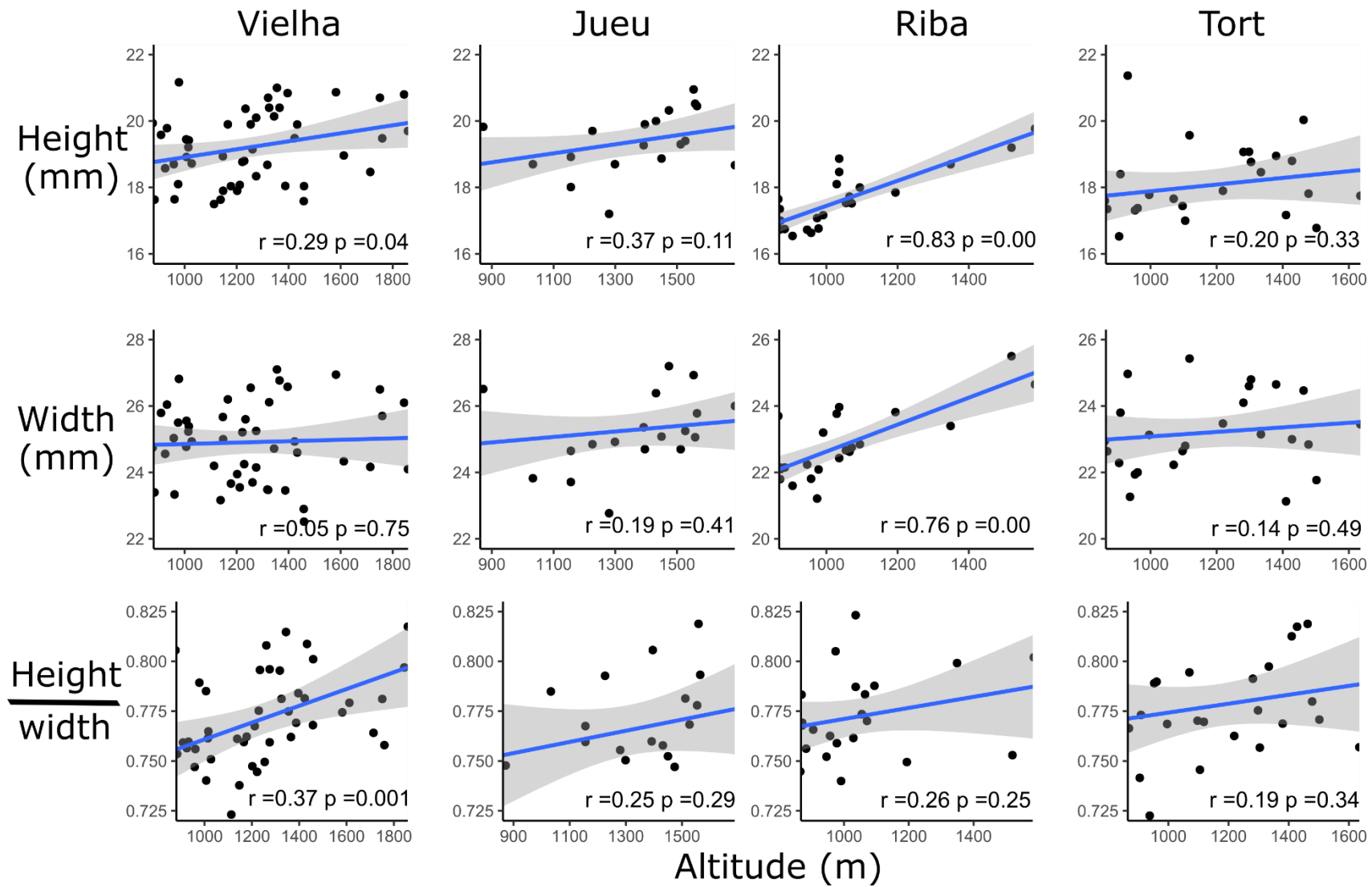


Figure S4.3. Scatterplots showing the present-day relationship between altitude and size and shape of shells in four Pyrenean valleys. Regression line and confidence intervals are shown, alongside the Pearson coefficient and p value.

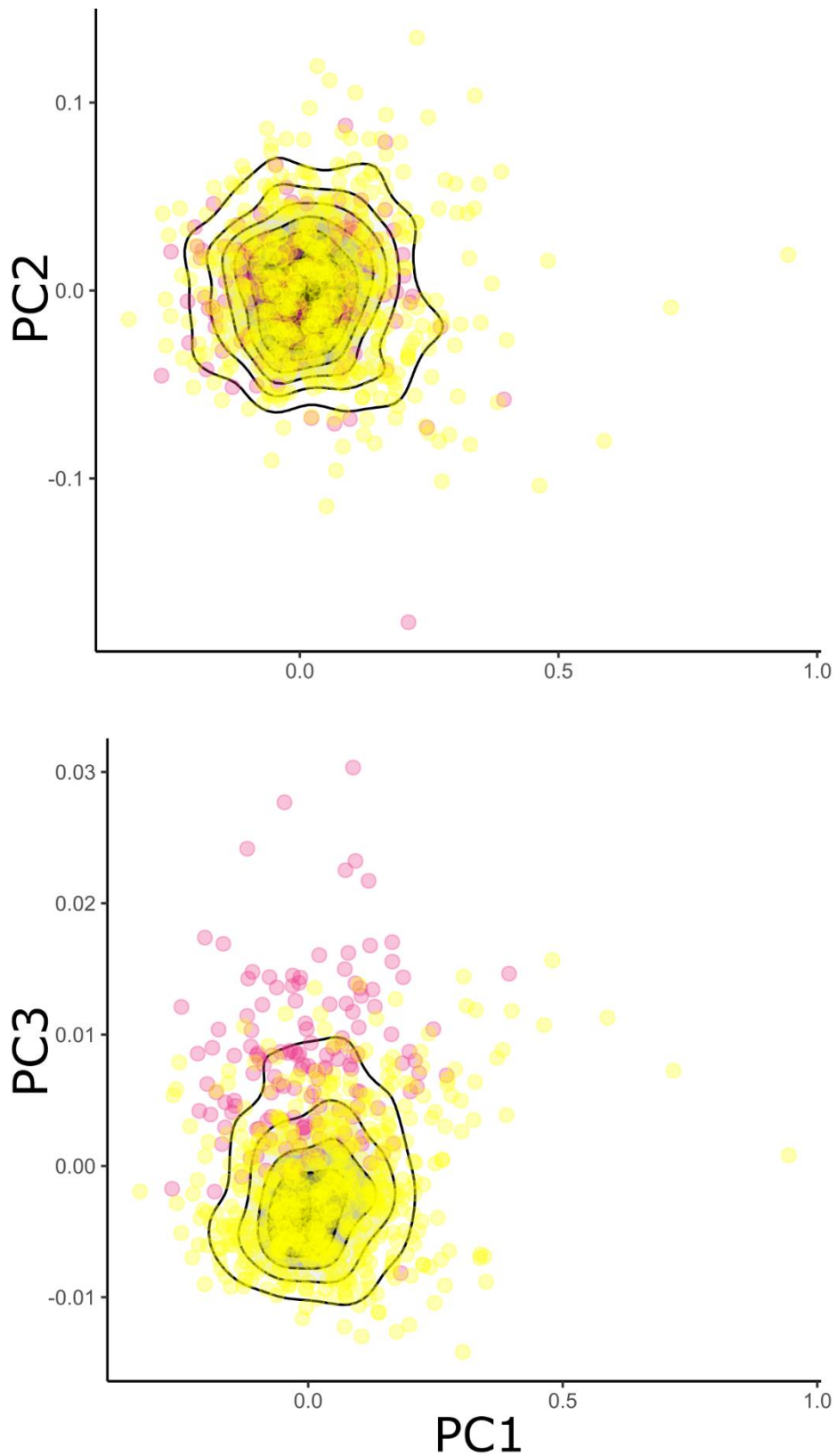


Figure S4.4. Scatterplot showing variation of visual space coordinates, xyz, on three principal component axes, using shells from Vielha and Jueu valleys in the Pyrenees. Units are in JNDs. Points are coloured according to human-scored classification of the shell, either yellow or pink.

Table S4.1. Summary of the sampling collection of *C. nemoralis* in 2017 and 2018. Details of location, habitat and shell phenotypes with its frequencies are reported.

Code	Latitude	Longitude	Altitude	Habitat classification	Total snails	Yellow	Pink	Brown	Unbanded	Mid-banded	Five-banded	Other banding
2017 collection												
DRG1	42.69676	0.81278	1014	2	34	22	12	0	5	2	23	4
DRG2	42.69723	0.81273	1027	1	9	9	0	0	2	0	5	2
DRG3	42.69939	0.82452	1016	1	14	7	6	0	5	0	9	0
DRG4	42.70123	0.92666	1458	1	30	18	12	0	3	0	27	0
DRG5	42.70094	0.92759	1459	2	46	26	20	0	2	4	36	4
DRG6	42.69719	0.93143	1433	2	12	10	2	0	4	0	8	0
DRG7	42.69985	0.91832	1318	2	22	13	10	0	9	2	11	0
DRG8	42.69996	0.91832	1321	1	8	6	2	0	3	0	4	1
DRG9	42.70002	0.91755	1344	2	9	5	4	0	1	1	7	0
DRG10	42.70415	0.90238	1275	2	23	15	8	0	2	1	15	5
DRG11	42.70504	0.90342	1234	1	17	2	15	0	2	0	15	0
DRG12	42.69854	0.86332	1129	1	21	11	10	0	10	2	8	1
DRG13	42.70004	0.84889	1113	2	62	41	21	0	5	0	55	2
DRG14	42.67835	0.87315	1261	1	37	37	0	0	20	0	14	3
DRG15	42.68278	0.87539	1259	2	23	22	1	0	21	0	2	0
DRG16	42.69085	0.87381	1202	2	18	13	5	0	3	2	12	1
DRG17	42.69048	0.87416	1178	3	63	42	21	0	32	3	27	1
DRG18	42.69539	0.87371	1138	1	43	31	10	0	5	2	30	6
DRG19	42.68952	0.78683	1193	2	1	1	0	0	1	0	0	0
DRG20	42.67758	0.78686	1229	1	16	16	0	0	14	0	0	2
DRG21	42.67866	0.78779	1212	1	15	15	0	0	10	0	5	0
DRG22	42.68685	0.78983	1166	1	10	8	2	0	4	0	2	4
DRG23	42.68785	0.79002	1148	1	14	16	0	0	6	2	4	2
DRG24	42.6988	0.79402	1006	1	39	35	4	0	10	1	26	2
DRG25	42.69666	0.79275	978	2	14	15	2	0	2	1	9	2
DRG26	42.70031	0.80295	958	1	13	8	5	0	4	0	5	4
DRG27	42.70686	0.79624	961	2	56	35	19	0	3	2	49	2
DRG28	42.72042	0.79612	1007	3	30	21	8	0	5	6	18	1
DRG29	42.72947	0.79178	1147	2	10	9	1	0	1	0	9	0
DRG30	42.72604	0.79948	1222	2	10	7	3	0	8	1	1	0

DRG31	42.72174	0.79331	975	2	4	3	1	0	1	2	1	0
DRG32	42.7265	0.78439	925	2	43	13	30	0	9	2	31	1
DRG33	42.72649	0.78841	932	1	22	18	4	0	10	0	12	0
DRG34	42.73341	0.77671	909	1	22	15	7	0	1	1	20	0
DRG35	42.73886	0.76158	884	2	10	5	5	0	1	4	5	0
DRG36	42.73657	0.76037	877	2	24	16	8	0	13	1	6	4
DRG37	42.70649	0.80882	1423	1	10	7	3	0	0	0	8	2
DRG38	42.74539	0.70552	823	2	17	7	10	0	4	3	6	4
DRG39	42.73815	0.72204	838	3	16	8	8	0	7	0	9	0
DRG40	42.73626	0.72043	872	3	11	4	7	0	0	0	10	1
DRG41	42.7158	0.72163	1035	3	3	2	1	0	2	1	0	0
DRG42	42.70236	0.71194	1156	1	204	184	20	0	39	27	54	84
DRG43	42.6972	0.70773	1226	1	6	5	1	0	1	0	1	4
DRG44	42.67711	0.70696	1396	3	9	9	0	0	9	0	0	0
DRG45	42.68214	0.70667	1432	1	23	21	2	0	23	0	0	0
DRG46	42.68289	0.70754	1280	3	18	16	2	0	12	0	6	0
DRG47	42.71797	0.72336	1033	1	30	26	3	0	10	5	14	1
DRG48	42.7061	0.913922	1387	1	15	7	8	0	0	0	15	0
DRG49	42.70468	0.924582	1612	1	20	8	12	0	2	0	18	0
DRG50	42.5639	0.75003	1349	2	33	32	1	0	33	0	0	0
DRG51	42.55828	0.74746	1297	2	2	0	2	0	2	0	0	0
DRG52	42.55217	0.74768	1243	2	10	9	1	0	9	0	1	0
DRG53	42.54617	0.73439	1206	2	1	0	1	0	1	0	0	0
DRG54	42.54703	0.74149	1194	2	16	16	0	0	16	0	0	0
DRG55	42.54463	0.73038	1164	1	1	1	0	0	1	0	0	0
DRG56	42.54065	0.72912	1094	2	17	9	7	1	16	0	1	0
DRG57	42.53904	0.72736	1055	2	9	8	0	1	9	0	0	0
DRG58	42.53669	0.72622	1071	2	23	23	0	0	23	0	0	0
DRG59	42.53588	0.72553	1065	2	17	14	3	0	15	0	2	0
DRG60	42.51323	0.71942	1036	1	11	11	0	0	9	0	2	0
DRG61	42.513	0.71964	1036	2	19	10	0	9	18	0	1	0
DRG62	42.5064	0.71806	991	2	29	23	1	5	27	0	2	0
DRG63	42.41283	0.74002	883	1	43	28	8	7	13	3	22	5
DRG64	42.41867	0.73595	870	3	21	31	0	0	20	0	0	1
DRG65	42.41888	0.73597	865	2	5	5	0	0	3	0	0	2
DRG66	42.42711	0.72841	871	2	4	1	0	3	4	0	0	0
DRG67	42.43095	0.72259	869	2	11	11	0	0	11	0	0	0

DRG68	42.43537	0.71466	905	2	10	10	0	0	8	0	2	0
DRG69	42.43527	0.71464	892	2	10	5	0	5	9	0	1	0
DRG70	42.44844	0.71035	957	1	12	9	0	3	12	0	0	0
DRG71	42.45884	0.70997	937	2	14	12	2	0	8	0	6	0
DRG72	42.46839	0.71497	1029	2	3	0	0	3	3	0	0	0
DRG74	42.48304	0.71561	974	2	13	5	1	7	10	0	3	0
DRG75	42.48171	0.7147	978	2	16	3	0	13	16	0	0	0
DRG77	42.4792	0.71395	946	2	31	17	2	12	23	0	8	0
DRG78	42.43259	0.73986	905	2	44	35	4	5	23	1	13	7
DRG79	42.43479	0.74287	862	2	17	16	1	0	12	3	2	0
DRG80	42.44119	0.74672	909	1	10	10	0	0	8	1	1	0
DRG81	42.44796	0.7519	869	1	12	12	0	0	6	1	4	1
DRG82	42.45299	0.75418	941	2	17	15	2	0	8	0	7	2
DRG83	42.45321	0.75442	938	2	12	7	1	0	2	0	4	6
DRG84	42.45633	0.75849	996	1	32	35	0	0	6	3	15	8
DRG85	42.45556	0.75928	953	3	40	37	3	0	3	2	32	3
DRG86	42.45626	0.76009	961	1	47	45	2	0	8	1	29	9
DRG87	42.46047	0.76597	931	1	6	6	0	0	3	2	1	0
DRG88	42.49438	0.784053	1115	2	24	22	2	0	7	1	12	4
DRG89	42.49937	0.78319	1189	2	5	5	0	0	0	0	5	0
DRG90	42.49679	0.78401	1173	2	44	43	1	0	7	5	32	0
DRG91	42.49706	0.78695	1118	2	10	10	0	0	6	1	3	0
DRG92	42.56332	0.84286	1070	1	19	16	0	3	10	3	5	1
DRG93	42.5569	0.83714	1428	3	14	14	0	0	8	3	1	2
DRG94	42.54425	0.83964	1374	1	3	2	1	0	1	0	0	2
DRG95	42.52676	0.83342	1298	1	12	12	0	0	0	2	10	0
DRG96	42.52313	0.83568	1304	2	14	14	0	0	0	3	11	0
DRG97	42.52317	0.83659	1309	1	11	11	0	0	0	1	10	0
DRG98	42.52018	0.84257	1380	1	19	19	0	0	0	0	19	0
DRG99	42.51924	0.84682	1463	2	6	6	0	0	0	0	6	0
DRG100	42.52649	0.82871	1219	1	22	21	1	0	1	3	16	2
DRG101	42.51701	0.81945	1105	1	41	35	6	0	11	8	18	4
DRG102	42.50738	0.80655	1097	2	42	41	1	0	4	2	34	2
2018 collection												
DRG103	42.67786	0.705514	1474	2	19	12	7	0	15	0	4	0

DRG104	42.67605	0.705895	1480	2	6	6	0	0	6	0	0	0
DRG105	42.67509	0.702944	1494	1	6	6	0	0	2	0	4	0
DRG106	42.67439	0.702068	1559	2	27	27	0	0	27	0	0	0
DRG107	42.6747	0.7013	1527	2	19	19	0	0	19	0	0	0
DRG108	42.674	0.6999	1555	2	12	11	1	0	12	0	0	0
DRG109	42.6697	0.6999	1688	2	16	16	0	0	16	0	0	0
DRG110	42.6665	0.6947	1921	2	3	3	0	0	3	0	0	0
DRG111	42.6697	0.7089	1554	2	6	6	0	0	6	0	0	0
DRG112	42.674	10.7122	1565	2	14	14	0	0	14	0	0	0
DRG113	42.6751	0.7075	1512	3	6	6	0	0	6	0	0	0
DRG114	42.67762	0.707189	1482	3	10	8	2	0	3	0	6	1
DRG115	42.68255	0.70815	1450	2	13	13	0	0	3	0	3	7
DRG116	42.6907	0.708	1392	2	7	7	0	0	6	0	1	0
DRG117	42.7024	0.7123	1299	2	10	8	2	0	2	0	4	4
DRG118	42.70423	0.93945	1714	2	5	5	0	0	1	0	4	0
DRG119	42.70345	0.94682	1760	2	3	3	0	0	3	0	0	0
DRG120	42.70115	0.944631	1751	2	3	3	0	0	3	0	0	0
DRG121	42.699	0.9461	1844	2	1	1	0	0	1	0	0	0
DRG122	42.703	0.9433	1859	2	2	2	0	0	2	0	0	0
DRG123	42.72038	0.916398	1582	1	28	13	15	0	1	0	27	0
DRG124	42.6214	0.765843	1586	2	22	12	10	0	15	0	4	3
DRG125	42.62202	0.764279	1520	2	5	0	4	1	2	1	1	1
DRG126	42.7211	0.9142	1396	1	29	21	8	0	0	0	27	2
DRG127	42.71366	0.914242	1365	2	24	11	13	0	0	0	24	0
DRG128	42.7122	0.9104	1355	2	15	15	0	0	5	0	9	1
DRG129	42.7113	0.905847	1325	1	11	8	3	0	0	0	11	0
DRG130	42.7007	0.8628	1254	1	49	34	15	0	4	3	41	1
DRG131	42.5693	0.8465	1635	2	3	3	0	0	0	0	3	0
DRG132	42.5693	0.8465	1635	2	2	2	0	0	0	0	1	1
DRG133	42.56637	0.845173	1502	2	19	19	0	0	16	1	2	0
DRG134	42.56669	0.845923	1524	2	10	10	0	0	6	0	4	0
DRG135	42.56332	0.84286	1478	2	24	23	1	0	8	5	10	1
DRG136	42.55371	0.83521	1410	2	18	16	2	0	14	1	2	1
DRG137	42.54425	0.83964	1334	2	21	20	1	0	7	0	14	2
DRG138	42.5311	0.8346	1281	2	18	17	1	0	3	0	15	4

Sites from 2017 resampled in 2018

DRG10	42.70415	0.90238	1275	2	30	19	11	0	3	0	27	0
DRG42	42.70236	0.71194	1156	2	73	70	3	0	14	13	46	24
DRG75	42.48171	0.7147	978	2	26	8	0	18	25	0	1	0
DRG77	42.4792	0.71395	946	2	46	23	0	23	40	0	6	0
DRG100	42.52649	0.82871	1219	1	17	17	0	0	0	0	17	0

Total summary of resampled sites

DRG10	42.70415	0.90238	1275	2	53	34	19	0	5	1	42	5
DRG42	42.70236	0.71194	1156	2	277	254	23	0	53	40	100	84
DRG75	42.48171	0.7147	978	2	42	11	0	31	41	0	1	0
DRG77	42.4792	0.71395	946	2	77	40	2	35	63	0	14	0
DRG100	42.52649	0.82871	1219	1	39	38	1	0	1	3	33	2

Habitat classification; 1 = Open (shrubland, walls, grassland), 2 =Hedgerow or tall herbs, 3 = Woodland or shaded areas.

Table S4.2. Summary of the historical data for *C. nemoralis* . Details of location, habitat and shell phenotypes with its frequencies are reported.

Code	Year	Latitude	Longitude	Altitude	Total snails	Yellow	Pink	Brown	Unbanded	Mid-banded	Five-banded
Arnold, RW 1968 Phil.Trans.R.Soc.Lond B 253, 549-593											
AR1	1962	42.8631	0.7464	683	40	15	25	0	6	3	31
AR2	1962	42.8381	0.7306	722	28	6	22	0	1	7	20
AR3	1962	42.8106	0.7107	837	29	16	13	0	2	6	21
AR4	1962	42.7959	0.6993	772	27	20	7	0	2	0	25
AR5	1962	42.7891	0.6956	873	54	37	17	0	4	7	43
AR6	1962	42.7755	0.6866	788	36	27	9	0	5	3	28
AR7	1962	42.76139	0.6858	931	36	21	15	0	5	5	26
AR8	1962	42.75	0.7031	941	35	15	20	0	3	5	27
AR9	1962	42.7407	0.7146	849	51	29	22	0	14	2	35
AR10	1962	42.7389	0.7278	936	59	39	20	0	12	3	44
AR11	1962	42.7381	0.7455	905	51	29	22	0	8	3	40
AR12	1962	42.7392	0.7579	940	42	24	18	0	5	1	36
AR13	1962	42.7345	0.7724	1100	27	11	16	0	4	1	22
AR14	1962	42.723	0.7807	1016	39	19	20	0	3	2	34
AR15	1962	42.7256	0.7862	1217	41	23	18	0	3	5	33
AR16	1962	42.7142	0.7963	1186	61	39	22	0	21	4	36
AR17	1962	42.7089	0.7949	1186	35	20	15	0	1	3	31
AR18	1962	42.7006	0.7989	1073	32	18	14	0	4	0	28
AR19	1962	42.6976	0.8095	1067	45	18	27	0	2	6	37
AR20	1962	42.6974	0.8229	1126	39	23	16	0	7	0	32
AR21	1962	42.6998	0.835	1217	74	63	11	0	23	5	46
AR22	1962	42.7001	0.8466	1306	58	31	27	0	2	1	55
AR23	1962	42.7007	0.8628	1254	58	27	31	0	4	2	52
AR24	1962	42.7012	0.8683	1232	65	32	33	0	8	3	54
AR25	1962	42.7025	0.8868	1256	70	37	33	0	5	0	65
AR26	1962	42.7059	0.8921	1273	76	43	33	0	9	2	65
AR27	1962	42.7067	0.9012	1321	44	20	24	0	0	0	44
AR28	1962	42.7027	0.9119	1426	43	18	25	0	6	0	37

AR29	1962	42.7004	0.9179	1548	83	43	40	0	27	4	52
AR30	1962	42.6994	0.9213	1493	45	32	13	0	26	1	18
AR31	1962	42.6981	0.9259	1522	32	28	4	0	23	0	9
AR32	1962	42.6973	0.929	1522	63	52	11	0	54	2	7
AR33	1962	42.6949	0.9369	1793	66	61	5	0	64	0	2
AR34	1962	42.6916	0.9404	1534	28	23	5	0	26	0	2
AR35	1962	42.732	0.7265	1197	48	43	5	0	19	4	25
AR36	1962	42.722	0.7248	1103	29	25	4	0	7	8	14
AR37	1962	42.7086	0.717	1508	47	42	5	0	19	2	26
AR38	1962	42.6958	0.7091	1465	49	25	24	0	41	6	2
AR39	1962	42.6723	0.7047	1527	44	44	0	0	43	0	1
AR40	1962	42.7419	0.7551	1085	37	35	2	0	6	3	28
AR41	1962	42.7466	0.7593	1418	29	29	0	0	13	0	16
AR42	1962	42.7519	0.7625	1169	26	25	1	0	24	0	2
AR43	1962	42.7587	0.772	1278	9	9	0	0	8	0	1
AR44	1962	42.7655	0.7756	1720	21	13	8	0	20	0	1
AR45	1962	42.7667	0.7799	1367	23	21	2	0	22	0	1
AR46	1962	42.7193	0.8017	1280	51	27	24	0	8	6	37
AR47	1962	42.7208	0.8051	1280	25	18	7	0	2	0	23
AR48	1962	42.7242	0.8089	1554	68	63	5	0	19	0	49
AR49	1962	42.7288	0.8162	1357	29	29	0	0	16	1	12
AR50	1962	42.7305	0.82	1586	30	28	2	0	17	1	12
AR51	1962	42.731	0.8248	1586	37	37	0	0	35	1	1
AR52	1962	42.7328	0.8216	1586	36	36	0	0	33	1	2
AR53	1962	42.7338	0.8204	1731	32	32	0	0	25	0	7
AR54	1962	42.7362	0.8214	1731	49	49	0	0	49	0	0
AR55	1962	42.7399	0.8221	1731	24	24	0	0	24	0	0
AR56	1962	42.7426	0.8226	1951	17	17	0	0	17	0	0
AR57	1962	42.6891	0.7932	1473	48	40	8	0	21	6	21
AR58	1962	42.6947	0.7904	1110	44	37	7	0	19	6	19
AR59	1962	42.6898	0.7897	1358	87	80	7	0	56	9	22
AR60	1962	42.6859	0.7887	1358	20	20	0	0	18	1	1
AR61	1962	42.6794	0.7876	1531	65	64	1	0	48	7	10

AR62	1962	42.6779	0.7863	1531	37	37	0	0	33	0	4
AR63	1962	42.6757	0.7787	1268	6	6	0	0	6	0	0
AR64	1962	42.6754	0.7749	1401	42	42	0	0	42	0	0
AR65	1962	42.6783	0.7689	1401	29	29	0	0	29	0	0
AR66	1962	42.6748	0.765	1552	43	43	0	0	43	0	0
AR67	1962	42.6967	0.8735	1338	32	27	5	0	25	0	7
AR68	1962	42.6953	0.872	1338	45	44	1	0	39	1	5
AR69	1962	42.6922	0.873	1338	36	36	0	0	36	0	0
AR70	1962	42.69	0.8757	1798	25	25	0	0	20	0	5
AR71	1962	42.687	0.8733	1396	23	23	0	0	18	0	5
AR72	1962	42.68	0.8724	1432	28	18	10	0	23	0	5
AR73	1962	42.675	0.8733	1566	32	32	0	0	27	0	5
AR74	1962	42.67	0.8699	1566	27	27	0	0	11	3	13
AR75	1962	42.666	0.8673	1584	24	24	0	0	6	6	12
AR76	1962	42.7122	0.9104	1619	52	38	14	0	5	0	47
AR77	1962	42.7211	0.9142	1520	41	36	5	0	28	1	12
AR78	1962	42.7488	0.9143	1836	46	44	2	0	20	2	24
AR79	1962	42.7583	0.9111	2070	31	31	0	0	30	0	1
AR80	1962	42.7626	0.9122	2307	38	38	0	0	32	0	6
AR81	1962	42.6982	0.9167	1493	54	52	2	0	29	3	22
AR82	1962	42.693	0.9146	1447	28	27	1	0	26	0	2
AR83	1962	42.6832	0.9153	1610	28	28	0	0	25	1	2
AR84	1962	42.6793	0.9153	1610	33	31	2	0	31	1	1
AR85	1962	42.7007	0.937	1803	21	21	0	0	17	1	3
AR86	1962	42.703	0.9433	1859	39	39	0	0	38	0	1
AR87	1962	42.7065	0.955	1918	34	34	0	0	34	0	0
AR88	1962	42.7056	0.9659	2006	30	30	0	0	30	0	0
AR89	1962	42.786	0.7098	1265	21	14	7	0	2	7	12
AR90	1962	42.7605	0.705	1447	24	16	8	0	0	2	22
AR91	1962	42.746	0.7306	1247	31	29	2	0	0	0	31
AR92	1962	42.7447	0.7361	1201	37	23	14	0	0	0	37
AR93	1962	42.743	0.7416	1201	20	12	8	0	3	1	16
AR94	1962	42.7371	0.7766	1269	36	33	3	0	2	2	32

AR95	1962	42.7268	0.7896	1217	54	35	19	0	2	2	50
AR96	1962	42.7228	0.7943	1085	71	49	22	0	5	0	66
AR97	1962	42.7133	0.7908	971	59	54	5	0	10	0	49
AR98	1962	42.7059	0.7886	972	70	40	30	0	4	2	64
AR99	1962	42.6956	0.7995	1055	41	31	10	0	4	5	32
AR100	1962	42.7087	0.9076	1376	48	29	19	0	1	0	47
AR101	1962	42.7107	0.91	1619	66	53	13	0	4	0	62
AR102	1962	42.7112	0.9125	1619	61	40	21	0	1	1	59
AR103	1962	42.7125	0.9151	1619	40	36	4	0	2	0	38
AR104	1962	42.7133	0.9174	1885	35	27	8	0	1	0	34
AR105	1962	42.7138	0.919	1885	34	29	5	0	9	0	25
AR106	1962	42.714	0.9204	1885	42	32	10	0	18	0	24
AR107	1962	42.7146	0.9221	1885	30	30	0	0	22	1	7
AR108	1962	42.6953	0.9395	1793	57	56	1	0	41	0	16
AR109	1962	42.697	0.9429	1998	34	33	1	0	27	0	7
AR110	1962	42.699	0.9461	1998	33	33	0	0	33	0	0
AR111	1962	42.7003	0.9517	1918	28	28	0	0	28	0	0
AR112	1962	42.7021	0.9589	2006	54	51	3	0	54	0	0
AR113	1962	42.6978	0.7057	1256	33	27	6	0	21	0	12
AR114	1962	42.7557	0.7629	1169	11	10	1	0	8	0	3
AR115	1962	42.7642	0.7694	1278	22	22	0	0	22	0	0
AR116	1962	42.7252	0.8068	1304	67	61	6	0	8	2	57
AR117	1962	42.6976	0.7892	1110	29	23	6	0	7	2	20
AR118	1962	42.6786	0.7854	1531	32	28	4	0	8	2	22
AR119	1962	42.6963	0.8753	1464	33	21	12	0	0	0	33
AR120	1962	42.6954	0.8772	1464	38	35	3	0	16	1	21
AR121	1962	42.6942	0.8777	1464	90	81	9	0	15	4	71
AR122	1962	42.7207	0.9151	1520	59	42	17	0	7	0	52
AR123	1962	42.7408	0.8209	1731	26	26	0	0	25	0	1

Cameron RAD, Carter, MA, Haynes, FN 1973 Heredity 31, 43-74

CA1	1966	42.7304	0.7256	1197	24	20	4	0	4	3	17
CA2	1966	42.7297	0.7284	1197	27	23	4	0	9	5	13

CA3	1966	42.7201	0.7275	1271	24	19	5	0	15	3	6
CA4	1966	42.7145	0.7234	1508	36	32	4	0	20	0	16
CA5	1966	42.712	0.7229	1508	75	57	18	0	19	10	46
CA6	1966	42.7106	0.7197	1508	58	24	34	0	11	17	30
CA7	1966	42.7084	0.7175	1508	84	80	4	0	25	8	51
CA8	1966	42.7042	0.7142	1299	26	25	1	0	7	0	19
CA9	1966	42.7027	0.7132	1299	81	73	8	0	16	3	62
CA10	1966	42.6995	0.7133	1465	30	27	3	0	18	2	10
CA11	1966	42.6861	0.7117	1736	36	19	17	0	36	0	0
CA12	1966	42.6751	0.7046	1512	37	37	0	0	37	0	0
CA13	1966	42.6751	0.7027	1512	43	43	0	0	43	0	0
CA14	1966	42.6747	0.7013	1527	25	25	0	0	25	0	0
CA15	1966	42.674	0.6999	1655	22	22	0	0	22	0	0
CA16	1966	42.6751	0.7108	1915	27	27	0	0	27	0	0
CA17	1966	42.674	0.7122	1943	47	47	0	0	46	0	1
CA18	1966	42.3367	0.7703	1165	19	7	12	0	12	2	5
CA19	1966	42.6294	0.7703	1845	14	1	13	0	9	1	4
CA20	1966	42.6277	0.7731	1845	13	4	9	0	12	0	1
CA21	1966	42.6244	0.766	1651	42	18	24	0	33	0	9
CA22	1966	42.6074	0.7691	1824	22	4	18	0	22	0	0
CA23	1966	42.5862	0.7596	1769	47	46	1	0	47	0	0
CA24	1966	42.5752	0.7631	1805	71	69	2	0	71	0	0
CA25	1966	42.5718	0.756	1445	46	40	0	6	46	0	0
CA26	1966	42.5616	0.7476	1301	47	25	2	20	47	0	0
CA27	1966	42.5549	0.7453	1333	60	60	0	0	60	0	0
CA28	1966	42.5481	0.7298	1149	57	39	8	10	57	0	0
CA29	1966	42.5447	0.7226	1258	27	19	8	0	27	0	0
CA30	1966	42.5404	0.7203	1070	49	28	15	6	49	0	0
CA31	1966	42.5184	0.7191	1143	74	71	0	3	53	14	7
CA32	1966	42.5082	0.7138	1068	84	68	5	11	84	0	0
CA33	1966	42.4879	0.7155	1044	30	12	1	17	29	0	1
CA34	1966	42.4726	0.7119	1090	45	21	0	24	43	0	2
CA35	1966	42.482	0.7155	1008	29	28	1	0	21	2	6

CA36	1966	42.5803	0.8596	2435	16	16	0	0	9	0	7
CA37	1966	42.5566	0.8365	1815	13	13	0	0	10	2	1
CA38	1966	42.5515	0.8369	1815	34	29	5	0	27	1	6
CA39	1966	42.5274	0.8298	1447	32	29	3	0	8	2	22
CA40	1966	42.521	0.8274	1327	108	108	0	0	53	1	54
CA41	1966	42.5099	0.8007	1109	136	128	8	0	18	14	104
CA42	1966	42.4989	0.7903	1198	77	73	4	0	12	4	61
CA43	1966	42.476	0.775	1330	42	41	1	0	15	3	24
CA44	1966	42.4689	0.7698	1037	50	50	0	0	8	4	38
CA45	1966	42.465	0.7579	1107	21	21	0	0	20	0	1
CA46	1966	42.4591	0.7441	1261	36	29	7	0	22	4	10
CA47	1966	42.4472	0.7369	1006	37	34	3	0	32	1	4
CA48	1966	42.4342	0.7298	1020	97	88	4	5	86	2	9
CA49	1969	42.7418	0.7042	941	27	19	8	0	6	1	20
CA50	1969	42.7432	0.7075	941	102	56	46	0	15	6	81
CA51	1969	42.743	0.7099	1136	57	45	12	0	8	0	49
CA52	1969	42.7382	0.7108	849	39	28	11	0	6	4	29
CA53	1969	42.7365	0.7142	849	34	28	6	0	4	1	29
CA54	1969	42.7184	0.726	1271	29	22	7	0	14	5	10
CA55	1969	42.7159	0.7246	1508	39	36	3	0	3	14	22
CA56	1969	42.7095	0.7184	1508	36	30	6	0	18	2	16
CA57	1969	42.7024	0.7123	1299	49	25	24	0	12	9	28
CA58	1969	42.6995	0.7134	1465	43	34	9	0	24	2	17
CA59	1969	42.6971	0.7124	1465	30	29	1	0	10	1	19
CA60	1969	42.6946	0.708	1256	53	52	1	0	19	7	27
CA61	1969	42.6935	0.7108	1465	18	14	4	0	12	4	2
CA62	1969	42.6903	0.7113	1736	8	2	6	0	8	0	0
CA63	1969	42.6907	0.708	1392	38	35	3	0	16	0	22
CA64	1969	42.685	0.7096	1736	51	33	18	0	51	0	0
CA65	1969	42.6835	0.7104	1736	40	29	11	0	39	1	0
CA66	1969	42.6697	0.6999	1655	20	20	0	0	20	0	0
CA67	1969	42.6655	0.6966	2180	28	28	0	0	28	0	0
CA68	1969	42.6665	0.6947	2180	17	17	0	0	17	0	0

CA69	1969	42.6697	0.7089	1943	20	20	0	0	20	0	0
CA70	1969	42.6672	0.7056	1527	27	27	0	0	27	0	0
CA71	1969	42.663	0.7122	2155	25	25	0	0	25	0	0
CA72	1969	42.6623	0.7108	2155	27	27	0	0	27	0	0
CA73	1969	42.6609	0.7099	2155	23	23	0	0	23	0	0
CA74	1969	42.6751	0.7075	1512	30	30	0	0	30	0	0
CA75	1969	42.6294	0.7667	1845	36	20	16	0	36	0	0
CA76	1969	42.5955	0.7638	1783	16	7	9	0	16	0	0
CA77	1969	42.5815	0.7631	1805	65	60	5	0	65	0	0
CA78	1969	42.5781	0.7627	1805	40	40	0	0	40	0	0
CA79	1969	42.5693	0.7536	1445	22	22	0	0	22	0	0
CA80	1969	42.5642	0.7488	1301	37	26	9	2	37	0	0
CA81	1969	42.5515	0.7388	1296	26	26	0	0	26	0	0
CA82	1969	42.5481	0.725	1149	58	35	1	22	58	0	0
CA83	1969	42.5274	0.7179	1130	53	23	11	19	53	0	0
CA84	1969	42.5057	0.7174	1418	44	34	3	7	43	0	1
CA85	1969	42.4926	0.716	1135	62	23	5	34	61	0	1
CA86	1969	42.4794	0.7143	1008	33	13	0	20	33	0	0
CA87	1969	42.4599	0.706	969	67	33	4	30	60	6	1
CA88	1969	42.432	0.7179	924	75	72	3	0	71	1	3
CA89	1969	42.4294	0.7274	878	41	19	0	22	40	0	1
CA90	1969	42.4065	0.7369	886	51	47	1	3	47	0	4
CA91	1969	42.3735	0.7262	941	43	43	0	0	19	15	9
CA92	1969	42.5693	0.8465	1823	16	16	0	0	6	1	9
CA93	1969	42.5608	0.8441	1986	9	9	0	0	3	0	6
CA94	1969	42.5447	0.8417	1512	41	37	4	0	20	2	19
CA95	1969	42.5311	0.8346	1787	24	24	0	0	8	2	14
CA96	1969	42.5167	0.8227	1208	41	41	0	0	20	3	18
CA97	1969	42.5057	0.7953	1095	38	37	1	0	7	2	29
CA98	1969	42.496	0.7822	1138	23	23	0	0	9	3	11
CA99	1969	42.4706	0.7738	1037	60	58	2	0	33	4	23
CA100	1969	42.465	0.7619	1023	35	33	2	0	34	0	1
CA101	1969	42.4616	0.7477	1261	71	71	0	0	13	1	57

CA102	1969	42.4557	0.7405	1108	40	38	2	0	24	3	13
CA103	1969	42.4401	0.7346	923	68	41	20	7	41	2	25

Table S4.3. Direction of change in shell morph frequencies, from 1960s to 2017/2018 in the Pyrenees.

Morphs	Vielha			Jueu			Riba			Tort		
	Increase	No change	Decrease									
Yellow	17	6	14	4	6	2	12	1	6	10	3	6
Pink	14	6	17	2	6	4	7	5	7	3	6	10
Brown	0	0	0	0	0	0	4	5	10	2	16	1
Unbanded	15	3	19	2	5	5	3	5	11	5	2	12
Mid-banded	13	13	11	0	7	5	1	15	3	6	10	3
Banded	22	0	15	6	5	1	12	5	2	12	2	5

No Change = +/-3%

Table S4.4. Statistical summary of shell altitudinal distribution in each valley; correlations (Pearson, parametric; Kendall, non-parametric).

	Vielha			Jueu		
	Correlation	Parametric	P-value	Correlation	Parametric	P-value
Present (2017/2018)						
Yellow	0.136	Yes	0.357	0.755**	No	0.002
Unbanded	0.165	No	0.455	0.678**	No	0.001
Banded	0.058	No	0.111	-0.687**	No	0.001
Spectrophotometry (2017/2018)						
Yellow	-0.081	No	0.588	0.668*	No	0.013
PC1	0.103***	No	0.000	-0.015	No	0.833
PC2	-0.088**	No	0.001	0.414***	No	0.000
PC3	-0.089	No	0.056	0.397***	No	0.000
Past (1962/1969)						
Yellow	0.482***	No	0.000	0.492***	No	0.000
Unbanded	0.517***	No	0.000	0.858***	No	0.000
Banded	-0.480***	No	0.000	-0.834***	No	0.000

*p < 0.05. **p < 0.01. ***p < 0.001

	Riba			Tort		
	Correlation	Parametric	P-value	Correlation	Parametric	P-value
Present (2017/2018)						
Yellow	-0.235	No	0.429	0.265*	No	0.025
Unbanded	0.326	No	0.179	-0.203	No	0.111
Banded	-0.070	No	0.562	0.335*	No	0.029
Spectrophotometry (2017/2018)						
Yellow	n/a	n/a	n/a	n/a	n/a	n/a
PC1	n/a	n/a	n/a	n/a	n/a	n/a
PC2	n/a	n/a	n/a	n/a	n/a	n/a
PC3	n/a	n/a	n/a	n/a	n/a	n/a
Past (1962/1969)						
Yellow	-0.321	No	0.362	0.338	No	0.062
Unbanded	-0.059	No	0.088	-0.164	Yes	0.434
Banded	0.226	No	0.129	0.170	Yes	0.416

*p < 0.05. **p < 0.01. ***p < 0.001

Chapter 5:

Thinking process leading towards the Region-based Fully Convolutional Networks (R-FCN)

Taking the spectra data from all the samples used in chapter four as well as those from the characterization study of the colour variation in *C. nemoralis* (Davison et al., 2019), the next step was to generate a system to classify the colour of each individual, in the three classic discrete colours; yellow, pink and brown. They proposed a Gaussian mixture modelling to find cluster on the chromatic coordinate data. However, this method failed to separate pink from brown shells. Therefore, the first strategy was to apply all the different machine-learning algorithms, which could potentially work with this kind of data. K-means, Hdbscan, K-nearest neighbors (KNN), Naïve bayes, Partitioning around medoids algorithms were applied with similar results. Thereafter, I research through the engineering literature, which showed how deep learning algorithms pushed the boundaries found by machine learning in image colour processing by improving prediction performance using huge amount of data and plentiful computing resources. Therefore, in 2018 Fast-CNN (Girshick, 2015) was one of the main algorithm used in image detection. When testing this method in our data, the prediction performance improved considerably. However, the results were still under 80% accuracy. More research in the field and the discovery of a recent developed algorithm called 'Region-based Fully Convolutional Networks (R-FCN)', made our method to achieve further accuracy in prediction and classification as shown in chapter 5.

Supporting training metrics: The training metrics used in the deep learning algorithm to evaluate the test.

Figure S5.1. This collage shows example images from the training dataset. Each row displays the 7 main phenotype groups selected and each column the 8 different backgrounds (habitats where *C. nemoralis* can be found) used in all dataset.

Figure S5.2. These figures illustrate examples of prediction results in challenging scenarios such as various lighting, shell angles, distances, poses, blurriness,

enclosed and occluded shell pictures.

S5.1. Supporting training metrics.

DONE (t=0.81s).

Average Precision (AP) @[IoU=0.50:0.95 | area= all | maxDets=100] = 0.544
Average Precision (AP) @[IoU=0.50 | area= all | maxDets=100] = 0.764
Average Precision (AP) @[IoU=0.75 | area= all | maxDets=100] = 0.718
Average Precision (AP) @[IoU=0.50:0.95 | area= small | maxDets=100] = 0.700
Average Precision (AP) @[IoU=0.50:0.95 | area=medium | maxDets=100] = 0.610
Average Precision (AP) @[IoU=0.50:0.95 | area= large | maxDets=100] = 0.579
Average Recall (AR) @[IoU=0.50:0.95 | area= all | maxDets= 1] = 0.607
Average Recall (AR) @[IoU=0.50:0.95 | area= all | maxDets= 10] = 0.728
Average Recall (AR) @[IoU=0.50:0.95 | area= all | maxDets=100] = 0.731
Average Recall (AR) @[IoU=0.50:0.95 | area= small | maxDets=100] = 0.700
Average Recall (AR) @[IoU=0.50:0.95 | area=medium | maxDets=100] = 0.708
Average Recall (AR) @[IoU=0.50:0.95 | area= large | maxDets=100] = 0.771

INFO:tensorflow:Finished evaluation at 2020-06-25-09:45:17

I0625 09:45:17.481955 140686583383936 evaluation.py:275] Finished evaluation at 2020-06-25-09:45:17

INFO:tensorflow:Saving dict for global step 10000: DetectionBoxes_Precision/mAP = 0.5436208, DetectionBoxes_Precision/mAP (large) = 0.57905686, DetectionBoxes_Precision/mAP (medium) = 0.6099704, DetectionBoxes_Precision/mAP (small) = 0.7, DetectionBoxes_Precision/mAP@.50IOU = 0.7640599, DetectionBoxes_Precision/mAP@.75IOU = 0.71781445, DetectionBoxes_Recall/AR@1 = 0.6070529, DetectionBoxes_Recall/AR@10 = 0.72803134, DetectionBoxes_Recall/AR@100 = 0.73080885, DetectionBoxes_Recall/AR@100 (large) = 0.77087796, DetectionBoxes_Recall/AR@100 (medium) = 0.70782596, DetectionBoxes_Recall/AR@100 (small) = 0.7, Loss/BoxClassifierLoss/classification_loss = 0.11253723, Loss/BoxClassifierLoss/localization_loss = 0.04197678, Loss/RPNLoss/localization_loss = 0.006537688, Loss/RPNLoss/objectness_loss = 0.004196453, Loss/total_loss = 0.16524817, global_step = 10000, learning_rate = 0.0003, loss = 0.16524817

I0625 09:45:17.482253 140686583383936 estimator.py:2049] Saving dict for global step 10000: DetectionBoxes_Precision/mAP = 0.5436208, DetectionBoxes_Precision/mAP (large) = 0.57905686, DetectionBoxes_Precision/mAP (medium) = 0.6099704, DetectionBoxes_Precision/mAP (small) = 0.7, DetectionBoxes_Precision/mAP@.50IOU = 0.7640599, DetectionBoxes_Precision/mAP@.75IOU = 0.71781445, DetectionBoxes_Recall/AR@1 = 0.6070529, DetectionBoxes_Recall/AR@10 = 0.72803134, DetectionBoxes_Recall/AR@100 = 0.73080885, DetectionBoxes_Recall/AR@100 (large) = 0.77087796, DetectionBoxes_Recall/AR@100 (medium) = 0.70782596, DetectionBoxes_Recall/AR@100 (small) = 0.7, Loss/BoxClassifierLoss/classification_loss = 0.11253723, Loss/BoxClassifierLoss/localization_loss = 0.04197678, Loss/RPNLoss/localization_loss = 0.006537688, Loss/RPNLoss/objectness_loss = 0.004196453, Loss/total_loss = 0.16524817, global_step = 10000, learning_rate = 0.0003, loss = 0.16524817

INFO:tensorflow:Saving 'checkpoint_path' summary for global step 10000: training/model.ckpt-10000

I0625 09:45:17.496410 140686583383936 estimator.py:2109] Saving 'checkpoint_path' summary for global step 10000: training/model.ckpt-10000

INFO:tensorflow:Performing the final export in the end of training.

I0625 09:45:17.497366 140686583383936 exporter.py:410] Performing the final export in the end of training.

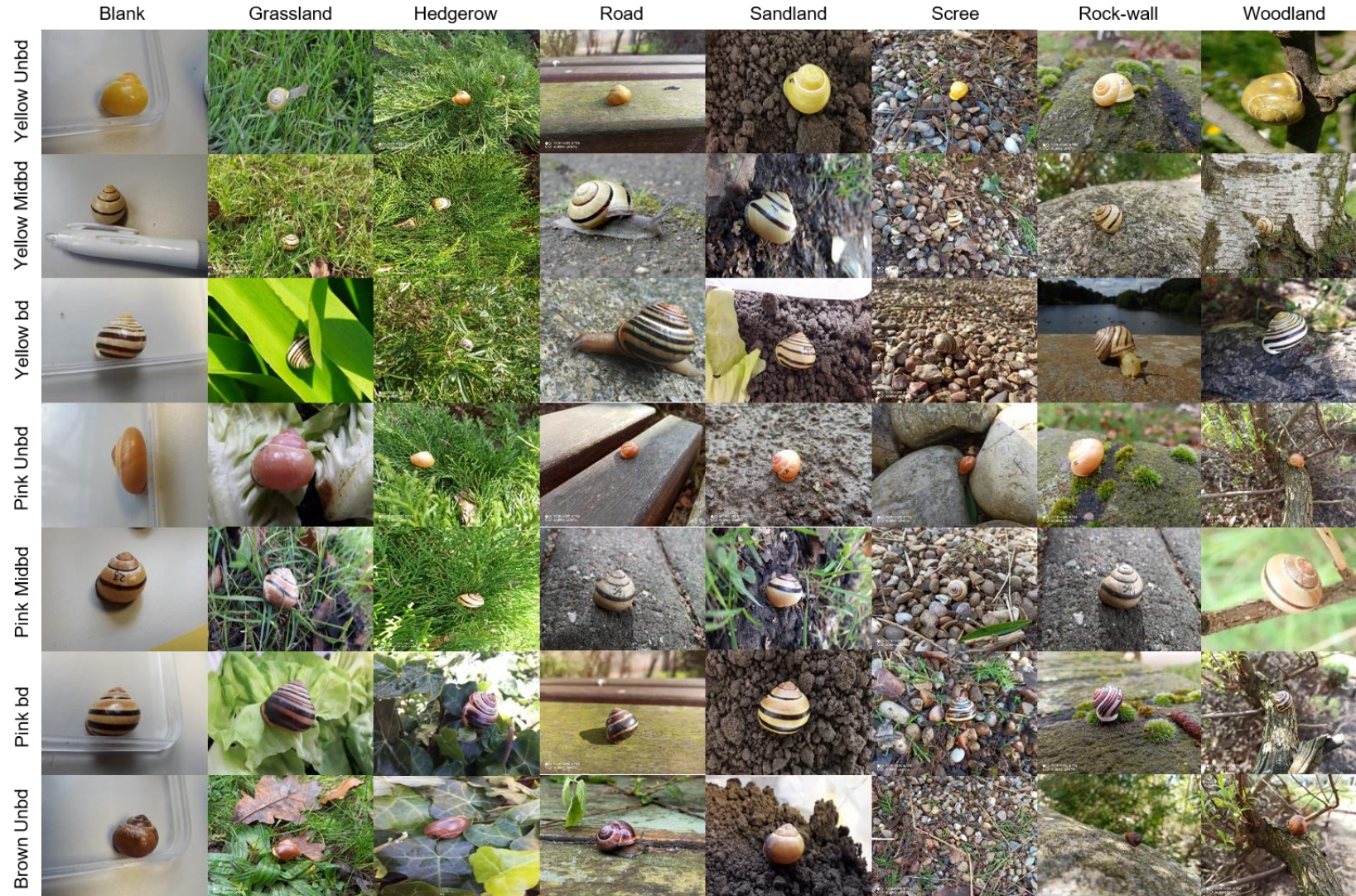


Figure S5.1. This collage shows example images from the training dataset. Each row displays the 7 main phenotype groups selected and each column the 8 different backgrounds (habitats where *C. nemoralis* can be found) used in all dataset.

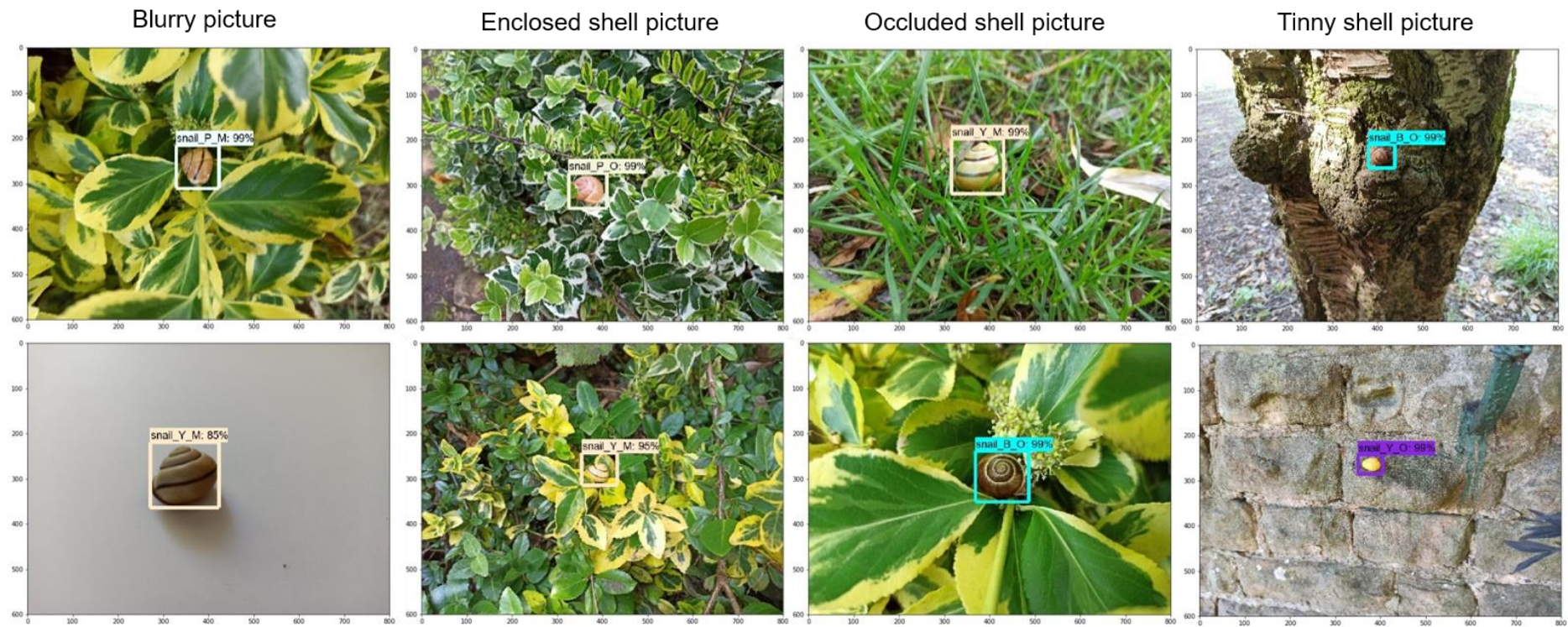


Figure S5.2. These figures illustrate examples of prediction results in challenging scenarios such as various lighting, shell angles, distances, poses, blurriness, enclosed and occluded shell pictures.